Investigation into the effect of compliant response on fluid flow in an ex vivo heart perfusion test system

by

Katie Gwendlyn Cameron

A thesis submitted in partial fulfillment of the requirements for the degree of

Master of Science

Department of Biomedical Engineering
University of Alberta

Abstract

Demand for heart transplants far exceeds supply. This is often attributed to the high percentage of donor hearts that are discarded due to cell injury and to the narrow six-hour time window currently available for transplantation. A method called *ex vivo* heart perfusion (EVHP) enables the use of damaged donor hearts and extends the available time window by preserving the heart's beating function outside the body from the time of donation until transplantation. To-date, research efforts have focused on controlling the metabolic environment required to maintain cardiac tissue health. However, the effect of the fluid mechanics of the system on cardiac performance has yet to be investigated. The region of the system where the fluid mechanics are most complex and the potential for adverse organ-machine interaction is highest is the region following the left ventricle where, *in vivo,* blood is ejected into the body's largest and most compliant artery, the aorta. The well-understood expansion-recoil function of the aorta plays the crucial roles *in vivo* of ensuring forward blood flow in the peripheral vasculature and reducing cardiac workload. These functions help mitigate the fatigue and remodeling of cardiac muscle that occur in response to elevated cardiac workload. It is likely that the introduction of compliant aortic response into the EVHP system would have a similarly positive effect on cardiac performance, but this idea has not been explored prior to this investigation.

This work has been undertaken to study of aortic compliant response in a mechanical flow loop analogous to the left side of the EVHP system in order to determine the impact of compliance on system performance. To this end, two experiments were performed; one established a fundamental case and the other explored a physiological case. The first experiment studied the pulsatile flow from a peristaltic pump in the analog system to establish a fundamental case of compliant response in a pulsatile flow regime. This experiment also compared the response of a Newtonian fluid to that of non-Newtonian fluid to ascertain whether or not non-Newtonian effects in the system warrant further investigation. The second experiment generated a simulated cardiac flow through the system using a commercial ventricular assist device (VAD). This experiment addressed the effect of compliance in a physiological pulsatile flow regime. For both experiments, three parameters were used to assess the impact of compliance on system performance: pressure, tube response and downstream velocity fields. Pressure was monitored at the inlet and outlet of the compliant section, as well as downstream where the velocity fields were obtained. Tube response was monitored with a camera and the downstream flow fields were captured using time-resolved particle imaging velocimetry (PIV). These parameters were used to assess the performance of the pump by applying unsteady Bernoulli analysis to the system and comparing these values to those obtained with a rigid test section.

In the case of the peristaltic pump experiment, it was found that the introduction of compliance into the system smoothed out the pressure and velocity responses and increased the energy applied by the pump for both fluids. The relationship between pulse frequency and pump energy was different for each fluid; the Newtonian case reached a peak at a pulse frequency of 1.67 Hz, while the non-Newtonian case maintained a positive linear relationship across the range of tested frequencies.

For the VAD experiment, the introduction of compliant response into the system was found to improve all evaluated system performance parameters. The compliant mock aorta case demonstrated healthier pressure waveform profiles, less downstream reverse flow and lower pump energy requirements. This is an important finding, as is suggests that the introduction of aortic response into the EVHP system is likely to have a positive impact on cardiac performance. Further, this work on pump energy requirements may serve as a useful proxy for quantifying cardiac performance in future work.

Preface

This thesis is original work by Katie Cameron. Part of the content contained in Chapter 4 and 5 of this thesis are published as Cameron, K., Freed, D.H., Nobes, D.S. (2016) *Time-resolved PIV of the pulsatile flow from an ex vivo heart perfusion model* in the proceedings of the 18th International Symposium on the Application of Laser and Imaging Techniques to Fluid Mechanics. Part of the content contained in Chapter 5 is under review for being published as Cameron K., Yu, B., Freed, D.H., Nobes, D.S. (2017) *Time-resolved PIV of the pulsatile flow field downstream of a mock aorta in an ex vivo heart perfusion model* in the proceedings of the ASTFE 2nd Thermal and Fluid Engineering Conference.

Acknowledgements

First and foremost, I would like to acknowledge that financial support for this project was provided by the Natural Sciences and Engineering Research Council (NSERC) of Canada, the Canadian Foundation of Innovation (CFI), the Canadian National Transplant Research Program (CIHR/CNTRP) and the University Hospital Foundation (UHF).

I would like to thank my co-supervisors Dr. Darren H. Freed and Dr. David S. Nobes for their unyielding support throughout my studies. To Dr. Freed, I would like to express gratitude for providing me with this great opportunity and instilling in me a love of the field of biomedical engineering. His investment in me pursuing this project and his guidance throughout is greatly appreciated. To Dr. Nobes, I would like to express appreciation for the patient guidance he provided every step of the way and for providing me with the resources and skills I needed to accomplish my goals. His dedication to training students is admirable and I have grown immensely as an engineer-in-training under his supervision.

I am also grateful to Bona Yu and Joshua Mulder who dedicated their summers to helping with this project. Their hard work went a long way to pushing this project forward and their contributions are greatly appreciated. The help and support of my friends and lab mates are also greatly appreciated. A special thanks is owed to Jake Hadfield and Mike Bayans who always lent a hand when I need assistance with in the lab.

Finally, I would like to send out a loving thank you to my parents for their unconditional support, and to my fiancé who has been my rock throughout this experience. Thank you all for being so supportive of my dreams!

Table of Contents

List of Tables

List of Figures

List of Symbols

Symbol	Description	Unit
α	Womersley number	--
α^*	Complex Womersley number for non-Newtonian fluid	--
A_{max}	Maximum tube cross sectional area	mm^2
A_{min}	Minimum tube cross sectional area	mm^2
cAI_x	Central aortic augmentation index	--
d	Distensibility	$mmHg^{-1}$
D	Diameter	m
De	Deborah number	--
$\frac{\partial p(t)}{\partial z}$	Axial pressure gradient	mmHg/m
E	Young’s modulus	mmHg
f	Pulse frequency	Hz
$\emptyset_n$	Phase change angles for unsteady component of axial pressure gradient	rad
g	Acceleration due to gravity	m/s^2
$\dot{\gamma}$	Shear rate	s^{-1}
h	Tube wall thickness	mm
I	Intensity	--

v	Kinematic viscosity	m^2/s
J_0	Zeroth order Bessel function	--
k	Flow consistency of a power-law fluid	$Pa.s^n$
L	Tube length	m
L_{eff}	Effective length of fluid column	m
μ	Viscosity	Pa.s
n	Flow index of a power-law fluid	--
N	Number of harmonic components of a periodic function included in the Fourier expansion	--
ω	Frequency	rad/s
$\omega_{Al\ pump}$	VAD experiment afterload pump speed	RPM
P	Pressure	mmHg
P_0	Steady component of axial pressure gradient	mmHg
P_1	Value of first occurring peak on central aortic pressure waveform	mmHg
P_2	Value of second occurring peak on central aortic pressure waveform	mmHg
$\bar{P}_a$	Mean arterial pressure	mmHg
$P_{Ao}(t)$	Aortic pressure waveform	mmHg
P_{ch}	Mock aorta chamber pressure	mmHg
P_d	Diastolic pressure	mmHg
P_n	Unsteady axial pressure gradient component coefficients	mmHg

P_p	Pulse pressure	mmHg
P_s	Systolic pressure	mmHg
r	Radial distance	m
R	Radius	m
ρ	Density	kg/m^3
t	Time	s
τ	Pulse cycle time	s
t_{ch}	Characteristic relaxation time	s
τ_{rz}	Shear stress	Pa
u	Velocity	m/s
$u_z(r,t)_{unsteady}$	Unsteady component of velocity in pulsatile flow regime	m/s
$u_z(r)_{steady}$	Steady component of velocity in pulsatile flow regime	m/s
V	Voltage	V
x	Horizontal coordinate in image	pixel
y	Vertical coordinate in image	pixel
z	Elevation	m

Glossary of Terms

Abbreviation	Description
AV	Aortic valve
DAQ	Data acquisition
DBD	Donation after brain death
DCD	Donation after circulatory death
EVHP	Ex vivo heart perfusion
FFT	Fast Fourier Transform
FIC	Flow indicating controller
FOV	Field of view
FT	Flow transmitter
LA	Left atrium
LV	Left ventricle
MV	Mitral valve
P1	Pump 1 (preload pump) in the EVHP system
P2	Pump 2 (afterload pump) in the EVHP system
PIV	Particle imaging velocimetry
PT	Pressure transmitter
PTV	Particle tracking velocimetry
PV	Pulmonary valve
PWV	Pulse wave velocity
RA	Right atrium

RV	Right ventricle
TV	Tricuspid valve
VAD	Ventricular assist device

Chapter 1. Literature Review

1.1 Introduction

Heart transplantation is the gold standard treatment for end stage heart failure patients [1] but demand for viable donor hearts far outweighs supply. In Europe and the United States, 10-12% of patients on the heart transplant waitlist die prior to receiving a heart [2] and there are many others who are removed from the waitlist due to irreversible disease degeneration. The critical shortage of donor hearts is often attributed [1], [3], [4] to three factors: high discard rate amongst available donor hearts, the limited time window available for transplantation, and the non-utilization of hearts from Donation after Circulatory Death (DCD) donors.

Currently, the only reliable source of donor hearts is Donation after Brain Death (DBD) donors but there are issues associated with hearts from donors of this type. During the process of brain death, donor organs experience an increased intracranial pressure which leads to a compensatory response of vasoconstriction and tachycardia, known as a “catecholamine storm” [5]. Although the majority of the myocardium is intact and healthy, this compensatory response often results in localized cell injury that can preclude donor hearts from being viable for transplantation [1], [5]. In North America only 36-39% of available donor hearts are successfully transplanted [6], [7]. In cases where the rest of the cardiac tissue is healthy, the localized cell injury is repairable [1] but the current method of donor heart storage and transportation does not facilitate this rehabilitation.

The current standard of donor heart storage is hypothermic static storage [8]. It involves lowering the temperature of the heart to reduce its metabolic demands and mitigate the effects of ischemia and hypoxia that result from removing the heart from its native environment [9]. While this method is the standard for organ transplant storage and transportation, it presents significant challenges that contribute to the shortage of available donor hearts. First, it imposes a six hour limitation on the time window available for transplantation [9]. Also, in addition to not facilitating rehabilitation of existing tissue injuries, the method can expose the organs to mechanical injuries [8]. Due to these limitations of the current method, there is a need to look for both a better method of preserving the available hearts and another reliable source of donor hearts.

Another source of donor hearts that remains largely untapped is Donation after Circulatory Death (DCD) donors. DCD donors are patients whose deaths are confirmed using circulatory criteria but not necessarily using neurological criteria [10]. This occurs most often in patients who have suffered cardiac arrest after being taken off life support but maintain brainstem response. In such cases, there is a short period of time after the heart stops beating and blood supply has terminated that the heart experiences oxygen deprivation while still at body temperature; this is known as the warm ischemic time [11]. The warm ischemic time is much longer for DCD donors than for DBD donors, therefore the risk of tissue damage is higher. This is the primary reason why DCD donor organ usage has yet to be widely accepted into clinical practice [3].

In order to reconcile demand for heart transplants with supply, the donor pool must be expanded. Three important opportunities to do so involve facilitating repair of tissue injury, extending the time window available for transplantation, and using hearts from DCD donors. *Ex vivo* heart perfusion (EVHP) has been proposed [1], [12], [13] as a method by which damaged donor hearts, from DBD or DCD donors, can be resuscitated, preserved and monitored. This method provides an opportunity to repair damaged hearts, extend the time window available for transplantation and utilize hearts from DCD donors [1]. It involves connecting a donor heart to a mechanical system that maintains its natural beating function outside the body. While the heart is operating, metabolic and mechanical conditions can be controlled in response to monitored changes in cardiac performance. This ability to functionally assess heart performance *ex vivo* is crucial for determining transplantation viability and providing the opportunity for resuscitation and preservation of donated hearts that is unique to this method [1]. Existing transplant technologies have not addressed these aspects of EVHP so there is great opportunity for further research into device optimization.

In order to maintain the heart's natural beating function, the flow loop of the EVHP system currently being researched [1] is set up to mimic the two circulatory loops in the body: pulmonary circulation and systemic circulation. The circulatory systems are shown in Figure 1-1, in which red and blue lines denote pathways of oxygenated and deoxygenated blood, respectively. The heart is comprised of two receiving chambers and two pumping chambers, the left and right atrium (LA & RA) and the left and right ventricle (LV & RV), respectively. The left atrium receives oxygenated blood from the lungs and the left ventricle pumps that blood to the body's organs against the resistance of the body's vasculature. Following delivery to the organs, the now deoxygenated blood is returned to the right atrium. This loop of oxygenated blood being delivered to the organs and deoxygenated blood being returned to the heart is called systemic circulation. Similarly, the right ventricle pumps deoxygenated blood to the lungs and the newly oxygenated blood is delivered to the left atrium. This flow loop, which encompasses the oxygenating of blood in the lungs and corresponding delivery to the left atrium, is called pulmonary circulation.

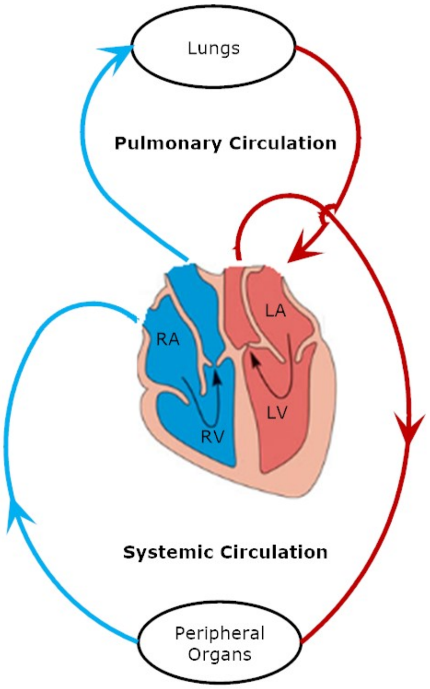

Figure 1-1: Schematic representation of *in vivo* circulatory systems, adapted from [14]

In the EVHP system, the heart is connected to a mechanical flow loop via four connection points: LA, LV, RA, RV. As the heart beats via pacemaker stimulation, blood flows through the system; this allows the heart to receive and eject blood in its natural beating cycle. Current research is being conducted with porcine hearts, which have traditionally been used to represent human heart behavior in research environments. The current flow loop components, including the heart and mechanical components, are shown in Figure 1-2. The system is comprised of a pacemaker-implanted heart, a reservoir, arterial filter, two centrifugal pumps, an oxygenator and a series of tubes, as shown in Figure 1-2. Pump 1 (P1) supplies flow to the left and right atria of the heart which, upon pacemaker stimulation, contract. This ejects perfusate, a mixture of blood and support nutrients, into ⅜” and ½” tubing in the mock systemic and pulmonary circulatory loops, respectively. Pump 2 (P2) simulates vascular afterload by supplying a constant flow against the direction of ventricular ejection. This provides resistance to the flow and a back pressure that allows the aortic valve to close. Flow ejected from the left ventricle combines with flow supplied by P2, passes through an oxygenator, then combines with flow from the right ventricle and finally, returns to the reservoir. Pressure and flow monitoring at several locations provides direct feedback of the conditions and performance of the heart.

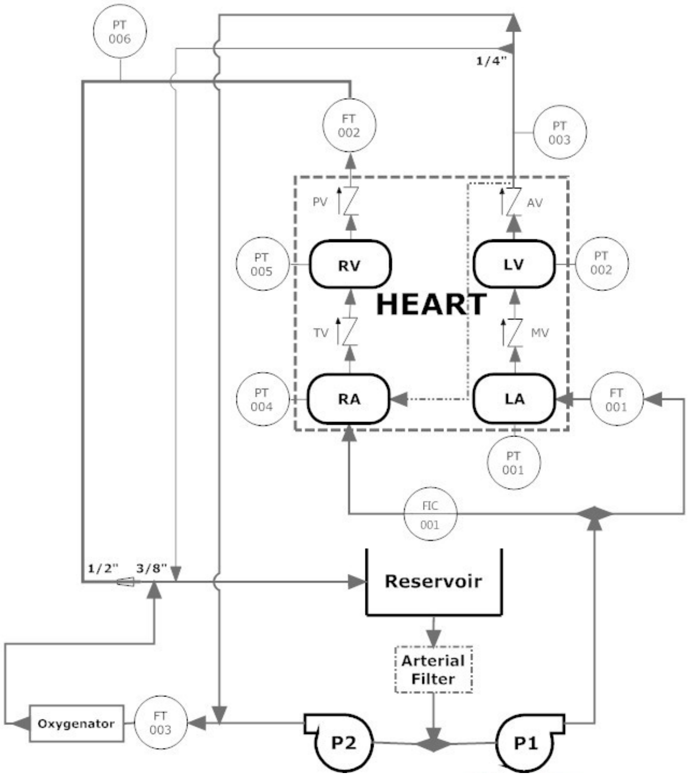

Heart	
LA	Left Atrium
MV	Mitral Valve
LV	Left Ventricle
AV	Aortic Valve
RA	Right Atrium
TV	Tricuspid Valve
RV	Right Ventricle
PV	Pulmonary Valve

EVHP System	
FIC	Flow Indicating Controller
FT	Flow Transmitter
PT	Pressure Transmitter

Figure 1-2: Schematic of the current EVHP system setup

To date, research efforts have been largely focused on controlling the metabolic environment required to sustain cardiac performance and on developing monitoring procedures [1], [12], [13]. The fluid mechanics of the system and their corresponding impact on cardiac performance have yet to be investigated. The most complex region of flow in the system is the left flow loop which simulates *in vivo* systemic circulation. Immediately following the heart's primary pumping chamber, the left ventricle, is the body's largest artery, the aorta. During the cardiac cycle, the aorta exhibits a compliant response in response to the pressure pulse generated by the heart, which is known as the Windkessel effect [15]. This compliant response is not currently present in the EVHP system as a consequence of the attachment method in which the explanted donor heart aortic root is connected to the device with rigid tubing. It is likely that the lack of elastic response in this region of flow is impairing cardiac performance of donor hearts. However, this impact has not been quantified and the possibility of adding a mock aorta into the system to replicate the Windkessel effect has not been explored prior to this investigation. The remainder of this chapter will provide an overview of the relevant topics and literature that were reviewed during this work.

1.2 Cardiac cycle

The heart undergoes a well-defined mechanical contraction-relaxation process known as the cardiac cycle [16]. The pressure pulse generated by the heart during contraction is impacted both by the intrinsic properties of the heart muscle, such as contractility, and by the hemodynamic conditions in the vasculature, such as blood pressure. Information about cardiac performance and cardiovascular health is most commonly understood through interpretation of pressure waveforms in the peripheral arteries, those that are far away from the heart. While this is common clinical practice due to the non-invasive nature of such measurement, more important information about cardiovascular function can be obtained from central aortic pressure waveforms that are obtained directly in the aorta [17]. Understanding the values that can be obtained from central aortic pressure waveforms provides a foundation upon which to study cardiovascular flow.

A labelled diagram of a generic central aortic pressure waveform is shown in Figure 1-3.The cardiac cycle occurs in two stages called systole and diastole which represent ventricular contraction and relaxation, respectively. When the LA receives oxygenated blood from the lungs, left atrial pressure rises until it exceeds left ventricular pressure at which point the MV opens and blood flows into the LV. Once left ventricular pressure exceeds left atrial pressure the MV closes. Once the MV is closed, the LV receives an electrical impulse which induces it to contract. The minimum pressure of the cycle occurs just prior to ejection and is referred to as the diastolic foot [18]. This initiation of isovolumetric contraction marks the beginning of mechanical systole, the period of ventricular ejection which, under ideal conditions, lasts approximately one third of the cardiac cycle duration. The LV pressure rise continues until the LV pressure exceeds the back pressure of the systemic vasculature, at which point the aortic valve opens and blood is ejected into the aorta. During this stage, there is a rapid increase in aortic pressure. The corresponding rise in pressure on the aortic pressure waveform is referred to as the anacrotic limb during which time the compliant aorta expands to store a portion of the ejected blood. Once the ventricle is finished contracting and the systolic peak is reached, both left ventricular and aortic pressure begin to drop. Once left ventricular pressure drops below aortic pressure, the aortic valve closes which marks the end of systole. When the aortic valve closes, there is a momentary rise in aortic pressure due to the elastic recoil of the aortic wall against a closed aortic valve [16]; this is referred to as the dicrotic notch. Now that both the mitral and aortic valves are closed, the ventricle undergoes isovolumetric relaxation, which marks the beginning of diastole. This period of ventricular relaxation and aortic pressure drop is referred to as the dicrotic limb on the aortic pressure waveform. Once the ventricle relaxes to a pressure lower than the left atrial pressure, the mitral valve opens and left ventricular filling begins again. During this period, aortic pressure is decreasing as blood is being delivered to the body's organs, and it will continue to do so until the aortic valve opens and systole begins again. At the same time, blood flows through the coronary ostia behind the aortic valve into the coronary arteries, allowing nourishment and oxygenation of the heart tissue.

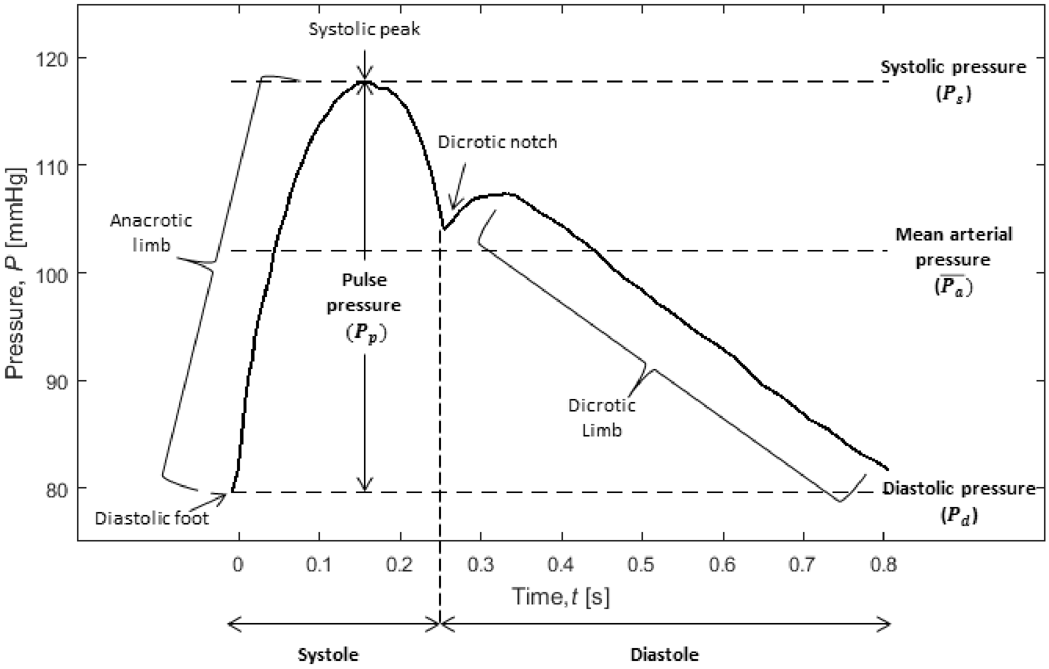

Figure 1-3: Labelled diagram of a generic central aortic waveform, adapted from waveform presented in [16]

There are four important pressure readings that can be determined from Figure 1-3: diastolic pressure (P_d), systolic pressure (P_s), mean arterial pressure ($\bar{P}_a$) and pulse pressure (P_p). Diastolic pressure is the minimum pressure in the cycle, which occurs at the diastolic foot prior to aortic valve opening and ventricular ejection. Systolic pressure is the maximum pressure achieved during the cycle, which occurs at the systolic peak. Mean arterial pressure is a consequence of peripheral arterial vasculature and is calculated as the mean pressure of the aortic pressure waveform [19]:

$$\bar{P}_a = \int_0^{t_c} P_{Ao}(t)dt \tag{1-1}$$

where t_c is the cycle time [s] and $P_{Ao}(t)$ is the periodic aortic pressure waveform function. Lastly, pulse pressure is defined as the difference between the systolic peak pressure and diastolic pressure:

$$P_p = P_s - P_d \tag{1-2}$$

The generic central aortic waveform presented in Figure 1-3 provides a simplified understanding of the pressure responses seen in the aorta during the cardiac cycle. The nuances of this waveform will vary based on specific hemodynamic conditions, but understanding the definitions of the pressure values represented on this waveform enables a general understanding of the systemic pressure cycle pertinent to this investigation. The nature of this pressure waveform produced by the heart greatly influences systemic flow conditions, and while pressure waveforms are often used as the sole basis for evaluating cardiovascular health, the resulting flow conditions can also provide important information about cardiac performance. A review of cardiovascular flow properties will be discussed in the following sections.

1.3 Non-Newtonian nature of blood

The pressure fluctuations involved in the cardiac cycle induce flow with a time-varying shear rate. Blood is a non-Newtonian fluid, meaning that such variations in shear rate induce non-linear changes in the fluid's viscosity [20]. There are a number of models that can be used to describe non-Newtonian fluid behaviour, but the one of concern to this investigation is the Ostwald-de Waele power-law model [20], [21] which defines the relationship between viscosity and shear rate as:

$$\mu = k(\dot{\gamma})^{n-1} \tag{1-3}$$

where μ is the fluid viscosity [Pa.s], k is the flow consistency [Pa.s^n], $\dot{\gamma}$ is the shear rate [s^{-1}] and n is the flow index. Flow index and consistency are determined using the log-log relationship between viscosity and shear rate:

$$\log(\mu) = (n-1)\log(\dot{\gamma}) + \log(k) \tag{1-4}$$

The slope of this relationship, $(n-1)$, is used to determine the flow index of the fluid, n, and the intercept, $\log(k)$, is used to determine the flow consistency, k. Based on the value of n, non-Newtonian fluids are classified as either shear thickening or shear thinning. Shear thickening fluids are characterized by a positive relationship between shear rate and viscosity as indicated by $n > 1$ in the power-law model. Shear thinning fluids exhibit decreasing viscosity at increasing shear rates, described in the power-law model by $n < 1$. Fluids with $n = 1$ are classified as Newtonian fluids.

Blood is classified as a shear-thinning fluid due to its reduced viscosity at high shear rates [22]. Examples of viscosity vs. shear rate plots for whole blood, obtained from [23], [24], are shown in Figure 1-4. The value of n is strongly related to the percentage red blood cell composition, the hematocrit, of the blood but typical values of n for human blood can vary between 0.67-0.72 for normal hematocrit ranges[23], [24]. Prolonged changes in blood viscosity can have significant consequences to overall health. In particular, plasma hyperviscosity has been associated with conditions such as hypertension, heart disease and stroke [22] due to its effect of increasing peripheral resistance and cardiac workload [25].

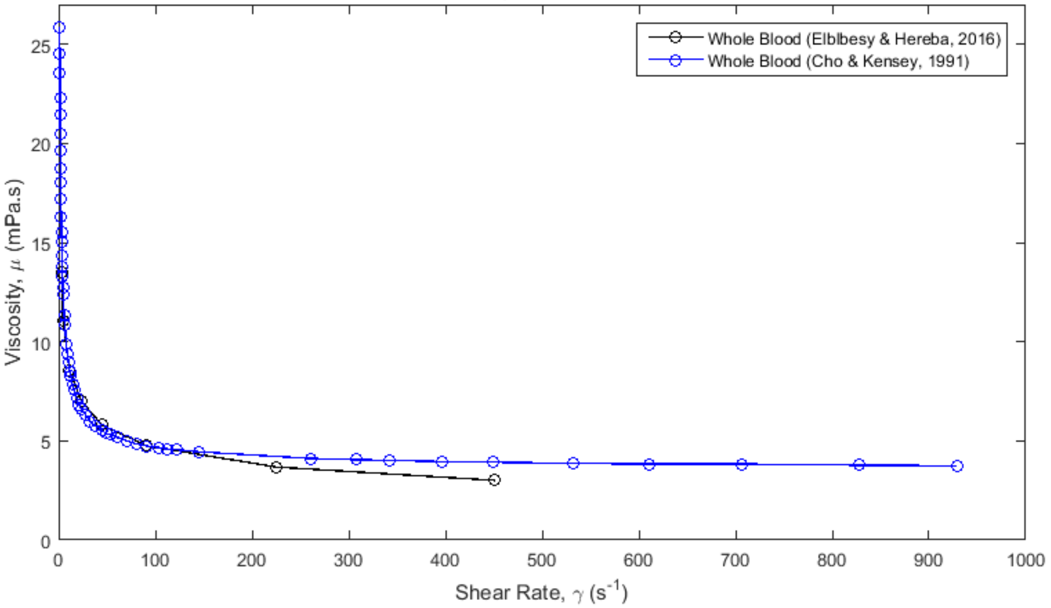

Figure 1-4: Plot of viscosity vs. shear rate of whole blood [23], [24]

Traditionally, the shear thinning behavior of blood has only been considered in small arteries where flow velocities, and therefore shear rates, are low. In the large arteries, shear rates are often greater than 100 s^{-1} [25]–[27] and non-Newtonian effects are neglected because at such high shear rates blood reaches its Newtonian limit viscosity of approximately 3.4-3.7 mPa.s [22]–[25], [28], [29]. However, a recent model [30] suggests that while this assumption holds during systole, it likely does not provide a complete picture of velocity distributions or wall shear stresses throughout the cardiac cycle because it does not account for the impact of the low shear rates during diastole. To the author's knowledge, there has been minimal experimental investigation into this model in an *ex vivo* large compliant artery model.

Due to the opaque appearance of blood, investigations involving fluid imaging techniques require the use of transparent blood analog fluids to study the impact of blood's viscoelastic properties on flow fields. The most common blood analogs used for experimental investigations are aqueous polyacrylamide and xanthan gum/glycerol solutions [31]. Polyacrylamide provides a good representation of the viscous component of blood's shear thinning behavior but has been shown to have a larger elastic component than blood [31]. A log-log plot of the viscosity-shear rate relationship for a 0.1 wt.% aqueous polyacrylamide solution is compared to that of blood in Figure 1-5, and their n and k values are summarized in Table 1-1.

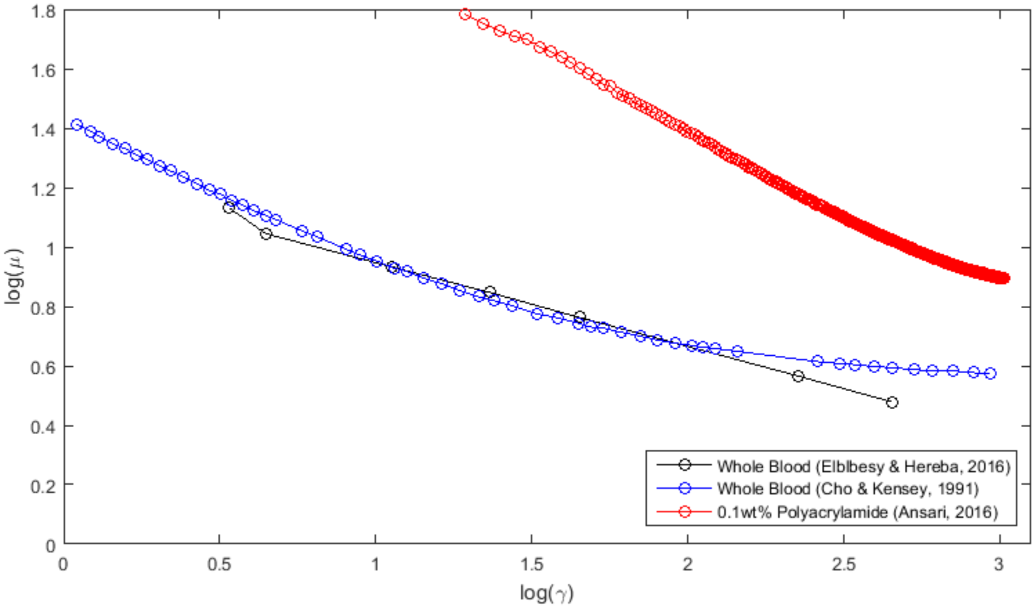

Figure 1-5: Log-log plot of viscosity vs. shear rate for whole blood and 0.1 wt.% polyacrylamide solution [20], [23], [24]

Table 1-1: Summary of flow index and flow consistency values for blood and 0.1 wt.% aqueous polyacrylamide solution

Fluid	Flow Index, n [--]	Flow Consistency, k [Pa.s^n]
Whole Blood [23], [24]	0.7050 – 0.7054	0.0180 – 0.0203
0.1 wt.% aqueous polyacrylamide solution [20]	0.469	0.054

1.4 Pulsatile flow

The periodic pressure gradient produced by the heart induces a pulsatile flow through the systemic arteries. Understanding the flow fields induced in the vasculature due to the heart's pumping cycle provides crucial information about the efficiency of the heart and about arterial health. Flow information can aid in determining how much energy is being successfully imparted to the fluid and how arterial properties affect cardiac workload.

The theory behind pulsatile flow is well-understood [26], [32]–[34]. The axial pressure gradient driving flow along a length of tube is a periodic function that consists of a steady component and an overlaid oscillatory component [35]:

$$\frac{\partial p(t)}{\partial z}=\frac{p_1(t)-p_2(t)}{L} \tag{1-5}$$

where $p_1(t)$ and $p_2(t)$ are the inlet and outlet pressure waveforms, respectively and L is the distance between the pressure measurement points. The axial pressure gradient can then be deconstructed into its steady and unsteady components using a Fourier expansion [36] such that:

$$\frac{\partial P(t)}{\partial z}=P_0+\sum_{n=1}^{N} P_n\, e^{i2\pi f t n_H-\emptyset_n} \tag{1-6}$$

where P_0 is the steady component of the pressure gradient, P_n is the array of wave amplitudes for the unsteady component of the pressure gradient, f is the pulse frequency [Hz], t is time [s], n_H is the number of the harmonic of each term of the expansion, N is the total number of harmonics of the wave being included in the expansion and $\emptyset_n$ is the array of wave phase changes for the unsteady component of the pressure gradient.

The time-dependent axial pressure gradient induces a periodic flow through the vasculature that also has a steady and an unsteady component. A method for quantifying the velocity and flow rate of this pulsatile flow in a straight, rigid circular pipe subjected to a known unsteady pressure gradient was first developed by Womersley [32]. At that time, the non-dimensional Womersley number, α, was defined to describe the relationship between unsteady and viscous effects in a pulsatile flow regime [32]:

$$\alpha=\frac{D}{2}\sqrt{\frac{\rho\omega}{\mu}} \tag{1-7}$$

where *D* is the tube diameter [m], ρ is the fluid density [kg/m^3], ω is the pulse frequency [rad/s] and μ is the fluid's dynamic viscosity [Pa.s]. This non-dimensional number is now widely accepted as the foremost dynamic similarity parameter used for scaling pulsatile flow experiments [37]. Flow of Newtonian fluids through rigid tubes in laminar pulsatile flow regimes is well-described [32], [35], [38]–[41] and it has been suggested that α = 10 is the limit where the fluid behavior varies significantly from the quasi-static case [42]. In human aortas, α ranges from approximately 12-20 [26], [43], [44].

Womersley numbers are much lower in the peripheral arteries; for example, $\alpha \cong 4$ in the femoral artery [43]. For these low α regimes present in small arteries, the flow has a dominant steady component and is therefore well-represented by Bernoulli's equation defined at points 1 and 2 in a fluid system [45]:

$$P_1 + \rho g z_1 + \frac{\rho {u_1}^2}{2} = P_2 + \rho g z_2 + \frac{\rho {u_2}^2}{2} \tag{1-8}$$

where P_1 and P_2 are the pressures at points 1 and 2, respectively, g is the acceleration due to gravity [m/s^2], z_1 and z_2 are the elevations of points 1 and 2, respectively and u_1 and u_2 are the flow speeds at points 1 and 2, respectively. This equation represents the conservation of energy in a fluid system under steady, incompressible flow conditions.

In high α flows, there are significant local changes in acceleration caused by the unsteady component of the pressure gradient. These changes in acceleration impact the energy in the system, therefore an extra term must be added to the Bernoulli equation to correctly represent the conservation of energy in a high α regime [33]:

$$P_1 + \rho g z_1 + \frac{\rho {u_1}^2}{2} + \int_0^1 \frac{du_1}{dt} ds = P_2 + \rho g z_2 + \frac{\rho {u_2}^2}{2} + \int_0^2 \frac{du_2}{dt} ds \tag{1-9}$$

where $\frac{du_1}{dt}$ and $\frac{du_2}{dt}$ are the flow accelerations at points 1 and 2, respectively being integrated along a streamline, *ds*. The integral terms of this equation represent how the fluid acceleration changes in the axial direction in response to the fluctuating pressure gradient. Previous investigations [33], [46], [47] have employed the use of this equation in cardiovascular analog flow regimes to relate the forces acting on the fluid to the temporal and convective accelerations that those forces induce using the assumption of uniform tube thickness from point 1 to point 2:

$$\Delta P(t) - P_{losses} = \rho L_{eff} \frac{du_2}{dt} + \frac{1}{2}\rho({u_2}^2 - {u_1}^2) \tag{1-10}$$

where $\Delta P(t)$ is the time-varying pressure gradient between the two locations in the system, p_{losses} are the frictional losses that occur along the tube length, and L_{eff} is the length of the fluid column being accelerated. This form of the equation is useful for understanding the types of energy present in systemic circulation. During ventricular contraction, work is done by the heart on the blood. The resulting energy of the fluid can then be expressed as the sum of its potential, kinetic and hemodynamic energy [48]. These concepts are useful to this investigation because, through the collection of pressure information and time-resolved velocity data, the energy relationship between pumping energy and fluid energy can be ascertained. This can then be used as a basis for assessing system performance which can be used as a proxy for understanding stress conditions of the heart.

1.4.1 Profiles of velocity

Velocity profiles are commonly used for assessing flow behaviour. While basic flow conditions can be determined from centerline velocities, which can be obtained from standard flow meter measurements, velocity profiles allow evaluation of more specific flow characteristics. They show directional changes across the tube geometry which indicate the locations of shear regions and provide information about the system's resistance to flow. Analysis of velocity profiles is particularly important in a pulsatile flow regime where the time-dependent pressure fluctuations often result in flow directional changes. This impact of pressure fluctuations is dependent on the relative magnitudes of the Womersley (unsteady) and Poiseuille (steady) component. For low α flows, velocity profiles closely resemble parabolic profiles characteristic of steady laminar flows. For high α regimes, the significant Womersley component will induce stronger regions of reverse flow [40], [42], resulting in high shear regions away from the boundary. The presence of such shear regions often produces flow instabilities which *in vivo* have been associated with atherosclerosis [44]. The presence of such flow instabilities occurs as a result of flow deceleration in the aorta during diastole [37], [44], [49] and is therefore strongly influenced by the compliant behavior of the aorta. Previous experimental investigations [50]–[54] have studied the velocity distributions through compliant phantoms using particle imaging velocimetry (PIV) and particle tracking velocimetry (PTV). To the author's knowledge, the effect of physiological aortic compliance on downstream flow fields has yet to be investigated experimentally. The following sections outline the theory behind Newtonian and non-Newtonian pulsatile profiles of velocity.

1.4.1.1 Newtonian Velocity Profiles

The steady flow component for a Newtonian pulsatile flow regime is defined by the equation of motion of fully developed laminar flow [45]:

$$\frac{\partial^2 u}{\partial r^2} + \frac{1}{r}\frac{\partial u}{\partial r} + \frac{1}{\mu}P_0 = 0 \tag{1-11}$$

where *u* is the fluid velocity [m/s], and *r* is the radial distance [m] from the tube axis. The resulting solution for the steady component of a pulsatile flow velocity profile is therefore:

$$\left[u_z(r)_{steady}\right]_{Newt} = \frac{1}{4\mu}P_0(R^2 - r^2) \tag{1-12}$$

where *R* is the radius of the tube [m].

For the unsteady component, since the pressure gradient is periodic in time, the governing equation of motion is [32]:

$$\frac{\partial^2 w}{\partial r^2}+\frac{1}{r}\frac{\partial w}{\partial r}-\frac{1}{\nu}\frac{\partial w}{\partial t}=-\frac{P_{n_H}}{\mu}e^{-in_H\omega t} \tag{1-13}$$

where w is the axial velocity of the fluid [m/s] and v is the kinematic viscosity of the fluid [m^2/s].

Since the pressure gradient is harmonic, the resulting velocity will also be described by a periodic function, $w = ue^{in_H\omega t}$. Substituting this into the equation of motion gives:

$$\frac{\partial^2 u}{\partial r^2}+\frac{1}{r}\frac{\partial u}{\partial r}-\frac{in_H}{\nu}u=-\frac{P_n}{\mu} \tag{1-14}$$

The solution for the Womersley component of the velocity profile is therefore:

$$\left[u_z(r,t)_{unsteady}\right]_{Newt}=\Re\left[\frac{i\omega}{\rho}\left(1-\frac{J_0\left(\alpha i^{3/2}\frac{r}{R}\right)}{J_0\left(\alpha i^{3/2}\right)}\right)P_n e^{in_H\omega t-\emptyset_n}\right] \tag{1-15}$$

where J_0 is a zeroth order Bessel function.

Combining this solution with the steady solution produces the complete velocity profile equation for a Newtonian fluid in a pulsatile flow regime [32], [33], [42], [55]:

$$u_z(r,t)=\frac{1}{4\mu}p_0(R^2-r^2)+\Re\left[\frac{i\omega}{\rho}\left(1-\frac{J_0\left(\alpha i^{3/2}\frac{r}{R}\right)}{J_0\left(\alpha i^{3/2}\right)}\right)P_n e^{in_H\omega t-\emptyset_n}\right] \tag{1-16}$$

This equation provides a theoretical comparison for the experimentally obtained Newtonian velocity profiles obtained during investigation.

1.4.1.2 Non-Newtonian Velocity Profiles

The steady flow component for a power-law fluid pulsatile flow regime is defined by the same equation of motion as the Newtonian case, but the presence of a shear-rate varying viscosity yields a velocity profile equation that is dependent on the flow index and consistency of the power law fluid, as defined for this case in Section 1.3. The resulting steady component of the velocity profile for a power-law fluid in a pulsatile flow regime is [34]:

$$\left[u_z(r)_{steady}\right]_{non-Newt} = \left(-\frac{1}{2}P_0\frac{1}{kL}\right)^{1/n}\left(\frac{n}{n+1}\right)\left[R^{\frac{n+1}{n}} - r^{\frac{n+1}{n}}\right] \tag{1-17}$$

For the unsteady component, both the pressure gradient and the shear rate are periodic in time, and the governing equation of motion can be expressed using the Maxwell model momentum equation for viscoelastic flow in a tube [34]:

$$\alpha^2\frac{\partial u_z}{\partial t} = -\frac{\partial P}{\partial z} + \frac{1}{r}\frac{\partial}{\partial r}(r\tau_{rz}) \tag{1-18}$$

where α is the Womersley number and τ_{rz} is shear stress [Pa]. For a power law fluid, this becomes:

$$\mathrm{De}\frac{\partial\tau_{rz}}{\partial t} + \tau_{rz} = \dot{\gamma} \tag{1-19}$$

where De=$\frac{t_{ch}}{\tau}=\frac{t_{ch}}{1/f}$ is the Deborah number, where t_{ch} is the characteristic relaxation time of the fluid as defined by the time taken for the stress vs strain rate plot of the fluid to reach its asymptotic value [s], τ is the characteristic time of the flow, the cycle time, [s], and f is the pulse frequency [Hz] [56].

Solving this ordinary differential equation with harmonic solutions for pressure, velocity and shear stress gives the resulting equation for the unsteady component of the velocity profile, which is [32]:

$$\left[u_z(r,t)_{unsteady}\right]_{non-Newt} = \Re\left[\frac{i\omega}{\rho}\left(1 - \frac{J_0\left(\alpha^* i^{3/2}\frac{r}{a}\right)}{J_0\left(\alpha^* i^{3/2}\right)}\right)P_n e^{in_H\omega t}\right] \tag{1-20}$$

where $\alpha^*=\alpha\sqrt{\frac{\omega(1+i\mathrm{De})}{\nu}}=\omega\sqrt{(1+i\mathrm{De})}$ is the complex Womersley number.

Combining this solution with the steady solution yields the complete velocity profile equation for a power-law fluid in a pulsatile flow regime:

$$u_z(r,t) = \left(-\frac{1}{2}P_0\frac{1}{kL}\right)^{1/n}\left(\frac{n}{n+1}\right)\left[R^{\frac{n+1}{n}} - r^{\frac{n+1}{n}}\right] + Re\left[\frac{i\omega}{\rho}\left(1 - \frac{J_0\left(\alpha^* i^{3/2}\frac{r}{a}\right)}{J_0\left(\alpha^* i^{3/2}\right)}\right)P_n e^{in_H\omega t}\right] \tag{1-21}$$

This section outlined the theoretical flow response of a pulsatile system to a known unsteady pressure gradient. The derived theoretical velocity profile equations provide a basis for comparing the response of the test system to the measured axial pressure gradients in the rigid and compliant cases. The presence of compliance in the system alters the axial pressure gradient, so the theoretical profiles of the rigid and compliant cases are expected to differ. This difference is expected to be particularly pronounced when highly compliant vessels such as the aorta are being considered. The next section outlines the theory behind the compliant function of the aorta and its clinical significance.

1.5 Aorta function

There have been many numerical and experimental investigations into pulsatile flows through rigid tubes [35], [37], [39], [57], but these are ultimately limited in their physiological relevance because *in vivo*, blood interacts with compliant arteries. This compliant response is particularly pronounced in the aorta, which expands to 120-160% of its end diastolic volume [53] during systole and stores approximately 50% of the stroke volume [15].

1.5.1 Elastic response

The amount of expansion is determined by the intrinsic and operative distensibility of the tissue [58] as well as the difference between the pulse pressure generated by the LV and the pressure surrounding the aorta, the transmural pressure. Typical aortic distensibility values range from approximately 1.33 - 8.90 x 10^{-3} mmHg^{-1} [59], [60] depending on the person's age and health. Although the physical meaning of distensibility is percent expansion per mmHg of internal fluid pressure, the literature [59]–[61]most commonly represents it in units of mmHg^{-1} so that is the unit that will be adopted in this thesis. During diastole, the aorta recoils, inducing forward flow of blood to the periphery. This expansion-recoil response of the aorta is thought to serve the primary purpose of dampening out pressure fluctuations from the heart's ejection in order to sustain nearly constant peripheral blood flow [62] which prevents damage to the peripheral vessels [63] and insufficient organ perfusion [64]. During systole, the heart ejects against the resistance of the body's vasculature which is essentially an incompressible column of blood. The aorta expands to make room for the stroke volume and stores some of the ejection energy as elastic energy. When the aorta recoils, the pressure increase creates the pressure gradient required to maintain forward blood flow to the periphery [15], [64]–[66].

The elastic response of the aorta is theoretically characterized by Windkessel theory, which models the aorta as a capacitor in parallel with a resistor representing the peripheral vessels [15]. Windkessel theory has been investigated using two-element, three-element and four-element models [65] which have been applied through the use of pulse contour wave analysis wherein *in vivo* central aortic waveforms are derived using generalized transfer functions of peripheral waveforms [67]. These models and corresponding analysis make the assumption of simultaneous pressurization of all points in the system and therefore fall short in being able to account for wave propagation effects or independent local changes in aortic compliance [65], [67].

1.5.2 Wave propagation

In reality, aortic compliance has a significant impact on pressure wave propagation effects *in vivo* so variations in aortic compliance are widely recognized as having a significant impact on overall cardiovascular health [67]–[69]. Aortic stiffening has been associated with cardiovascular diseases [70] such as hypertension [58], [67], [71], coronary artery disease [58], [63], [72], left ventricular hypertrophy [63], stroke, heart attack and organ damage [71]. A few metrics are used to clinically assess aortic health. The first is the speed at which pressure waves propagate through the aortic tissue, known as pulse wave velocity (PWV). PWV is defined by the Moens-Korteweg equation as [73]:

$$\mathrm{PWV} = \sqrt{\frac{Eh}{D\rho}} \tag{1-22}$$

where *E* is the Young's modulus of the tissue [Pa] and *h* is the vessel wall thickness [m]. PWV is dependent on the geometry of the aorta and the Young's modulus of the tissue. It is a clinically significant marker of cardiovascular health because it provides information about overall vascular resistance and about the impact of pressure wave transmission speed on hemodynamic conditions.

A large PWV indicates a large Young's modulus and therefore stiff aortic tissue. Stiffness reduces the amount of stroke volume that can be stored during ejection and therefore increases the amount of energy the heart has to expend to overcome the high inertial forces of the vascular afterload. This manifests in an elevated pulse pressure and, over time, the development of pathophysiology associated with heart disease [64].

In addition to aortic stiffness increasing overall vascular resistance, changes in aortic compliance induce changes in systemic pressure waveforms and therefore flow conditions. In a body with a healthy compliant aorta, there exists a steep stiffness gradient between the aorta and peripheral vessels. Stiffening of aortic tissue decreases this stiffness gradient, and since the aorta stiffens much quicker than the peripheral vessels [74], stiffness gradient decreases with age [75] and often reverses[59]. Typical values of PWV for various age groups [59], [76] are presented in Table 1-2 to provide a basis for evaluating the mock aorta used in this investigation.

Table 1-2: Average pulse wave velocity (PWV) values by age group

Age [yrs]	13 – 17	20 – 29	30 – 39	40 – 49	50 – 59	60 – 69	70 +
PWV [m/s]	5.1 – 5.2	6.2 ± 0.7	6.7 ± 1.0	8.8 ± 1.9	9.5 ± 1.8	12.8 ± 3.9	13.8 ± 5.3

The PWV of the aorta has a significant impact on the shape of central aortic waveforms, which are interpreted as a summation of the forward traveling pressure pulse from the heart's ejection and a backward traveling wave that is reflected from peripheral sites of vessel impedance mismatch [64], [75], [77]–[79]. As such, the overall pressure waveform is most commonly analyzed using frequency domain analysis which describes the pressure wave as a summation of sinusoidal harmonic components [77]. Investigations have found that using Fast Fourier transform (FFT) filtering or zero-phase filtering with cutoff frequencies between the 6th and 15th harmonics adequately distinguishes the features required to perform central aortic waveform assessment [77], [80]–[83].

1.5.3 Central aortic pressure waveform analysis

In addition to the key features of a central aortic pressure waveform discussed in Section 1.2, wave reflections introduce other important features. While the systolic peak is the global maximum of the pressure waveform, reflected waves introduce a second local peak pressure. The anacrotic notch, an inflection point that marks the arrival of the reflected wave, identifies the location of this reflected wave. The relationship between the incident and reflected wave is clinically used to assess aortic and overall cardiovascular health. The parameter commonly used to do such assessment is central augmentation index, cAI_x, calculated as:

$$cAI_x = \frac{P_2 - P_1}{P_s - P_d} = \frac{P_2 - P_1}{P_p} \qquad \textbf{(1-23)}$$

where P_1 is the first occurring peak and P_2 is the second occurring peak.

Central aortic pressure waveforms are typically classified into one of three categories: Type A, Type B or Type C based on the relationship between the incident and reflected wave and corresponding value of cAI_x [81], [84]. This is referred to as Murgo's classification scheme. Labeled diagrams of each of these waveform types are shown in Figure 1-6, Figure 1-7 and Figure 1-8.

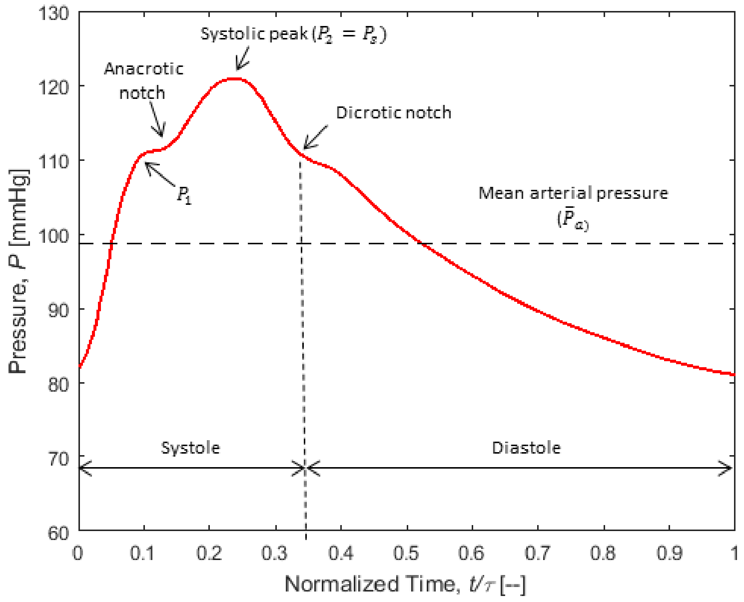

Figure 1-6: Labelled plot of Murgo's Types A central aortic pressure waveform [85]

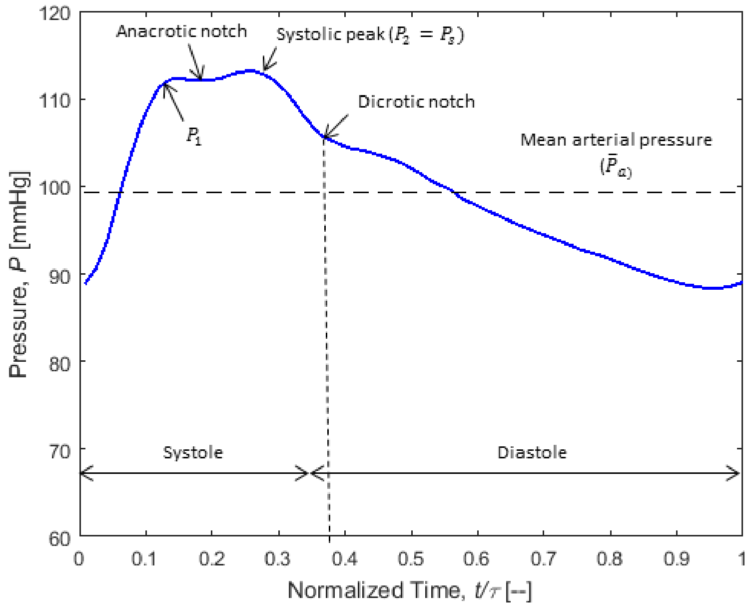

Figure 1-7: Labelled plot of Murgo's Types B central aortic pressure waveform [86]

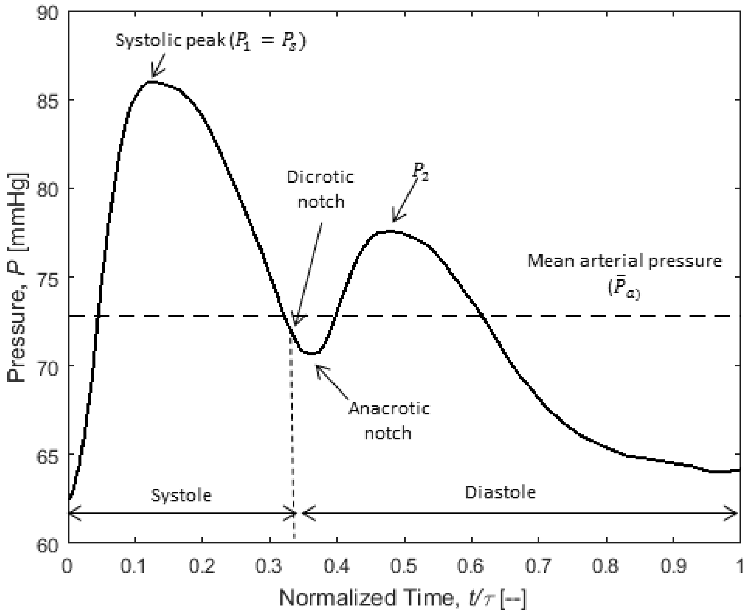

Figure 1-8: Labelled plot of Murgo's Types C central aortic pressure waveform[85]

Each of these waveform types have unique characteristics that are associated varying degrees of cardiac performance. Type C waveforms represent the healthiest, most compliant case so it will be discussed first. Type C waveforms are characterized by a peak systolic wave occurring in early systole, followed by a well-defined reflected wave [81], resulting in a $cAI_x < 0$. This indicates a slow traveling reflected wave which is characteristic of a young patient with a healthy, compliant aorta. Due to the dampening effect of the compliant aorta, the reflected wave arrives back at the heart during diastole [48]. This assists coronary perfusion which is imperative for maintaining healthy cardiac tissue. It also helps maintain relatively low systolic and pulse pressure values, as shown in Figure 1-6. Type B waveforms are characterized by an early systolic reflected wave followed by a late systolic peak, resulting in a cAI_x between 0 and 12 [81]. When compared to Type C waveforms, Type B waveforms have slightly elevated systolic pressures due to the early arrival of the reflected wave slightly augmenting systolic peak pressure. Type A is similarly characterized by a reflected wave that occurs in early systole followed by a systolic peak occurring in late systole. However, for a type A waveform, $cAI_x > 12$. This is typical for older patients whose aortas have high PWV, resulting in a fast moving reflected wave. In this case, the reflected wave arrives back at the heart during early systole causing it to significantly augment the forward traveling wave. This results in elevated afterload and therefore greater workload on the heart. This increased systolic load is often also associated with prolonged systolic duration, which can impair diastolic relaxation [86]. Additionally, a strong relationship has been found between stiffness gradient and aortic reverse flow; low or reverse stiffness gradients have been associated with increased flow reversal in the aorta and increased risk of stroke [70]. It has been suggested that this is a consequence of systolic flow suppression due to the early arrival of the reflected wave [70].

There has been a great deal of clinical investigation into wave propagation effects *in vivo* [78], and into experimental investigations of flow fields through compliant phantoms in low α regimes [50], [51], [54], but, to the author's knowledge, there has been little experimental investigation into controlled changes in aortic compliance within a physiological range in an *ex vivo* environment. The impact of such compliant response on peripheral flow fields and upstream pump performance has also not been evaluated.

1.6 Research objectives

This research sought to understand the impact of introducing a compliant mock aorta into an EVHP test system on the pressure waveforms, peripheral flow fields, and on the work done by the pump. To accomplish this objective, a fundamental understanding of the fluid mechanics involved in a pulsatile flow interacting with compliant vessels, in both Newtonian and non-Newtonian flow regimes, was required. Therefore, the first experiment established a fundamental case by comparing the downstream flow fields and pressure waveforms obtained in a EVHP analog system with a compliant tube to those obtained with a rigid tube. This was undertaken using a peristaltic pump which delivered a known stroke volume at a fixed rate. In this way, the effect of compliance in a pulsatile flow regime could be determined in a well-defined, reliable system. The potential impact of non-Newtonian effects in such an *ex vivo* environment could also be discovered to determine whether or non-Newtonian exploration is warranted in future experiments.

After establishing this fundamental case which quantified the phenomena of the fluid mechanics involved and established an experimental methodology, a more complex physiologically accurate case was explored. This case employed the use of a commercial ventricular assist device (VAD) (Thoratec® Corporation) to generate a simulated contraction-relaxation cycle. The VAD delivered a fixed stroke volume at a variable rate that was dependent on the afterload conditions of each individual experiment since the preload conditions were fixed. This more accurately reflected *in vivo* conditions, which respond to changing hemodynamic conditions, but made isolated control over variables difficult. The objectives of this case were aimed at understanding the energy requirements on the VAD, the analog heart, when compliant tubing was introduced as compared to the rigid case. In this way, this experiment sought to provide experimental verification of Windkessel theory and corresponding clinical theory about the effect of PWV on cardiac workload in the context of their potential application in the EVHP system. Central aortic pressure waveforms as well as peripheral flow fields were used to quantify the impact of compliance on flow conditions and pump performance.

1.7 Content & outline of thesis

The content of this thesis is organized into five additional chapters. Chapter 2 provides a detailed explanation of the two experimental setups used for this investigation. In addition, it includes a detailed overview of the design and manufacturing procedure involved in making the compliant tube used for both experiments, as well as an overview of the optical measurement technique used to obtain flow field data. Chapter 3 outlines the processing methodology used to obtain results from each experiment. Chapter 4 presents the results obtained from the first experiment. It investigates the impact of compliance and non-Newtonian effects in the system subjected to the well-controlled pulsatile flow from a peristaltic pump. Chapter 5 presents the results obtained from the second experiment. It compares system performance parameters of a rigid and compliant mock aorta test section subjected to the physiological pulsatile flow from a VAD. Finally, Chapter 6 outlines conclusions that can be drawn from the results presented in previous chapters and proposes directions for future research.

Chapter 2. Experimental Setup

The general approach to this experimental setup was to simulate the left side of the EVHP system in order to facilitate testing of tubing compliance on downstream flow fields and upstream pump performance. The basic components of the setup were a pump, a compliant test section and an imaging section[1]. The performance of the compliant test section was compared with that of the rigid test section through monitoring of pressure waveforms, tube expansion response, and peripheral flow fields.

The fluid mechanics involved in a physiological flow field with compliant vessels are complex due to wave propagation effects, so two different versions of this analog system were used to establish both a fundamental case and a physiological case. The first experiment involved the use of a peristaltic pump to generate a well-controlled low flow rate pulsatile flow and the second utilized a VAD to generate a physiological pulsatile flow. The goal of the first setup was to obtain a fundamental case of compliant tube response in a simplified pulsatile flow regime and compare these behaviors using Newtonian and non-Newtonian fluids. Since the peristaltic pump delivered a fixed stroke volume at a fixed rate, quantification of system behavior was reliable and provided a good basis for verifying future results from the physiological flow. The second setup was then able to address a more complex physiological flow environment with the goal of understanding the impact of a compliant mock aorta on peripheral flow and pump performance.

This chapter provides a detailed outline of both experimental setups. The first three sections address those aspects that were common to both setups: the mock aorta, the Camera 1 setup and the method of flow field acquisition, PIV. The final two sections offer detailed descriptions of both experimental setups.

---

[1] Detailed drawings of the imaging section base and lid are provided in Appendices A-2.1 and A-2.2

2.1 Mock aorta development

Previous investigations have established that silicone rubbers can demonstrate similar elastic response as human arteries under physiological pressure conditions [87]. Off-the-shelf silicones are commonly used to mimic small arterial properties but for the purposes of this investigation, more compliant response was required so a two-part silicone (Ecoflex® 00-50, Smooth-On Inc.) was chosen. The extent to which silicone tubes can reflect *in vivo* response is largely based on tube thickness and diameter, so a custom-made tube was designed and molded in-house to reflect *in vivo* aortic compliant conditions in for use in this experiment. The tube design and molding process are outlined in the following sections.

2.1.1.1 Tube design

The mock aorta, shown in Figure 2-1, was designed to accommodate the range of typical *in vivo* distensbility values reported in Section 1.5.1. The material and geometric properties are summarized in Table 2-1. The length of the tube was selected using an average length across all aortic sections based on geometric data obtained from CT images reported by [53] scaled to fit the tube diameter used in the experimental setup which was chosen to ensure consistency with the current EVHP experiment. In future experiments, this could be scaled to accommodate other geometries. Given the material properties of the base silicone material, the desired distensibility range and expected P_p from the VAD, an optimal wall thickness was calculated using distensibility equations [53], [60]:

$$d = \frac{A_{max} - A_{min}}{A_{min}} \times \frac{1}{P_p} = \cdots = \frac{\Delta D}{D} \times \frac{1}{P_p} \tag{2-1}$$

$$d = \frac{1}{E\left(\frac{h}{D}\right)} \tag{2-2}$$

where d is tube distensibility [mmHg^{-1}] and A_{min} and A_{max} are the minimum and maximum cross sectional areas of the tube, respectively [mm^2]. The tube was designed to have a flange with four clearance holes on the top, as shown in Figure 2-1(a) to facilitate connection to the bracket that connected the experiment to the optical rail. The flange was connected to a square piece with threaded holes that were mounted to the bracket. A square sleeve was placed on the other side of the flange to provide extra security to the connection[2].

---

[2] Detailed drawings of the connector and sleeve are provided in Appendices A-2.6 and A-2.7, respectively

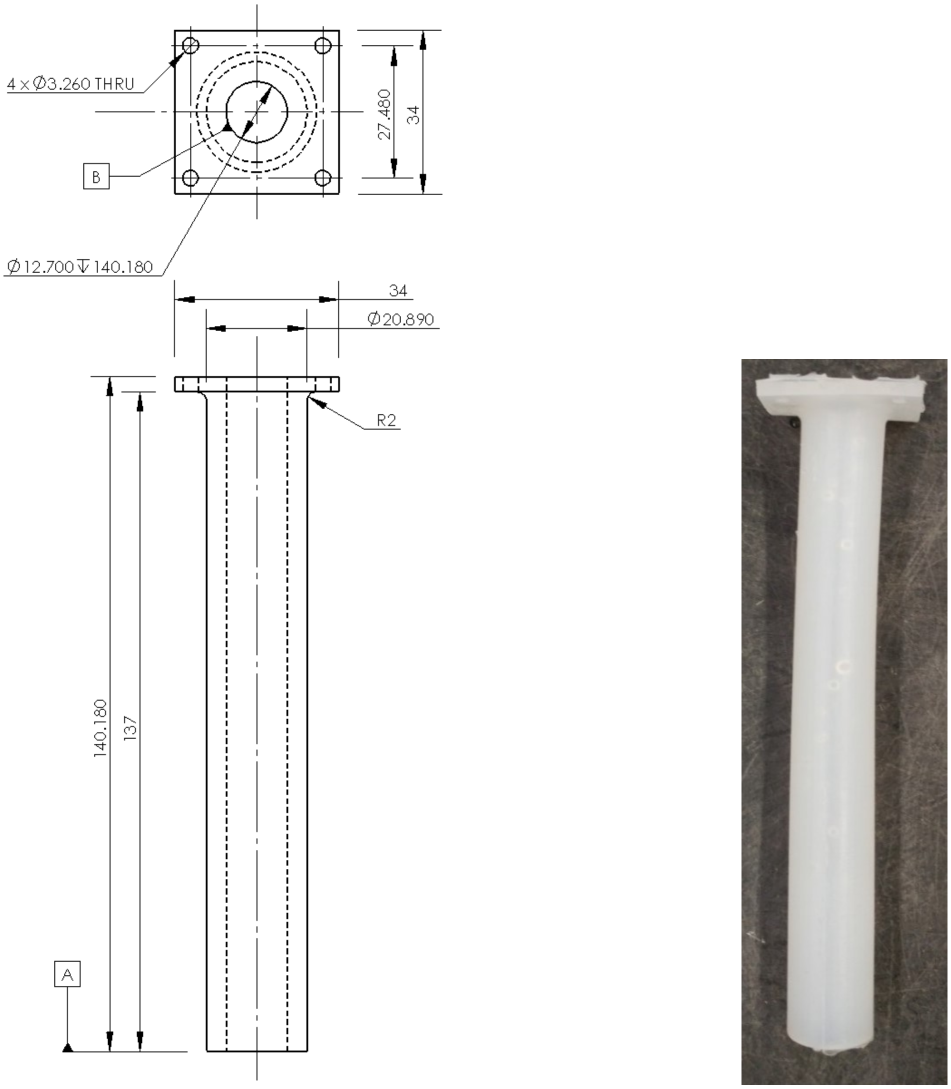

(a) **(b)**

Figure 2-1: Mock aorta (a) labelled side and top view and (b) image

Table 2-1: Mock Aorta Properties

Property	Value	Unit
Length	137	mm
Inner diameter	12.7	mm
Wall thickness	4.1	mm
100% modulus [88]	621	mmHg
PWV	5.1	m/s

2.1.1.2 Moulding process

A mould was 3D printed (Form 2, Formlabs®) for manufacturing the mock aorta. The mould was comprised of three pieces: the base piece, side piece and center piece[3]. Figure 2-2 provides (a) a section and top view of the mould assembly as well as (b) a labelled image of the mould. The inside surface of the base and side pieces formed the outside diameter of the tube and the center piece formed the desired inner diameter, as depicted in Figure 2-2. The mould was assembled by first fitting the side piece into the groove at the bottom of the base piece, shown in Figure 2-2(b). Then, the center piece was inserted in the space between the two previously assembled pieces. Included in the bottom of the base piece was a groove, visible in Figure 2-2(a), into which the center piece was fit to ensure its proper alignment.

The moulding process involved several steps. First, the mould was sprayed with a release agent (Easy Release 200, Smooth-On Inc.) and left to dry for 30 minutes. Next, one-third of the required silicone was mixed and degassed within the 18-minute pot life of the silicone. Once the silicone was degassed and the mould release agent was dry, the silicone was poured into the top of the mould. A stirring stick was used to puncture any visible bubbles generated during the pouring process. To aid in the removal of air bubbles an air bleed line, shown in Figure 2-2(b), was included in the base piece. This first third of the silicone was left to partially cure for 90 minutes to minimize the potential for bubbles developing with subsequent pours. This process was repeated for the remaining 2/3 of required silicone and then the tube was left to cure of 3 hours following the final pour.

---

[3] Detailed drawings of each of these components are provided in Appendices A-2.3, A-2.4 and A-2.5

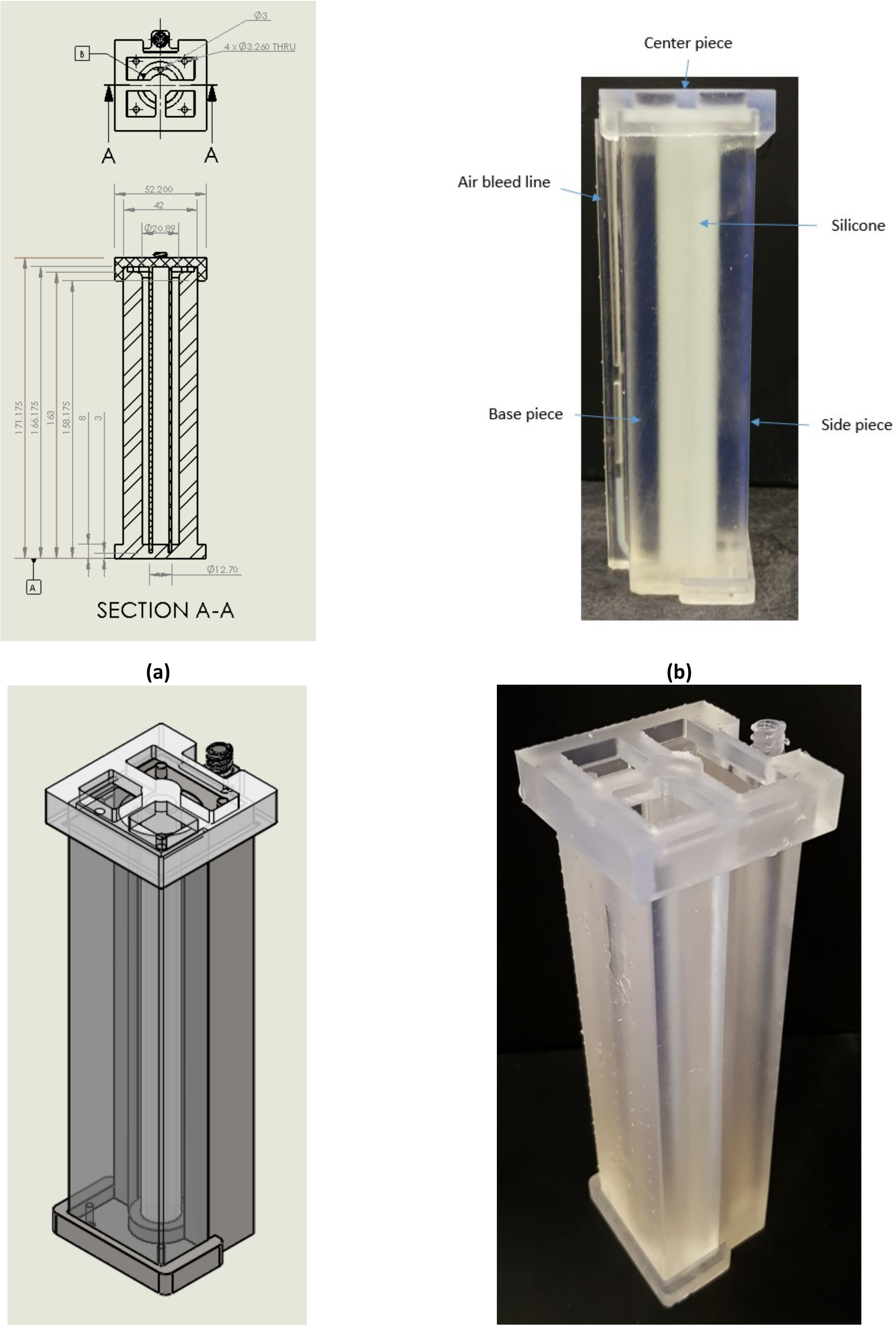

(a) (b)

(c) (d)

Figure 2-2: 3D printed mould (a) dimensioned section view, (b) image (side view) (c) 3D rendering (isometric view) and (d) image (isometric view)

2.2 Mock aorta imaging setup

In both experiments, a camera (Basler pioneer®, Basler Vision Technologies) with a resolution of 648 x 488 pixels was used to acquire images of the mock aorta that were used to quantify the tube's compliant response over multiple pulse cycles. A labelled schematic of the optical setup is shown in Figure 2-3, in which the camera is labelled Camera 1. The camera was positioned to image a field of view (FOV) at the approximate axial mid-point of the tube. All results were expressed as percent expansions, so the size of the field of view in millimeters was not calibrated. Instead, an image was taken prior to beginning the experiment of the tube in its unloaded position and the tube width was calculated in pixels. This provided the relaxed diameter required to calculate percent expansion without requiring a pixel to millimeter conversion factor. The camera frame rate was controlled by Function Generator 1 which was set to output a 113 Hz square wave function for the peristaltic pump experiment and a 210 Hz square wave function for the VAD experiment. This output signal was split to both trigger the camera and be collected by the DAQ (data acquisition) system used in the setup. The image acquisition was triggered by in-house software (LabWindows CVI, National Instruments) on Computer 1.

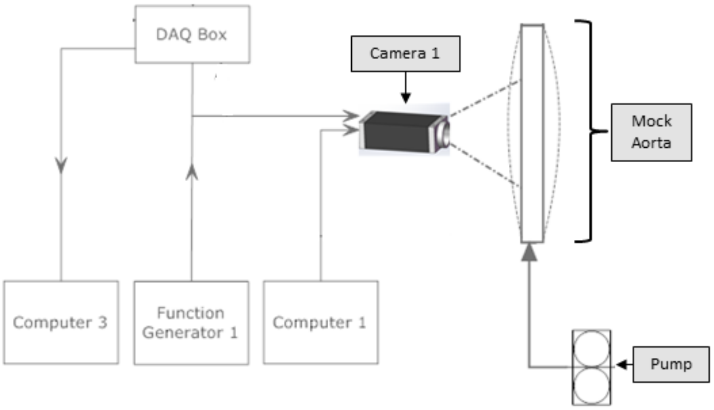

Figure 2-3: Labelled schematic of Camera 1 optical setup

2.3 Particle imaging velocimetry (PIV)

The technique used to obtain the downstream flow fields in this investigation is time-resolved PIV which is a method of flow visualization that is used to obtain instantaneous fluid velocity measurements [89]. A standard PIV setup includes tracer particles, a laser and a high-speed camera. The flow is seeded with small, neutrally buoyant tracer particles that are assumed to have minimal inertia such that they only follow the flow, not affect it. A high-speed camera is focused on a small field of view in the center of the flow and a laser illuminates the tracer particles. As the fluid moves, the camera triggers simultaneously with the laser pulses to capture images of the illuminated particles. An alternative to traditional PIV is shadowgraph PIV [90], which uses an LED backlight instead of a laser sheet to illuminate the particles. A basic schematic of a shadowgraph PIV setup is displayed in Figure 2-4. The LED, situated behind the flow channel, illuminates tracer particles in a thin focal plane in the center of the channel. The high-speed camera captures images of the illuminated particles from a small field of view in the focal plane. Shadowgraph PIV was employed in this investigation for the sake of experiment portability and for overcoming the limited access that comes with introducing a laser light sheet into the system.

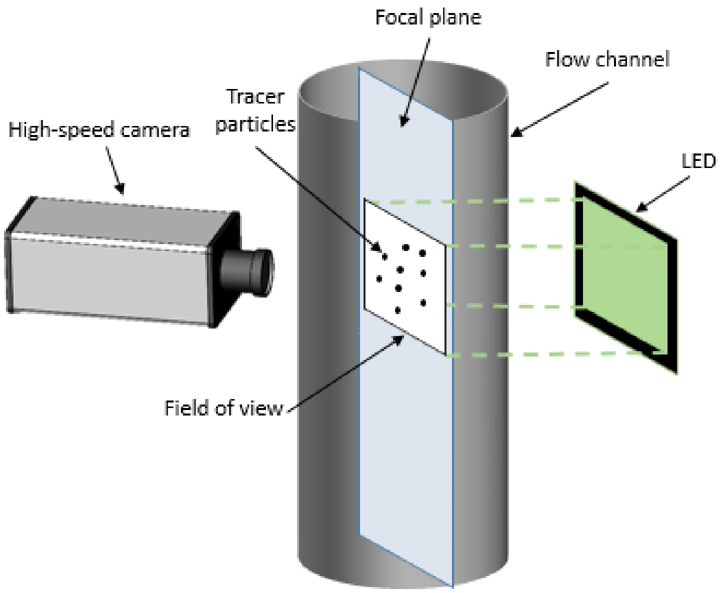

Figure 2-4: Labelled schematic of basic components of shadowgraph PIV setup

With an appropriate seeding density, the images can be processed using a cross-correlation algorithm to determine average particle displacement over a specific region in the image from frame to frame. With known displacement and known time, velocity is calculated. PIV is advantageous for studying pulsatile flow because it is non-intrusive and capable of capturing a complete flow field instantaneously at several instances in time so the time-variant behavior of the fluid can be observed and quantified. For this reason, PIV is commonly used to study velocity distributions in cardiovascular flow [49].

Several experimental investigations have been performed to study pulsatile flow through compliant phantoms [50], [51], [53], [54], [91], [92], including simulated stenosed arteries [61], [93]. Additionally, PIV has been used to study flow dynamics in the LV [94] and around the aortic valve [95]–[97]. In this study, PIV is appealing because time-resolved velocity data provides the opportunity for understanding the time-dependent changes in flow behavior and enables the understanding of changes in a fluid's kinetic energy over time. PIV was used in both experimental setups used during this investigation but different variations of the setup had to be employed to accommodate the vastly different flow rates in each case. Detailed descriptions of both optical setups are included in the following sections which describe the components and procedures involved in both experimental setups.

2.4 Peristaltic pump experimental setup

The focus of this experimental setup, shown in the schematic in Figure 2-5 and the digital image in Figure 2-6, was to investigate the flow fields downstream from a mock aortic test section. Velocity distributions were compared for a Newtonian and non-Newtonian case using both rigid and compliant test sections. Deionized water and a 0.1 wt.% aqueous solution of polyacrylamide were used for the Newtonian and non-Newtonian case, respectively. For the purposes of this investigation, polyacrylamide was the most reliable blood analog given the confidence in preparation procedure and the nature of the optical techniques used. The polyacrylamide solution was prepared with commercial anionic polyacrylamide powder (BASF SE, Germany) using the procedure outlined in [20]. The pulsatile flow was generated using a peristaltic pump (L/S® 07523-80, Masterflex®), which used rollers to deliver a fixed stroke volume at the rate set by the pump. The pump has four rollers, so the pulse rate of the flow was equal to four times the speed of the pump.

The pressure data from the transducers (Edwards® Truwave Disposable Pressure Transducers, Edwards Lifesciences Corporation), labeled PT001 and PT002, along with the trigger signals of both cameras were collected using the same DAQ to facilitate coupling of pressure, velocity and tube response results. Once the pulse rate of the pump was set, acquisition of pressure data was started using in-house code on Computer 3 and the data was collected for 15 seconds at a sampling rate of 1000 Hz. Within that time period, Camera 1 was triggered as discussed in Section 2.2 and Camera 2 was triggered by turning on the output channel of Function Generator 2. Camera 1 collected 800 images of the tube at a frame rate of 113 Hz and Camera 2 collected 300 images in the middle of the imaging section at a frame rate of 113 Hz. This experimental procedure was repeated for nine pulse frequencies between 1.00 and 2.33 Hz (60 – 140 BPM).

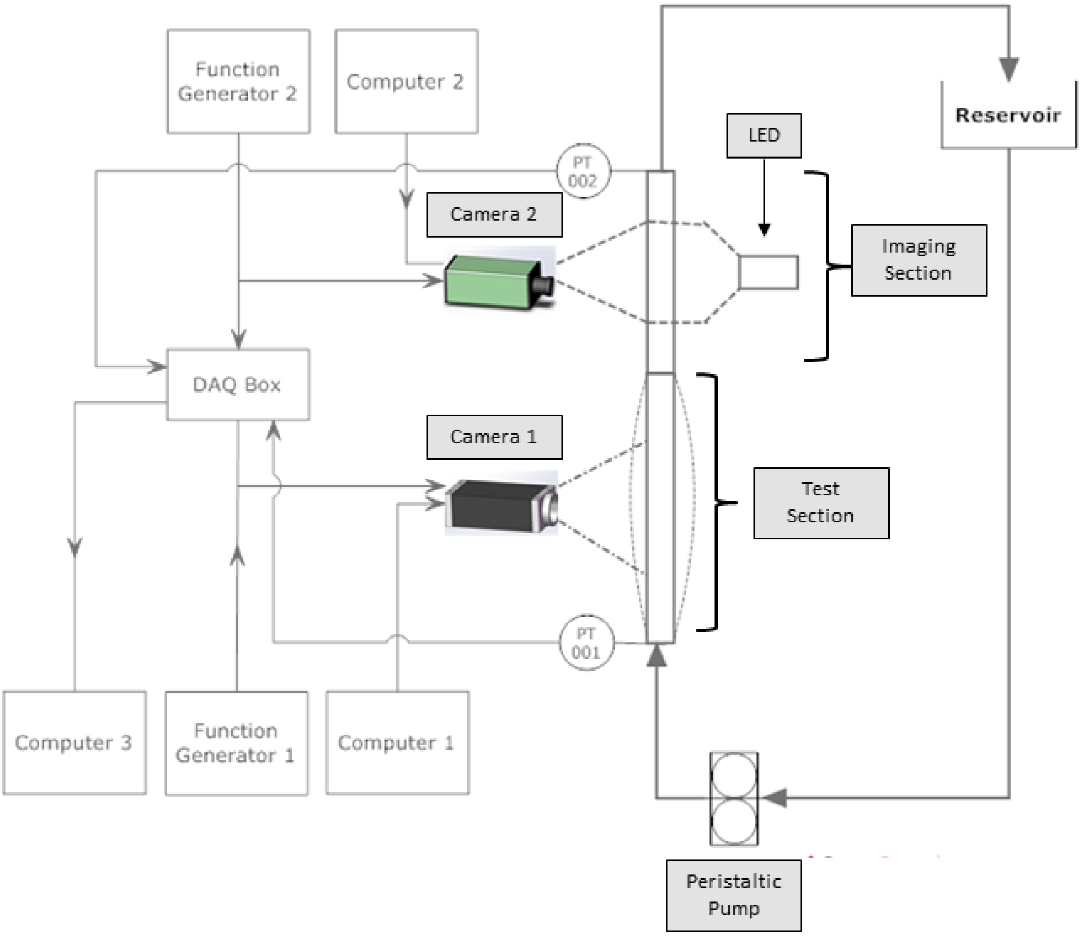

Figure 2-5: Labelled schematic of peristaltic pump experimental setup

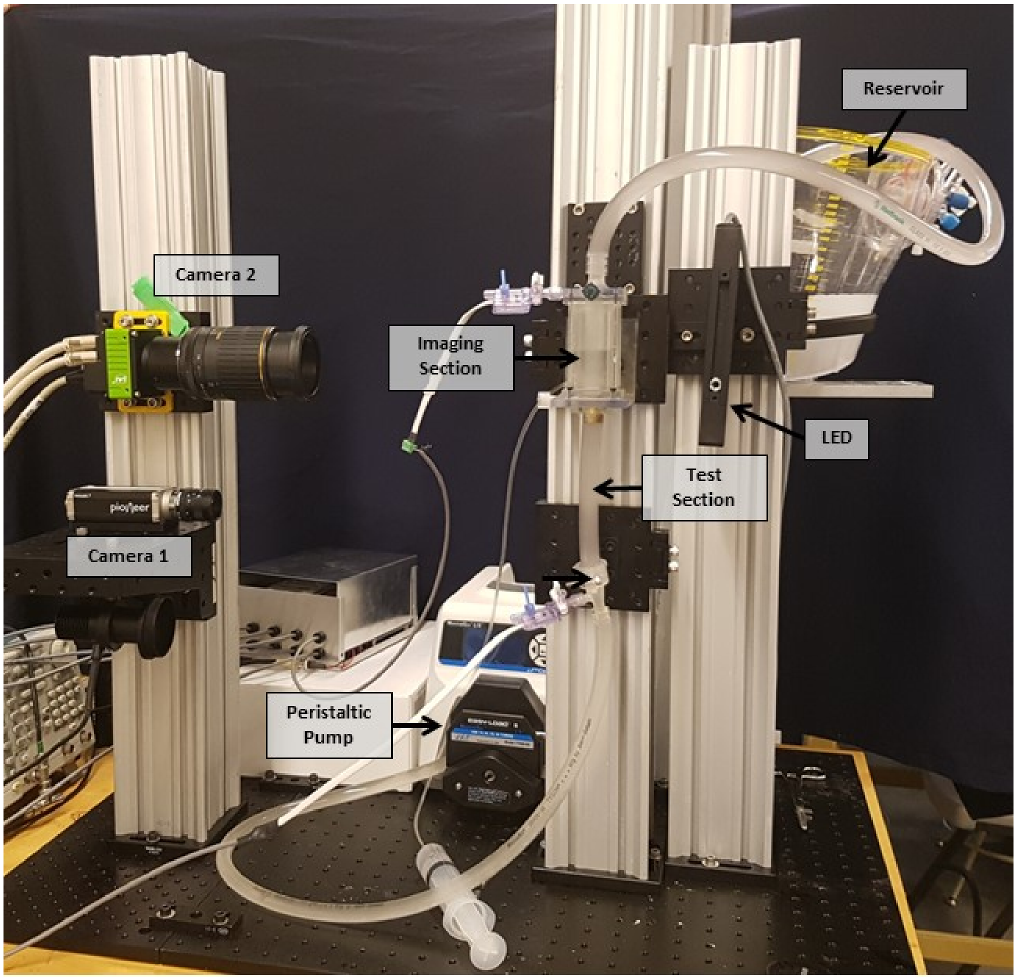

Figure 2-6:Labelled image of peristaltic pump experimental setup

2.4.1 Camera 2 optical setup

The velocity fields were captured using Camera 2 (SP-5000M-PMCL-CX; JAI Inc.) with a resolution of 2000x1800 pixels that captured 300 images at a collection rate of 113 fps. The flow was seeded with 18 μm borosilicate glass microspheres (ASTM C169, Potters Industries Inc.) with bulk density of 0.49 gcm^{-3}. A 90 mm SLR lens set at *f*#2.8 was used to image a 24.3 x 12.7 mm field of view in the middle of the imaging section with a resolution of 0.014 mm/pixel, an average particle size of approximately 1.3 pixels and a focal plane thickness of approximately 0.5 mm. A low *f*# was used to define the region of interest on the center plane of the imaging section. The custom made imaging section[4] was filled with deionized water for improved refractive index matching. Images were collected in back-illumination/shadowgraph mode using a high current green 4”x4” side-fired LED backlight (BX0404-520nm, Advanced Illumination

---

[4] Detailed drawings of the imaging section are provided in Appendices A-2.1 and A-2.2

Inc.). The camera was controlled by Function Generator 2 (TDS 2024B, Tektronix Inc.) and the trigger signal was fed to the DAQ system used to collect the pressure data.

2.5 VAD experimental setup

The focus of this experimental setup, shown in Figure 2-7 and Figure 2-8, was to investigate the impact of compliance on the peripheral flow and pump performance using a mock aorta in a physiological cardiovascular flow. The physiological flow was generated using a VAD, which produced a pulsatile cycle akin to that seen *in vivo* at a pulse rate that varied depending on the afterload conditions of the experiment[5]. The mock aorta was surrounded by a custom-made air pressure chamber that was used to control the magnitude of compliant response. This compliant response was imaged using the optical setup described in Section 2.2. The pressure data from the transducers PT001, PT002 and PT003, along with the 210 Hz and 1000 Hz trigger functions of Camera 1 and Camera 2, respectively, were collected using the same DAQ to facilitate coupling of pressure, velocity and tube response results. In addition, the trigger signal of Camera 2, which was controlled by output channel 2 of Function Generator 2, was collected by the DAQ. This set of experiments was performed with a rigid test section and with the compliant mock aorta discussed in Section 2.1. The two experimental conditions that were altered were the afterload pump speed ($\omega_{Al\,pump}$) and, for the compliant mock aorta case, the chamber pressure (P_{ch}). The VAD was turned on first, following immediately by the afterload pump which was set to the desired speed for the given experiment. After giving the VAD a few seconds to adjust its pulse frequency accordingly, pressure data acquisition was initiated for 15 seconds at a sampling rate of 4000 Hz. Then, within the 15 seconds, Camera 2 acquisition was initiated by turning on output channel 2 of Function Generator 2 and Camera 1 acquisition was initiated by turning on the trigger function channel of Function Generator 1 and beginning image acquisition from the software on Computer 1. This process was repeated for two mock aorta chamber pressures, 103 and 155 mmHg, and 4-5 afterload pump speeds depending on how much tube distension the chamber could hold before the tube made contact with the wall. Varying $\omega_{Al\,pump}$ altered the back pressure conditions of the system, which impacted systolic ejection time and pulse pressure, while varying P_{ch} allowed control over the magnitude of compliant response.

---

[5] The VAD was mounted to the optical rail using a custom-made mount. A detailed drawing of this mount is provided in Appendix A-2.10.

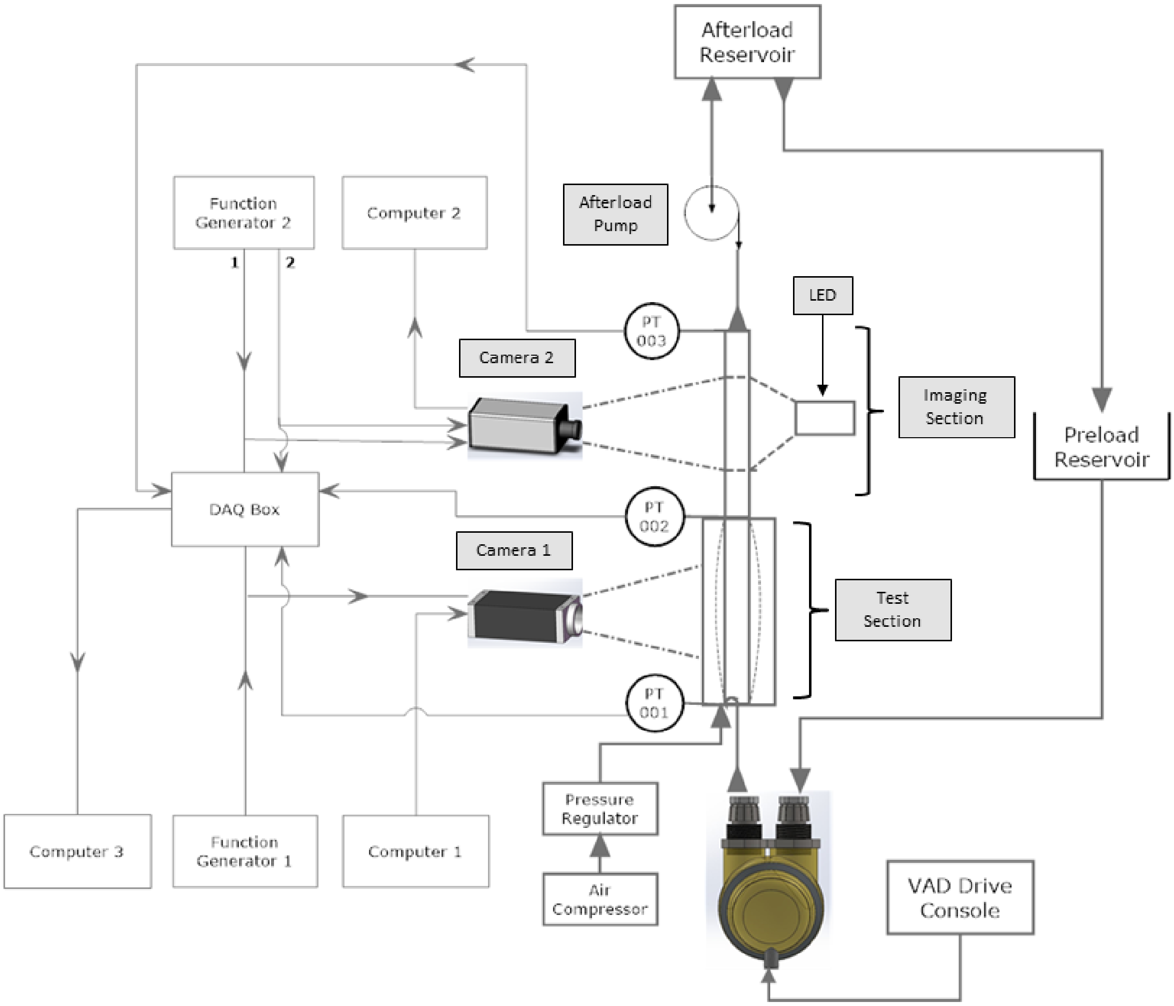

Figure 2-7: Schematic of VAD experimental setup

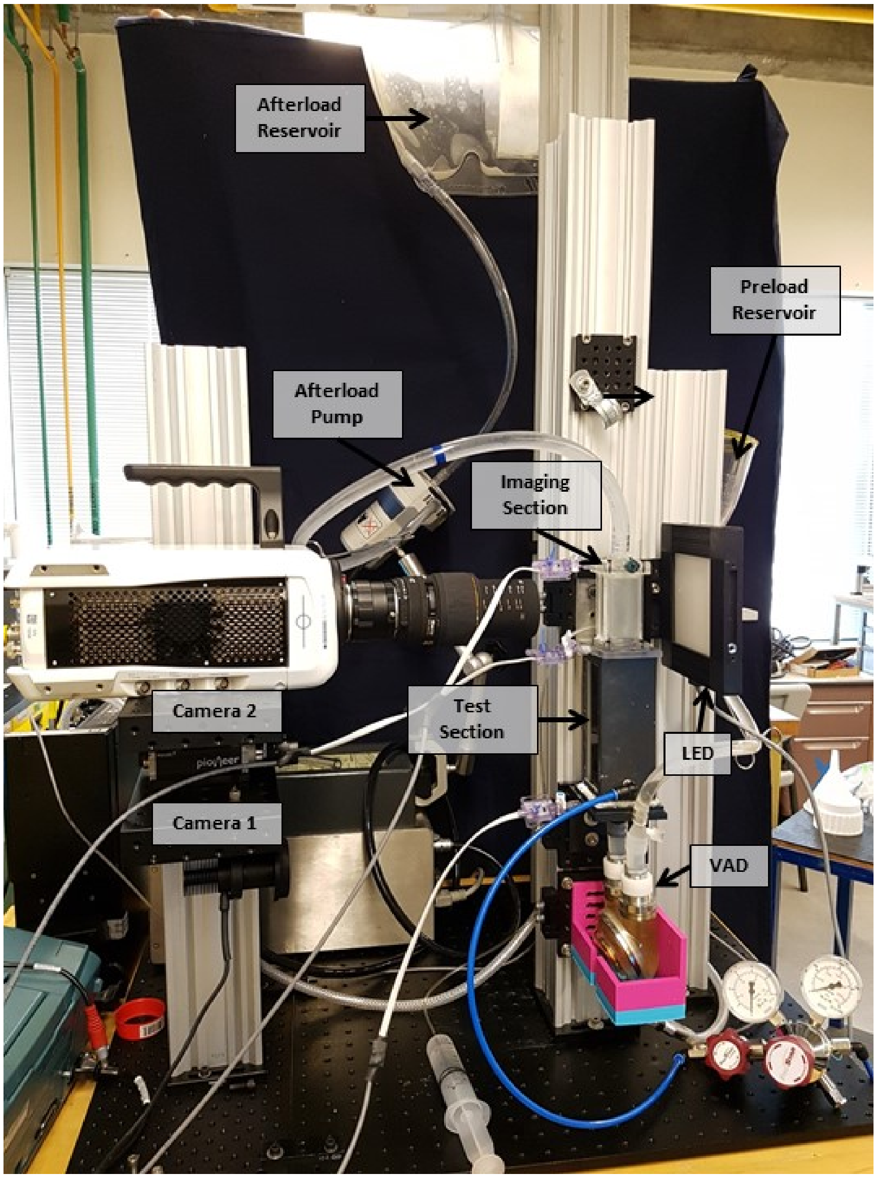

Figure 2-8: Labelled image of VAD experimental setup

2.5.1 Ventricular assist device (VAD)

A diagram [98] and an image of a VAD used to generate the simulated cardiac flow in this experiment is shown in Figure 2-9(a) and (b), respectively. A VAD is a prosthetic ventricle comprised of a polyurethane pumping sac, and two Bjork-Shirley tilting disc valves, one for inflow and one for outflow. Expansion and compression of the sac is controlled by a pneumatic drive console which alternatively applies positive and vacuum pressure to compress and expand the sac, respectively [99].

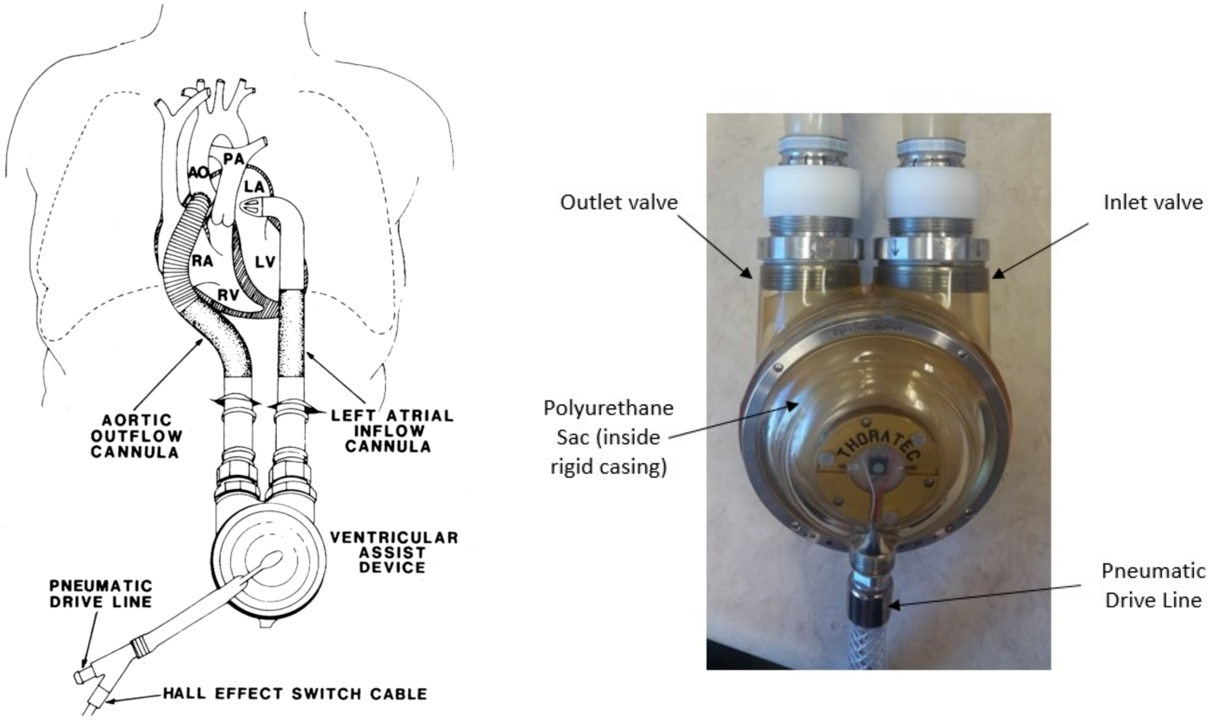

(a) **(b)**

Figure 2-9: VAD (a) diagram [98] and (b) labelled image

In vivo, the vacuum pressure and left atrial pressure drive flow through the inlet valve into the sac. Clinically, the vacuum pressure is set at -10 to -30 mmHg on the drive console and left atrial pressure is approximately 4-12 mmHg, resulting in a net filling pressure gradient of 14-42 mmHg. The Hall effect cord shown in Figure 2-9(a) sends a signal back to the controller when the sac is full, indicating that is it time for ejection. Under ideal conditions, systolic ejection is set to last 30% of the cycle, and filing is set to 70% of the cycle [98]. For this experiment, the VAD was operated in volume (full-to-empty) mode [99], wherein the full 65 mL stroke volume was ejected with every beat, resulting in a variable pulse rate depending on the afterload conditions.

The filling and ejection times are dictated by the filling pressure gradient and exit pressure gradient, respectively, as shown in Figure 2-10, adapted from [98]. For this experiment, the preload reservoir was set approximately 360 mm above the inlet valve of the VAD, generating approximately 26 mmHg of filling pressure due to static pressure head. This coupled with the 10-15 mmHg of vacuum pressure being applied created a filling pressure gradient of approximately 40 mmHg and therefore a fixed filling time of 0.41 seconds for this set of experiments.

The ejection time of the VAD is determined by the difference between the maximum driveline pressure and the arterial pressure [98]. In the case of this experiment, since the driveline pressure was fixed, the ejection time depended on the amount of back pressure generated by the afterload pump, as dictated by its speed which was varied throughout this experiment. Due to the fixed nature of the driveline pressure and the configuration of the setup, the VAD produced hypertensive conditions in this experiment. While systolic pressures were elevated with respect to typical *in vivo* values, experiments were performed to study a range of pulse pressures, both high and within a physiological range. The investigation was focused on determining the impact of mock aortic compliance on the system performance, so the extreme conditions of the setup only made the differences between the rigid and compliant cases more discernible but should not have an impact the conclusions drawn from the results.

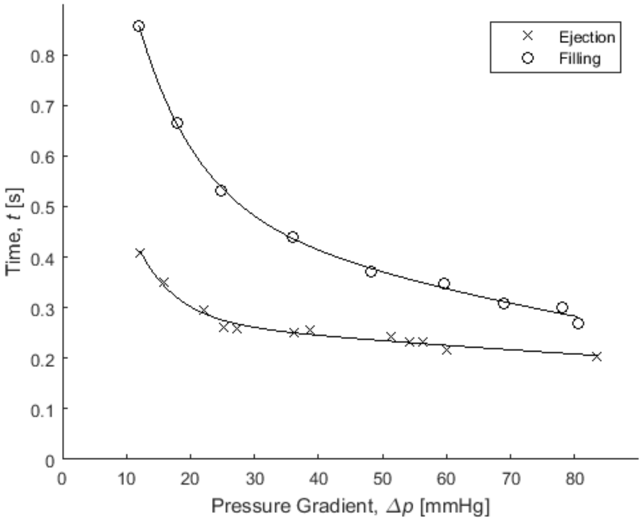

Figure 2-10: VAD ejection and filling times as a function of inlet and outlet pressure gradients [98]

2.5.2 Pressure chamber design & regulation

To facilitate control over the magnitude of compliant response, the mock aorta was contained within an air pressure chamber, shown in Figure 2-11(a) & (b). The chamber was 3D printed (Form 2, Formlabs®) in two parts: the base bracket and the top piece[6]. The base piece included a bracket that was used to mount the chamber onto an optical rail, and a groove in which the top piece was press-fit, as shown in Figure 2-11(a). Printed into the top surface of the top piece was an o-ring groove, shown in Detail A of Figure 2-11(a). This was done to facilitate the use of a custom-made o-ring to prevent leaking between the pressure chamber and the imaging section. The top piece also included a groove into which an 1/8"

---

[6] Detailed drawings of the pressure chamber base bracket and top piece are provided in Appendices A-2.8 and A-2.9, respectively

acrylic window could be inserted to enable viewing of the mock aorta by Camera 1. The edges of this window and the interface between the base and top piece were sealed with off-the-shelf silicone sealant. At the top inner surface of the top piece and top surface of the base piece were barbed connectors that were used the attach the mock aorta. To ensure security of the connection, custom made clamps were attached to each end. In addition to the barbed connector on the top surface of the base bracket, there was another one on the bottom surface to facilitate connection to the VAD outlet tubing. Air was delivered to the chamber through the pressure supply port on the side of the top piece and the pressure transducers were attached to the bracket by means of a luer lock connector printed onto the side of the base bracket piece.

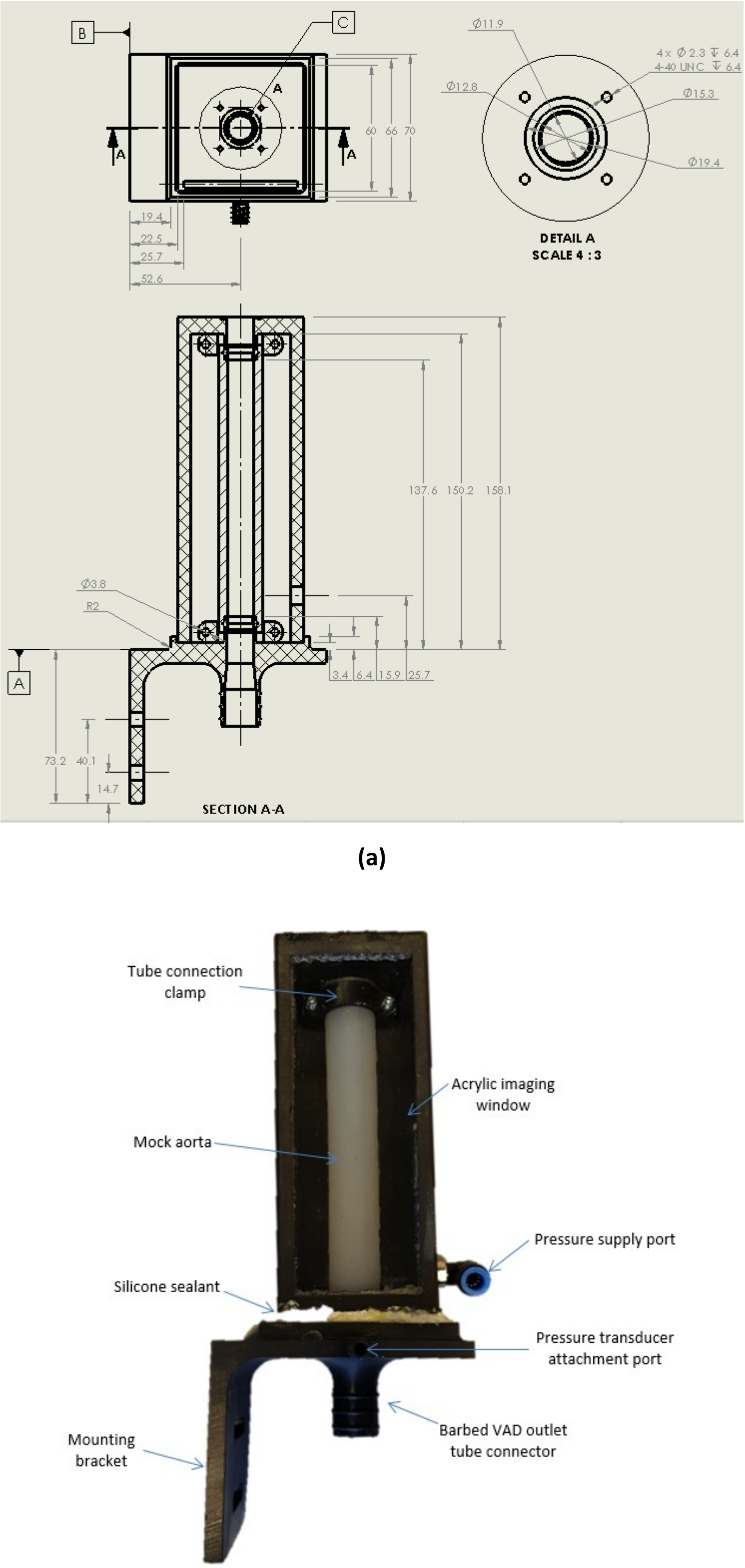

(a)

(b)

Figure 2-11: Pressure chamber (a) dimensioned section view and (b) labelled image

2.5.3 Camera 2 optical setup

The velocity fields were captured using a camera (Phantom® v611, Vision Research, Inc.) with a resolution of 1280x800 pixels that captured 1054 images at a collection rate of 1000 fps. The flow was seeded with 30-50 μm solid glass spheres (Spheriglass 3000, Potters Industries Inc.). PIV usually requires the use of neutrally buoyant particles but this larger sized particle was necessary for particle resolution and, given the high ejection velocities involved with this experiment, these particles were deemed acceptable. A 105 mm lens set at *f*#2.8 was used to image a 9.8x12.7 mm field of view in the middle of the imaging section with a resolution of 0.012 mm/pixel, an average particle size of approximately 3.3 pixels and a focal plane thickness of approximately 0.45 mm. Images were collected in back-illumination/shadowgraph mode using a high current green 4”x4” side-fired LED backlight (BX0404-520nm, Advanced Illumination Inc.). The camera was controlled by a function generator (TDS 2024B, Tektronix Inc.); the trigger signal was fed to the DAQ system used to collect the pressure data so the exact time stamp of each image could be known with respect to the pressure waveform.

Chapter 3. Data Processing Methodology

The experiments monitored three responses: pressure, tube distension and velocity fields. After acquisition, the pressure data was filtered to get rid of noise in the signal. The tube response was captured by Camera 1 and processed using in-house intensity peak detection code (Matlab, Mathworks,Inc.) to find the percent expansion of the tube with respect to time. Images of the downstream flow fields from Camera 2 were collected as AVI files and processed using commercial PIV software (DaVis Imaging Software, 8.1.4, LaVision GmbH). This chapter outlines the techniques used to collect and process the data obtained from both experiments.

3.1 Processing of pressure data

Producing the pressure waveforms was a three-step process that involved: collecting the voltage data from the DAQ using in-house code (LabWindows CVI, National Instruments), converting the output voltages to pressures using in-house calibration results, and then filtering the pressure signal using zero-phase digital filtering. As discussed in Section 2.4, for the peristaltic pump experiment the voltage data from the transducers was collected for 15 seconds at a sampling rate of 1000 Hz. The trigger functions from the output channels of the function generators controlling the cameras' frame rates were also captured by the DAQ. An example output voltage data set is shown in Figure 3-1(a). Close-up views of the 113 Hz square wave functions controlling the frame rates of each camera are shown Figure 3-1(b) and (c), respectively[7].

---

[7] The code used to generate Figure 3-1 is provided in Appendix A-3.2

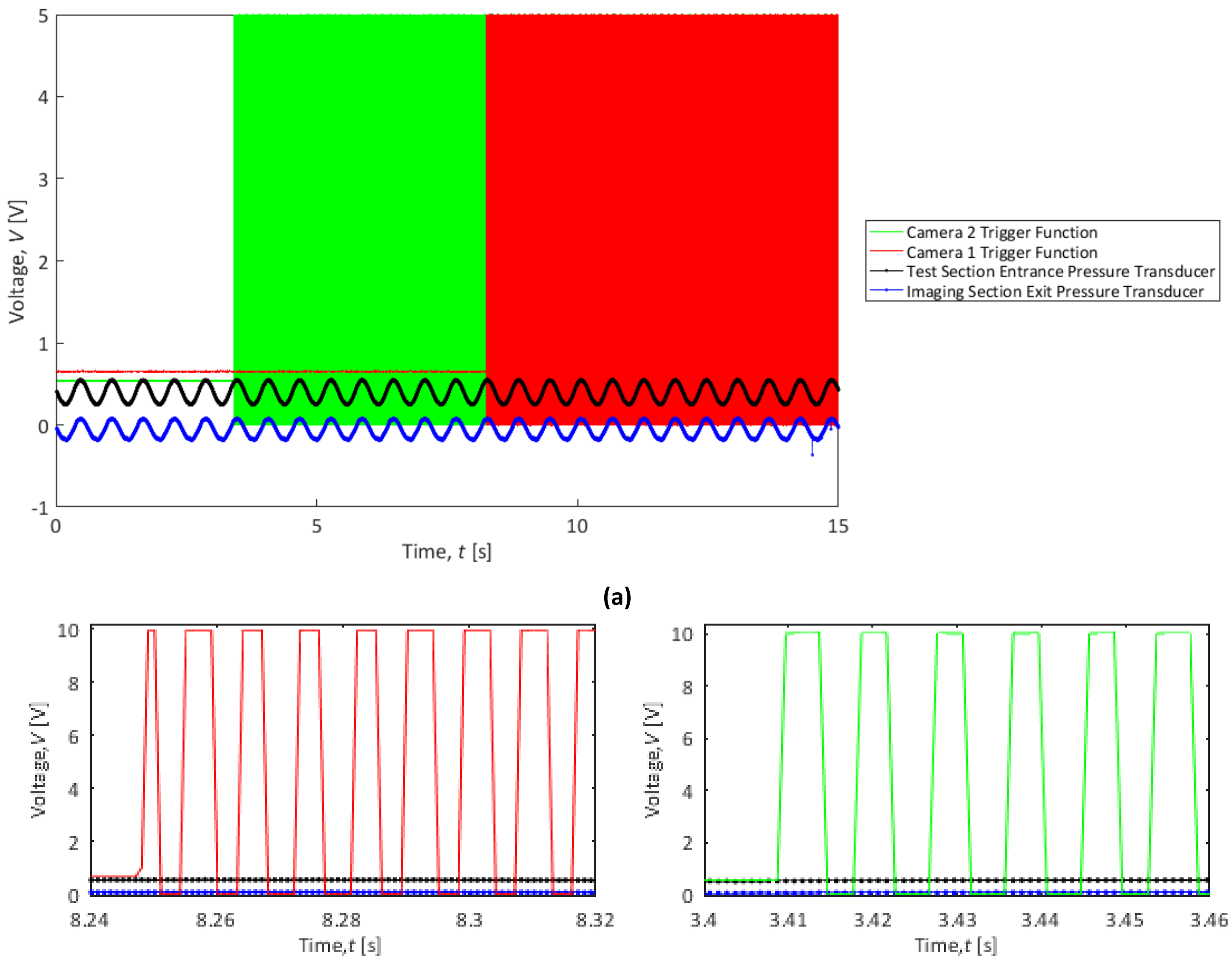

(a)

(b) (c)

Figure 3-1: Plot of peristaltic pump experiment voltage data from DAQ (1.67 Hz compliant case) for (a) complete dataset, (b) 113 Hz Camera 1 trigger function and (c) 113 Hz Camera 2 trigger function

The same methodology was applied to processing data from the VAD experiment, but the data was collected at a higher sampling rate of 4000 Hz because the frame rates of both cameras were higher than those used in the peristaltic pump experiment. As discussed in Section 2.5, for the VAD experiments the DAQ captured 15 seconds of voltage data from the transducers, the 210 Hz trigger function controlling the Camera 1 frame rate, the 1000 Hz signal controlling the Camera 2 frame rate and the trigger signal controlling the initiation of Camera 2 acquisition. The trigger signal was available in this experiment because in this case the Camera 2 trigger signal was directly controlled by the function generator rather than by the software, as was the case with Camera 2 used for the peristaltic pump experiment. An example voltage data set from the VAD experiment is presented in Figure 3-2(a). Close-up views of the 210 Hz Camera 1 trigger function and of the 1000 Hz Camera 2 trigger signal and trigger function are shown in Figure 3-2(b) and (c), respectively[8].

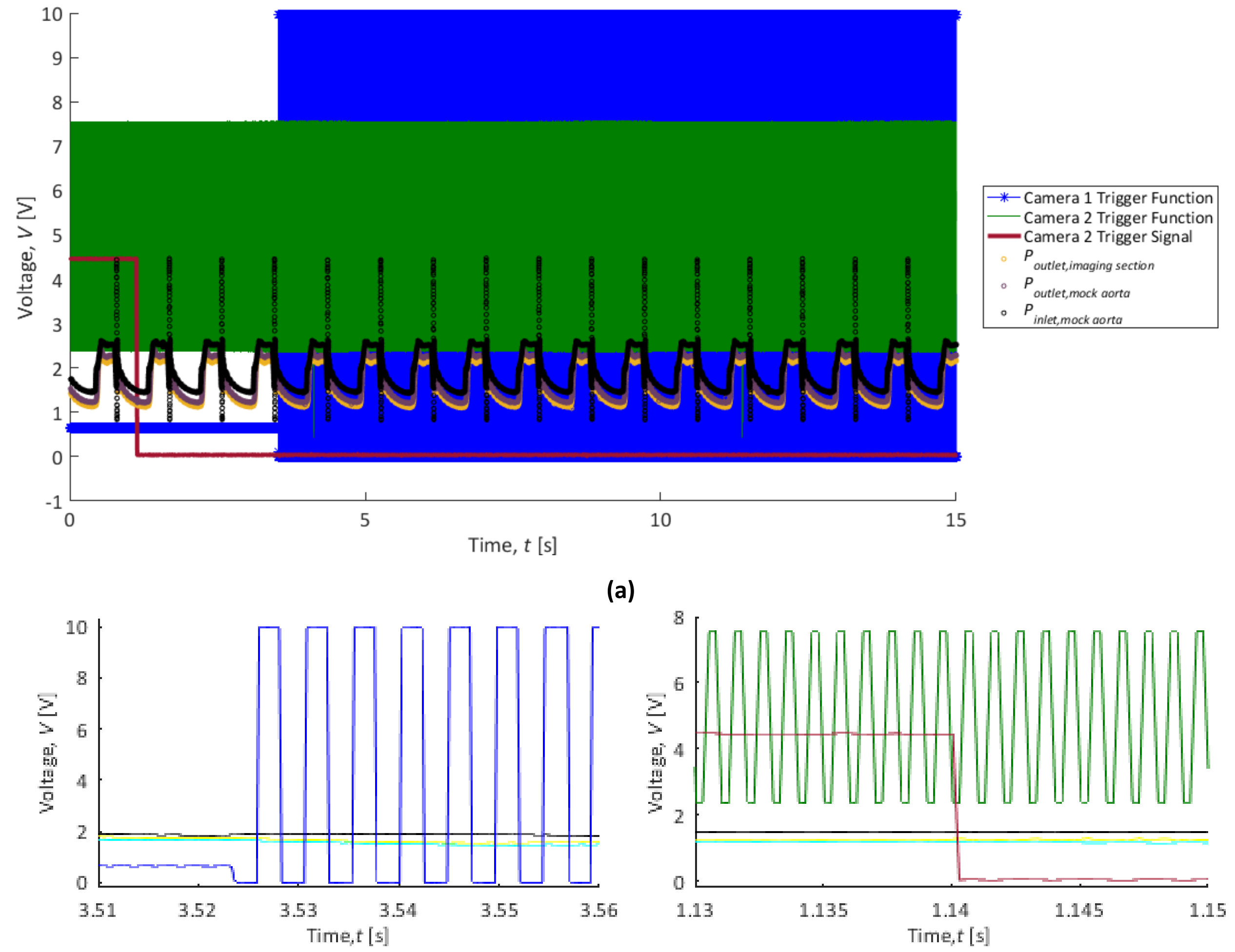

(a)

(b) **(c)**

Figure 3-2: Plot of VAD experiment raw voltage data from DAQ ($\omega_{AL\ pump}$ = 1235 RPM, P_{ch} = 103 mmHg mock aorta case) for (a) complete dataset, (b) 210 Hz Camera 1 trigger function and (c) 1000 Hz Camera 2 trigger function (green) and trigger signal (red)

The second step in processing the pressure data from the transducers was to convert the voltages into pressures. For both experiments, this conversion was done using in-house calibration data collected prior to beginning the experiment. These calibration values were obtained by collecting voltage data from the transducers under five known pressures, as summarized in Table 3-1. Output voltage was plotted as a function of pressure to obtain the slope and intercept of the resulting linear relationship. This plot for both transducers used in the experiment is shown in Figure 3-3 along with derived linear

---

[8] The code used to generate Figure 3-2 is provided in Appendix A-3.2

equations. The slopes and intercepts of these relationships were used to convert output voltage data from the experiments into pressure values.

Table 3-1: Summary of Pressure Transducer Calibration Data

Water Height [m]	Pressure [mmHg]	Mock Aorta Inlet Transducer Voltage [V]	Imaging Section Outlet Transducer Voltage [V]
0	0	0.065	0.019
0.5	37	0.615	0.563
1.0	73	1.156	1.104
1.5	110	1.702	1.651
2.0	147	2.252	2.198
2.5	184	2.801	2.740
3.0	220	3.348	3.291

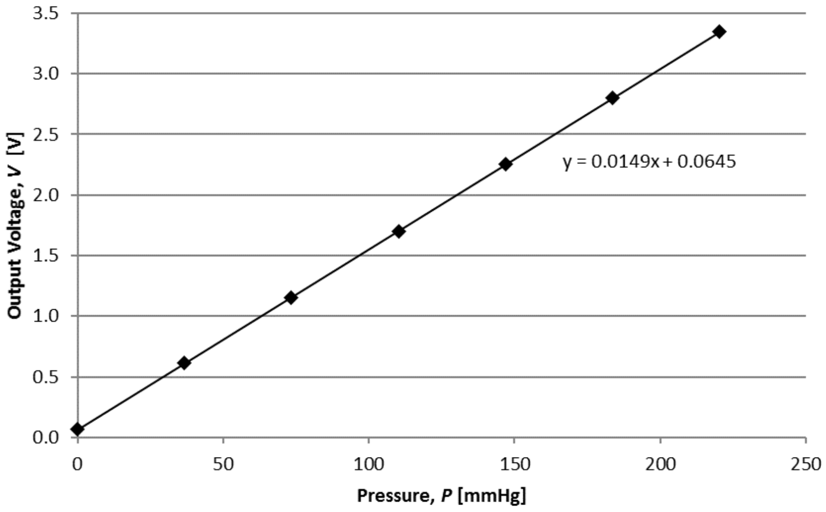

(a)

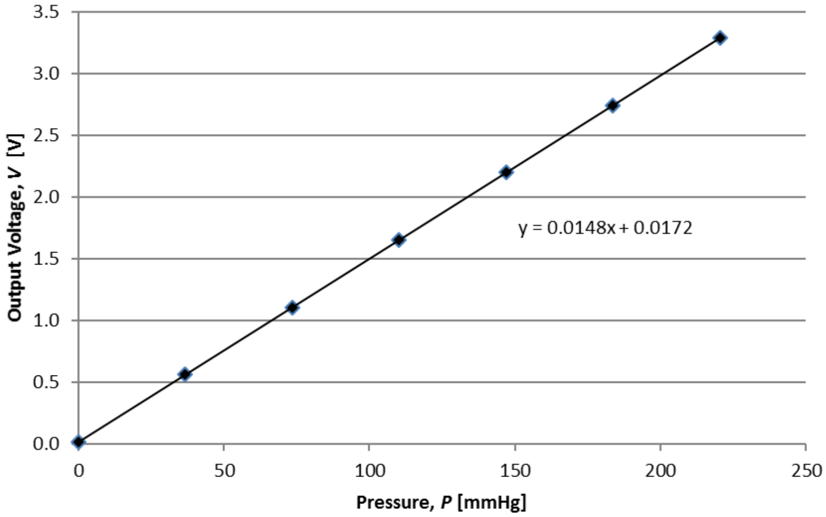

(b)

Figure 3-3: Plot of pressure transducer calibration data for (a) mock aorta inlet transducer and (b) imaging section outlet transducer

After converting the output voltages to pressure values, the pressure data was filtered to eliminate noise from the signal. This was done using a zero phase digital filtering technique (Matlab, Mathworks, Inc.)[9]. For the peristaltic pump experiment, 4 harmonics of the waveform were sufficient to provide an accurate representation of the pressure response. An example of a filtered waveform superimposed on the unfiltered data from the peristaltic pump experiment is shown in Figure 3-4(a) where it can be seen that the filtered waveform closely follows the unfiltered data. For the VAD experiment, 10 harmonics of the waveform were included in accordance with the literature discussed in Section 1.5.3. An example

---

[9] The code that was used to perform this filtering is provided in Appendix A-3.1

comparing a filtered mock aorta inlet pressure waveform to the corresponding unfiltered data from the VAD experiment is shown in Figure 3-4 (b). The filtered pressure waveform closely follows the data along the anacrotic limb and accurately reflects the shapes of the incident and reflected waves. The filtered waveform excludes the noise generated during the valve closure event, which first occurs at approximately 0.42 seconds, but still clearly marks the dicrotic notch. For both experiments, the filtered pressure waveforms can be expressed as continuous lines due to the high sampling frequency at which the data was collected, and they will be expressed as such in the results presented in Chapters 4 and 5.

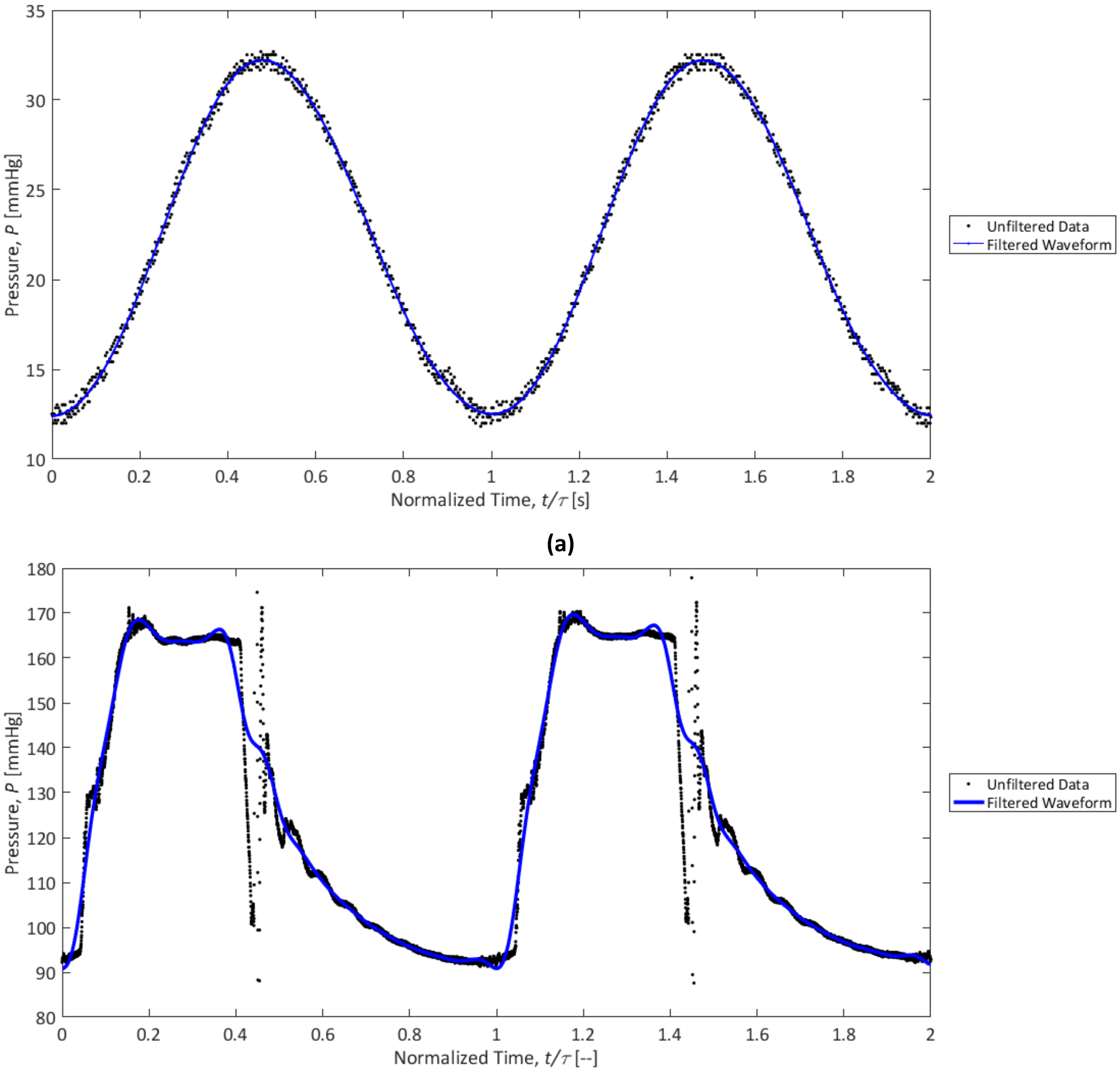

(a)

(b)

Figure 3-4: Plot comparing raw data to filtered pressure waveforms over two normalized pump cycles for (a) the peristaltic pump experiment (compliant f = 1.67 Hz case) and (b) the VAD experiment ($\omega_{AL\ pump}$ = 1235 RPM, P_{ch} = 103 mmHg mock aorta case)

3.2 Processing of Camera 1 mock aorta images

The second system behavior that was monitored is compliant tube expansion response. Collecting images of the tube throughout the pumping cycle at a frequency approximately one hundred times that of the pulse frequency allowed visualization of the tube response to pressure variations in the system. An annotated Camera 1 image obtained from the peristaltic pump experiment is presented in Figure 3-5. Camera 1 was focused on the side edges of tube; a black background was set behind the tube to enhance contrast and allow sharp visualization of the tube edges. During image processing, the tube width was calculated at a location in the middle of the image, shown as a blue line in Figure 3-5.

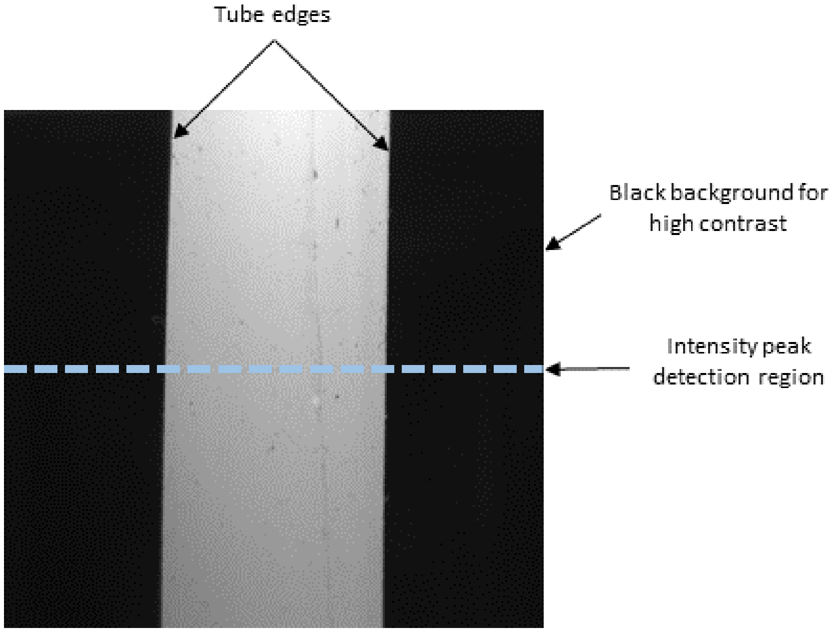

Figure 3-5: Raw image of mock aorta obtained from camera 1

All collected images were processed using an in-house peak intensity detection code (Matlab, Mathworks, Inc.) that ran through all of the Camera 1 images tracking the locations of peak intensity changes, *dI,* across the width of the images, *x* at the axial location denoted by a dashed blue line in Figure 3-5. An example plot of *x* vs. *dI* is provided in Figure 3-6[10]. The black lines in the figure represent the locations of highest contrast in the image, which occur at the tube edges. The red line is the minimum intensity threshold which ensures that if there are additional peaks in the image due to noise, they are not picked up in the code. The red squares confirm that the correct peak has been detected. Once the correct tube edges were properly detected, the distance between the two locations was

---

[10] The peak intensity detection code used to generate Figure 3-6 and calculate tube distension from Camera 1 images is provided in Appendix A-3.13

calculated. The value was then expressed as a percent expansion, *ΔD/D*, by dividing the calculated value by the pixel width of the tube in its unloaded position, a value that was obtained prior to beginning the experiment. This processing methodology was the same for both experiments except for the difference in the Camera 1 frame rate at which the images were collected.

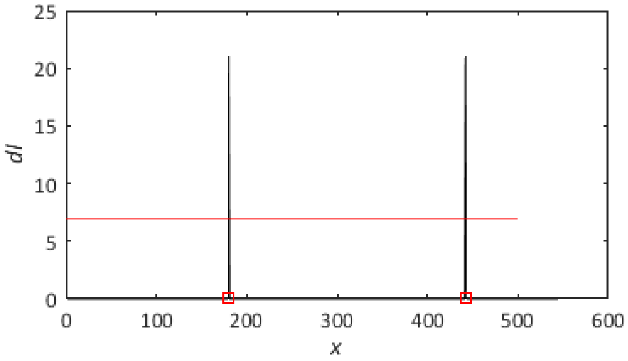

Figure 3-6: Plot of maximum intensity peak tracking over width of Camera 1 image showing the locations of intensity peaks (black lines & red squares) and minimum intensity threshold (red)

In order to prevent pixelation of the results, the code included a curve fitting algorithm that allowed detection of the sub-pixel x locations of each intensity peak. A plot comparing the pixelated results to the curve-fitted sub-pixel results is shown in Figure 3-7. This figure demonstrates that in cases where the distension values are small, without the sub-pixel curve fitting algorithm, the calculated values of tube distension would snap to whole pixel values rather than represent the actual shape of the tube distension waveform.

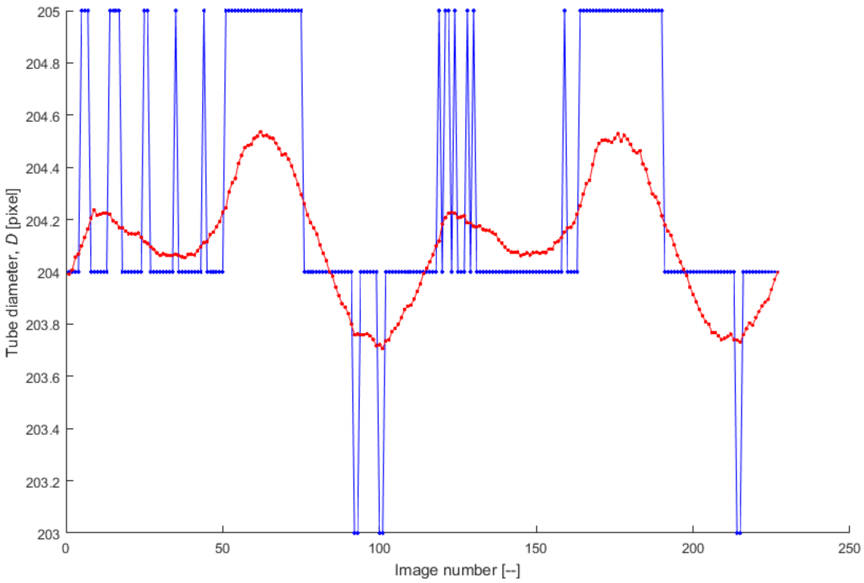

Figure 3-7: Plot comparing pixelated (blue) and curve-fitted sub-pixel (red) tube distension results

3.3 Processing of flow field images

The third response that was monitored during the experiment is the peripheral, or downstream, flow field. The AVI files that were generated from the collected Camera 2 images were processed using commercial PIV software (DaVis Imaging Software, 8.1.4, LaVision GmbH). First, the images were inverted and a geometric mask was applied to constrain the image to the desired field of view. Decreasing multi-pass time series cross-correlation was applied to generate the vector map. For the peristaltic pump experiment, the first two passes were 256x256 square windows with 50% overlap and the third and fourth passes were 16x16 square 4:1 ellipsoid windows with 50% overlap. For the VAD experiment, the first three passes were 256x256 square windows with 50% overlap and the last three passes were 32x32 4:1 ellipsoid windows with 75% overlap. In both experiments, the ellipsoid shape was used in the final passes to improve spatial resolution in the near-wall region. After applying the processing scheme, vector maps were obtained, as shown in Figure 3-8 (a), (b), (c) and (d)[11]. Figure 3-8(a) & (b) are vector fields obtained from the peristaltic pump experiment during the acceleration and deceleration phase of the cycle, respectively. Figure 3-8(c) & (d) are vector fields obtained from the VAD experiment during systole and diastole, respectively. Note the different velocity scales in the VAD systole and diastole vector maps. All four vector maps are normalized by the width of the channels in both the radial and axial directions and are displayed from $y/D = 0 - 0.5$ in the axial direction.

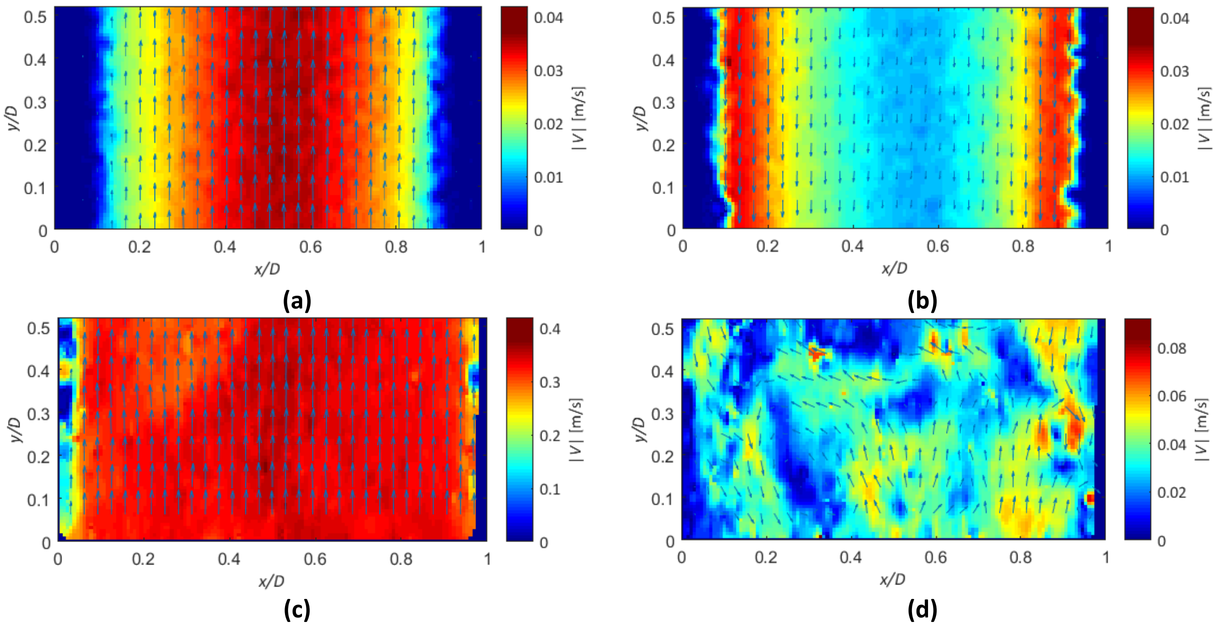

(a) (b)

(c) (d)

Figure 3-8: Vector field images with a background color map of velocity magnitude obtained from processing Camera 2 images from (a) the peristaltic pump experiment (systole), (b) peristaltic pump experiment (diastole), (c) VAD experiment (systole) and (d) VAD experiment (diastole)

---

[11] The code used to generate Figure 3-8 is provided in Appendix A-3.4

In both experiments, the vector arrays produced by DaVis® were imported into Matlab to obtain centerline velocities and velocity profiles. Centerline velocities were averaged over a region that spanned the full axial length of the image and approximately 70 pixels on both radial sides of the image center. For the peristaltic pump results, averaging over a region rather than taking the value at one location did not make much of a difference to the obtained value of centerline velocity due to the uniform nature of the flow fields in the axial direction. However, for the VAD, there was often a significant presence of secondary flows and therefore non-uniformities in the axial direction during diastole. Therefore, averaging vector values over a region was important for obtaining reliable VAD centerline velocity results.

Similarly, profiles of velocity were obtained from these vector field results by averaging the vectors at each *x/D* location over the full axial length of the image. Since the flow was uniform in the axial direction, obtaining the profiles of velocity in such a manner provided reliable and repeatable results. Due to the non-uniformity of VAD vector fields in the axial direction, velocity profiles were not used as a basis for comparing those results.

3.4 Generation of theoretical profiles of velocity

Theoretical velocity profiles and centerline velocity plots were generated based on equation (1-16) to compare against the PIV data results collected from this experiment[12]. The Newtonian equation was used for both the Newtonian and non-Newtonian profiles because all shear rates were low enough that polyacrylamide behaved as a Newtonian fluid. The axial pressure gradient input to the equation was the difference between measured pressures at the test section inlet and imaging section outlet minus the static pressure difference between the two transducer locations, expressed in units of pascal. An example of the axial pressure gradient used to calculate the velocity profile for the f = 1.67 Hz compliant case is shown in Figure 3-9. This periodic function was decomposed into its steady and unsteady components using a Fourier series expansion. The steady component was found to be extremely sensitive to the value of static head used in the equation. Within as little as 0.05 mmHg, P_0 changed by a factor of 10, causing the steady component to either dominate the response or disappear. This is likely due to small errors in the transducer measurements which caused errors in the subsequent calculation of axial pressure gradient. Errors in the transducer measurements are likely because they were

---

[12] The code used to calculate the theoretical centerline velocity and velocity profile results is provided in Appendix A-3.5

calibrated in mmHg but the velocity profile calculations were performed in Pa; any small error in mmHg corresponds to a large error in pascal.

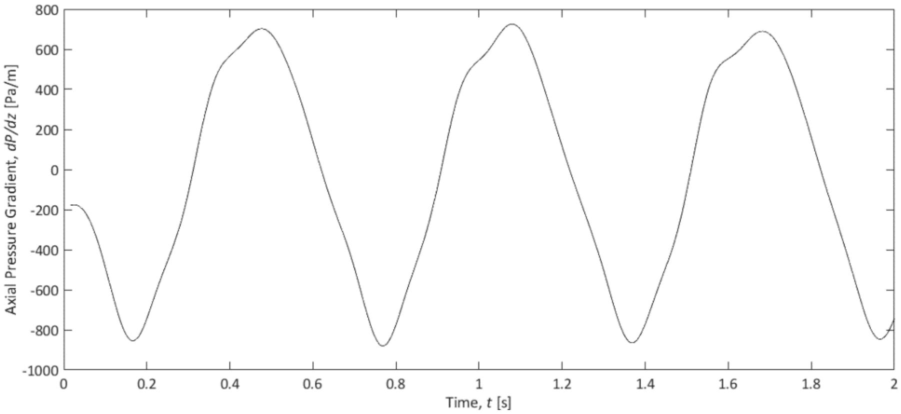

Figure 3-9: Plot of axial pressure gradient (*dP/dz*) from *f* = 1.67 Hz case of peristaltic pump experiment

In spite of the sensitivity of the theoretical velocity profiles shapes to axial pressure gradient measurements, the resulting phase angle between pressure gradient and velocity remained consistent for each tested value of static pressure. The centerline velocity was found to lead the pressure gradient for all pulse frequencies tested in this experiment. However, the phase angle was slightly different for each pulse frequency. Due to the consistency in the phase angle result for each pulse frequency, this phase angle was used for syncing experimental pressure and velocity measurements in the peristaltic pump experimental results.

3.5 Process of syncing system performance parameters

To interpret the relationship between pressure, tube expansion and downstream velocity, the three responses were synced in time. For the peristaltic pump experiment, the minimum of the pressure waveform was used as a reference point. It was assumed that the pressure and tube diameter minimas would coincide, so these two locations were synced. For the velocity results, the pressure and velocity responses were synced based on the theoretically obtained phase angle between pressure and velocity, as mentioned in the previous section. For the VAD experiment, the dicrotic notch was visible on both the tube distension and pressure plots so these two locations were synced. The pressure and velocity plots were synced by finding the index location of Camera 2 trigger signal in the raw voltage data and the first pressure minimum occurring after the trigger signal. The time index of this pressure minimum was matched with the Camera 2 image corresponding to that time stamp[13].

---

[13] The codes used to perform this phase syncing function is provided in Appendix A-3.7

3.6 Summary

This chapter outlined the methodologies used to process the pressure waveforms, compliant tube distension response and peripheral velocity fields collected during this experimental investigation. The pressure data was processed to produce filtered waveforms which allowed interpretation of pressure responses in each experiment. The images collected by Camera 1 were processed to obtain percent expansion values of the tube throughout multiple pumping cycles to determine the nature of its distension in response to fluctuating pressure gradients. Images obtained by Camera 2 downstream from the test section were processed to obtain vector fields. Theoretical velocity plots were generated to compare against experimentally obtained PIV results and to calculate the phase angle between pressure and velocity required to sync experimental responses in the peristaltic pump experiment. The next two chapters discuss the processed results obtained from the peristaltic and VAD experiment and explore the relationship between the three responses in each case.

Chapter 4. Impact of Compliant Tubing on EVHP Test Flow Loop Using Peristaltic Pump

4.1 Introduction

Peristaltic pumps are commonly used in the medical field for applications such as heart-lung machines to supply controlled pulsatile flow in a physiological environment. Due the well-controlled nature of the stroke volume delivery, peristaltic pumps are useful tools for studying the phenomena involved in high α pulsatile flow regimes with compliant response. In this study, a peristaltic pump was used to provide a foundational study into the effect of compliance in the EVHP analog test system using Newtonian and non-Newtonian fluids. This was done for a range of physiological pulse frequencies: 1.00 to 2.33 Hz (60 to 140 BPM).

This chapter summarizes the results obtained from the f = 1.67 Hz (100 BPM) case of the peristaltic pump experiment. The first three sections present the experimentally obtained results for the three behaviors of interest: pressure waveforms, compliant tube response and peripheral flow fields. The following section addresses the relationship between these three responses by viewing them together over one pumping cycle. Following that discussion, experimentally obtained velocity profiles are presented and comparisons are made between the rigid and compliant case for both fluids. Additionally, theoretical velocity profiles are presented and compared to the experimentally obtained profiles. Finally, an exploration of the effect of compliance on flow behavior and pump performance with respect to changing pulse frequency is presented. Results from this experiment are intended to illustrate the impact of compliant tubing both on the downstream flow fields and on the pump performance in a Newtonian and non-Newtonian regime.

4.2 Pressure response

The obtained pressure waveforms are the first basis for comparing the system response under rigid and compliant test section conditions. Figure 4-1(a) and (b) compare the rigid to compliant pressure waveforms at the inlet of the test section for the Newtonian and non-Newtonian case, respectively. The phase time (t) is normalized by the cycle time (τ)[14]. All cycles have been indexed to begin at the initiation of the pressure pulse. For both fluids, the rigid and compliant case demonstrate consistent signals across

---

[14] The code used to generate Figure 4-1 is provided in Appendix A-3.2

multiple cycles. Also, for both fluids the compliant case waveforms are significantly smoother than their rigid counterparts, implying that the introduction of compliance into the system dampens the pressure response and minimizes acoustic effects. In addition, the compliant waveforms peak later in the cycle than do the rigid waveforms, indicating that the compliant test section delays pressure pulse transmission through the system. There are also notable differences between the Newtonian and non-Newtonian pressure waves in both the rigid and compliant cases. For the Newtonian fluid, the mean pressure is approximately the same for the rigid and compliant cases but for the non-Newtonian fluid, the compliant mean pressure is higher than the rigid mean pressure but the amplitude is smaller. The rigid Newtonian waveform has more peaks in the waveform than the rigid non-Newtonian waveform, indicating that the increased viscosity of the non-Newtonian fluid reduces acoustic effects.

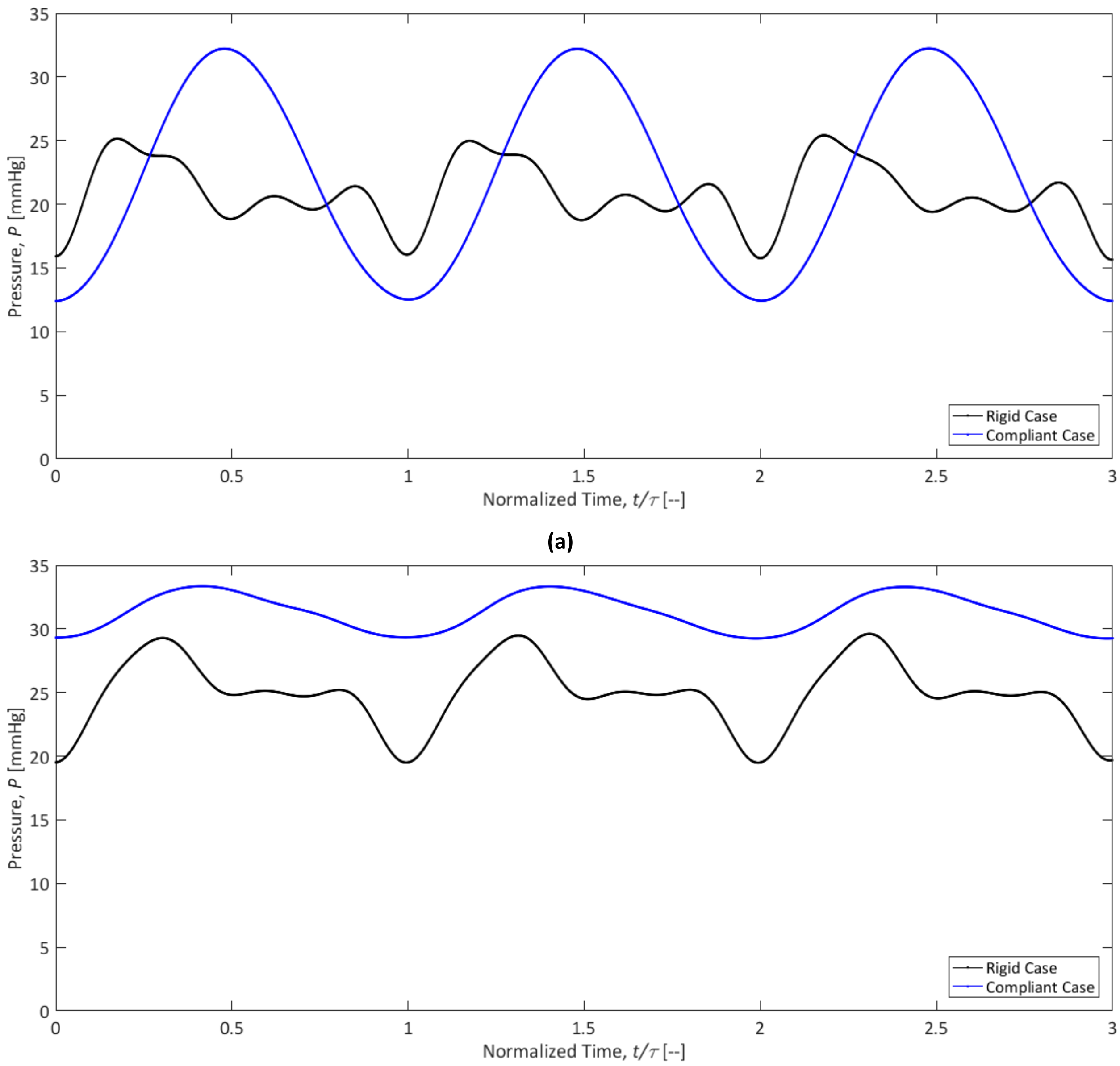

(a)

(b)

Figure 4-1: Plot comparing rigid and compliant case inlet pressure waveforms obtained from the *f* = 1.67 Hz case of the peristaltic pump experiment over multiple normalized pump cycles for (a) the Newtonian fluid and (b) the non-Newtonian fluid

4.3 Compliant tube response

As a pressure pulse is delivered by the pump, the compliant test section expands and stores some of the delivered stroke volume. How much the tube distends impacts the pressure waveforms and downstream flow fields. Figure 4-2 displays the compliant tube response as a percentage of relaxed diameter over two normalized pump cycles for the (a) Newtonian and (b) non-Newtonian case[15]. For both cases, results are consistent across multiple cycles. While the tube response is similar in shape for

---

[15] The code used to generate Figure 4-2 is provided in Appendix A-3.13

both fluids, the magnitudes vary significantly. The amount of tube distension resulting from the static pressure is higher for the non-Newtonian case than for the Newtonian case but the pulse pressure distension is lower. For the Newtonian fluid, the distension due to the static loading of the fluid column is approximately 1.75%, while for the non-Newtonian fluid it is 4.3%. Once there is an increase in pressure in the system, the Newtonian case distends by approximately 2.05% while the non-Newtonian fluid only distends an additional 0.4%.

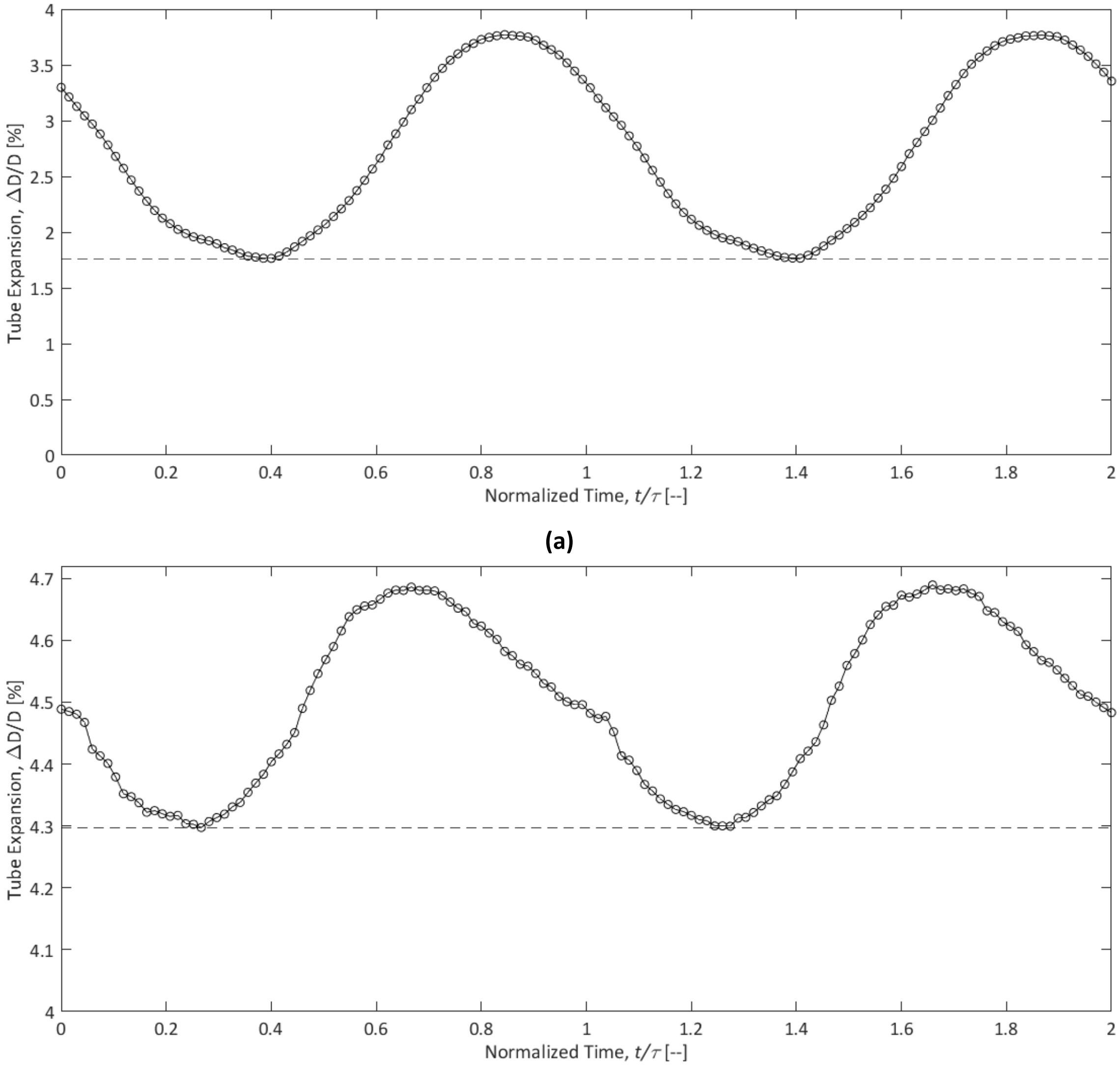

(a)

(b)

Figure 4-2: Plot of tube distension for the *f* = 1.67 Hz compliant case over multiple normalized pump cycles for (a) Newtonian case and (b) non-Newtonian case

4.4 Downstream flow response

The shapes of the pressure waveforms coupled with the compliant tube response affect the downstream flow behavior. Figure 4-3 compares the changes in downstream centerline velocity over three normalized pump cycles for the rigid and compliant test section using (a) the Newtonian fluid and (b) the non-Newtonian fluid[16]. Velocity data is consistent across multiple cycles for both cases of both fluids and, similar to the pressure waveforms, the compliant cases demonstrate much smoother responses than do the rigid cases. There are several differences between the rigid and compliant responses of the Newtonian fluid. First, although they oscillate around approximately the same mean velocity, the amplitude of the compliant centerline velocity waveform is significantly larger than that of the rigid response. In addition, the rigid centerline velocity exhibits minimal reverse flow, but the compliant centerline velocity oscillates between a positive peak velocity of approximately 0.1 m/s and a negative peak centerline velocity of approximately -0.07 m/s. This perhaps implies that while the compliant tube delays pressure pulse transmission, smoothing out the pressure waveform, it also induces both forward and reverse flow when it recoils. There are similar comparisons to be made about the non-Newtonian centerline velocities. Both the rigid and compliant centerline velocities also appear to share a similar mean velocity, but unlike the Newtonian case, the rigid non-Newtonian response has a higher amplitude and larger negative and positive peak velocities than the compliant case. Comparisons can also be made between the Newtonian and non-Newtonian responses. For the rigid case, the shapes and magnitudes of the centerline velocity curves are approximately the same for both fluids. However, for the compliant case, the amplitude of the non-Newtonian response is nearly half that of the Newtonian response and there is significantly less reverse flow due to viscous effects.

---

[16] The code used to process and plot experimental centerline velocity results is provided in Appendix A-3.6

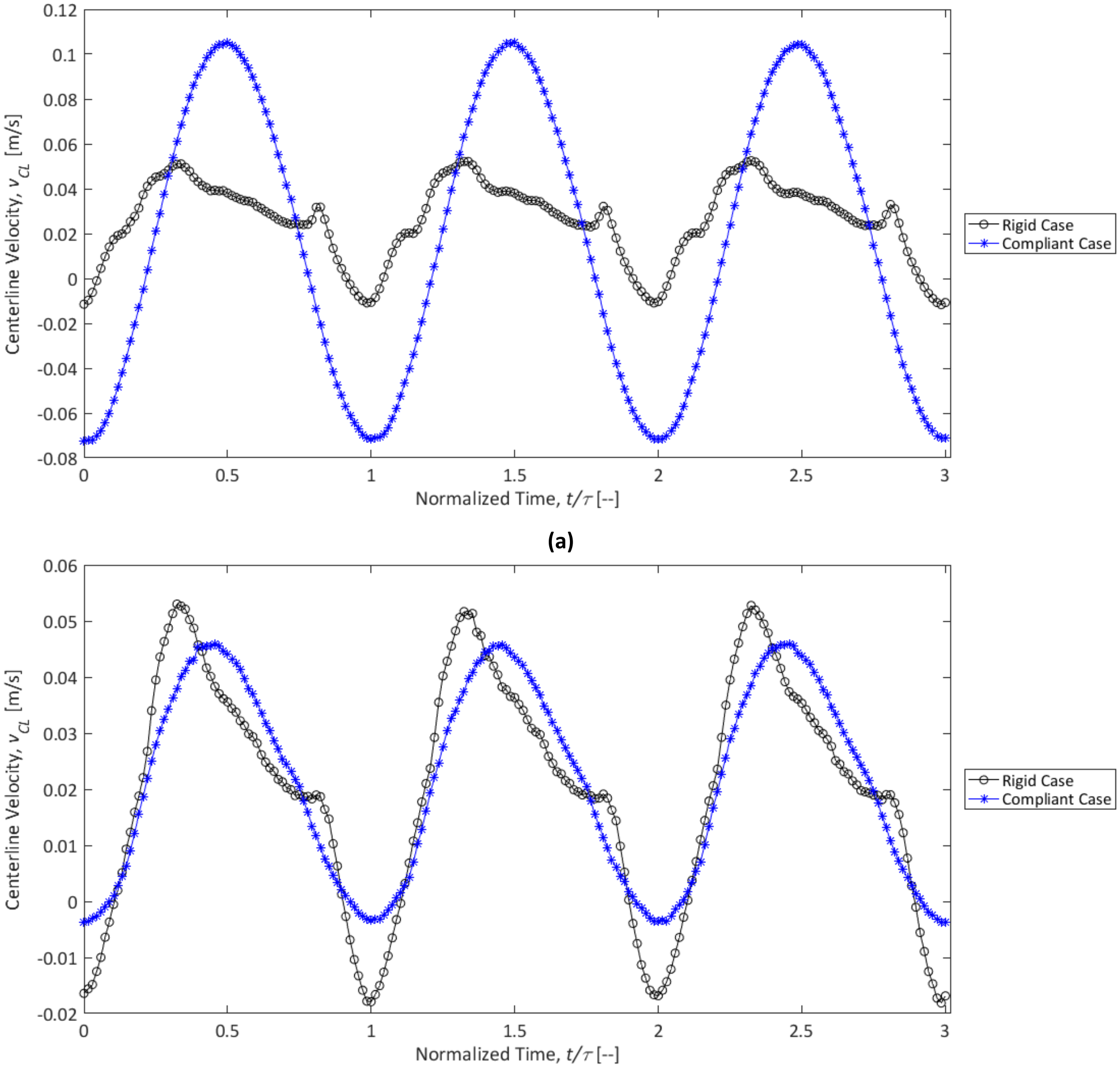

(a)

(b)

Figure 4-3: Plot of downstream centerline velocities for the *f* = 1.67 Hz case using rigid (black) and compliant (blue) test sections over multiple pump cycles with respect to normalized time for (a) Newtonian fluid and (b) non-Newtonian fluid

4.5 Comparison of system performance parameters over one pump cycle

The three aforementioned responses affect each other and impact system performance, so it is useful to view the relationships between them. Figure 4-4 provides a detailed view of the relationship between inlet pressure, tube distension and downstream centerline velocity over one normalized pump cycle for (a) the rigid Newtonian case, (b) the compliant Newtonian case, (c) the rigid non-Newtonian case and (d) the compliant non-Newtonian case[17,18]. Experimentally obtained centerline velocity results are represented by blue dots and theoretical centerline velocity responses are denoted by solid blue lines. In all four cases, the centerline velocity leads the pressure waveform. In both compliant cases, the shape of the tube distension response closely matches the pressure waveform shape as expected and the experimental centerline velocity curve agrees nicely with theoretical predictions. For both rigid cases, there are significant discrepancies between the theoretical and experimental centerline velocities. First, theory predicts a substantial decrease in centerline velocity immediately following peak velocity at approximately $t/\tau = 0.1$. This does not occur in the experimental plots; instead, centerline velocity remains positive until it reaches a secondary positive peak at approximately $t/\tau = 0.6$ and then decreases until it achieves its peak negative velocity at approximately $t/\tau = 0.7 - 0.8$ for both fluid cases. The shapes of the rigid theoretical centerline velocity curves closely mimic those of the pressure waveforms, which is not the case for the experimentally obtained results. Overall, the experimental centerline velocity results agree nicely with theory in the compliant cases but not in the rigid cases for both fluids. Due to the more complex nature of the rigid pressure waveforms and the presence of more acoustic effects, these discrepancies are likely due to sensitivity of the theoretical calculations to input axial pressure gradient.

---

[17] Normalized one cycle plots for other tested f values for the rigid and compliant cases are provided in Appendices A-1.1 and A-1.2, respectively

[18] The code used to plot Figure 4-4(a)&(c) is provided in Appendix A-3.7A-3.8 and the code used to plot Figure 4-4(b)&(d) is provided in Appendix A-3.9

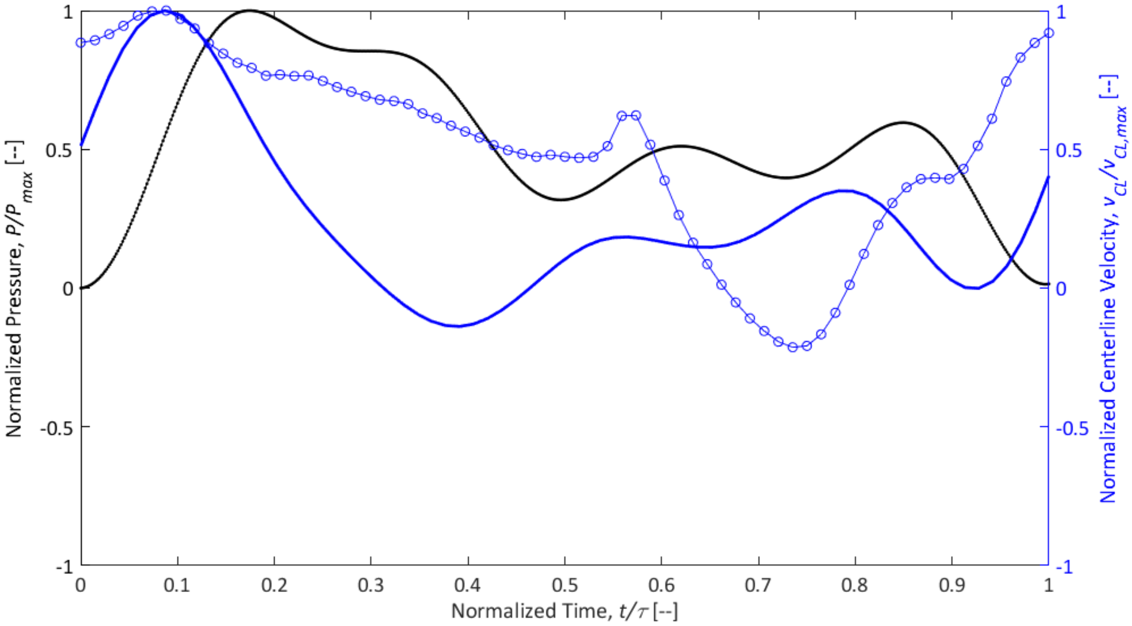

1
0.5
0
-0.5
-1
0
0.1
0.2
0.3
0.4
0.5
0.6
0.7
0.8
0.9
1
Normalized Pressure, P/P_{max} [--]
Normalized Time, t/τ [--]
Normalized Centerline Velocity, $v_{CL}/v_{CL,max}$ [--]

(a)

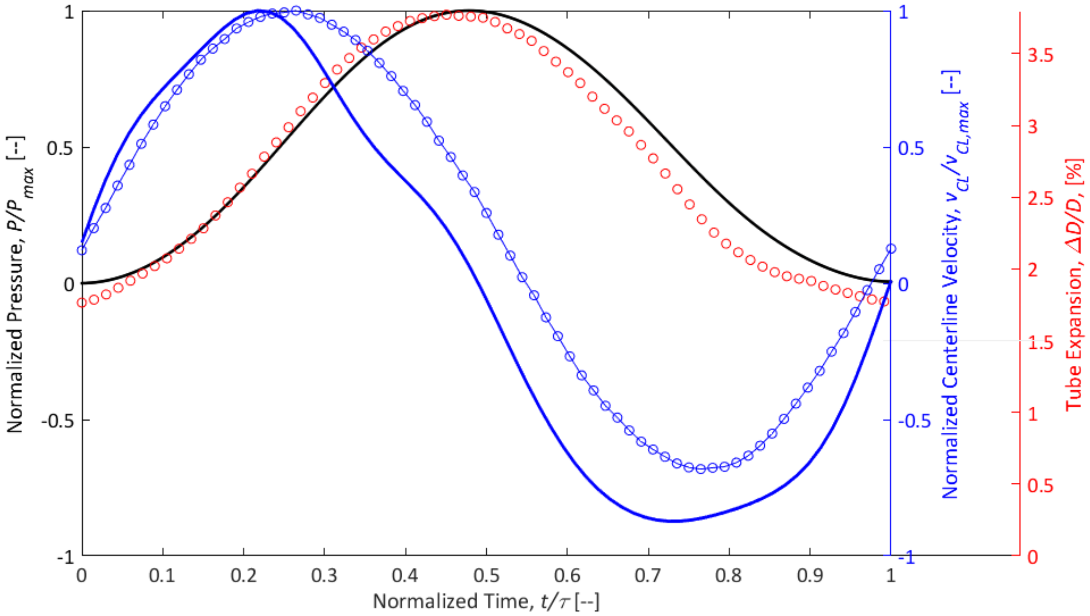

1
0.5
0
-0.5
-1
0
0.1
0.2
0.3
0.4
0.5
0.6
0.7
0.8
0.9
1
3.5
3
2.5
2
1.5
1
0.5
0
Normalized Pressure, P/P_{max} [--]
Normalized Time, t/τ [--]
Normalized Centerline Velocity, $v_{CL}/v_{CL,max}$ [--]
Tube Expansion, $\Delta D/D$, [%]

(b)

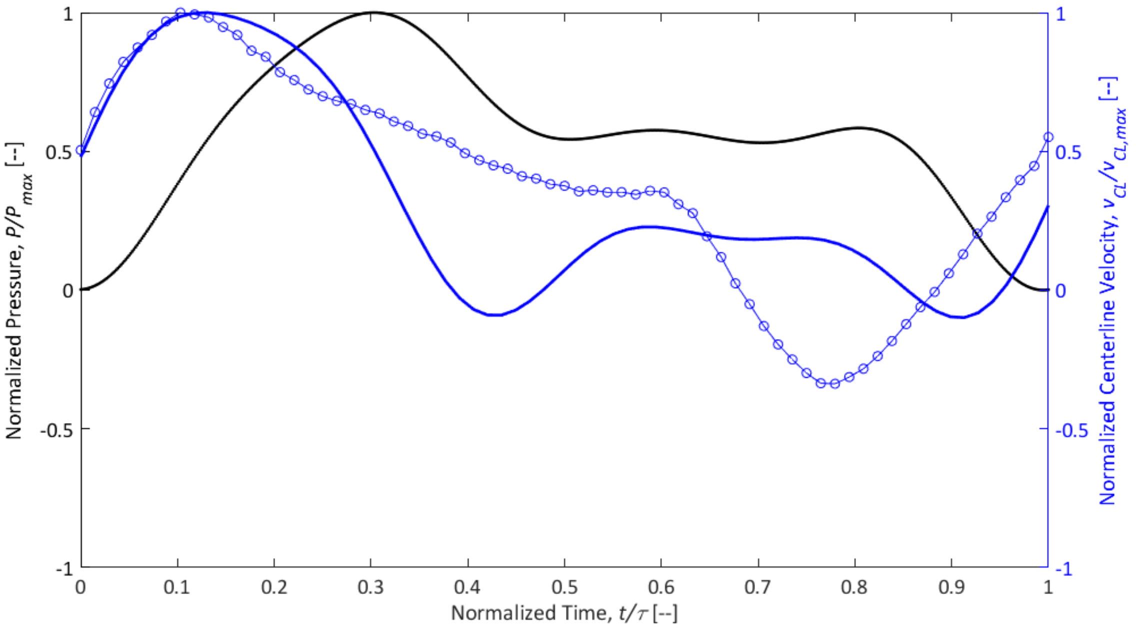

(c)

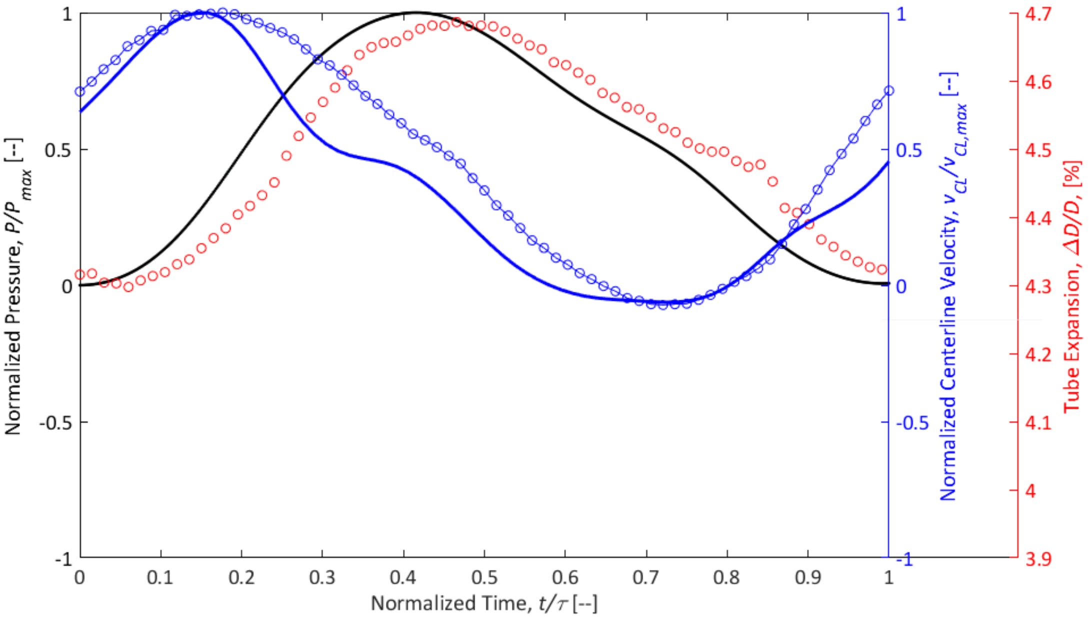

(d)

Figure 4-4: Normalized one cycle plot of pressure (solid black), theoretical centerline velocity (solid blue), experimental centerline velocity (blue circles) and tube distension (red circles) for (a) rigid Newtonian case, (b) Newtonian compliant case, (c) rigid non-Newtonian case, (d) compliant non-Newtonian case

4.6 Profiles of velocity

More detailed understanding of the downstream flow behavior under the four conditions of this study can be obtained by examining the profiles of velocity at various times throughout the cycle. This section presents non-dimensionalized velocity profiles obtained at ten time steps throughout the pumping cycle ($t/\tau = 0.0 - 0.9$) to compare the profiles resulting from the compliant test section to those obtained from the rigid test section. Four figures are presented for this comparison: a theoretical and experimental Newtonian plot, and a theoretical and experimental non-Newtonian plot.

4.6.1 Newtonian case

Figure 4-5 compares the non-dimensionalized experimental Newtonian velocity profiles obtained from the rigid (black) and compliant (blue) test section cases. The profiles are represented by solid lines due to the large number of data points defining the profile shape across the diameter of the tube. The first notable difference between the two cases is that there appear to be asymmetries in the compliant profiles that are not present in the rigid profiles. At the beginning of the cycle, the flow is accelerating and both profiles are developing. There is a phase difference between the two profiles attaining their maximum velocities. Due to the high α of the regime, unsteady effects are significant and neither profile has time to fully develop; the compliant profile develops into a much stronger top-hat profile than does the rigid profile. At the beginning of flow deceleration, which for the rigid case is $t/\tau = 0.1$ and for the compliant case is $t/\tau = 0.3$, both profiles begin to flatten, and at $t/\tau = 0.7$, they show reverse flow near the wall creating regions of high shear. This result is consistent with theoretical expectations from the literature for flows with $\alpha \geq 10$ [42] and with the theoretical expectations derived in this study, shown in Figure 4-6. The profiles in Figure 4-6 represent the theoretical profiles that were calculated based on the experimentally obtained axial pressure gradients. During the beginning of the cycle, from $t/\tau = 0.0 - 0.4$, the rigid and compliant experimental profile shapes are in excellent agreement with the theoretical expectations. During the deceleration phase, there are some discrepancies between the theoretical and experimental profile shapes, which are likely due to slight offsets in phase between the theoretical and experimental plots, as it is apparent that both the rigid and compliant profiles assume the predicted shapes during the cycle. Also, at $t/\tau = 0.8$, the theoretical profiles predict a laminar profile with no shear regions away from the wall, which implies that the theory predicts a stronger steady component than experimental findings would suggest for this flow regime.

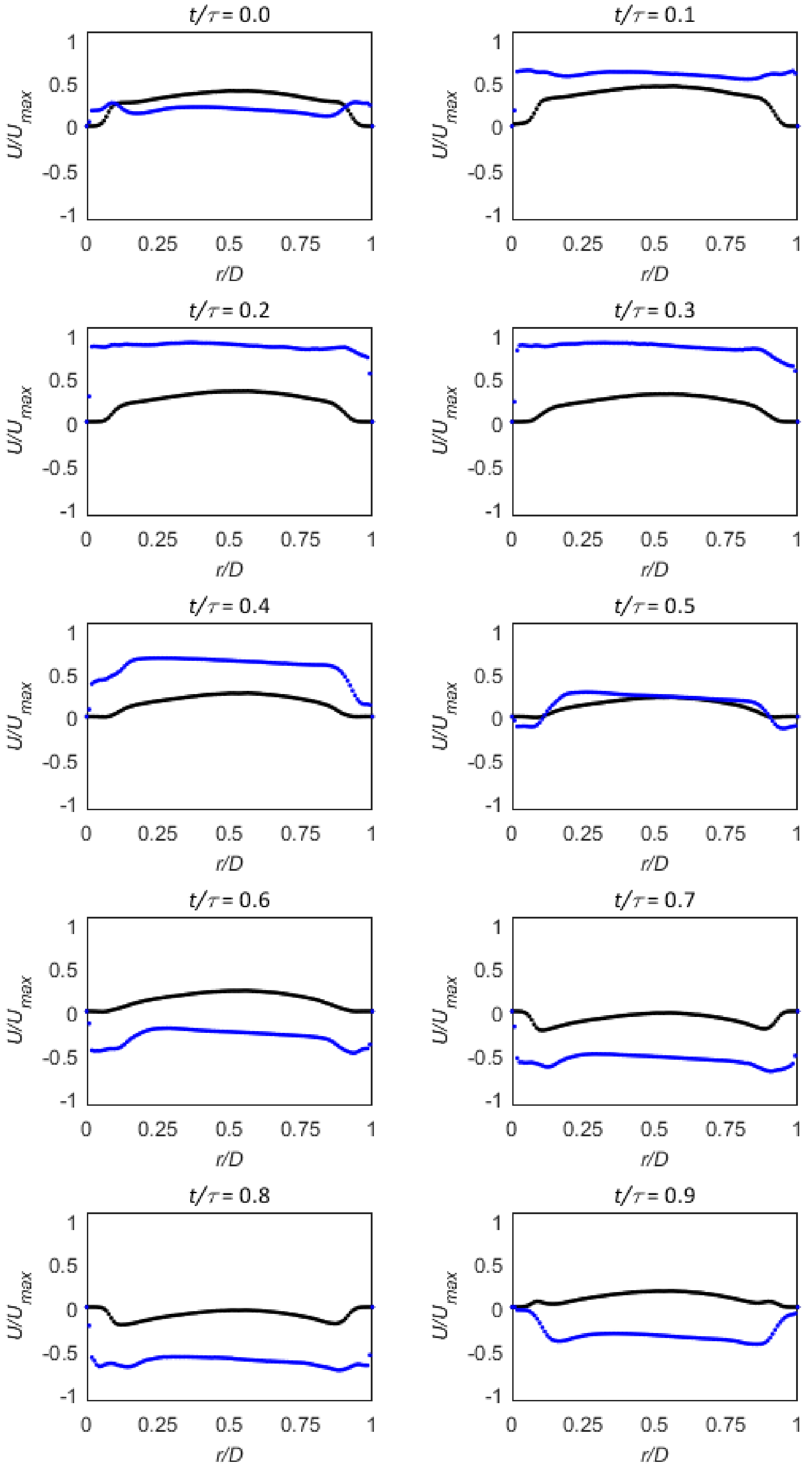
$t/\tau = 0.0$, $t/\tau = 0.1$, $t/\tau = 0.2$, $t/\tau = 0.3$, $t/\tau = 0.4$, $t/\tau = 0.5$, $t/\tau = 0.6$, $t/\tau = 0.7$, $t/\tau = 0.8$, $t/\tau = 0.9$

Figure 4-5: Non-dimensionalized experimental Newtonian velocity profiles for rigid (black) and compliant (blue) cases obtained at 10 time steps during pump cycle (t/τ = 0.1-0.9)

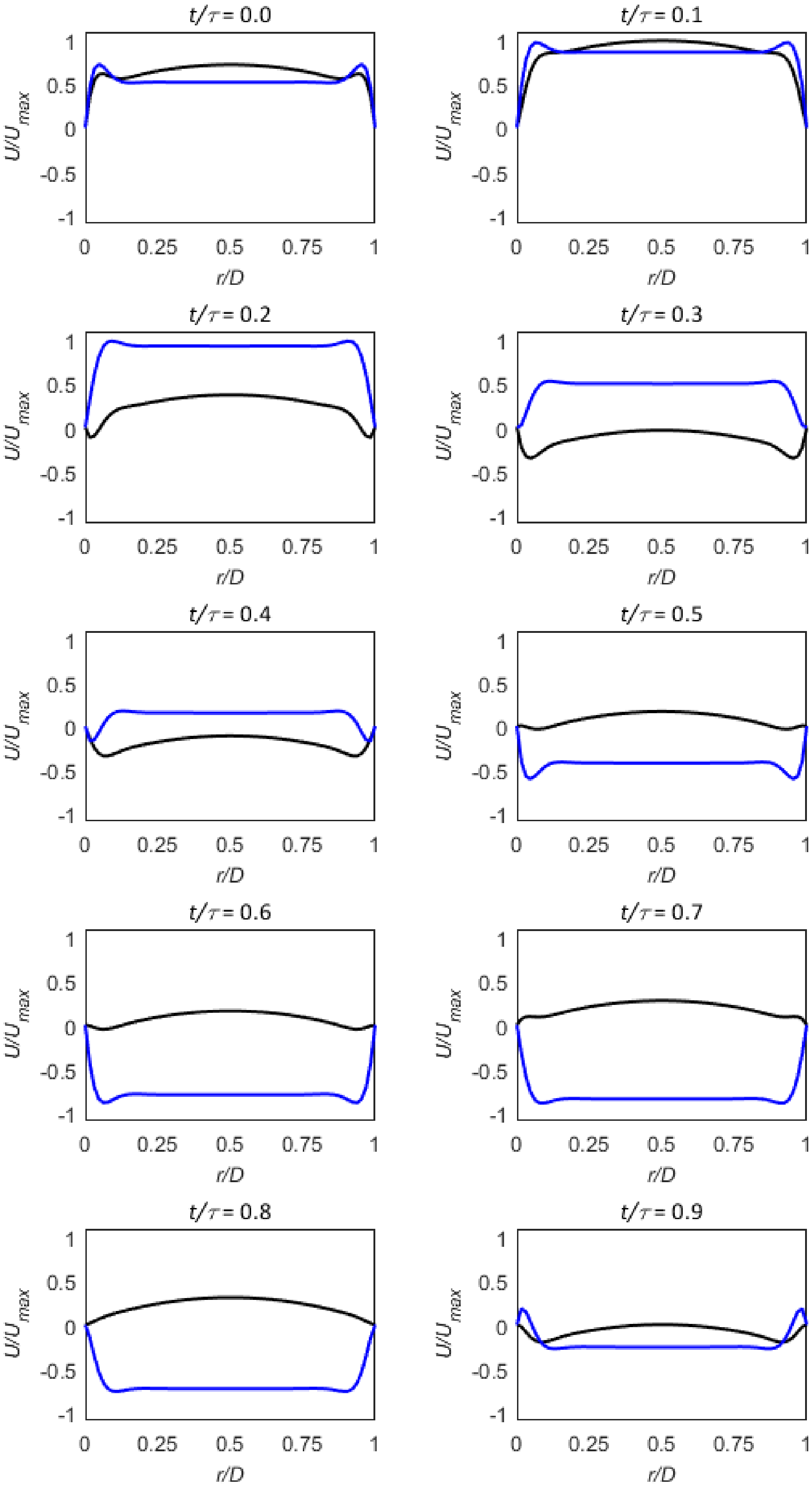

Figure 4-6: Non-dimensionalized theoretical Newtonian velocity profiles for rigid (black) and compliant (blue) cases obtained at 10 time steps during pump cycle (t/τ = 0.1-0.9)

4.6.2 Non-Newtonian case

Figure 4-7 compares the non-dimensionalized experimental non-Newtonian velocity profiles obtained from the rigid (black) and compliant (blue) test sections. As with the experimental Newtonian profiles, the profiles in Figure 4-7 are represented by solid lines due to the large number of data points defining the profile shapes across the diameter of the tube. For this case, both the rigid and compliant experimental profiles are symmetric about the center of the tube. Throughout the most of the cycle, the experimental rigid and compliant results overlap, indicating that compliance has little effect on the downstream flow behavior. Small differences in the experimental rigid and compliant profiles appear at $t/\tau = 0.6$ and $t/\tau = 0.8$, where the compliant case flow appears to be nearly stagnant and the rigid assumes a partially developed top-hat profile. In this case, it appears that the introduction of compliant tubing is preventing the reverse flow that is present at $t/\tau = 0.8$ in the rigid case. The shapes of these profiles are similar to those predicted by the theoretical non-Newtonian profiles presented in Figure 4-8, although the experimental profiles achieve a more parabolic-shaped profile than the theoretical results predict. The theoretical profiles assume a top-hat profile at maximum velocity and have regions of high shear away from the wall during deceleration that are less pronounced in the experimental profiles. This suggests that the steady component is stronger than the theory predicted according to the axial pressure gradient, or that the fluid is less viscous than the predicted viscosity. The slight differences in theoretical profile shapes from $t/\tau = 0.5 - 0.7$ are likely due to the small phase offsets in the results seen in Figure 4-4, but the shapes are similar for the theoretical rigid and compliant results during this phase of the cycle.

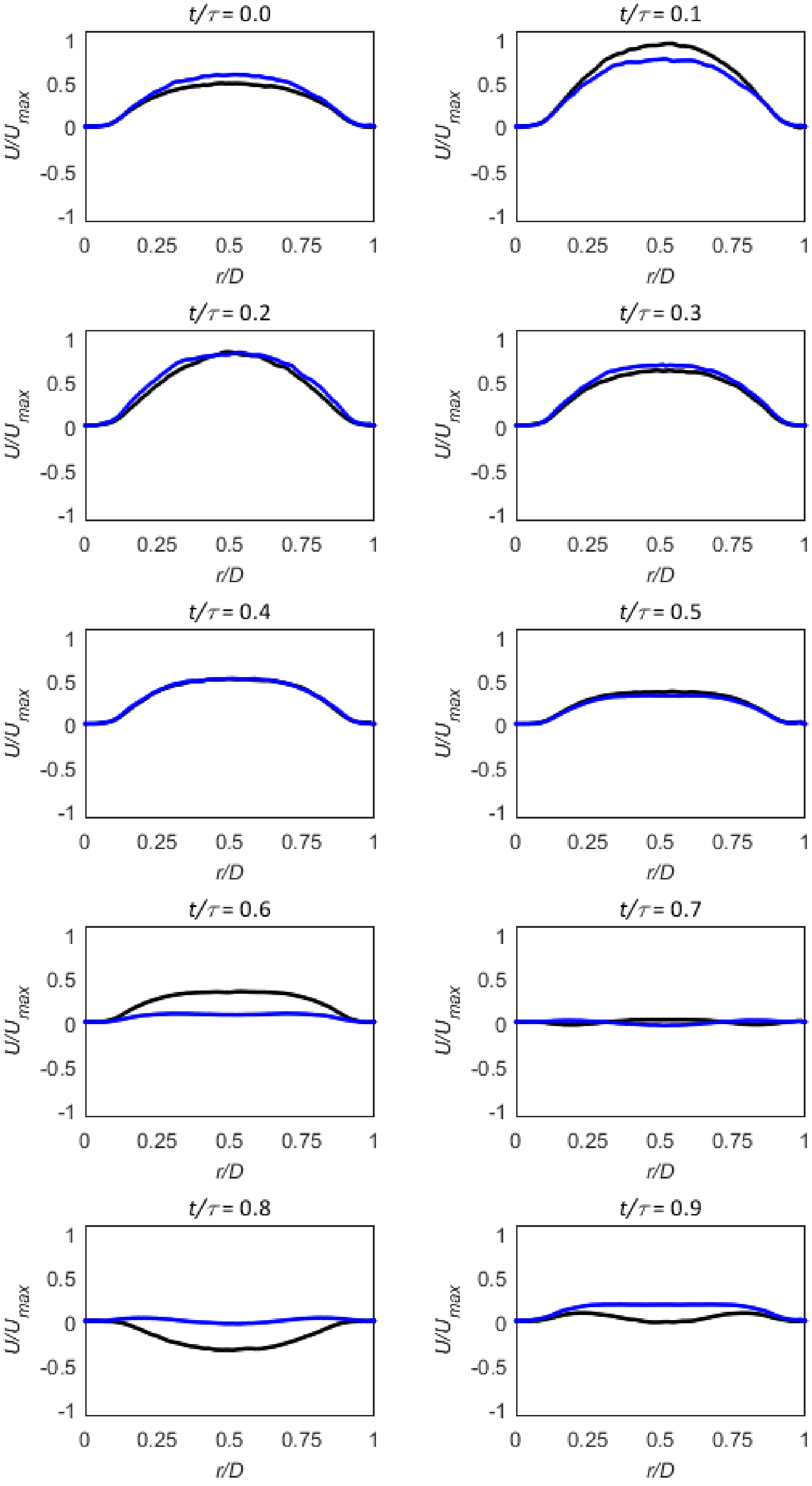

Figure 4-7: Non-dimensionalized experimental non-Newtonian velocity profiles for rigid (black) and compliant (blue) cases obtained at 10 time steps during the pump cycle (t/τ = 0.1-0.9)

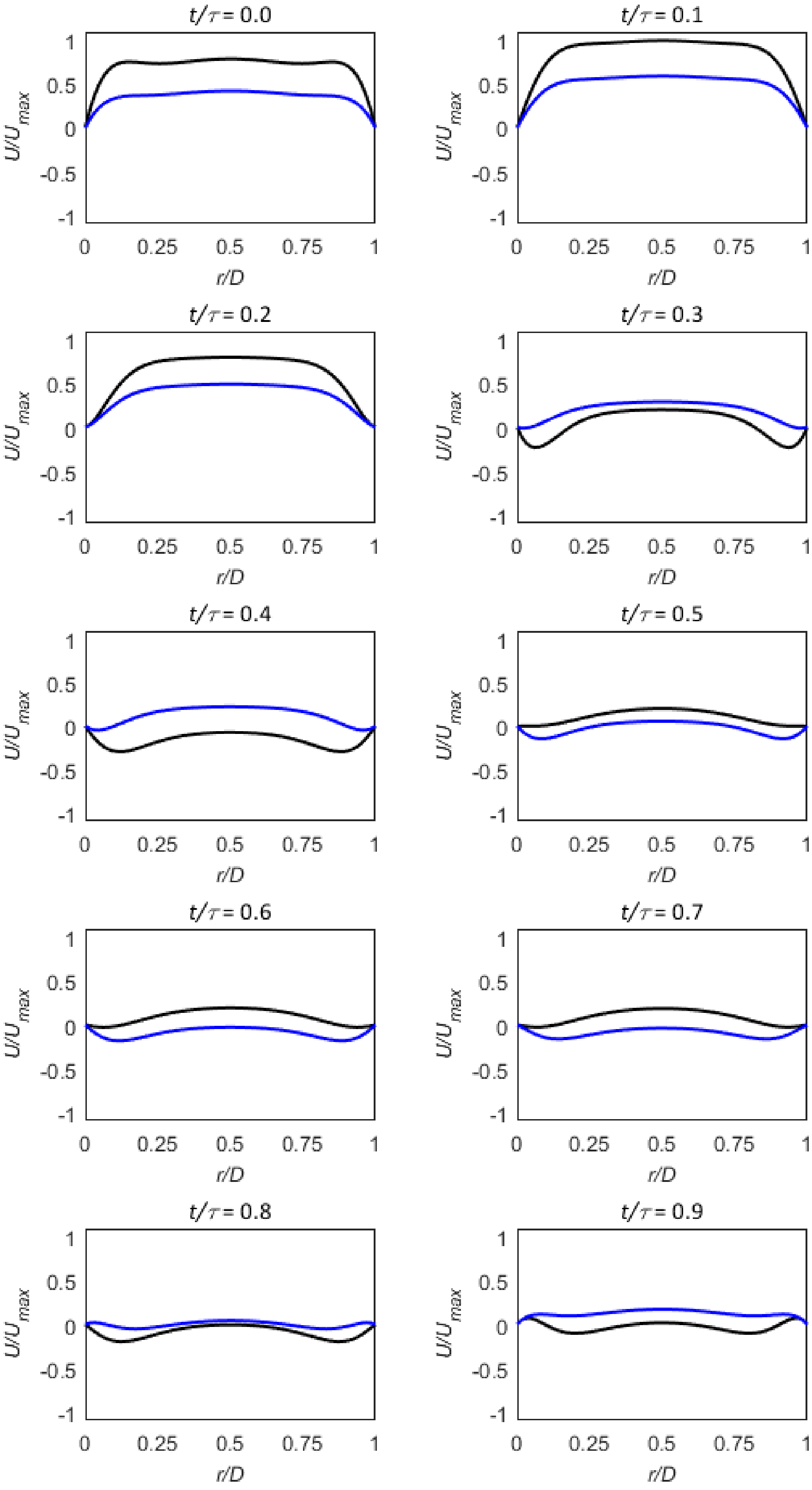

Figure 4-8: Non-dimensionalized theoretical non-Newtonian velocity profiles for rigid (black) and compliant (blue) cases obtained at 10 time steps during the pump (t/τ = 0.1-0.9)

4.6.3 Comparison of Newtonian and non-Newtonian profiles of velocity

A comparison of the rigid and compliant test section case has been presented for the Newtonian and non-Newtonian fluid[19,20]. Comparisons can also be made between the Newtonian and non-Newtonian profiles. The theoretical profiles predicted a similarly blunted top-hat profile for the Newtonian and non-Newtonian rigid cases in their most developed forms. Experimental results were consistent with this prediction for the Newtonian case, but non-Newtonian experimental profiles were notably more parabolic in shape. In addition, the theoretical and experimental profiles demonstrated pronounced forward and backward top-hat profiles for the compliant Newtonian case but not for the non-Newtonian compliant case. The compliant non-Newtonian profiles instead had regions of reverse flow near the walls creating high shear regions, similar to those seen in the rigid profiles of both fluids.

The experimental velocity profiles presented in this section are in good agreement with the theoretical profiles generated for this investigation, indicating that flow monitoring and modeling were reliable in this experiment. Examining the velocity profiles for this pulse frequency indicates that the presence of compliance alters the downstream flow fields far more significantly in a Newtonian regime than in a non-Newtonian regime. In the Newtonian case, the compliant test section introduced significant reverse flow into the system but this was not the case with the non-Newtonian fluid.

---

[19] The code used to generate Figure 4-5 and Figure 4-7 is provided in Appendix A-3.10

[20] The code used to generate Figure 4-6 and Figure 4-8 is provided in Appendix A-3.11

4.7 Effect of pulse frequency on system performance

The previous sections presented results for one pulse frequency case of the peristaltic pump experiment, and comparisons were made between the rigid and compliant case using both Newtonian and non-Newtonians fluids. Further understanding of system performance can be gleaned by looking at the effect of pulse frequency on system performance in terms of its impact on pressure waveform shape, tube distension, downstream centerline velocity and pump energy.

The range of pulse frequencies explored in this experiment is 1.00 – 2.33 Hz (60 – 140 BPM). The corresponding Womersley numbers for each experimental condition are summarized in Table 4-1. The Newtonian α was calculated using equation (1-7) and the non-Newtonian α was calculated as the real part of the complex Womersley number defined in equation (1-20) using a characteristic relaxation time of 0.11 seconds.

Table 4-1: Summary of Womersley numbers for peristaltic pump experiment

Frequency, f [Hz]	Newtonian Womersley number, α [--]	Non-Newtonian Womersley number, $\Re(\alpha^*)$ [--]
1.00	15.9	6.3
1.17	17.2	7.3
1.33	18.3	8.4
1.50	19.4	9.5
1.67	20.5	10.5
1.83	21.5	11.6
2.00	22.4	12.6
2.17	23.4	13.7
2.33	24.2	14.8

4.7.1 Effect of pulse frequency on pressure waveform shape

Figure 4-9 depicts the pressure waveforms obtained from the (a) rigid Newtonian case, (b) compliant Newtonian case, (c) rigid non-Newtonian case and (d) compliant non-Newtonian case at all tested pulse frequencies over one normalized pump cycle[21]. For the rigid Newtonian case, the pressure waveforms assume similar shapes at the lower frequencies, but after f = 1.83 Hz there is a shift in the location of the global maximum from $t/\tau \cong 0.2\text{-}0.3$ to $t/\tau \cong 0.8$. At the lower end of the tested range, increasing pulse frequency increases the amplitude of the first peak but after the peak reversal at f = 1.83 Hz, increasing pulse frequency causes an increase in height of the second peak. For the compliant Newtonian case, increasing pulse frequency smooths out the waveform shape. At f = 1.33 Hz, the waveform changes from having two peaks to only one; increasing pulse frequency increases the height and causes a

---

[21] The code used to generate Figure 4-9 is provided in Appendix A-3.3

leftward phase shift of that peak. After *f* = 1.67 Hz, the wave amplitude begins to decrease with increasing pulse frequency and the wave continues to shift to the left. For the rigid non-Newtonian case, the amplitudes of both peaks increase with increasing pulse frequency and the valley between the two peaks becomes more distinct. Finally, for the compliant non-Newtonian case, increasing pulse frequency smooths out the waveform and causes both an increased wave amplitude and a consistent rightward phase shift of the peak.

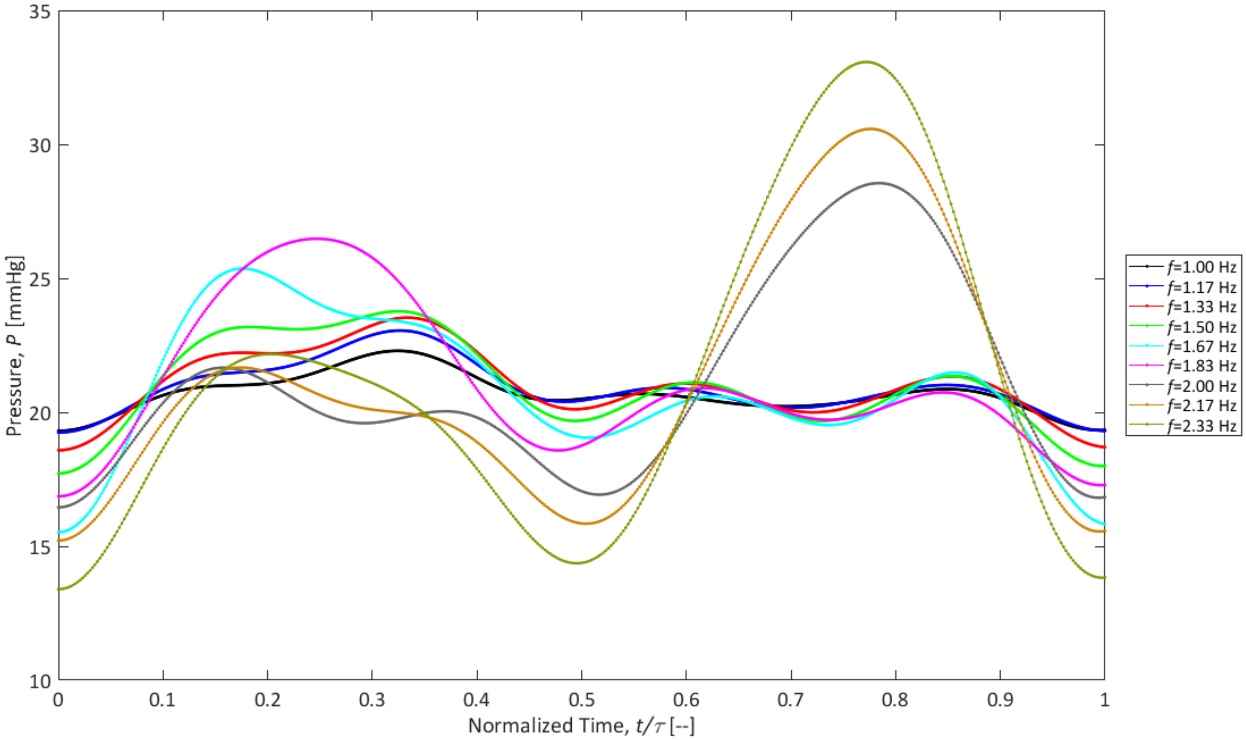
35
30
25
20
15
10
Pressure, P [mmHg]
0
0.1
0.2
0.3
0.4
0.5
0.6
0.7
0.8
0.9
1
Normalized Time, t/τ [--]
f=1.00 Hz
f=1.17 Hz
f=1.33 Hz
f=1.50 Hz
f=1.67 Hz
f=1.83 Hz
f=2.00 Hz
f=2.17 Hz
f=2.33 Hz

(a)

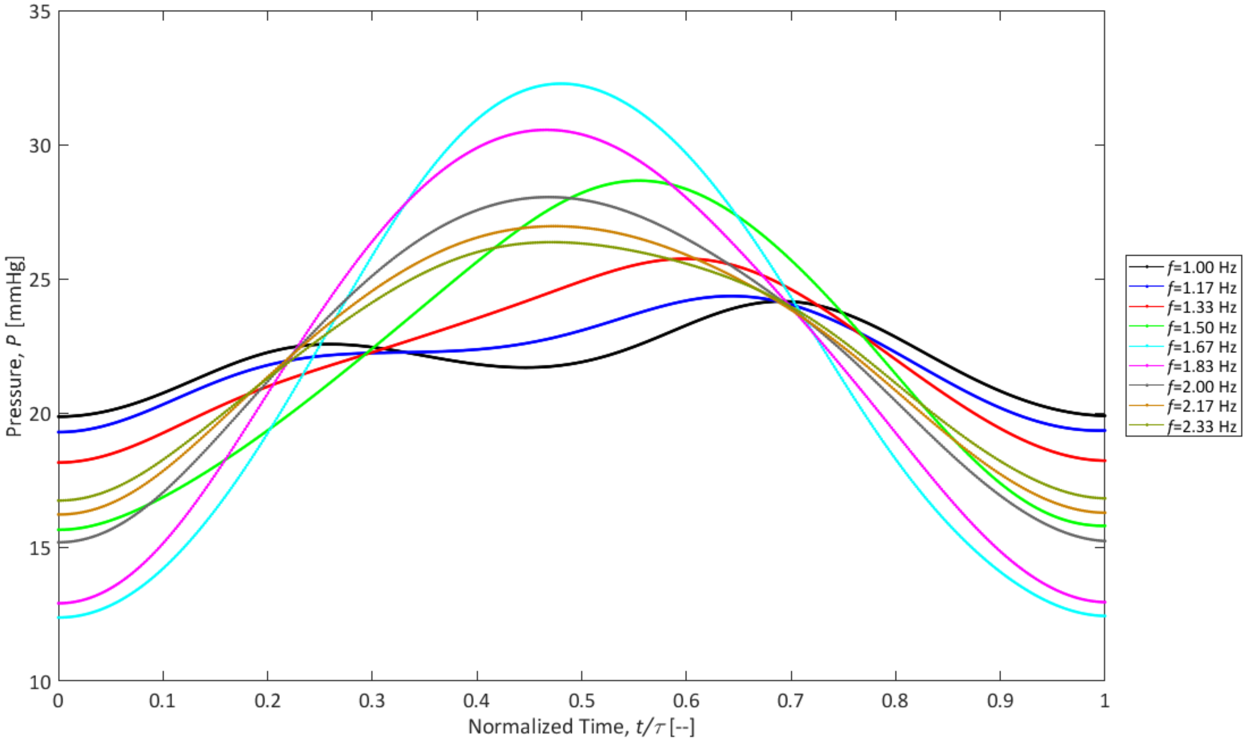
35
30
25
20
15
10
Pressure, P [mmHg]
0
0.1
0.2
0.3
0.4
0.5
0.6
0.7
0.8
0.9
1
Normalized Time, t/τ [--]
f=1.00 Hz
f=1.17 Hz
f=1.33 Hz
f=1.50 Hz
f=1.67 Hz
f=1.83 Hz
f=2.00 Hz
f=2.17 Hz
f=2.33 Hz

(b)

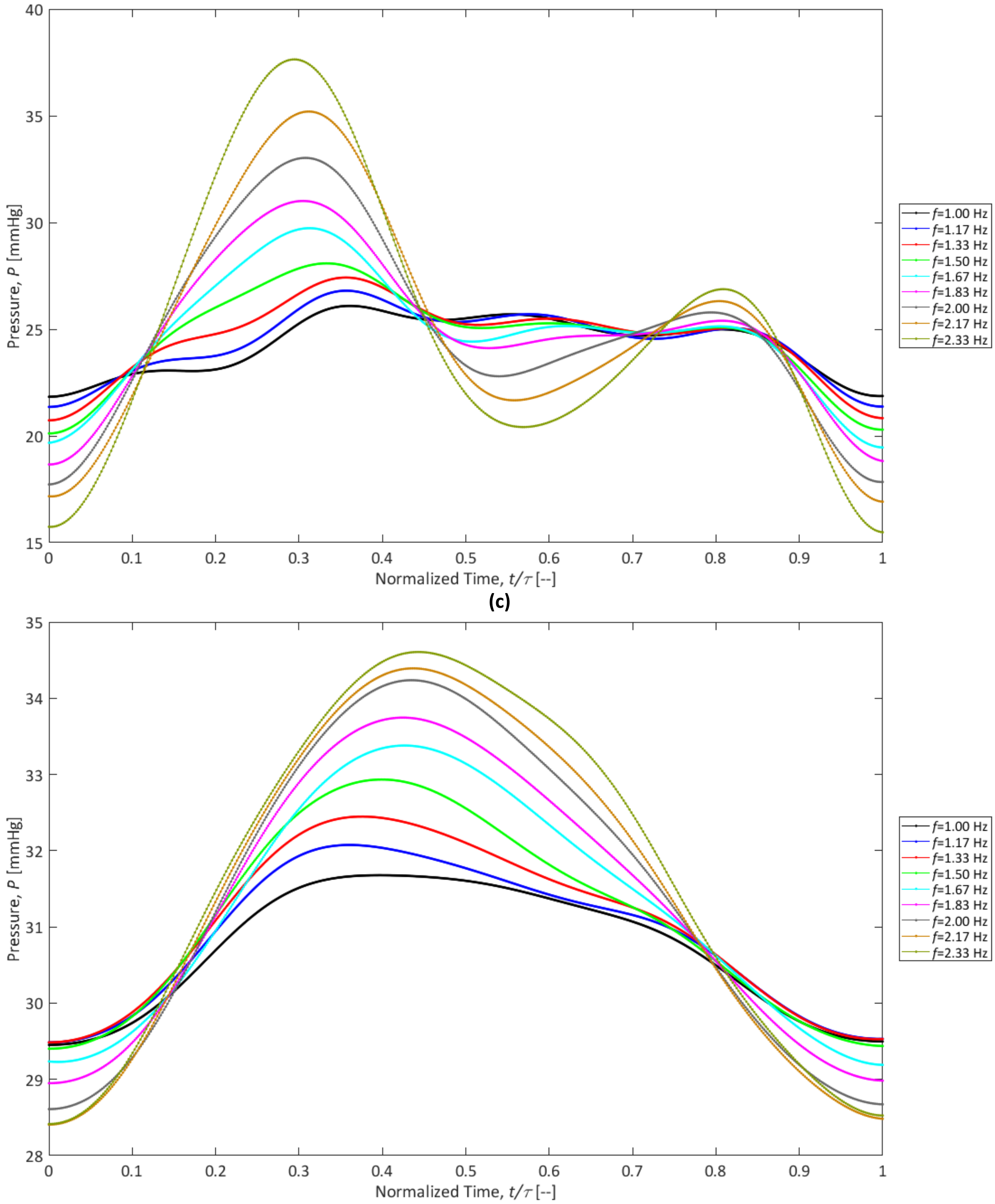

(c)

(d)

Figure 4-9: Plot comparing the changes in pressure waveform shapes that occur with changing pulse frequency

4.7.2 Effect of pulse frequency on compliant tube distension

Figure 4-10 establishes the relationship between pulse frequency and maximum tube distension achieved during the pulse cycle for the Newtonian and non-Newtonian case. The maximum tube distension demonstrates a positive relationship with pulse frequency for both fluids at the low frequencies. At 1.67 Hz (α = 20.5), the Newtonian case reaches its peak distension; at higher pulse frequencies maximum tube distension decreases with increasing pulse frequency. The non-Newtonian fluid demonstrates a different behavior and maintains a positive linear relationship throughout the range of tested pulse frequencies.

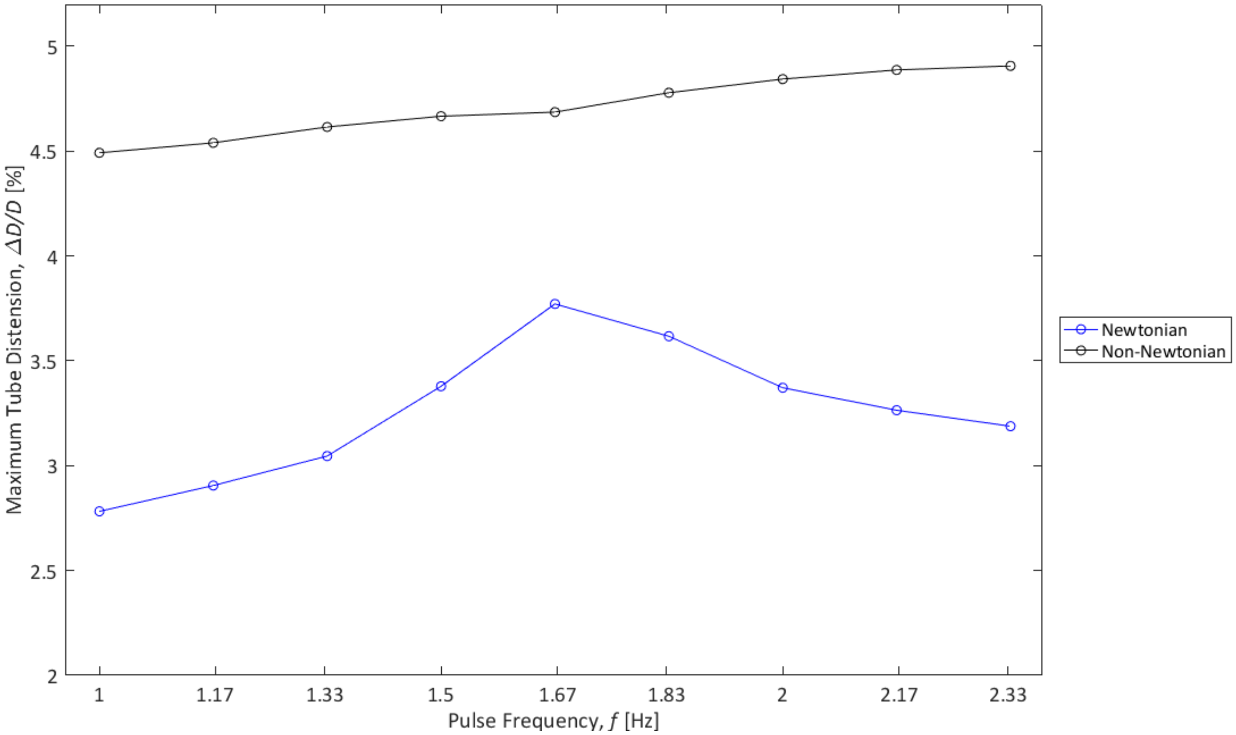

Figure 4-10: Plot comparing the effect of pulse frequency (*f*) on maximum tube distension (*ΔD/D*) in the compliant Newtonian and non-Newtonian cases

4.7.3 Effect of pulse frequency on downstream flow

To further understand the impact of compliance on system performance, the downstream centerline velocity was examined. Figure 4-11 depicts the relationship between pulse frequency and the maximum downstream centerline velocity achieved during the pump cycle for all four cases. While the rigid cases for both fluids display approximately the same linear relationship between pulse frequency and maximum centerline velocity, the compliant responses differ significantly. The maximum centerline velocity of the compliant Newtonian case increases with increasing pulse frequency in a non-linear fashion. It reaches its peak at 1.67 Hz then drops off non-linearly. The compliant non-Newtonian case however, demonstrates a positive linear relationship between pulse frequency and maximum centerline velocity until 2.17 Hz, at which point the centerline velocity slowly begins to decrease with increasing pulse frequency. These results indicate that with a rigid test section, non-Newtonian effects have minimal impact on the peak downstream velocity achieved during the cycle. In contrast, with a compliant test section non-Newtonian effects significantly dampen the maximum downstream velocity achieved during the pump cycle. This suggests that the compliant tube stores more fluid during the pressure pulse than it transmits forward. Notably, the frequency at which the largest maximum centerline velocity is achieved for the Newtonian case corresponds to the frequency at which maximum tube distension is reached, suggesting that for the low viscosity Newtonian fluid, the tube distension augments downstream flow until the flow exceeds $\alpha = 20.5$. At higher values of α, the tube does not have adequate time to expand and store as much volume and therefore downstream flow is not as significantly enhanced.

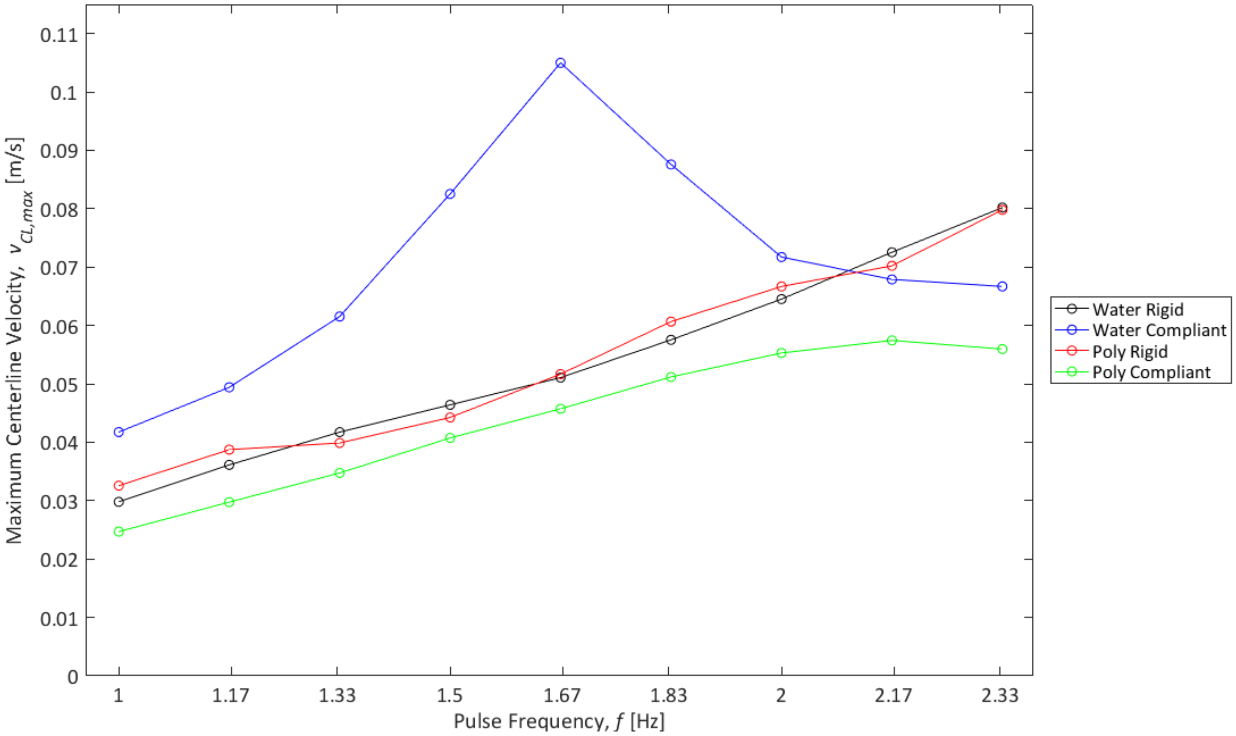

Figure 4-11: Plot of comparing the effects of pulse frequency (*f*) on maximum centerline velocity ($v_{CL,max}$) in the rigid and compliant cases with Newtonian and non-Newtonian fluids

4.7.4 Effect of pulse frequency on pump energy

The results presented in previous sections focused on the impact of compliance and non-Newtonian effects on specific flow conditions such as pressure and velocity. While these flow conditions provide information about certain aspects of system performance, combining them to understand pump performance is the most powerful tool for analyzing the effect of compliance on overall system performance. Based on equations (1-9) and (1-10), the energy output by the pump was determined based on the total energy in the fluid in region 2, the region of velocity data collection, integrated over the cycle time[22]. This calculation incorporates the pressure pulse energy, the kinetic energy, the static energy and the local acceleration energy such that:

$$E_{pp} = \underbrace{\frac{1}{\rho}\int_0^{t_c} \dot{m}_2(t)\, p_2(t)dt}_{\text{Pressure}} + \underbrace{\frac{1}{2}\int_0^{t_c} \dot{m}_2(t)\, [\bar{v}_2(t)]^2 dt}_{\text{Kinetic}} + \underbrace{g\Delta z \int_0^{t_c} \dot{m}_2(t)\, dt}_{\text{Static}} + \underbrace{L_{eff}\int_0^{t_c} \dot{m}_2(t) \left(\frac{dv}{dt}\right)_2 dt}_{\text{Local Acceleration}} \qquad \textbf{(4-1)}$$

where E_{pp} is the energy output by the peristaltic pump per pulse cycle [J/cycle], $\dot{m}_2(t)$ is the mass flow rate through the region of velocity data collection [kg/s], as calculated by: $\dot{m}_2(t) = \rho\left[\iint_0^D v(r)rdrd\theta\right] = \rho\left[\pi r\int_0^D v(r)dr\right]$, $p_2(t)$ is the pressure waveform obtained at point 2 [Pa], t_c is the cycle time [s], $\bar{v}_2(t)$ is the average velocity in region 2 [m/s], Δz is the height difference between the preload reservoir and point 2 [m], L_{eff} is the height difference between point 2 and the preload reservoir [m], and $\left(\frac{dv}{dt}\right)_2$ is the acceleration in region 2 [m/s^2] calculated from $\bar{v}_2(t)$.

Figure 4-12 depicts the relationship between pulse frequency and pump energy for the Newtonian rigid and compliant cases. Each type of energy is plotted to highlight its relative contribution to total pump energy. In both fluids, the local acceleration and kinetic energy are negligible and the static energy contribution is slightly negative. For both cases, the energy resulting from the pressure pulse dominates. At the lowest frequencies, the compliant and rigid energy requirements are approximately the same, but the responses begin to diverge after *f* = 1.33 Hz. For the rigid case, the pressure and total energy curves remain relatively consistent throughout the range of pulse frequencies, implying that without the presence of compliance in the system, pulse frequency has minimal impact on the energy requirements of the pump. For the compliant case however, the pressure and total pump energy functions assume similar shapes to what was seen in Figure 4-10 and Figure 4-11, which means that the energy requirements of the pump increase in this system as the magnitude of compliant response increases.

---

[22] The code used to perform the energy calculations is provided in Appendix A-3.12

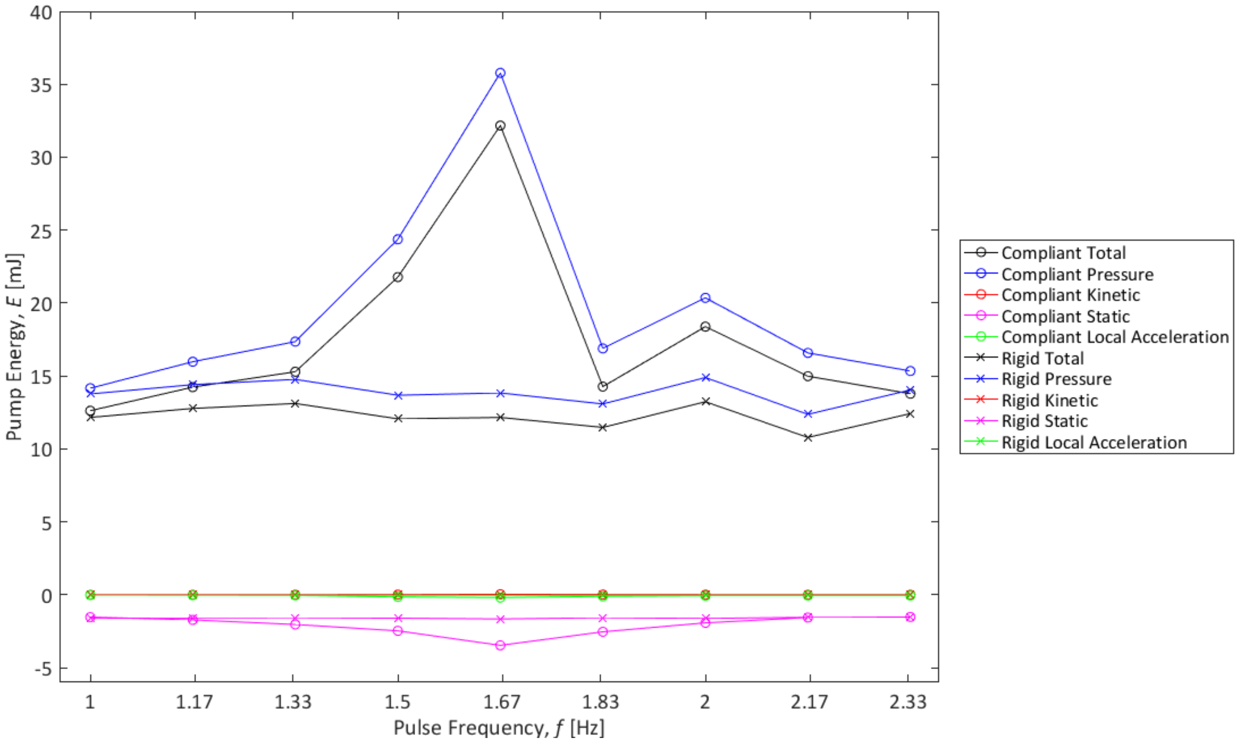

Figure 4-12: Plot comparing the effect of pulse frequency (*f*) on pump energy (*E*) for the Newtonian rigid and compliant cases

Figure 4-13 depicts the relationship between pulse frequency and pump energy for the non-Newtonian rigid and compliant cases. As in Figure 4-12, each type of energy is plotted to highlight its relative contribution to total pump energy and, like the Newtonian case, pressure pulse energy dominates. Unlike the Newtonian response, both the rigid and compliant non-Newtonian cases maintain fairly consistent total energy values across the range of tested frequencies, indicating that pulse frequency has minimal impact on pump energy requirements in a non-Newtonian regime whether compliant response is present or not. While both responses display similar shapes, the pump energy requirement of the compliant case is higher than that of the rigid case across the pulse frequency range. This finding is consistent with the Newtonian results that the introduction of compliance increases the pump energy requirements in this experimental setup.

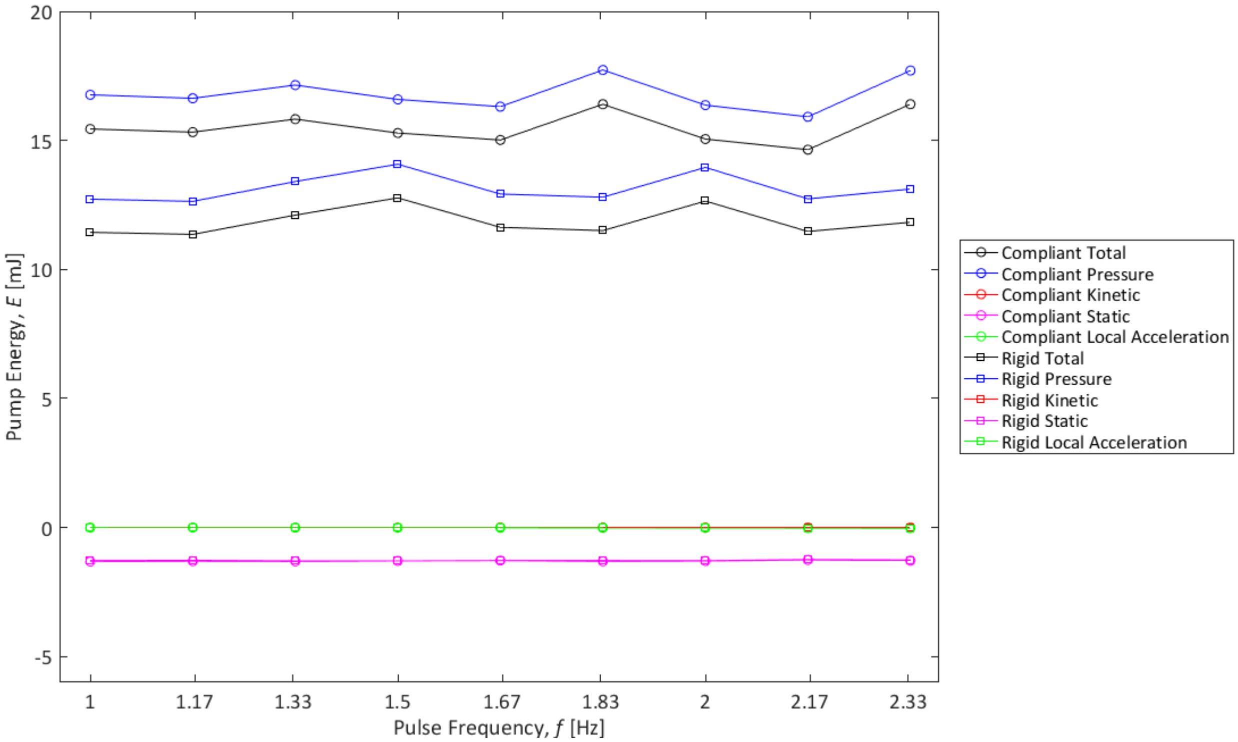

Figure 4-13: Plot comparing the effect of pulse frequency (*f*) on pump energy (*E*) for the non-Newtonian rigid and compliant cases

4.8 Conclusion

This chapter presented results from the peristaltic experiment in terms of the pressure, tube response and velocity results of the 1.67 Hz case in order to provide a comparison between the rigid and compliant test section cases. Results for each case were presented using a Newtonian and a non-Newtonian fluid and experimental velocity results were compared to theoretical results. Then, to gain broader understanding of the system behavior, results investigating the impact of pulse frequency on each of the tested system behaviours were presented, culminating in the examination of pump performance.

Pressure results indicate that the introduction of a compliant test section smooths out the pressure waveform at the inlet of the test section for both fluids, indicating the presence of more acoustic effects in the rigid case. This is supported by the presence of peaks in the rigid downstream centerline velocity responses presented in Section 4.4 that are not present in the compliant results. Looking at the range of tested pulse frequencies, the smoothing effect of the compliant test section was consistently present in both fluids but the magnitudes of the tube response were different. The Newtonian case demonstrated a larger tube response to pulse pressure which translated to a centerline velocity response that peaked at 1.67 Hz, the case of maximum tube distension. For the non-Newtonian case, no such peak existed and the relationship between pulse frequency, tube distension and downstream centerline velocity remained linear within the range of tested pulse frequencies. In terms of pump energy requirements, findings for both fluids indicated a higher pump energy requirement in the compliant test section conditions when compared to the rigid test section conditions. For the Newtonian fluid, the shape of this relationship mirrored that of tube distension with respect to pulse frequency, so the peak energy requirements occurred at 1.67 Hz. For the non-Newtonian fluid, pump energy requirements were fairly consistent across the tested values of pump frequency for the rigid and compliant case, indicating that pulse frequency has minimal impact on pump energy requirements in a non-Newtonian regime of this nature. However, consistent with the Newtonian findings, the pump energy requirements of the compliant case were consistently higher than those for the rigid cases.

Chapter 5. Impact of a Mock Aorta in an EVHP Test System

5.1 Introduction

In vivo, the Windkessel effect plays an important role in maintaining cardiac performance. This response is not present in the EVHP system and the potential consequences of its absence have yet to be addressed. The aim of this investigation was to study the impact of introducing a compliant mock aorta into a mechanical flow loop analogous to the left side of the EVHP system to determine the impact on system performance, particularly on the energy requirements of the pump. This was done through analysis and comparison of pressure waveforms, tube distension response and peripheral flow fields obtained from the rigid tubing case and the compliant mock aorta case using water as a Newtonian fluid. The first four sections of this chapter outline the pressure, tube distension and peripheral velocity results obtained from this experimental study under one set of conditions, where P_{ch} = 103 mmHg and $\omega_{AI\ pump}$ = 1235 RPM. This includes an analysis of the relationship between these three parameters over one pump cycle. The next three sections explore the relationship between $\omega_{AI\ pump}$ and the pressure, tube distension and peripheral flow conditions, respectively, for the rigid and mock aorta case at both tested values of P_{ch}. The final section discusses the energy requirements of the pump under each of the tested experimental conditions and the relationship between distensibility and pump energy.

5.2 Pressure response

Pressure waveforms were obtained at the mock aorta inlet and imaging section outlet. The waveform at the mock aorta inlet represents the central aortic waveform of the system, and is therefore the waveform that was used to assess pressure response. Figure 5-1 compares the pressure waveforms obtained from the rigid and the P_{ch} = 103 mmHg mock aorta case with $\omega_{AI\ pump}$ = 1235 RPM over three normalized pump cycles. Data is presented as solid lines rather than discrete points due to the high sampling frequency at which the data was collected.

The waveform shape in Figure 5-1 is consistent across multiple cycles for both cases but the two waveforms have significantly different shapes and magnitudes. The mock aorta waveform is much smoother than the rigid waveform and resembles a Murgo's Type C waveform, as presented in Section 1.5.3, with cAI_x = -0.037. However, the reflected wave arrives during systole, indicating that there is likely some systolic pressure augmentation. The incident and reflected waves are well-defined and the dicrotic notch is visible at approximately t/τ = 0.4. The diastolic, systolic and mean arterial pressures of the mock aorta case waveform are 91.7, 169 and 126 mmHg, respectively. The rigid waveform has more peaks, indicating that there are multiple reflected waves involved in the system response in contrast to the sole visible reflected wave in the compliant case. The diastolic, systolic and mean arterial pressures of the rigid case are 68.1, 215 and 134 mmHg, respectively. The significantly higher systolic pressure suggests substantial augmentation of systolic pressure by the reflected waves during early systole. The large valley in the rigid pressure wave is most likely caused by forceful reflected waves impeding the VAD outlet valve's closure.

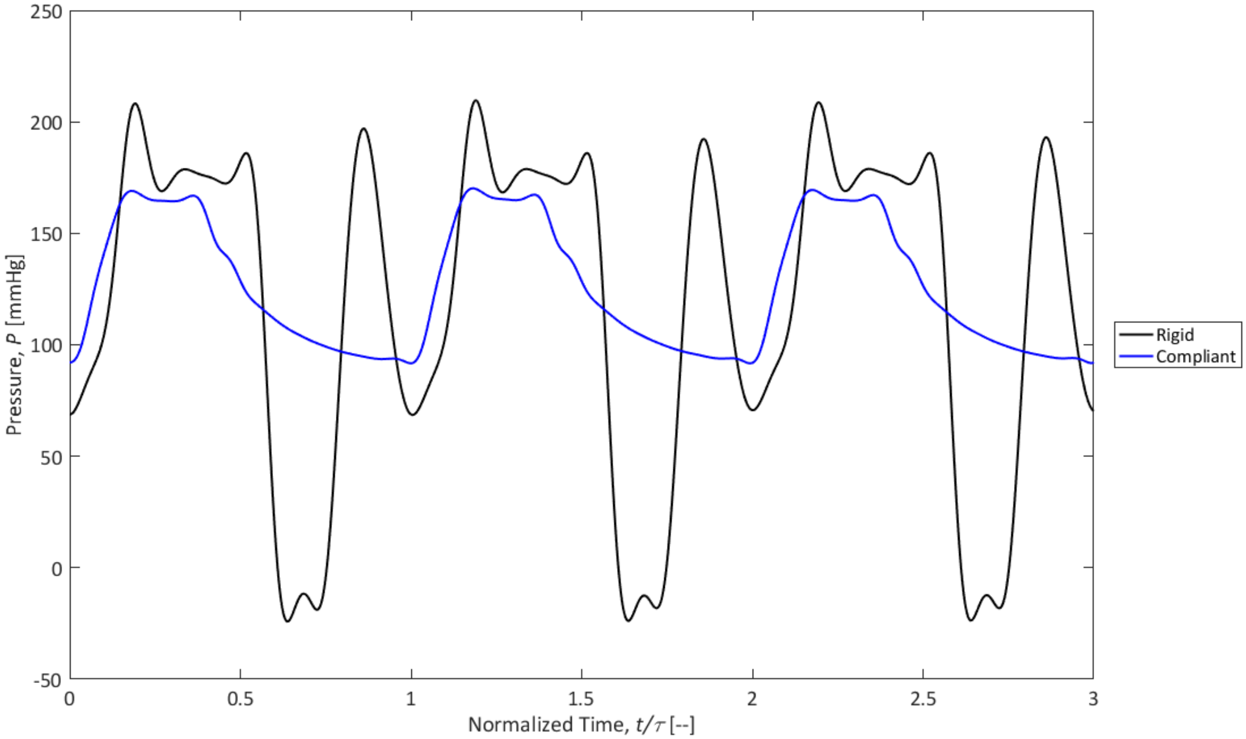

Figure 5-1: Plot of central aortic pressure waveforms for rigid ($\omega_{AL\ pump}$ = 1235 RPM) compliant mock aorta ($\omega_{AL\ pump}$ = 1235, P_{ch} = 103 mmHg) cases over three normalized pump cycles

In addition to there being differences between the rigid and compliant pressure values, the introduction of compliance into the system impacted the cycle time. The comparison between the pressure waveforms over one cycle shown in Figure 5-2 demonstrates this difference. The overall cycle time for the compliant case (0.89 s) is longer than for the rigid case (0.77 s), and therefore the pulse frequency is slower. Systolic duration for the compliant case is shorter (~0.38 secs) than for the rigid case (~0.48 secs) and diastole is longer. As discussed in Section 1.5, this combination of short systolic duration and long diastolic duration is positively associated cardiac performance. Conversely, the rigid waveform is shorter in duration and has a prolonged systolic ejection phase, which according to theory indicates higher cardiac workload and impaired cardiac function. These pressure waveform results indicate improved system performance at the same back pressure conditions for the compliant mock aorta case compared to the rigid case.

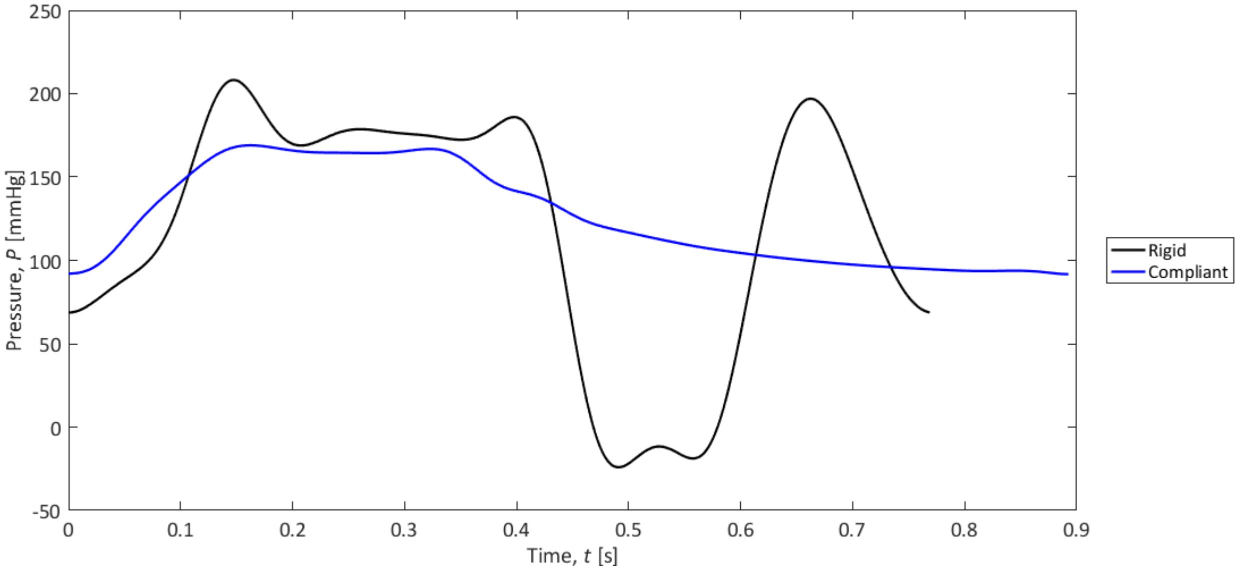

Figure 5-2: Plot of central aorta pressure waveforms of rigid ($\omega_{AL\ pump}$ = 1235 RPM) and compliant mock aorta ($\omega_{AL\ pump}$ = 1235 RPM, P_{ch} = 103 mmHg) cases over one cycle

5.3 Mock aorta compliant response with P_{ch} = 103 mmHg

The previous section presented results that indicate improved pressure response through the introduction of the mock aorta. This section discusses the compliant mock aorta's expansive response to the previously discussed pressure waveform. Figure 5-3 displays this distension response over three normalized pump cycles[23]. Two contributions to the tube expansion are shown in Figure 5-3: the tube distension resulting from $\overline{P}_a$ alone (dotted line), and from P_p (circles). The profile and magnitude of the response are consistent across multiple cycles. During diastole, the afterload pump distends the tube to 11.1% of its unloaded diameter. During systolic ejection, the tube expands quickly to approximately 28%, at which point the expansion rate decreases. The tube diameter continues to increase at the slower rate until it reaches its peak expansion of 38.7%. This change in slope of the expansion response is likely a result of the pressure waveform augmentation discussed in the previous section causing additional tube expansion in late systole. After reaching its peak, the tube begins to relax. Shortly after the beginning of relaxation there is a sharp momentary increase in tube diameter that signals the VAD outlet valve closure. After valve closure, the tube continues to relax to its end diastolic diameter.

---

[23] The code used to generate Figure 5-3 is provided in Appendix A-3.13

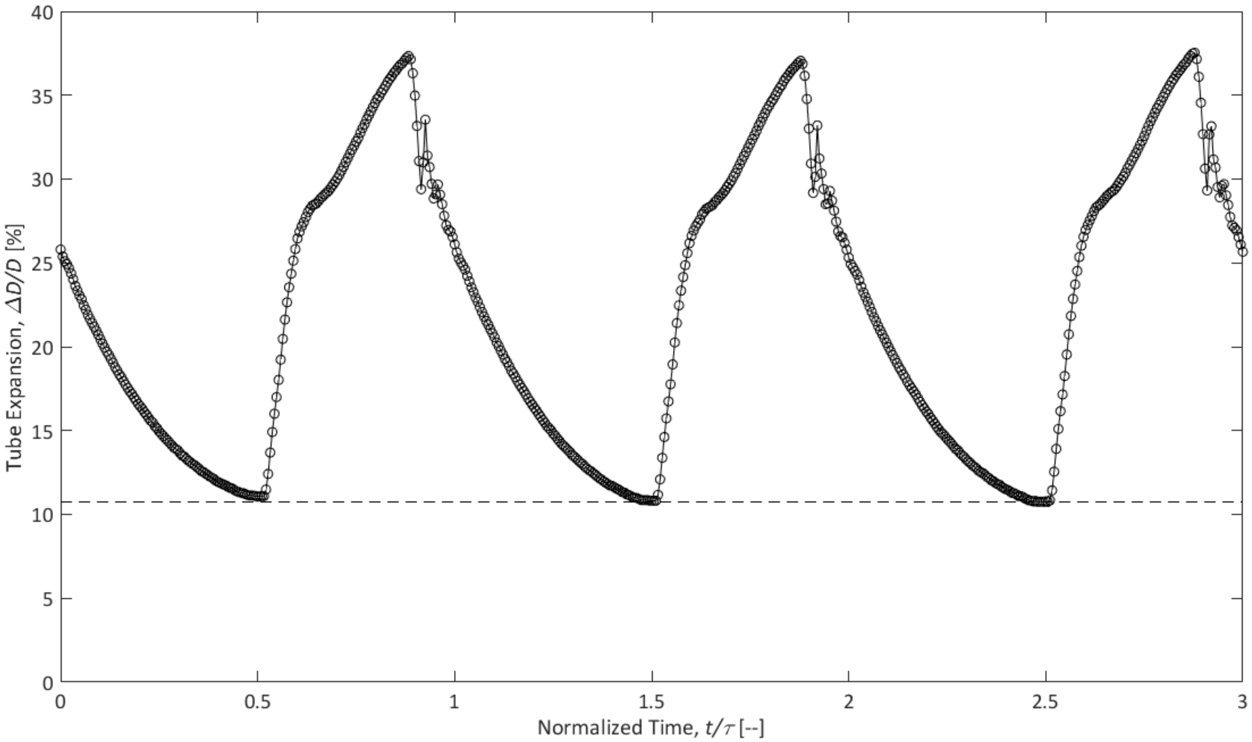

Figure 5-3: Plot of mock aorta pulse pressure (circles) and afterload (dotted line) tube distension over three normalized pump cycles

5.4 Peripheral flow response

The expansion-recoil response of the aorta *in vivo* significantly impacts the peripheral flow fields, as discussed in Section 1.5. This section compares the peripheral flow fields obtained from the compliant mock aorta to those obtained with a rigid test section. Figure 5-4 displays the peripheral centerline velocity fluctuations over one normalized pump cycle for the rigid and compliant cases[24]. Both response cycles are indexed to begin at the image corresponding to the first diastolic minimum after the Camera 2 trigger signal, as discussed in Section 3.5. There are significant differences between the two response shapes. First, the centerline velocity of the rigid case is less smooth than the compliant response, which is a byproduct of the multiple reflected waves passing through the system. The rigid case also reaches both a higher positive and negative peak velocity during the cycle and reaches its positive peak velocity later in the cycle than does the compliant case. The increased reverse flow in the rigid case indicates a high unsteady component in the pressure gradient driving the flow which is supported by the pressure waveform results discussed in Section 5.2. In the compliant case however, there is minimal reverse flow at the beginning of the cycle, indicating steadier peripheral flow.

---

[24] The code used to generate the centerline velocity results presented in Figure 5-4 is provided in Appendix A-3.16

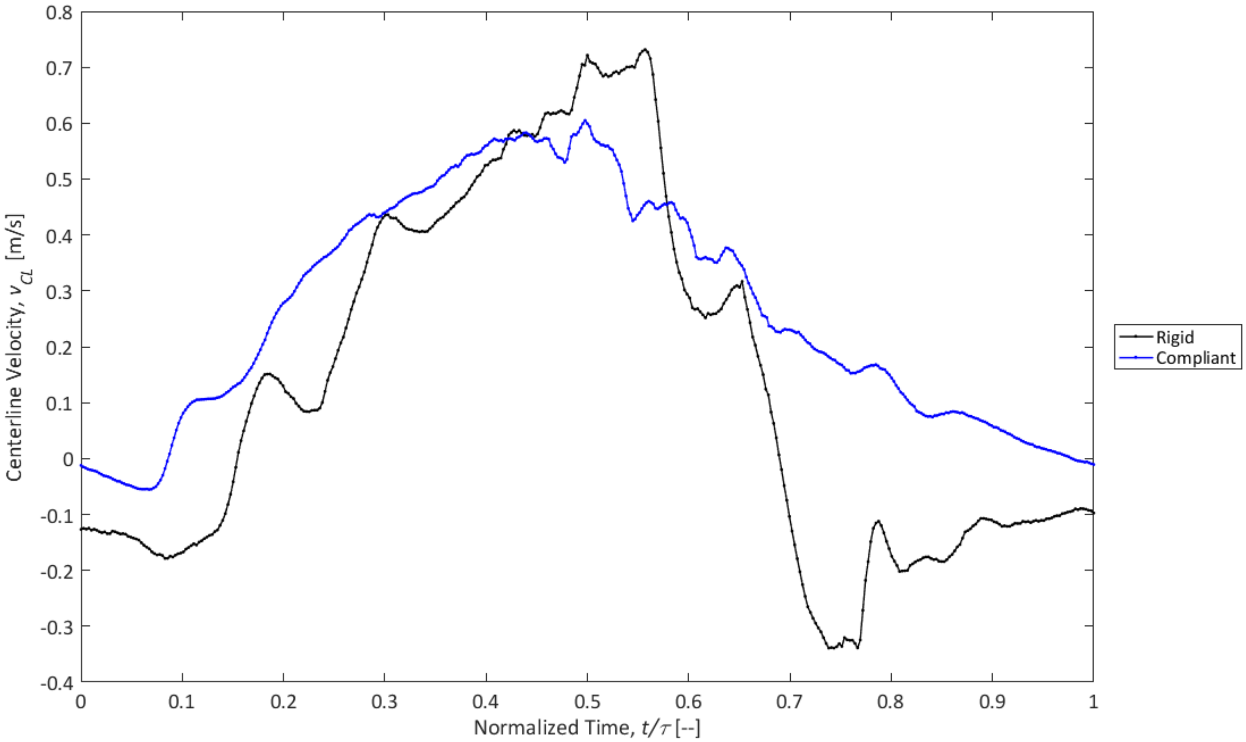

Figure 5-4: Plot of centerline velocities (v_{CL}) for rigid ($\omega_{AL\ pump}$ = 1235 RPM) and compliant mock aorta ($\omega_{AL\ pump}$ = 1235 RPM, P_{ch} = 103 mmHg) cases over one normalized pump cycle

5.5 Comparison of system performance parameters over one pump cycle

To understand the interaction between the three parameters discussed in previous sections, it is useful to view the parameters together over one pump cycle. Figure 5-5 depicts the relationship between the normalized pressure waveform and peripheral centerline velocity over one normalized pump cycle obtained from the rigid case[25,26,27]. The pressure waveform shows the occurrence of multiple reflected waves, the results of which are visible on the centerline velocity plot. The centerline velocity reaches its positive peak at the time of arrival of the third pressure peak, t/τ = ~0.55. It reaches its negative peak, that is nearly half the magnitude of the positive peak, at t/τ = ~0.75 and the velocity is negative for approximately half of the cycle time. The significant amount of reverse flow supports the observation that the peripheral flow in the rigid case is substantially impacted by the unsteady effects of the pressure pulse from the VAD.

---

[25] Normalized one cycle plots for other tested $\omega_{AL\ pump}$ values are provided in Appendix A-1.3

[26] The code used to generate one normalized cycle of the filtered pressure waveform in Figure 5-5 is provided in Appendix A-3.14

[27] The code used to plot Figure 5-5 is provided in Appendix A-3.17

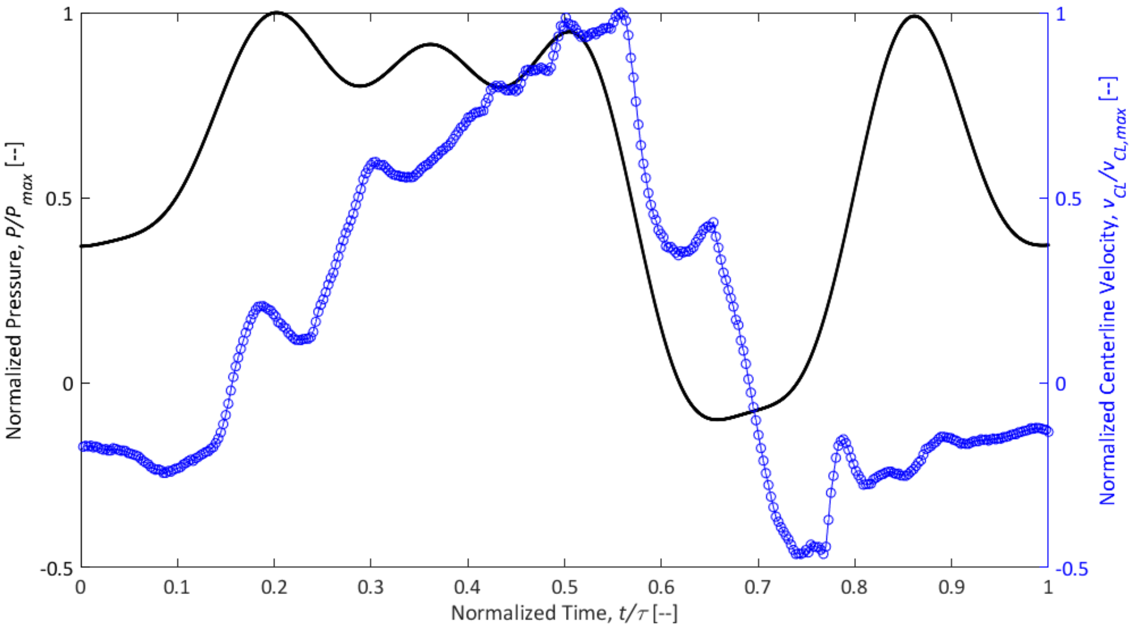

Figure 5-5: Normalized plot of central aortic pressure waveform (P/P_{max}) and peripheral centerline velocity ($v_{CL}/v_{CL,max}$) for the rigid case with $\omega_{AL\ pump}$ = 1235 RPM

Figure 5-6 depicts the relationship between normalized pressure waveform, normalized peripheral centerline velocity and tube distension for one normalized pump cycle obtained from the compliant mock aorta case[28,29,30]. The initial tube expansion occurs in phase with the systolic pressure pulse and then slows down, reaching its maximum around the moment of arrival of the reflected pressure wave, at t/τ = ~0.41. The pressure decrease coincides with a decrease in tube diameter, and the moment of valve closure is apparent on both waveforms, at t/τ = ~0.45. The peripheral centerline velocity response lags both the pressure and tube response, reaching its peak at t/τ = ~0.50. The centerline velocity is negative for approximately the first 10% of the cycle time, reaching a negative peak velocity that is 9% of the positive peak velocity at t/τ = 0.06. This minimal amount of reverse flow indicates that the full impact of the pressure pulse from the VAD is not being transmitted to the periphery. This is a substantial improvement over the significant amount of reverse flow in the rigid case operated at the same afterload pump speed.

---

[28] Normalized one cycle plots for other tested P_{ch} and $\omega_{AL\ pump}$ values are provided in Appendix A-1.4.

[29] The code used to generate one normalized cycle of the filtered pressure waveform in Figure 5-6 is provided in Appendix A-3.14

[30] The code used to plot Figure 5-6 is provided in Appendix A-3.18

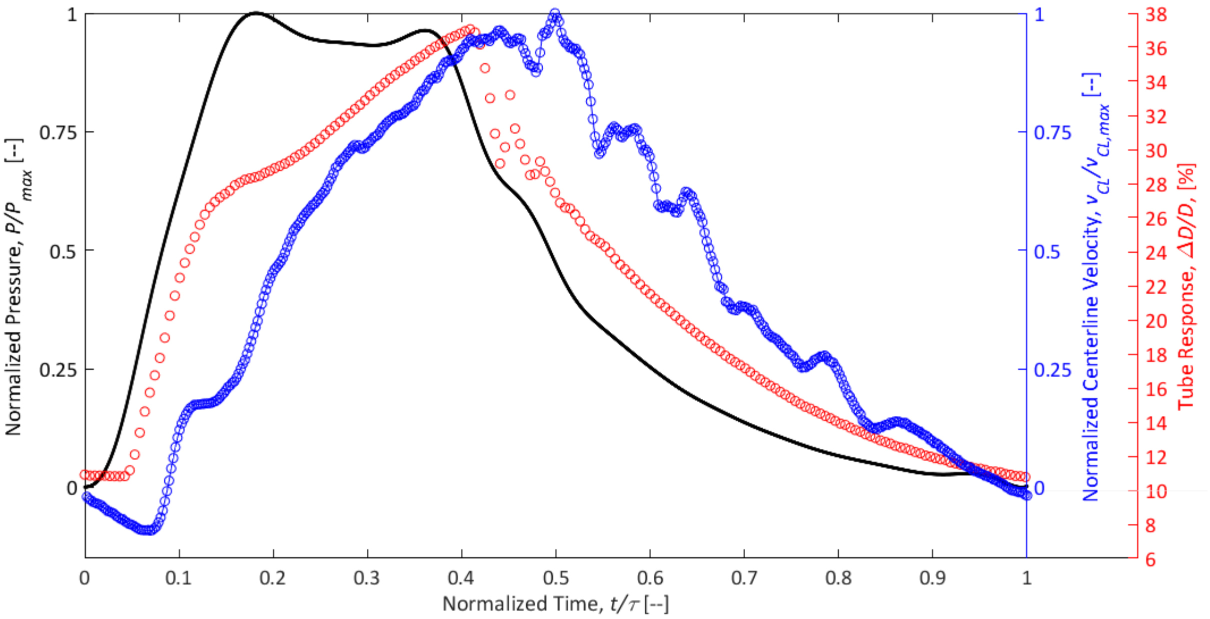

Figure 5-6: Plot of normalized central aortic pressure waveform (P/P_{max}), normalized peripheral centerline velocity ($v_{CL}/v_{CL,max}$) and tube distension ($\Delta D/D$) for mock aorta case with P_{ch} = 103 mmHg and $\omega_{AL\ pump}$ = 1235 RPM

5.6 Effect of experimental conditions on system performance

The previous sections of this chapter discussed the pressure, tube expansion and peripheral velocity results obtained at one set of experimental conditions. This section explores the impact of varying experimental conditions, $\omega_{AL\ pump}$ and P_{ch}, on system performance. First, the relationship between $\omega_{AL\ pump}$ and central aortic pressure values is discussed. Next, the changes in tube distension in response to varying $\omega_{AL\ pump}$ at the two tested values of P_{ch} are discussed. This is followed by a discussion of changes in peripheral centerline velocity that occur in response to changes in $\omega_{AL\ pump}$ and P_{ch}, in particular on the amount of reverse flow. Finally, these results are interpreted in terms of how the energy requirements on the VAD change based on the presence of rigid or compliant mock aorta conditions.

5.6.1 Effect of afterload conditions on VAD pulse frequency

The pulse rate of the VAD is dependent on the afterload conditions of the experiment, so as $\omega_{AL\ pump}$ changed, the pulse frequency changed. The range of experimental conditions and corresponding values of pulse frequency are summarized in Table 5-1[31]. Figure 5-7 depicts the resulting positive linear relationships between $\omega_{AL\ pump}$ and pulse frequency of the VAD, f, at each of the different mock aorta

---

[31] The code used to generate the values presented in Table 5-1 is provided in Appendix A-3.15

test section conditions investigated in this experiment. The figure illustrates that as $\bar{P}_a$ increases due to increased $\omega_{AL\ pump}$, the VAD pulse frequency increases linearly. The slope of this relationship is independent of the mock aorta conditions but the intercept, or the zero back pressure frequency of the VAD, varies based on the mock aorta conditions. This variation in pulse frequency based on afterload conditions mirrors *in vivo* cardiac response. *In vivo*, increased vascular resistance increases cardiac workload, inducing the heart to beat faster to sustain cardiac output.

Table 5-1: Summary of VAD pulse frequencies under the range of tested experimental conditions

Test Section Conditions	**Afterload pump speed, $\omega_{AL\ pump}$ [RPM]**	**Pulse Frequency, f [Hz]**
Rigid	980	1.20
	1065	1.23
	1235	1.30
	1450	1.40
	1540	1.42
Mock Aorta, P_{ch}=103 mmHg	980	1.07
	1065	1.09
	1235	1.12
	1450	1.17
Mock Aorta, P_{ch}=155 mmHg	980	1.12
	1065	1.12
	1235	1.17
	1450	1.21
	1540	1.23

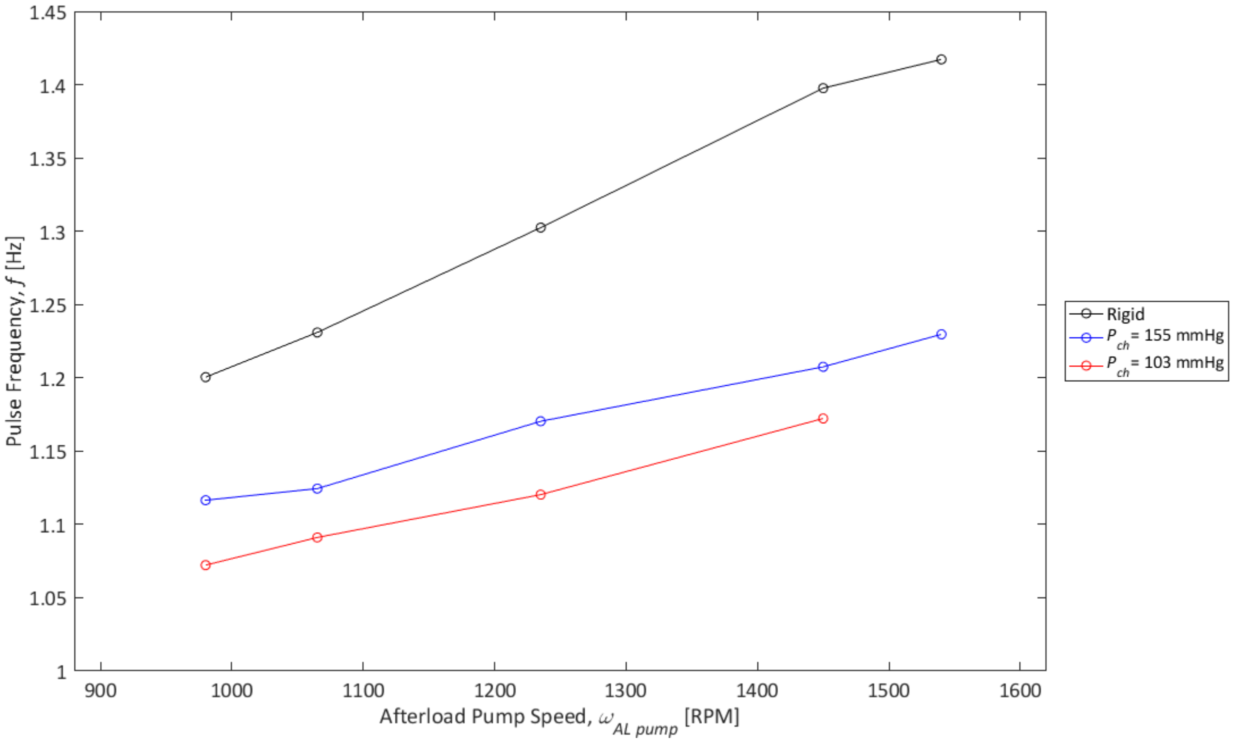

Figure 5-7: Plot comparing the effect of afterload pump speed ($\omega_{AL\ pump}$) on VAD pulse frequency (f) for three test section conditions: rigid (black), mock aorta with P_{ch} = 155 mmHg (blue) and mock aorta with P_{ch} = 103 mmHg (red)

5.6.2 Effect of afterload conditions on mock aorta inlet pressure response

Under the variable afterload conditions, the values of P_d, P_s and therefore P_p changed. The obtained pressure values at each of the tested experimental conditions are summarized in Table 5-2. Figure 5-8 depicts the changes in each of these three pressure values in response to changing $\omega_{AL\ pump}$ for the three test section conditions listed in Table 5-2[32]. For all cases, values of P_s remained relatively consistent across experimental conditions but P_d displayed a positive linear relationship with $\omega_{AL\ pump}$. Therefore, P_p decreased with increasing $\omega_{AL\ pump}$ for all test section conditions. The slope of the relationship for the rigid case is slightly steeper than those of the compliant cases, and all three cases have different intercepts. These results demonstrate that, for the same $\omega_{AL\ pump}$ setting, increased mock aortic compliance reduces VAD pulse pressure. As discussed in Section 1.5.2, low pulse pressure is a positive indicator of cardiac performance.

---

[32] The code used to generate the values presented in Table 5-2 is provided in Appendix A-3.15

Table 5-2: Summary of pressure values collected at each set of tested experimental conditions

Test Section Conditions	$\omega_{AL\ pump}$ [RPM]	Systolic Pressure, P_s [mmHg]	Diastolic Pressure, P_d [mmHg]	Pulse Pressure, P_p [mmHg]	Mean arterial pressure, $\overline{P_a}$ [mmHg]
Rigid	980	209.7	58.0	151.7	120.1
	1065	210.2	63.7	146.5	124.7
	1235	214.7	68.1	146.5	133.6
	1450	214.7	86.8	127.9	147.3
	1540	214.7	95.6	119.1	152.3
	1720	218.8	116.1	102.7	164.4
	2000	216.1	143.8	72.3	169.5
	2250	211.9	133.6	78.3	168.4
Mock Aorta, P_{ch}=103 mmHg	980	168.5	63.7	109.4	104.8
	1065	168.9	73.7	114.7	95.2
	1235	169.4	91.6	125.8	77.7
	1450	169.7	121.5	141.8	48.2
Mock Aorta, P_{ch}=155 mmHg	980	171.9	52.3	108.1	119.6
	1065	172.7	62.6	112.5	110.2
	1235	172.9	83.2	124.0	89.8
	1450	172.9	111.6	139.8	61.3
	1540	173.9	124.6	146.4	49.2

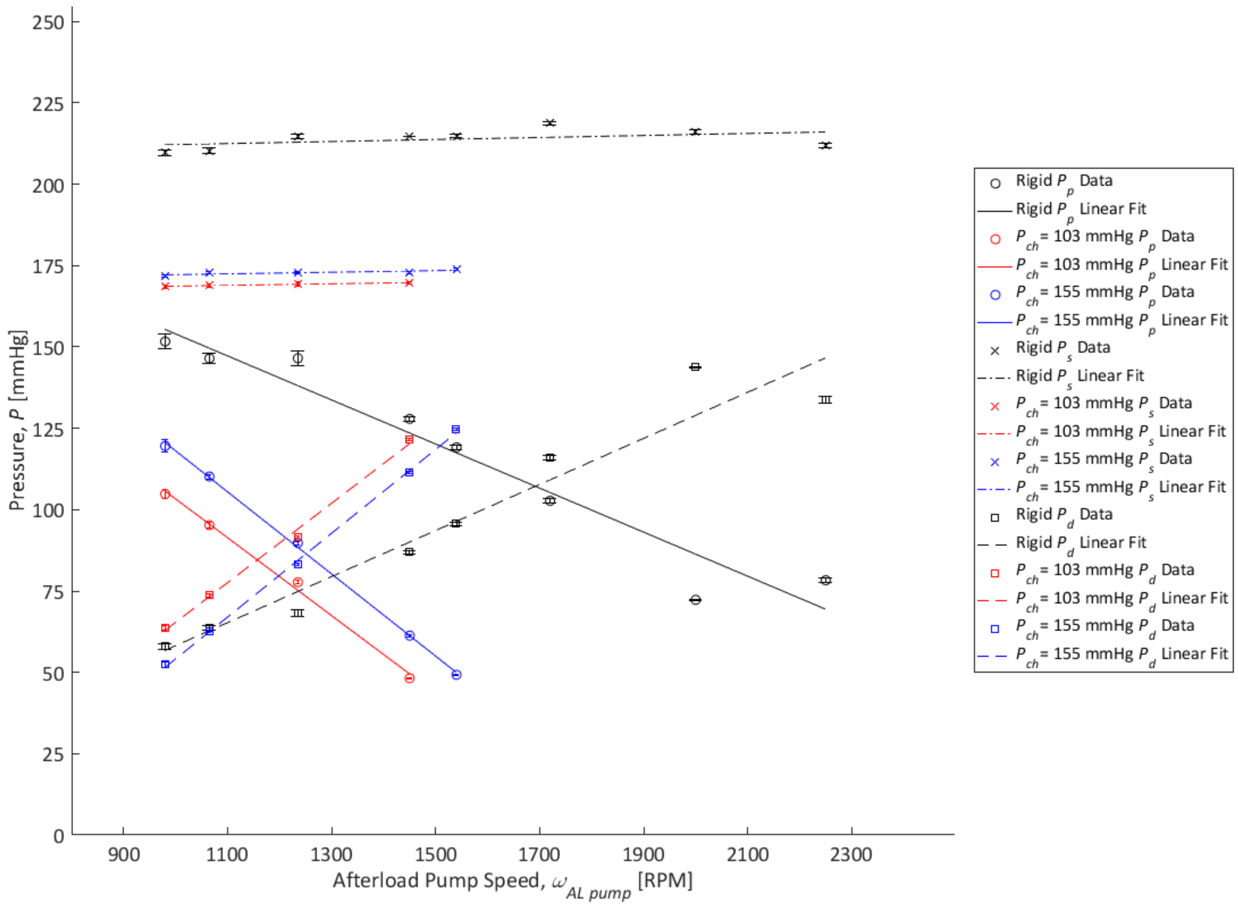

Figure 5-8: Plot comparing the effect of afterload pump speed ($\omega_{AL\ pump}$) on central aorta pressure measurements (P_d, P_s, P_p) for three test section conditions: rigid (black), mock aorta with P_{ch} = 155 mmHg (blue) and mock aorta with P_{ch} = 103 mmHg (red)

5.6.3 Tube response

In the compliant case, the mock aorta expands during systolic ejection. The values of distension, including the contribution of $\omega_{AL\ pump}$ and P_p to the total distension, are summarized in Table 5-3 for both tested chamber pressure settings. These results are displayed in Figure 5-9 which shows the relationship between $\omega_{AL\ pump}$ and tube distension response. The contributions of $\overline{P}_a$ and P_p to this distension, as well as the total distension are represented in the figure. As expected, the lower chamber pressure conditions yielded more distension due to reduced transmural pressure for all values of $\omega_{AL\ pump}$. The maximum distension of ~55% was achieved with the settings: $\omega_{AL\ pump}$ = 1450 RPM and P_{ch} = 103 mmHg. The afterload contribution to the overall tube response exhibits an exponential relationship with $\omega_{AL\ pump}$, which suggests that the tube might have non-linear properties. The pulse pressure contribution to the response exhibits a negative linear relationship with $\omega_{AL\ pump}$, likely due to the trend of reduced pulse pressure at higher $\omega_{AL\ pump}$ values that was presented in the previous section. The total distension response appears to be exponential in nature. At the highest $\omega_{AL\ pump}$ value, the afterload contribution exceeds the pulse pressure contribution to the response. This suggests that the active afterload pump filling of the mock aorta during diastole plays an important role in the reduction of pulse pressure associated with increased compliance in the mock aorta test section.

Table 5-3: Summarize of mock aorta tube distension results for both tested chamber pressure settings

		Distension, $\Delta D/D$ [%]		
Mock Aorta Chamber Pressure, P_{ch} [mmHg]	**$\omega_{AL\ pump}$ [RPM]**	**$\omega_{AL\ pump}$ Contribution**	**P_p Contribution**	**Total**
103	980	3.93	31.43	35.36
	1065	5.83	30.71	36.55
	1235	11.07	27.62	38.69
	1450	30.12	25.95	56.07
155	980	1.19	28.93	30.12
	1065	2.50	27.86	30.36
	1235	5.60	25.48	31.07

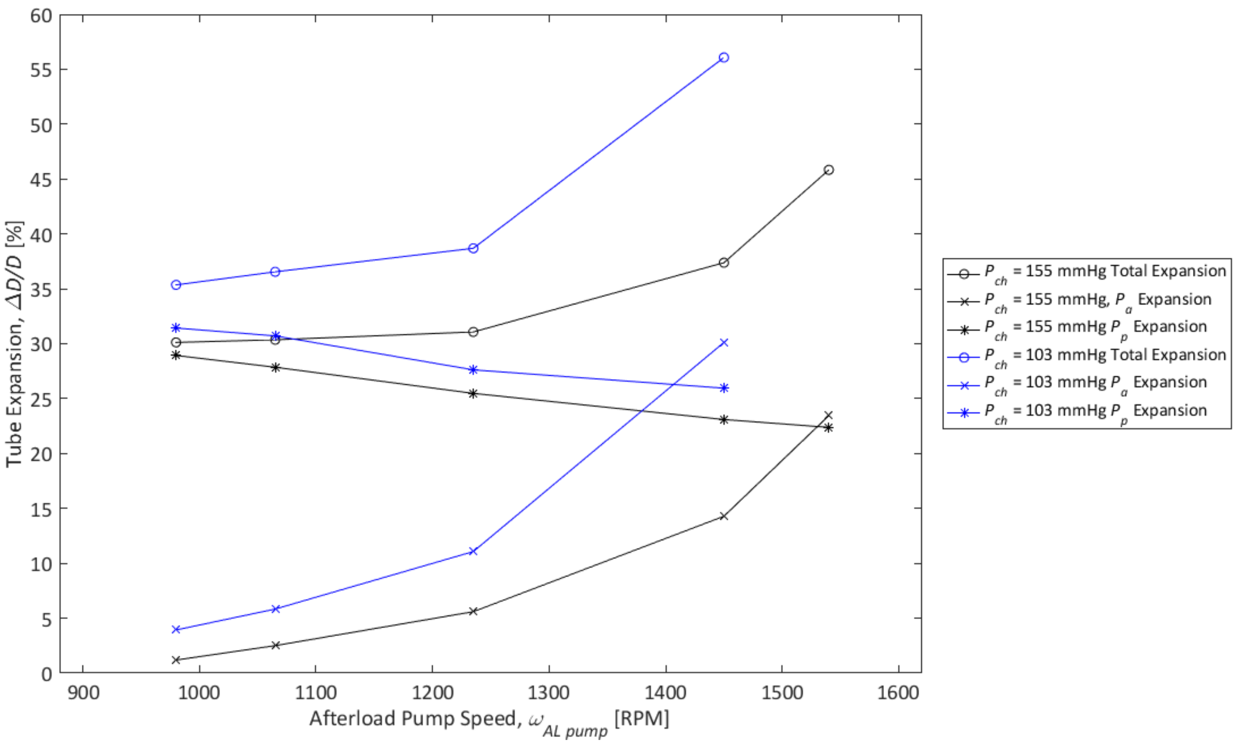

Figure 5-9: Plot comparing the effect of afterload pump speed ($\omega_{AL\ pump}$) on mock aorta distension ($\Delta D/D$) for two pressure chamber conditions: P_{ch} = 155 mmHg (black) and P_{ch} = 103 mmHg (blue)

5.6.4 Peripheral flow

The previous sections have addressed the impact of afterload pump speed on the pressure conditions of the system and the compliance of the mock aorta. This section addresses the impact of $\omega_{AL\ pump}$ on peripheral flow conditions and compares these relationships in the rigid and compliant cases. Figure 5-10 depicts the changes in maximum positive peak centerline velocity (circles) and negative peak centerline velocity (squares) that occur as a result in increasing $\omega_{AL\ pump}$ for the rigid case. On the secondary axis is the ratio between peak reverse flow during the cycle to peak positive flow ($v_{pk,(-)}/v_{pk,(+)}$). This is an indicator of how significantly the unsteady effects of the pressure pulse are transmitted to the periphery. The positive peak centerline velocity is shown to decrease with increasing $\omega_{AL\ pump}$, while the negative peak centerline velocity remains fairly constant. As a result, the peak flow ratio increases with increasing $\omega_{AL\ pump}$. Therefore, for the rigid case, increasing the afterload pump speed increases the strength of reverse flow in the system, as expected.

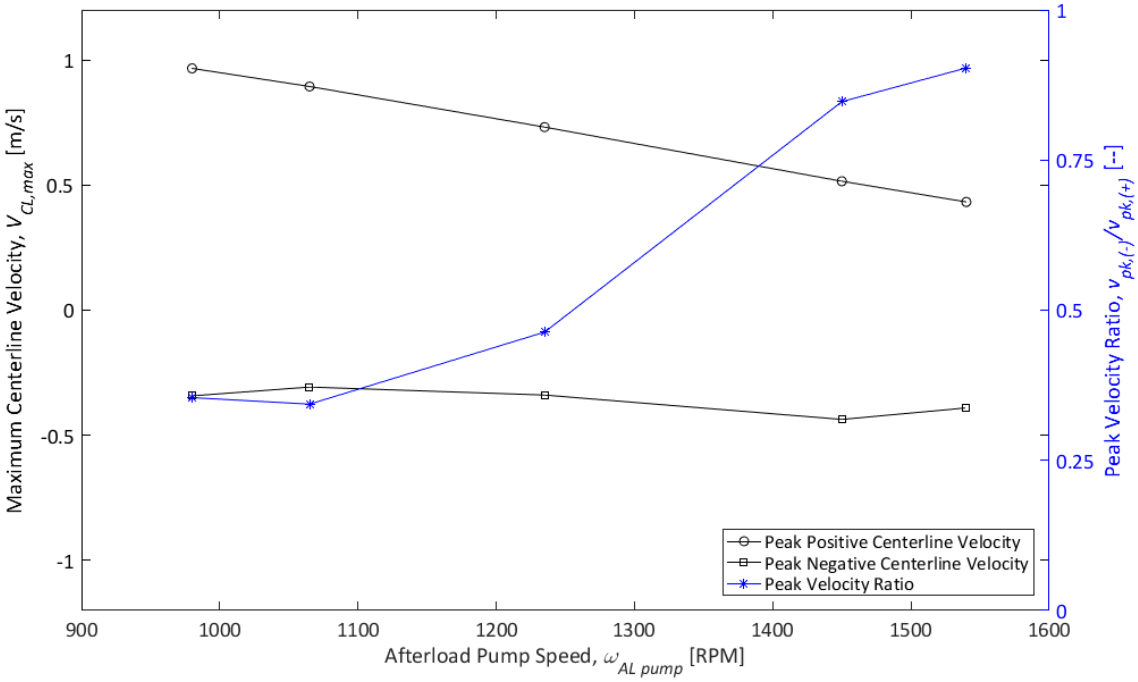

Figure 5-10: Plot representing the impact of $\omega_{AL\ pump}$ on maximum positive peripheral centerline velocity (black circles), maximum negative centerline velocity (black squares) and peak velocity ratio ($v_{pk,(-)}/v_{pk,(+)}$) (blue asterisk) for rigid case with $\omega_{AL\ pump}$ = 1235 RPM

Results discussed in previous sections indicate that the compliant mock aorta case demonstrates less reverse flow than does the rigid case. Therefore, for the compliant case, instead of expressing the positive and negative peak flow velocities as functions of $\omega_{AL\ pump}$, a comparison between distensibility, as defined by equation (2-1), and the positive and negative peak velocities is warranted. Figure 5-11 and Figure 5-12 plots mock aorta distensibility versus peak positive (circles) and negative (squares) centerline velocities for the cases where P_{ch} = 103 and 155 mmHg, respectively. As well, the peak velocity ratio defined in the previous section is plotted on the secondary y-axis. Both plots depict similar trends; as distensibility of the mock aorta increases, the magnitudes of the positive and negative peak peripheral velocities decrease. As a result, the peak velocity ratios decrease. This is an indication that the introduction of compliance into the system has a steadying effect on peripheral flow, as Windkessel theory suggests.

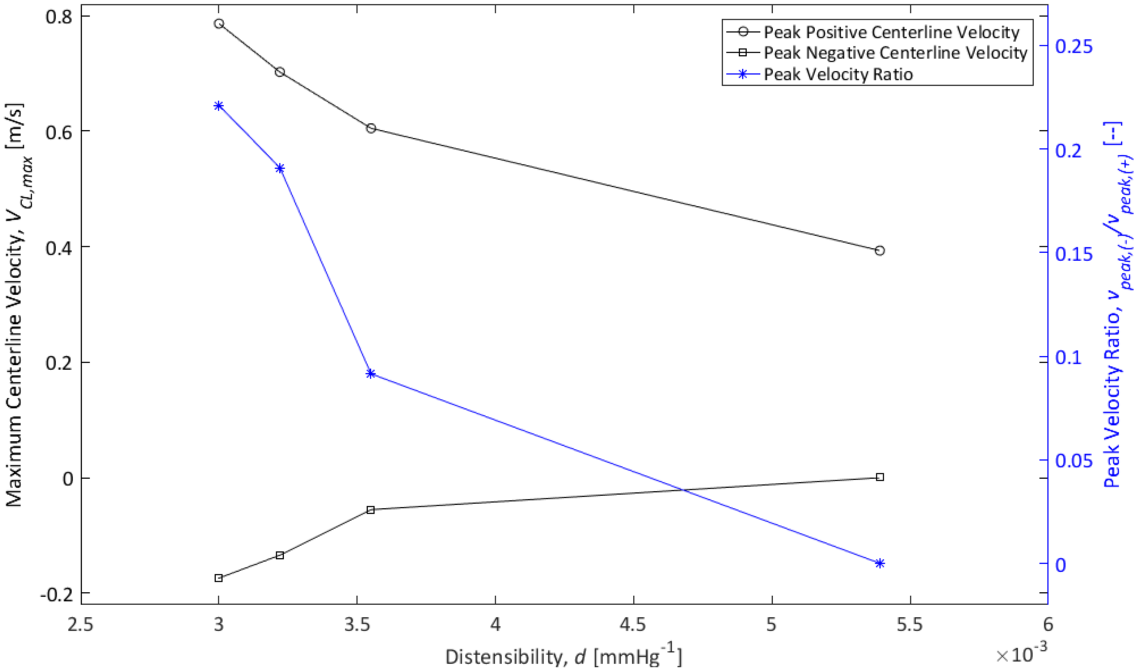

Figure 5-11: Plot representing the impact of mock aorta distensibility (*d*) on maximum positive peripheral centerline velocity (black circles), maximum negative centerline velocity (black squares) and peak velocity ratio ($v_{pk,(-)}/v_{pk,(+)}$) (blue asterisk) for the case where P_{ch} = 103 mmHg

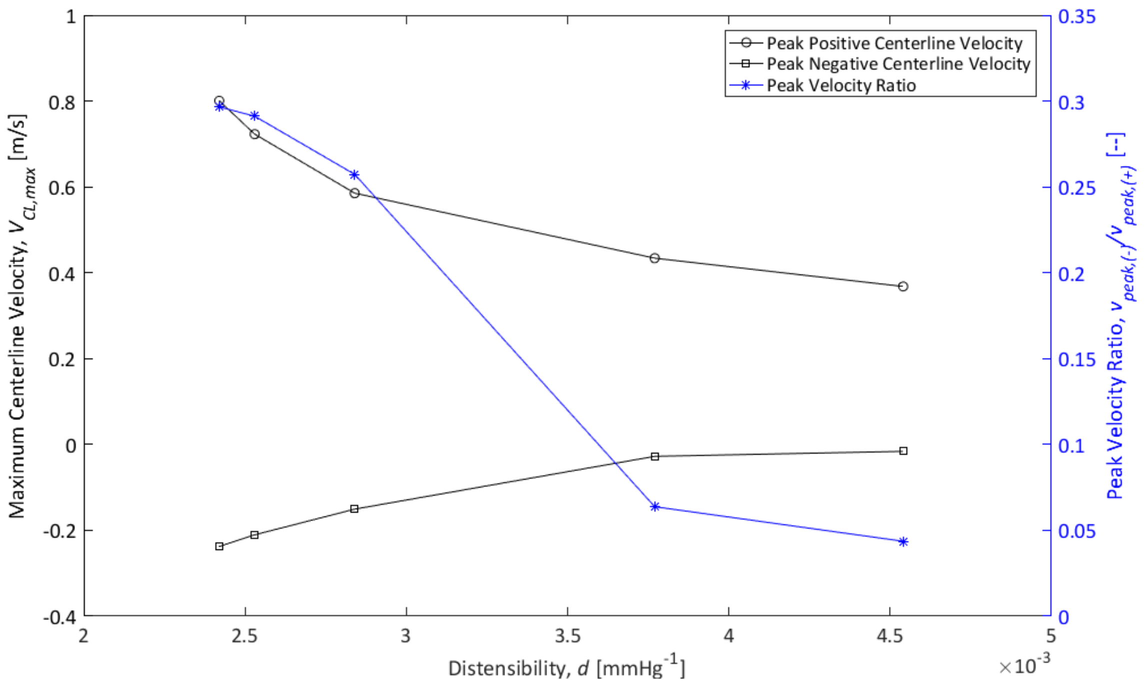

Figure 5-12: Plot representing the impact of mock aorta distensibility (*d*) on maximum positive peripheral centerline velocity (black circles), maximum negative centerline velocity (black squares) and peak velocity ratio ($v_{pk,(-)}/v_{pk,(+)}$) (blue asterisk) for the case where P_{ch} = 155 mmHg

5.6.5 Impact of compliance on pump energy

In order to understand how the parameters studied in this investigation impact pump performance, a form of the unsteady Bernoulli equation expressed in terms of energy was used to related the work done by the pump during systole to the energy in the blood in the region of velocity data collection during the systolic ejection period. Similar to the method used for performing energy analysis in the peristaltic pump experiment, the energy output of the VAD was determined using the total energy in region 2, the region of velocity data collection, in the system integrated over systolic ejection time[33]:

$$E_{VAD} = \underbrace{\frac{1}{\rho}\int_0^{t_s} \dot{m}_2(t)\,p_2(t)dt}_{\text{Pressure}} + \underbrace{\frac{1}{2}\int_0^{t_s} \dot{m}_2(t)\,[\bar{v}_2(t)]^2 dt}_{\text{Kinetic}} + \underbrace{gz_2\int_0^{t_s} \dot{m}_2(t)\,dt}_{\text{Static}} + \underbrace{L_{eff}\int_0^{t_s} \dot{m}_2(t)\left(\frac{dv}{dt}\right)_2 dt}_{\text{Local Acceleration}} \qquad (5\text{-}1)$$

where E_{VAD} is the energy imparted by the pump to the fluid per systolic ejection [J/ejection], $\dot{m}_2(t)$ is the mass flow rate through region 2 [kg/s], calculated by integrating the mean velocity profile of each Camera 2 image to get volume flow rate and then multiplying by density to get mass flow rate, according to: $\dot{m}_2(t)=\rho\left[\iint_0^D v(r)rdrd\theta\right]=\rho\left[\pi r\int_0^D v(r)dr\right]$, $p_2(t)$ is the pressure waveform obtained in

---

[33] The code used to perform the VAD energy calculations is provided in Appendix A-3.19

region 2 [Pa], $\bar{v}_2(t)$ is the average velocity in region 2 [m/s]. z_2 is the elevation of point 2 above the VAD outlet valve [m], L_{eff} is the height of the column of fluid being accelerated, which in this case is the height difference between the VAD outlet valve and point 2, and t_s is the systolic ejection time [s].

Table 5-4 presents a detailed breakdown of the experimental conditions and resulting distensibility values, cycle times, systolic ejection times and per-minute pump energies. For a given $\omega_{AL\ pump}$, the shortest cycle times and therefore the highest pulse frequencies occur in the rigid case, suggesting that the pump is working harder in the rigid cases than in the compliant cases. This implication of increased pump workload is supported by the result that the rigid cases also corresponds to the highest VAD energy requirements.

Table 5-4: Summary of VAD experiment per-ejection energy results

$\omega_{AL\ pump}$ [RPM]	Chamber pressure, P_{ch} [mmHg]	Distensibility, d [mmHg^{-1} x 10^{-3}]	Cycle Time, t_c [s]	Systolic Ejection Time, t_s [s]	Energy per ejection [J/ejection]
980	Rigid	0	0.84	0.51	1.81
	155	2.42	0.90	0.59	1.33
	103	3.00	0.93	0.56	1.35
1065	Rigid	0	0.82	0.51	1.72
	155	2.53	0.88	0.56	1.22
	103	3.23	0.92	0.51	1.29
1235	Rigid	0	0.78	0.49	1.44
	155	2.84	0.85	0.49	1.09
	103	3.55	0.89	0.40	1.22
1450	Rigid	0	0.72	0.46	1.01
	155	3.77	0.83	0.40	0.88
	103	5.39	0.85	0.40	0.98
1540	Rigid	0	0.70	0.47	0.82
	155	4.54	0.81	0.40	0.79

Figure 5-13 summarizes the impact of mock aorta distensibility on the energy output by the pump per minute for each of the tested $\omega_{AL\ pump}$ settings[34]. The energy values are presented per minute rather than per ejection because, as discussed in Section 5.6, both systolic ejection time and total cycle time

---

[34] The code used to generate Figure 5-13 is provided in Appendix A-3.20

vary based on $\omega_{AL\ pump}$ and P_{ch}. Therefore, looking at the per ejection energy alone provides only a partial picture of how the pump energy varies based on experimental conditions. In Figure 5-13, each $\omega_{AL\ pump}$ setting displays the same trend. The rigid case (d=0) places the highest energy demands on the pump then there is a substantial decrease in energy with the introduction of compliance. At a certain point after that initial decline in energy, all $\omega_{AL\ pump}$ cases demonstrate a small increase with the next increase in distensibility. This is most likely the point at which the flow supplied by the pump 2 ceases to be sufficient to fill the mock aorta, so the VAD requires more energy output to fill that extra volume. This idea is supported by the energy analysis results presented in Section 4.7.4 which showed a trend towards increasing pump energy with increasing tubing compliance in the absence of an active back pressure supply. In addition, the inflection point where energy begins to rise shifts left with decreasing $\omega_{AL\ pump}$ setting, indicating that with less afterload supply, more energy is required by the pump at lower distensibility values.

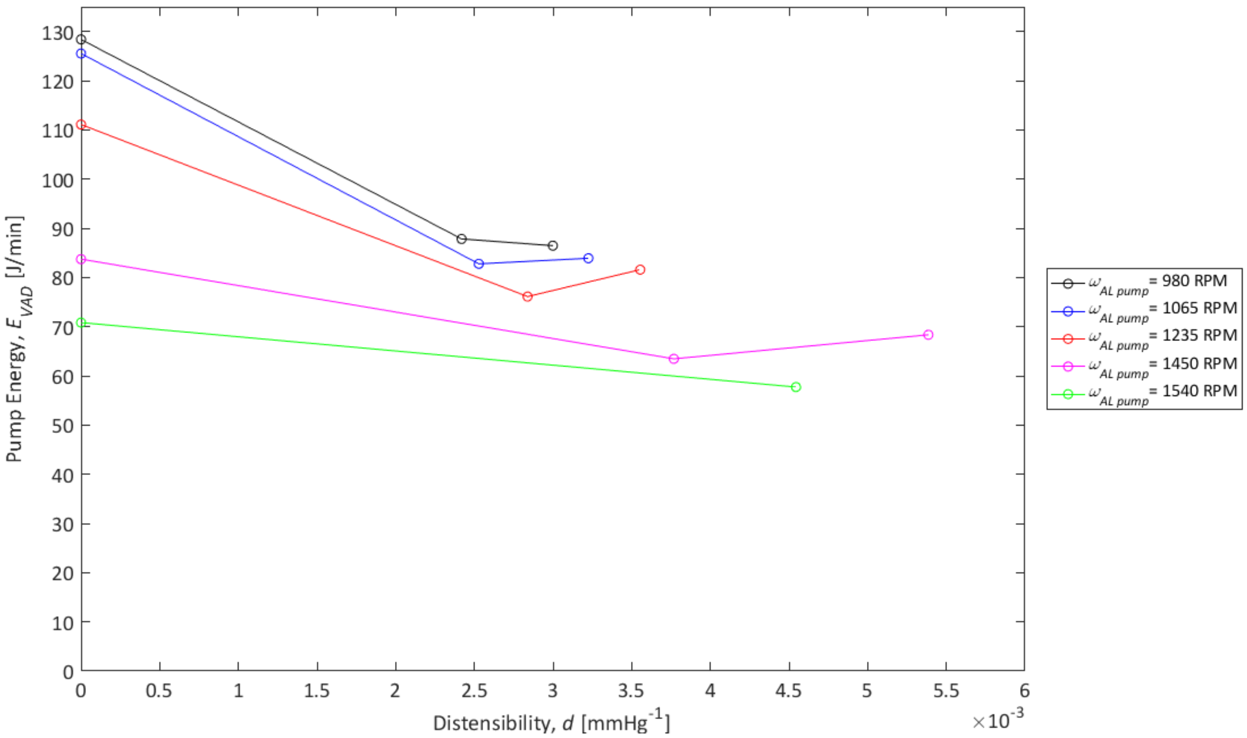

Figure 5-13: Plot representing the impact of mock aorta distensibility (d) on the energy expenditure of the VAD per minute (E_{VAD}) for each tested setting of $\omega_{AL\ pump}$

5.7 Conclusion

This chapter presented the results obtained using a rigid and compliant mock aorta in the VAD experimental setup. The impact of compliance was studied for one set of experimental conditions based on the pressure waveforms at the inlet of the mock aorta, the tube distension response and the peripheral flow response. After establishing the results from one case, a discussion of the effect of experimental conditions of the system responses under investigation was included. This culminated in an analysis of the pump energy requirements for the range of tested experimental conditions.

Overall, the compliant mock aorta conditions promoted better system performance. The pressure waveforms obtained with the rigid case showed the presence of multiple reflected waves that augmented the systolic pressures. The compliant case for the same experimental conditions more closely resembled typical *in vivo* central aortic waveforms with one incident and reflected wave, with significantly less systolic pressure augmentation that the rigid case. The tube response results indicated that the afterload pump plays a key role in distending the mock aorta, which works to alleviate the pulse pressure required from the VAD. The compliant mock aorta was also shown to have a positive impact on peripheral flow; peak velocity ratios were reduced with increasing mock aorta distensibility, which indicates the compliant response of the aorta dampened some of the unsteady effects, preventing them from being transmitted to the periphery. Finally, the expression of system performance in terms of energy requirements of the VAD allowed the evaluation of system performance in terms of all measured parameters expressed as one inclusive value. Consistent with theoretical expectations, the energy requirements of the VAD were significantly higher in the rigid cases compared to the compliant cases.

Chapter 6. Conclusions and Future Work

6.1 Conclusions

The aim of this work was to compare the behavior of an EVHP test system under the current conditions of rigid tubing in place of the *in vivo* aorta to more physiologically realistic conditions that include a compliant mock aorta. This was done in the interest of understanding the fluid mechanics of the EVHP system and using that knowledge to optimize system performance. Due to the complex nature of cardiovascular flow, two variations of the experimental setup were required; one was performed to establish a fundamental case, and the other was performed to test a physiological case that closely mimicked the left side of the EVHP system.

The first experimental setup utilized a peristaltic pump to establish the fundamental case. This set of experiments compared the pressure and downstream velocity responses resulting from rigid and compliant mock aorta sections, using both a Newtonian and non-Newtonian fluid. Tube response in the compliant case was monitored to compare the magnitude of the response under the various experimental conditions. Results from this experiment indicate that there are notable differences between the responses of the rigid and compliant tubing for both Newtonian and non-Newtonian fluids, but that compliance more significantly alters system performance in the Newtonian case. This is supported by the pump energy findings, which indicate that for both fluids, a higher pump energy is required in the compliant case, but these discrepancies in energy demands are higher in the Newtonian case. These findings are opposite to those that are expected in a physiological system, discussed in Section 1.5, most likely due to the low pressure pulses delivered by the peristaltic pump and the absence of significant back pressure in the system. In this experiment, because there is no significant source of back pressure, the work required to expand the compliant tube must be done by the pump. This results in higher pump energy requirements under more compliant conditions. This is not the case for a physiological flow with high pulse pressures and back pressures.

The second experiment utilized a VAD to simulate a physiological flow. This experiment compared the central aortic pressure waveforms and peripheral flows for range of $\omega_{AL\ pump}$ settings and, for the compliant mock aorta case, two P_{ch} settings. Tube response monitoring was performed to quantify the magnitude of compliant response in each case and visualize the transmission of the pressure pulse through the system. Results from this experiment support theoretical explanations of aortic function *in vivo*. In all cases, the introduction of compliance smoothed out the central aortic pressure waveforms as well as the peripheral flow. The peripheral velocities demonstrated a lower peak velocity ratio than the rigid cases, supporting the conclusion that the compliant mock aorta serves to dampen the pressure pulse transmission through the system and create quasi-steady flow in the periphery. Clinically, aortic compliance is associated with reduced cardiac workload, so this investigation used the total energy in the peripheral fluid to calculate the energy imparted by the pump for each experimental condition. It was found that the introduction of compliant response into the system improved all evaluated system performance parameters. The compliant mock aorta case demonstrated healthier pressure waveform profiles and less downstream reverse flow than the rigid cases. Most importantly, there was a significant decrease in energy output by the pump for each $\omega_{AL\ pump}$ setting when the compliant mock aorta was used. This result supports the clinical expectations discussed in Section 1.5 and suggests that the introduction of aortic response into the EVHP system is likely to have a positive impact on cardiac performance.

Findings from this study provide important experimental verification of Windkessel theory and provide a basis for future improvements to the EVHP system design. The results suggest that introducing a compliant mock aorta into the EVHP system could yield significant improvements in cardiac performance and therefore shelf life of the organs.

6.2 Future Work

Recommendations for further research in this area include:

- Develop a pulsatile flowmeter to enable flow measurements at pump inlet to facilitate system modeling
- Perform shadowgraph PIV on the actual EVHP system
- Test other mock aorta samples with different geometries and/or real aortic tissue
- Apply 3D flow visualization techniques to the peripheral flow fields, such as stereo-PIV or tomographic PIV to get 3D resolved velocity fields to study wall shear stress
- Test the VAD experiment with a non-Newtonian blood analog fluid
- Substitute Bjork-Shirley valves for porcine valves in VAD

References

[1] C. W. White, E. Ambrose, A. Müller, Y. Li, H. Le, B. Hiebert, R. Arora, T. W. Lee, I. Dixon, G. Tian, J. Nagendran, L. Hryshko, and D. Freed, "Assessment of donor heart viability during ex vivo heart perfusion," *Can. J. Physiol. Pharmacol.*, vol. 901, no. May, pp. 893–901, 2015.

[2] S. L. Longnus, V. Mathys, M. Dornbierer, F. Dick, T. P. Carrel, and H. T. Tevaearai, "Heart transplantation with donation after circulatory determination of death," *Nat Rev Cardiol*, vol. 11, no. 6, pp. 354–363, Jun. 2014.

[3] S. J. Messer, R. G. Axell, S. Colah, P. A. White, M. Ryan, A. A. Page, B. Parizkova, K. Valchanov, W. White, D. H. Freed, E. Ashley, M. Goddard, J. Parameshwar, C. J. Watson, T. Krieg, A. Ali, S. Tsui, S. R. Large, M. Ryan, A. A. Page, B. Parizkova, K. Valchanov, C. W. White, D. H. Freed, E. Ashley, J. Dunning, J. Parameshwar, C. J. Watson, T. Krieg, and A. Ali, "Functional Assessment and Transplantation of the Donor Heart Following Circulatory Death," *J. Hear. Lung Transplant.*, 2016.

[4] S. M. Minasian, M. M. Galagudza, Y. V. Dmitriev, A. A. Karpov, and T. D. Vlasov, "Preservation of the donor heart: from basic science to clinical studies," *Interact. Cardiovasc. Thorac. Surg.*, vol. 20, no. 4, pp. 510–519, 2015.

[5] D. W. McKeown, R. S. Bonser, and J. A. Kellum, "Management of the heartbeating brain-dead organ donor," *Br. J. Anaesth.*, vol. 108, no. SUPPL. 1, pp. 96–107, 2012.

[6] K. Hornby, H. Ross, S. Keshavjee, V. Rao, and S. D. Shemie, "Non-utilization of hearts and lungs after consent for donation: a Canadian multicentre study.," *Can. J. Anaesth.*, vol. 53, no. 8, pp. 831–7, 2006.

[7] J. E. Tuttle-Newhall, B. Munksgaard, R. S. Sung, J. Galloway, T. Mone, R. Laeng, C. E. Freise, P. S. Rao, and R. S. Sung, "Organ Donation and Utilization in the United States," *Am. J. Transplant.*, vol. 8, no. 2, pp. 922–934, 2008.

[8] J. F. McAnulty, "Hypothermic organ preservation by static storage methods: Current status and a view to the future," *Cryobiology*, vol. 60, no. 3 SUPPL., pp. S13–S19, 2010.

[9] M. J. Taylor, "Benefits of hypothermia in organ preservation," 2014.

[10] A. R. Manara, P. G. Murphy, and G. Ocallaghan, "Donation after circulatory death," *Br. J.*

Anaesth., vol. 108, no. SUPPL. 1, pp. 108–121, 2012.

[11] UC Davis Transplant Center, “Donation After Cardiac Death (DCD).” Sacramento, 2016.

[12] C. W. White, A. Ali, D. Hasanally, B. Xiang, Y. Li, P. Mundt, M. Lytwyn, S. Colah, J. Klein, A. Ravandi, R. C. Arora, T. W. Lee, L. Hryshko, S. Large, G. Tian, and D. H. Freed, “A cardioprotective preservation strategy employing ex vivo heart perfusion facilitates successful transplant of donor hearts after cardiocirculatory death.,” *J. Heart Lung Transplant.*, vol. 32, no. 7, pp. 734–43, 2013.

[13] C. W. White, D. Hasanally, P. Mundt, Y. Li, B. Xiang, J. Klein, A. Müller, E. Ambrose, A. Ravandi, R. C. Arora, T. W. Lee, L. V Hryshko, S. Large, G. Tian, and D. H. Freed, “A whole blood-based perfusate provides superior preservation of myocardial function during ex vivo heart perfusion.,” *J. Heart Lung Transplant.*, vol. 34, no. 1, pp. 113–21, 2015.

[14] Angelosscienceportfolio.wordpress.com, “Circulatory System.,” 2015. [Online]. Available: https://angelosscienceportfolio.wordpress.com/2013/04/30/circulatory-system/.

[15] G. G. Belz, “Elastic properties and Windkessel function of the human aorta.,” *Cardiovasc. Drugs Ther.*, vol. 9, no. November 1993, pp. 73–83, 1995.

[16] R. M. Berne, B. M. Koeppen, and B. A. Stanton, *Berne & Levy Physiology*. Philadelphia: Mosby/Elsevier, 2003.

[17] C.-H. Chen, E. Nevo, B. Fetics, P. H. Pak, F. C. P. Yin, W. L. Maughan, and D. A. Kass, “Estimation of Central Aortic Pressure Waveform by Mathematical Transformation of Radial Tonometry Pressure,” *Circulation*, vol. 95, no. 7, p. 1827 LP-1836, Apr. 1997.

[18] S. Emrani, T. S. Saponas, D. Morris, and H. Krim, “A Novel Framework for Pulse Pressure Wave Analysis Using Persistent Homology,” *IEEE Signal Process. Lett.*, vol. 22, no. 11, pp. 1879–1883, 2015.

[19] S. A. Esper, M. R. Pinsky, and C. Care, “Best Practice & Research Clinical Anaesthesiology Arterial waveform analysis,” vol. 28, pp. 363–380, 2014.

[20] S. Ansari, “Newtonian and Non-Newtonian Flows through Mini-channels and Micro-scale Orifices for SAGD Applications.” 2016.

[21] L. E. Bergman, K. J. DeWitt, R. C. Fernandez, and M. R. Botwin, “Effect of non-Newtonian behavior

on volumetric flow rate for pulsatile flow of blood in a rigid tube," *J. Biomech.*, vol. 4, no. 3, pp. 229–231, 1971.

[22] D. M. Eckmann, S. Bowers, M. Stecker, and a T. Cheung, "Hematocrit, volume expander, temperature, and shear rate effects on blood viscosity.," *Anesth. Analg.*, vol. 91, no. 3, pp. 539–545, 2000.

[23] M. A. Elblbesy and A. T. Hereba, "Computation of the Coefficients of the Power law model for Whole Blood and Their Correlation with Blood Parameters," *Appl. Phys. Res.*, vol. 8, no. 2, p. 1, 2016.

[24] Y. I. Cho and K. R. Kensey, "Effects of the non-Newtonian viscosity of blood on flows in a diseased arterial vessel. Part 1: Steady flows.," *Biorheology*, vol. 28, no. 3–4, pp. 241–262, 1991.

[25] A. M. Walker, *The Characterization of Common Cardiovascular Flow Regimes Using Newtonian and Non-Newtonian Fluids*. , University of Calgary Department of Mechanical and Manufacturing Engineering, 2013.

[26] D. N. Ku, "Blood Flow in Arteries," *Annu. Rev. Fluid Mech.*, vol. 29, pp. 399–434, 1997.

[27] M. K. Banerjee, R. Ganguly, and A. Datta, "Effect of Pulsatile Flow Waveform and Womersley Number on the Flow in Stenosed Arterial Geometry," *ISRN Biomath.*, vol. 2012, pp. 1–17, 2012.

[28] A. D. Anastasiou, A. S. Spyrogianni, K. C. Koskinas, G. D. Giannoglou, and S. V. Paras, "Experimental investigation of the flow of a blood analogue fluid in a replica of a bifurcated small artery," *Med. Eng. Phys.*, vol. 34, no. 2, pp. 211–218, 2012.

[29] B. Liu and D. Tang, "Influence of non-Newtonian properties of blood on the wall shear stress in human atherosclerotic right coronary arteries.," *Mol. Cell. Biomech.*, 2011.

[30] S. Karimi, M. Dabagh, P. Vasava, M. Dadvar, B. Dabir, and P. Jalali, "Effect of rheological models on the hemodynamics within human aorta: CFD study on CT image-based geometry," *J. Nonnewton. Fluid Mech.*, vol. 207, no. May 2014, pp. 42–52, 2014.

[31] K. A. Brookshier and J. M. Tarbel, "Evaluation of Transparent Blood Analogue Fluids — Aqueous Xanthan Gum Glycerin," *Biorheology*, no. JANUARY 1993, 1993.

[32] J. R. Womersley, "Method for the calculation of velocity, rate of flow and viscous drag in arteries

when the pressure gradient is known.," *J. Physiol.*, 1955.

[33] N. B. Wood, "Aspects of fluid dynamics applied to the larger arteries.," *J. Theor. Biol.*, vol. 199, no. 2, pp. 137–161, 1999.

[34] W. E. Langlois and M. O. Deville, *Slow Viscous Flow*. 2014.

[35] M. Özdinç Çarpinlioğlu and M. Yaşar Gündoğdu, "A critical review on pulsatile pipe flow studies directing towards future research topics," *Flow Meas. Instrum.*, 2001.

[36] A. P. and N. Fatouraee, "An analytical phantom for the evaluation of medical flow imaging algorithms," *Phys. Med. Biol.*, vol. 54, no. 6, p. 1791, 2009.

[37] C. A. Taylor and M. T. Draney, "Experimental and Computational Methods in Cardiovascular Fluid Mechanics," *Ann. Phys. (N. Y).*, vol. 36, pp. 197–231, 2004.

[38] S. Tsangaris and N. Stergiopulos, "The inverse Womersley problem for pulsatile flow in straight rigid tubes," *J. Biomech.*, vol. 21, no. 3, pp. 263–266, 1988.

[39] G. Pontrelli, "Pulsatile blood flow in a pipe," *Comput. Fluids*, vol. 27, no. 3, pp. 367–380, 1998.

[40] K. Haddad, Ö.̈ Ertunç, M. Mishra, and A. Delgado, "Pulsating laminar fully developed channel and pipe flows," *Phys. Rev. E - Stat. Nonlinear, Soft Matter Phys.*, vol. 81, no. 1, pp. 1–13, 2010.

[41] X. He, D. N. Ku, and J. E. Moore, "Simple calculation of the velocity profiles for pulsatile flow in a blood vessel using Mathematica.," *Ann. Biomed. Eng.*, 1993.

[42] C. Loudon and A. Tordesillas, "The use of the dimensionless Womersley number to characterize the unsteady nature of internal flow.," *J. Theor. Biol.*, vol. 191, no. 1, pp. 63–78, 1998.

[43] J. D. Bronzino, *The Biomedical Engineering Handbook 1*, 2nd Editio. New York: Springer Science & Business Media, 2000.

[44] A. F. Stalder, A. Frydrychowicz, M. F. Russe, J. G. Korvink, J. Hennig, K. Li, and M. Markl, "Assessment of flow instabilities in the healthy aorta using flow-sensitive MRI," *J. Magn. Reson. Imaging*, vol. 33, no. 4, pp. 839–846, 2011.

[45] Y. A. Cengel and J. M. Cimbala, *Fluid Mechanics Fundamentals and Applications, Second Edition*, 2nd ed. New York: McGraw-Hill, 2010.

[46] R. Y. Grimes, R. A. Levine, P. G. Walker, and A. P. Yoganathan, “Dynamics of Systolic Pulmonary Venous Flow in Mitral Regurgitation: Mathematical Modeling of the Pulmonary Venous System and Atrium,” *J. Am. Soc. Echocardiogr.*, 1995.

[47] A. Pasipoularides, J. P. Murgo, J. J. Bird, and W. E. Craig, “Fluid dynamics of aortic stenosis: mechanisms for the presence of subvalvular pressure gradients.,” *Am. J. Physiol.*, vol. 246, no. 4 Pt 2, pp. H542-50, 1984.

[48] M. E. J. Bridges, “Monitoring Arterial Blood Pressure: What You May Not Know,” vol. 22, no. 2, 2002.

[49] P. P. Sengupta, G. Pedrizzetti, P. J. Kilner, A. Kheradvar, T. Ebbers, G. Tonti, A. G. Fraser, and J. Narula, “Emerging trends in CV flow visualization,” *JACC Cardiovasc. Imaging*, vol. 5, no. 3, pp. 305–316, 2012.

[50] R. Yip, R. Mongrain, and A. Ranga, “Development of anatomically correct mock-ups of the aorta for PIV investigations,” no. 1, pp. 1–10, 2011.

[51] P. H. Geoghegan, N. A. Buchmann, C. J. T. Spence, S. Moore, and M. Jermy, “Fabrication of rigid and flexible refractive-index-matched flow phantoms for flow visualisation and optical flow measurements,” *Exp. Fluids*, vol. 52, no. 5, pp. 1331–1347, 2012.

[52] U. Gülan, B. Lüthi, M. Holzner, A. Liberzon, A. Tsinober, and W. Kinzelbach, “Experimental study of aortic flow in the ascending aorta via Particle Tracking Velocimetry,” *Exp. Fluids*, vol. 53, no. 5, pp. 1469–1485, 2012.

[53] L. Huetter, P. H. Geoghegan, P. D. Docherty, M. S. Lazarjan, D. Clucas, and M. Jermy, “Application of a meta-analysis of aortic geometry to the generation of a compliant phantom for use in particle image velocimetry experimentation,” in *IFAC-PapersOnLine*, 2015, vol. 48, no. 20, pp. 407–412.

[54] D. M. Amatya and E. K. Longmire, “Simultaneous measurements of velocity and deformation in flows through compliant diaphragms,” *J. Fluids Struct.*, vol. 26, no. 2, pp. 218–235, 2010.

[55] B. Giuma, V. Paramasivam, K. Osman, and M. R. Abdul, “Graphical User Interface (GUI) In MatLab for Solving the Pulsatile Flow in Blood Vessel,” vol. 1, no. July, pp. 50–58, 2009.

[56] F. J. Gijsen, E. Allanic, F. N. van de Vosse, and J. D. Janssen, “The influence of the non-Newtonian properties of blood on the flow in large arteries: unsteady flow in a 90 degrees curved tube.,” *J. Biomech.*, vol. 32, no. 7, pp. 705–713, 1999.

[57] M. Zácek and E. Krause, “Numerical simulation of the blood flow in the human cardiovascular system.,” *J. Biomech.*, vol. 29, no. 1, pp. 13–20, 1996.

[58] R. B. Hickler, “Aortic and large artery stiffness: current methodology and clinical correlations.,” *Clin. Cardiol.*, vol. 13, pp. 317–322, 1990.

[59] A. Redheuil, W. C. Yu, C. O. Wu, E. Mousseaux, A. De Cesare, R. Yan, N. Kachenoura, D. Bluemke, and J. A. C. Lima, “Reduced ascending aortic strain and distensibility: Earliest manifestations of vascular aging in humans,” *Hypertension*, vol. 55, no. 2, pp. 319–326, 2010.

[60] I. Voges, M. Jerosch-Herold, J. Hedderich, E. Pardun, C. Hart, D. D. Gabbert, J. H. Hansen, C. Petko, H.-H. Kramer, and C. Rickers, “Normal values of aortic dimensions, distensibility, and pulse wave velocity in children and young adults: a cross-sectional study,” *J. Cardiovasc. Magn. Reson.*, vol. 14, no. 1, p. 77, 2012.

[61] P. H. Geoghegan, N. A. Buchmann, J. Soria, and M. C. Jermy, “Time-resolved PIV measurements of the flow field in a stenosed, compliant arterial model,” *Exp. Fluids*, vol. 54, no. 5, p. 1528, 2013.

[62] G. S. Kassab, “Biomechanics of the cardiovascular system: the aorta as an illustratory example.,” *J. R. Soc. Interface*, 2006.

[63] A. M. Dart and B. A. Kingwell, “Pulse pressure--a review of mechanisms and clinical relevance.,” *J. Am. Coll. Cardiol.*, vol. 37, no. 4, pp. 975–84, 2001.

[64] M. Briet, P. Boutouyrie, S. Laurent, and G. M. London, “Arterial stiffness and pulse pressure in CKD and ESRD,” *Kidney Int.*, vol. 82, no. 10, pp. 388–400, 2012.

[65] N. Westerhof, J. W. Lankhaar, and B. E. Westerhof, “The arterial windkessel,” *Med. Biol. Eng. Comput.*, vol. 47, no. 2, pp. 131–141, 2009.

[66] C. Silva and A. H. Reis, “Structure and adaptation of arteries to pulsatile flow: the case of the ascending aorta,” *Med. Phys.*, vol. 41, no. 0094–2405 (Print), p. 63701, 2014.

[67] T. S. Manning, B. E. Shykoff, and J. L. Izzo, “Validity and reliability of diastolic pulse contour analysis (Windkessel model) in humans,” *Hypertension*, vol. 39, no. 5, pp. 963–968, 2002.

[68] A. Redheuil, W.-C. Yu, E. Mousseaux, A. A. Harouni, N. Kachenoura, C. O. Wu, D. Bluemke, and J. A. C. Lima, “Age-Related Changes in Aortic Arch Geometry,” *J. Am. Coll. Cardiol.*, vol. 58, no. 12, pp. 1262–1270, 2011.

[69] A. D. Hughes, C. Park, J. Davies, D. Francis, S. A. McG Thom, J. Mayet, and K. H. Parker, “Limitations of Augmentation Index in the Assessment of Wave Reflection in Normotensive Healthy Individuals,” *PLoS One*, vol. 8, no. 3, pp. 1–8, 2013.

[70] J. Hashimoto and S. Ito, “Aortic stiffness determines diastolic blood flow reversal in the descending thoracic aorta: Potential implication for retrograde embolic stroke in hypertension,” *Hypertension*, vol. 62, no. 3, pp. 542–549, 2013.

[71] M. F. O’Rourke and W. W. Nichols, “Aortic diameter, aortic stiffness, and wave reflection increase with age and isolated systolic hypertension,” *Hypertension*, vol. 45, no. 4 SUPPL., pp. 652–658, 2005.

[72] J. A. Chirinos, J. P. Zambrano, S. Chakko, A. Veerani, A. Schob, H. J. Willens, G. Perez, and A. J. Mendez, “Aortic pressure augmentation predicts adverse cardiovascular events in patients with established coronary artery disease,” *Hypertension*, vol. 45, no. 5, pp. 980–985, 2005.

[73] D. J. Farrar, H. D. Green, M. G. Bond, W. D. Wagner, and R. a Gobbeé, “Aortic pulse wave velocity, elasticity, and composition in a nonhuman primate model of atherosclerosis.,” *Circ. Res.*, vol. 43, no. 1, pp. 52–62, 1978.

[74] G. F. Mitchell, H. Parise, E. J. Benjamin, M. G. Larson, M. J. Keyes, J. A. Vita, R. S. Vasan, and D. Levy, “Changes in arterial stiffness and wave reflection with advancing age in healthy men and women: The Framingham Heart Study,” *Hypertension*, vol. 43, no. 6, pp. 1239–1245, 2004.

[75] M. Shimizu and K. Kario, “Role of the augmentation index in hypertension.,” *Ther. Adv. Cardiovasc. Dis.*, vol. 2, no. 1, pp. 25–35, 2008.

[76] G. S. Reusz, O. Cseprekal, M. Temmar, E. Kis, A. B. Cherif, A. Thaleb, A. Fekete, A. J. Szabó, A. Benetos, and P. Salvi, “Reference values of pulse wave velocity in healthy children and teenagers.,” *Hypertension*, vol. 56, no. 2, pp. 217–224, 2010.

[77] A. P. Avolio, L. M. Van Bortel, P. Boutouyrie, J. R. Cockcroft, C. M. McEniery, A. D. Protogerou, M. J. Roman, M. E. Safar, P. Segers, and H. Smulyan, “Role of pulse pressure amplification in arterial hypertension: Experts’ opinion and review of the data,” *Hypertension*, vol. 54, no. 2, pp. 375–383, 2009.

[78] P. Segers, J. Mynard, L. Taelman, S. Vermeersch, and A. Swillens, “Wave reflection: Myth or reality?,” *Artery Res.*, vol. 6, no. 1, pp. 7–11, 2012.

[79] N. Westerhof, P. Sipkema, G. C. Van Den Bos, and G. Elzinga, “Forward and backward waves in the arterial system,” *Cardiovasc. Res.*, vol. 6, no. 6, pp. 648–656, 1972.

[80] A. Yee, Y. Sakurai, S. G. Eskin, and L. V. McIntire, “A validated system for simulating common carotid arterial flow in Vitro: Alteration of endothelial cell response,” *Ann. Biomed. Eng.*, vol. 34, no. 4, pp. 593–604, 2006.

[81] J. P. Murgo, N. Westerhof, J. P. Giolma, and S. a Altobelli, “Aortic input impedance in normal man: relationship to pressure wave forms.,” *Circulation*, vol. 62, no. 1, pp. 105–116, 1980.

[82] A. Swillens and P. Segers, “Assessment of arterial pressure wave reflection: Methodological considerations,” *Artery Res.*, vol. 2, no. 4, pp. 122–131, 2008.

[83] L. Segadal and K. Matre, “Blood velocity distribution in the human ascending aorta,” 1987.

[84] R. Kelly, C. Hayward, A. Avolio, and M. O’Rourke, “Noninvasive determination of age-related changes in the human arterial pulse.,” *Circulation*, vol. 80, no. 6, pp. 1652–9, 1989.

[85] W. W. Nichols, “Clinical measurement of arterial stiffness obtained from noninvasive pressure waveforms,” *Am. J. Hypertens.*, vol. 18, no. 1 SUPPL., pp. 3–10, 2005.

[86] T. Weber, J. Auer, M. F. O’Rourke, C. Punzengruber, E. Kvas, and B. Eber, “Prolonged mechanical systole and increased arterial wave reflections in diastolic dysfunction.,” *Heart*, vol. 92, pp. 1616–1622, 2006.

[87] A. Benbrahim, G. J. L’Italien, B. B. Milinazzo, D. F. Warnock, S. Dhara, J. P. Gertler, R. W. Orkin, and W. M. Abbott, “A compliant tubular device to study the influences of wall strain and fluid shear stress on cells of the vascular wall,” *J. Vasc. Surg.*, vol. 20, no. 2, pp. 184–94, 1994.

[88] “Ecoflex 00-50,” 2016. [Online]. Available: https://www.smooth-on.com/products/ecoflex-00-

50/.

[89] A. Vogel and W. Lauterborn, “Time resolved particle image velocimetry,” *Opt. Lasers Eng.*, vol. 9, no. 3–4, pp. 277–294, 1988.

[90] R. Castrejon-Garcia, J. R. Castrejon-Pita, G. D. Martin, and I. M. Hutchings, “The shadowgraph imaging technique and its modern application to fluid jets and drops,” *Rev. Mex. Fis.*, vol. 57, no. 3, pp. 266–275, 2011.

[91] V. Deplano, Y. Knapp, L. Bailly, and E. Bertrand, “Flow of a blood analogue fluid in a compliant abdominal aortic aneurysm model: Experimental modelling,” *J. Biomech.*, vol. 47, no. 6, pp. 1262–1269, 2014.

[92] C. Stamatopoulos, Y. Papaharilaou, D. S. Mathioulakis, and A. Katsamouris, “Steady and unsteady flow within an axisymmetric tube dilatation,” *Exp. Therm. Fluid Sci.*, vol. 34, no. 7, pp. 915–927, 2010.

[93] P. H. Geoghegan, N. A. Buchmann, M. C. Jermy, D. Nobes, C. J. T. Spence, and P. D. Docherty, “SPIV and image correlation measurements of surface displacement during pulsatile flow in models of compliant, healthy and stenosed arteries,” in *15th International Symposium on Applications of Laser Techniques to Fluid Mechanics*, 2010, pp. 5–8.

[94] A. Kheradvar, H. Houle, G. Pedrizzetti, G. Tonti, T. Belcik, M. Ashraf, J. R. Lindner, M. Gharib, and D. Sahn, “Echocardiographic Particle Image Velocimetry: A Novel Technique for Quantification of Left Ventricular Blood Vorticity Pattern,” *J. Am. Soc. Echocardiogr.*, vol. 23, no. 1, pp. 86–94, 2010.

[95] W. L. Lim, Y. T. Chew, T. C. Chew, and H. T. Low, “Steady flow dynamics of prosthetic aortic heart valves: A comparative evaluation with PIV techniques,” *J. Biomech.*, vol. 31, no. 5, pp. 411–421, 1998.

[96] A. Falahatpisheh and A. Kheradvar, “High-speed particle image velocimetry to assess cardiac fluid dynamics in vitro: From performance to validation,” *Eur. J. Mech. B/Fluids*, vol. 35, pp. 2–8, 2012.

[97] Y. Shi, T. J. H. Yeo, Y. Zhao, and N. H. C. Hwang, “Particle Image Velocimetry Study of Pulsatile Flow in Bi-leaflet Mechanical Heart Valves with Image Compensation Method,” *J. Biol. Phys.*, vol. 32, no. 6, pp. 531–551, 2007.

[98] D. J. Farrar, P. G. Compton, J. H. Lawson, J. J. Hershon, and J. D. Hill, “Control Modes of a Clinical Ventricular Assist Device,” *IEEE Eng Med Biol*, vol. 5(1), no. March, pp. 19–25, 1986.

[99] D. J. Farrar and J. D. Hill, “Univentricular and biventricular thoratec VAD support as a bridge to transplantation,” *Ann. Thorac. Surg.*, vol. 55, no. 1, pp. 276–282, 1993.

Appendix

A-1. Additional Plots

A-1.1 Peristaltic Pump Experiment – Rigid Case

This appendix provides plots of normalized pressure, theoretical centerline velocity (solid blue lines) and experimental centerline velocity (blue circles) over one normalized pump cycle for additional cases of rigid peristaltic pump experiment.

Newtonian Cases

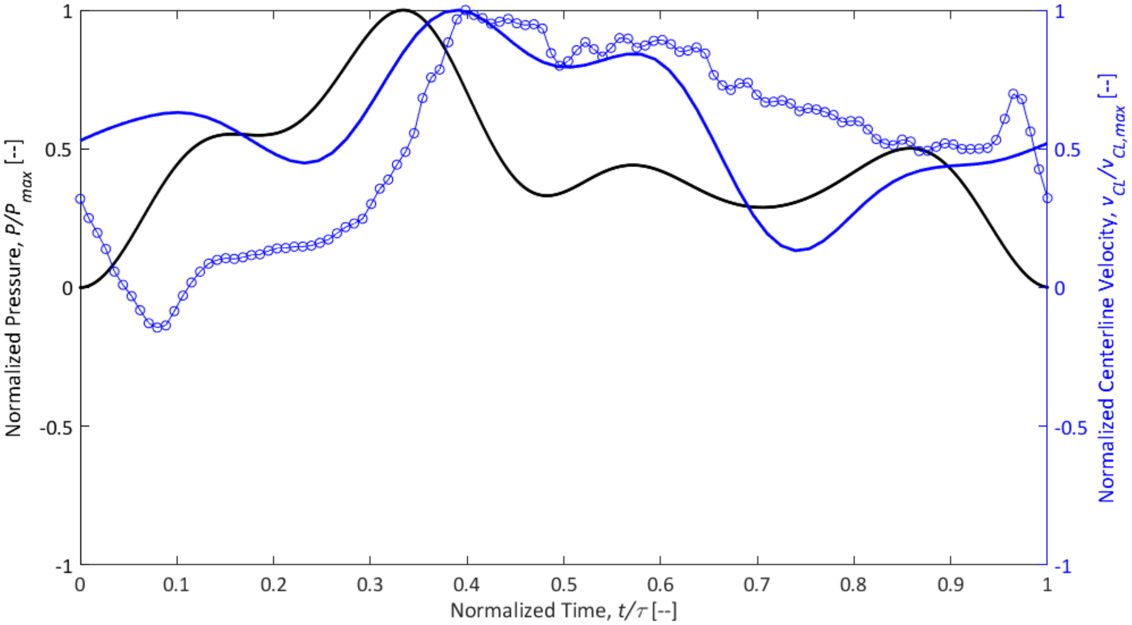

Figure A-1: Plot of normalized pressure and centerline velocity over one normalized pump cycle for rigid Newtonian *f* = 1.00 Hz (60 BPM) case

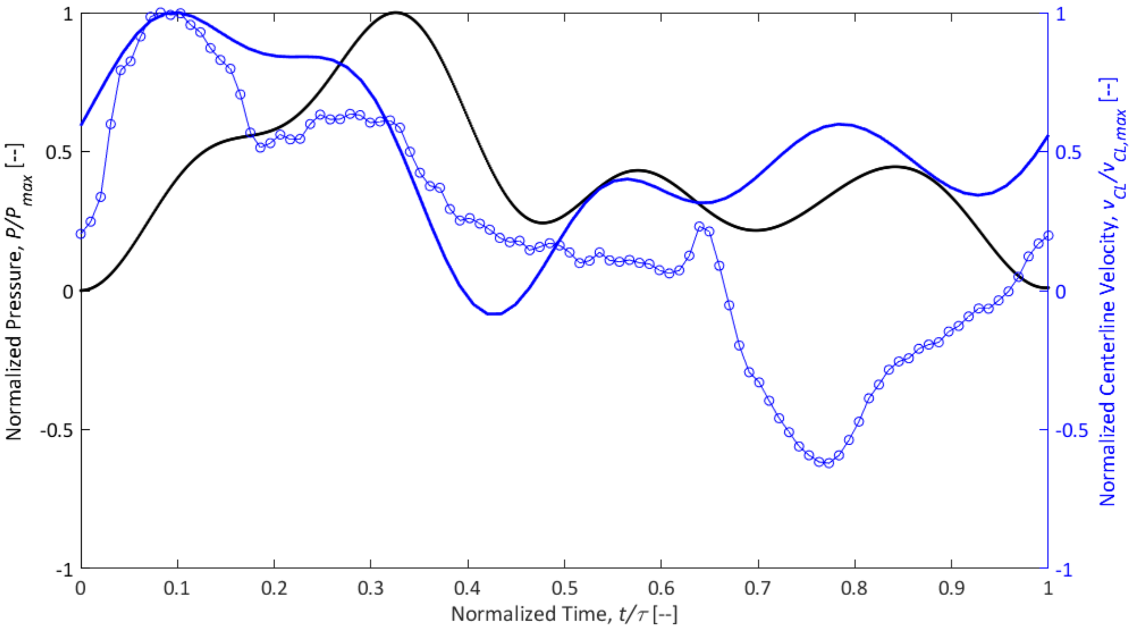

Figure A-2: Plot of normalized pressure and centerline velocity over one normalized pump cycle for rigid Newtonian *f* = 1.17 Hz (70 BPM) case

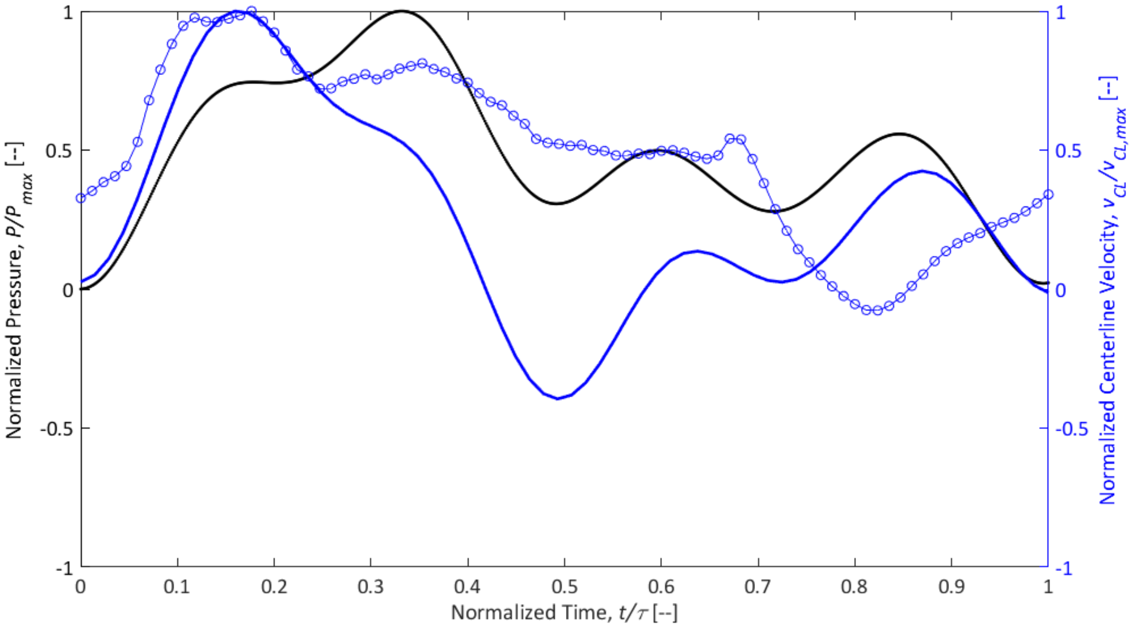

Figure A-3: Plot of normalized pressure and centerline velocity over one normalized pump cycle for rigid Newtonian *f* = 1.33 Hz (80 BPM) case

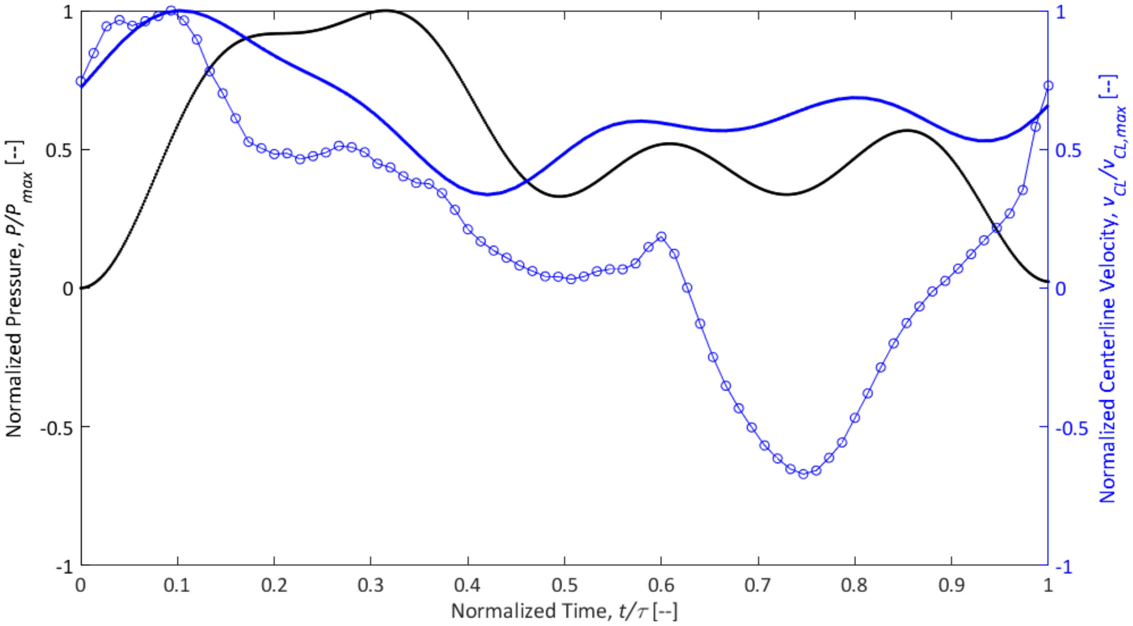

Figure A-4: Plot of normalized pressure and centerline velocity over one normalized pump cycle for rigid Newtonian *f* = 1.50 Hz (90 BPM) case

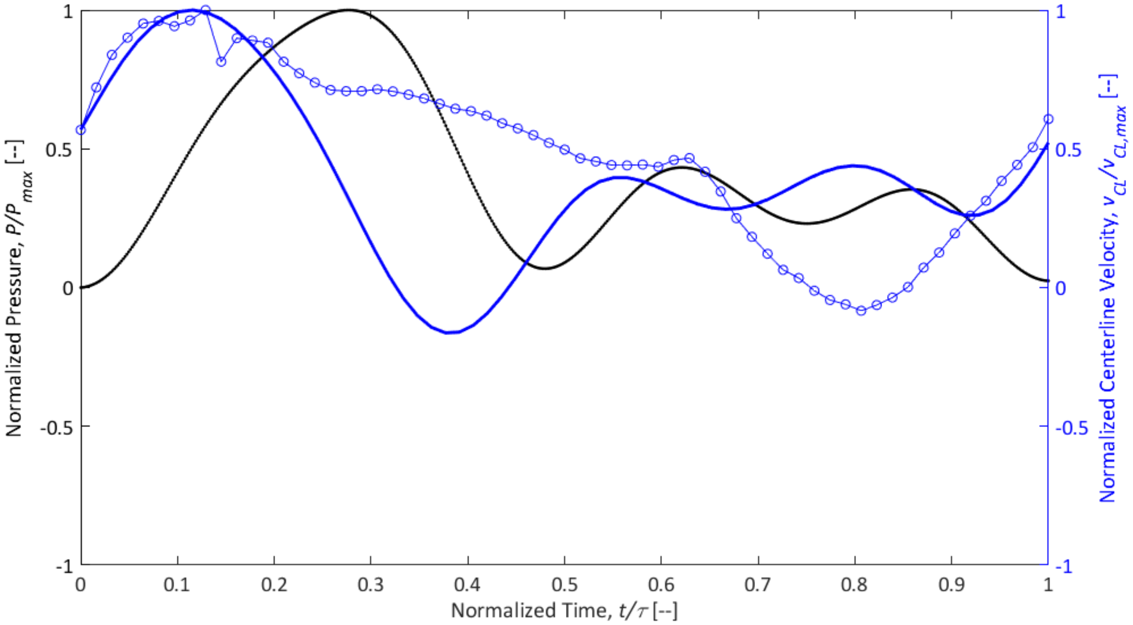

Figure A-5: Plot of normalized pressure and centerline velocity over one normalized pump cycle for rigid Newtonian *f* = 1.83 Hz (110 BPM) case

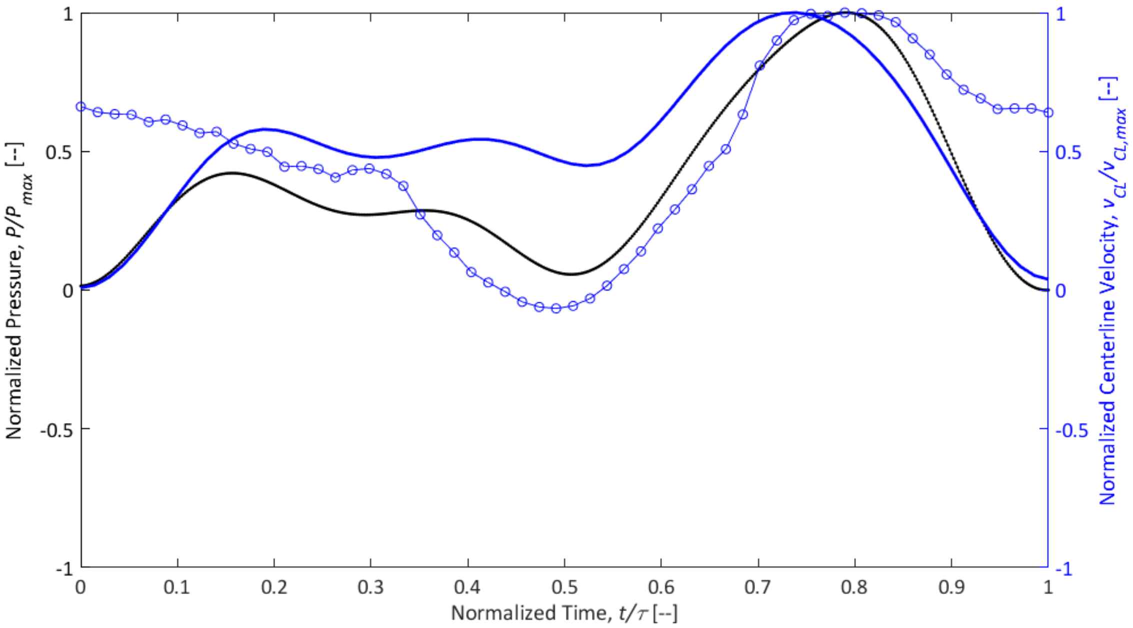

Figure A-6: Plot of normalized pressure and centerline velocity over one normalized pump cycle for rigid Newtonian *f* = 2.00 Hz (120 BPM) case

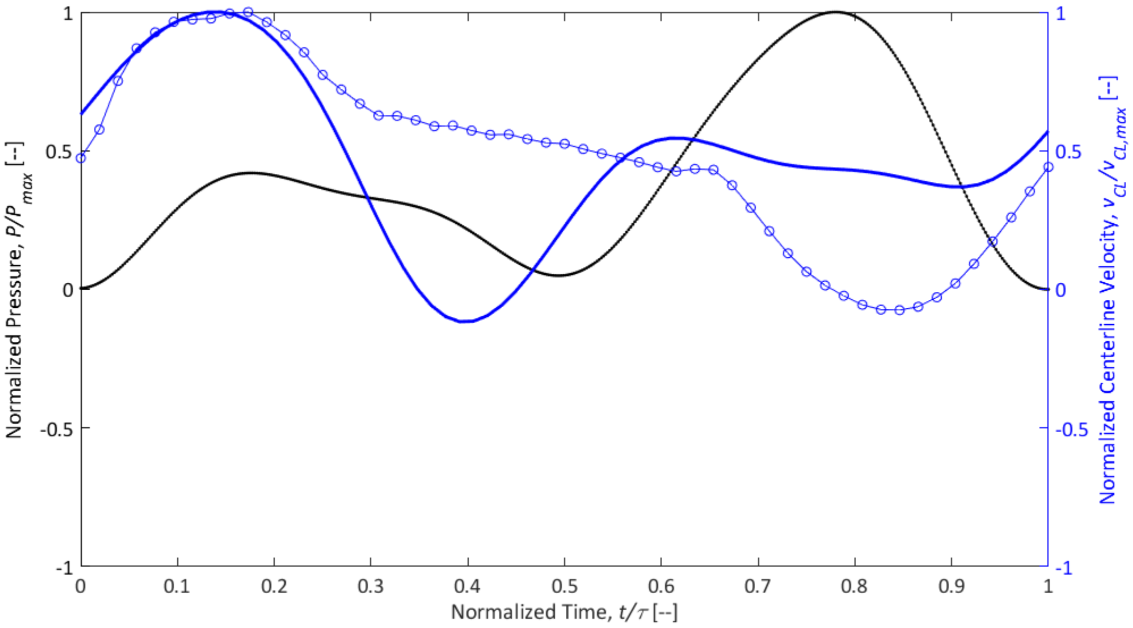

Figure A-7: Plot of normalized pressure and centerline velocity over one normalized pump cycle for rigid Newtonian *f* = 2.17 Hz (130 BPM) case

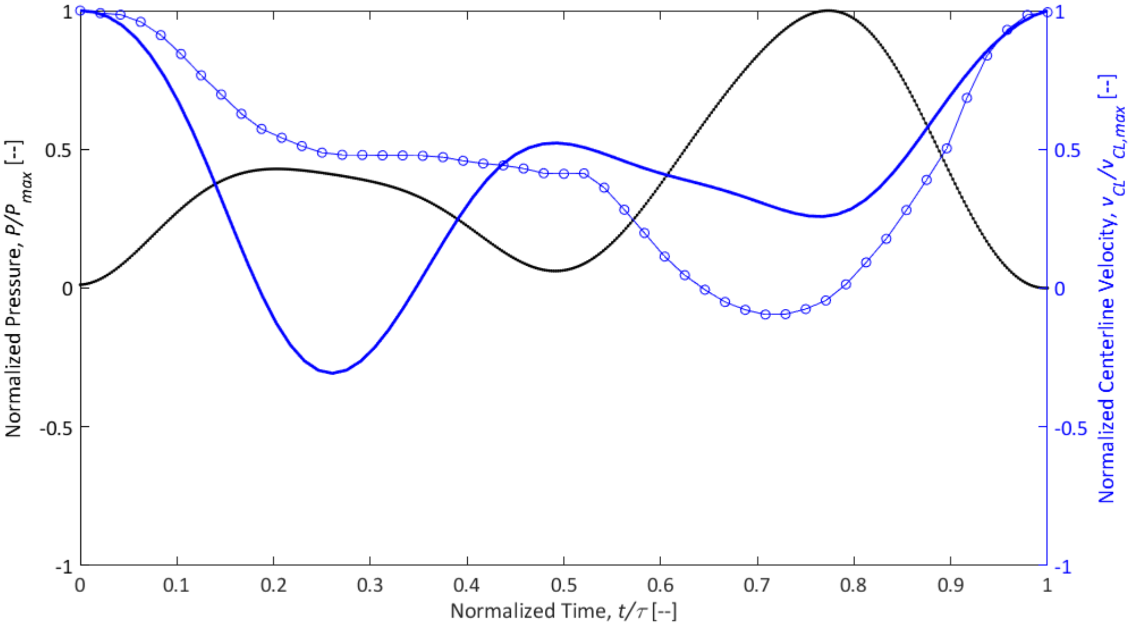

Figure A-8: Plot of normalized pressure and centerline velocity over one normalized pump cycle for rigid Newtonian f = 2.33 Hz (140 BPM) case

Non-Newtonian Cases

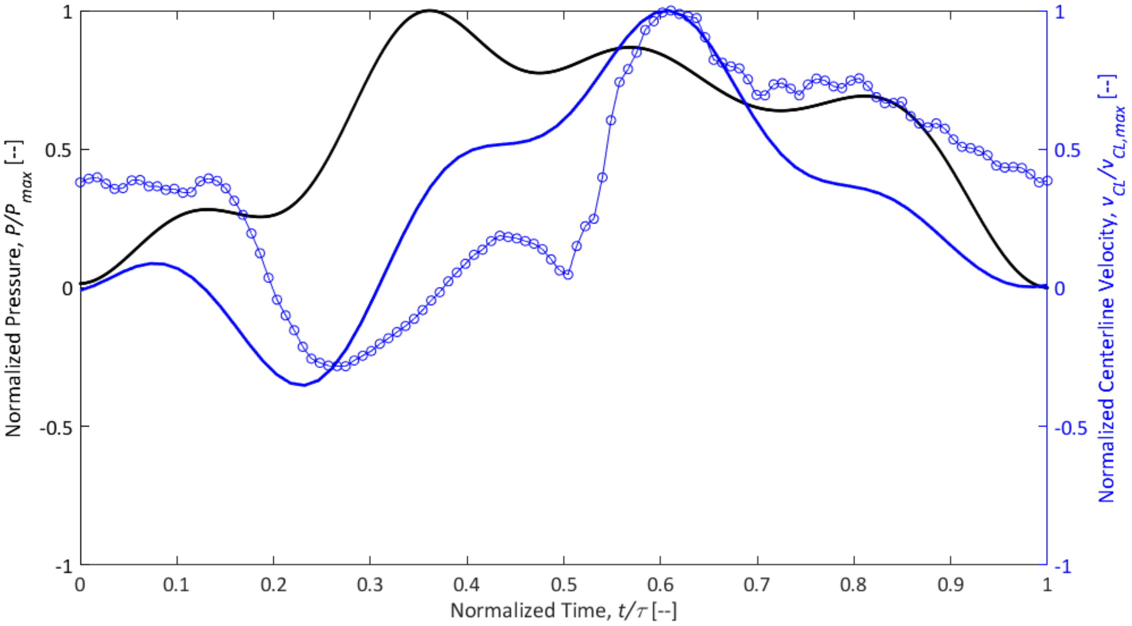

Figure A-9: Plot of normalized pressure and centerline velocity over one normalized pump cycle for rigid non – Newtonian f = 1.00 Hz (60 BPM) case

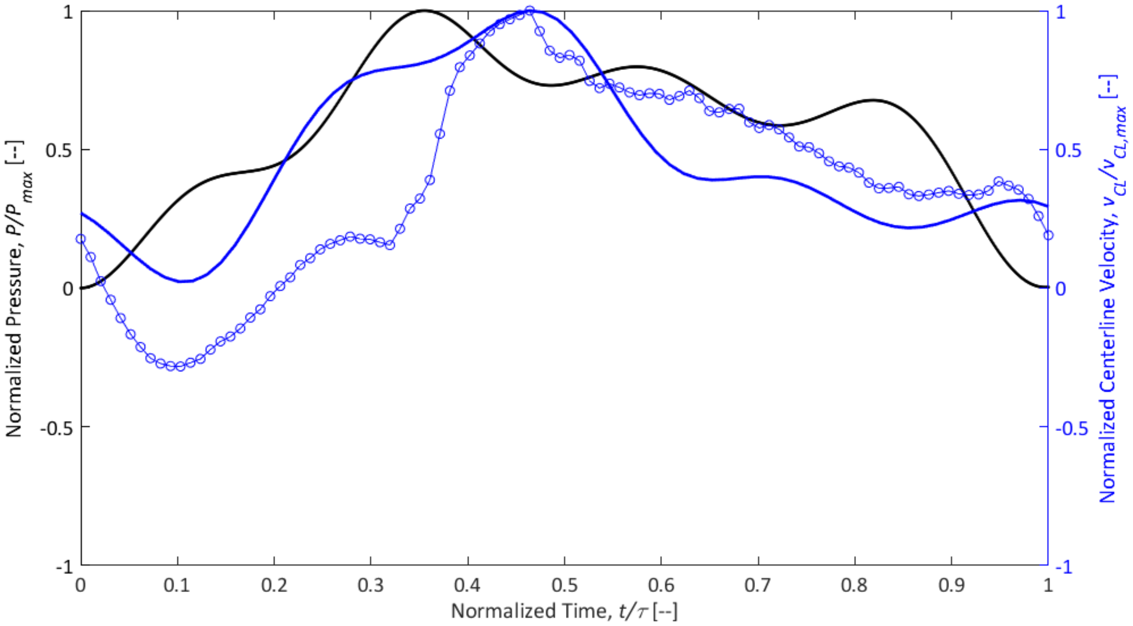

Figure A-10: Plot of normalized pressure and centerline velocity over one normalized pump cycle for rigid non – Newtonian *f* = 1.17 Hz (70 BPM) case

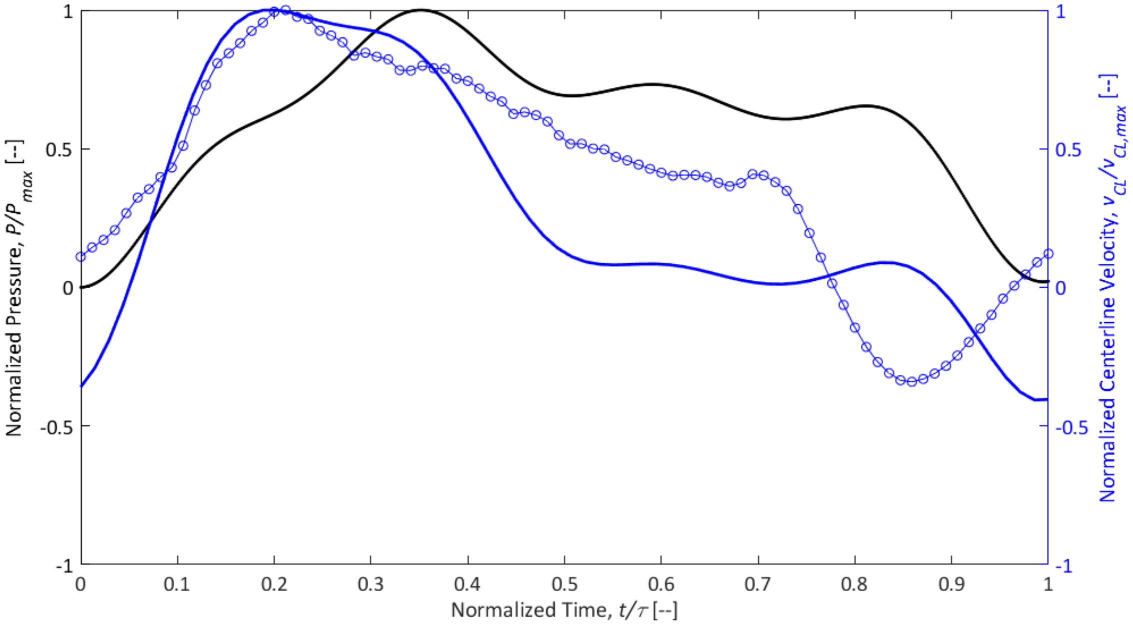

Figure A-11: Plot of normalized pressure and centerline velocity over one normalized pump cycle for rigid non – Newtonian *f* = 1.33 Hz (80 BPM) case

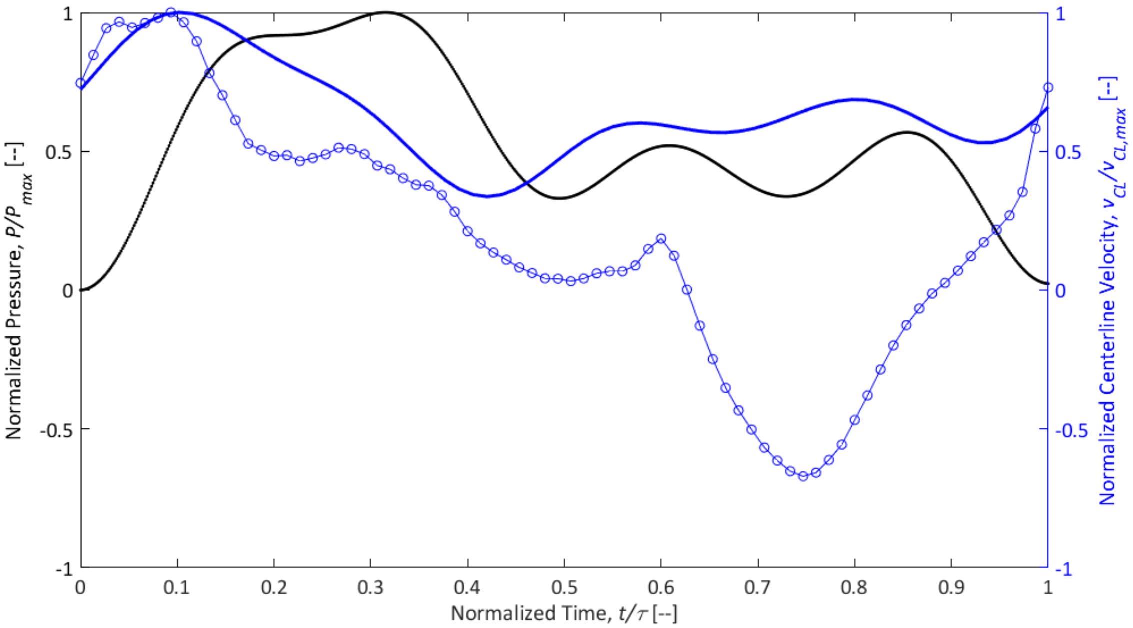

Figure A-12: Plot of normalized pressure and centerline velocity over one normalized pump cycle for rigid non – Newtonian *f* = 1.50 Hz (90 BPM) case

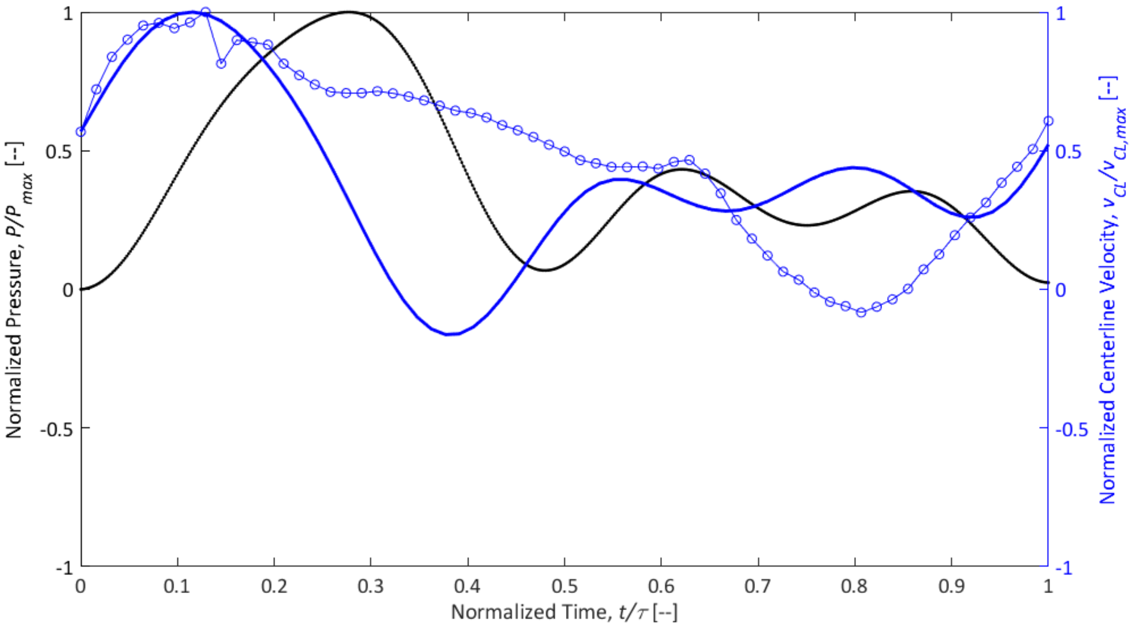

Figure A-13: Plot of normalized pressure and centerline velocity over one normalized pump cycle for rigid non – Newtonian *f* = 1.83 Hz (110 BPM) case

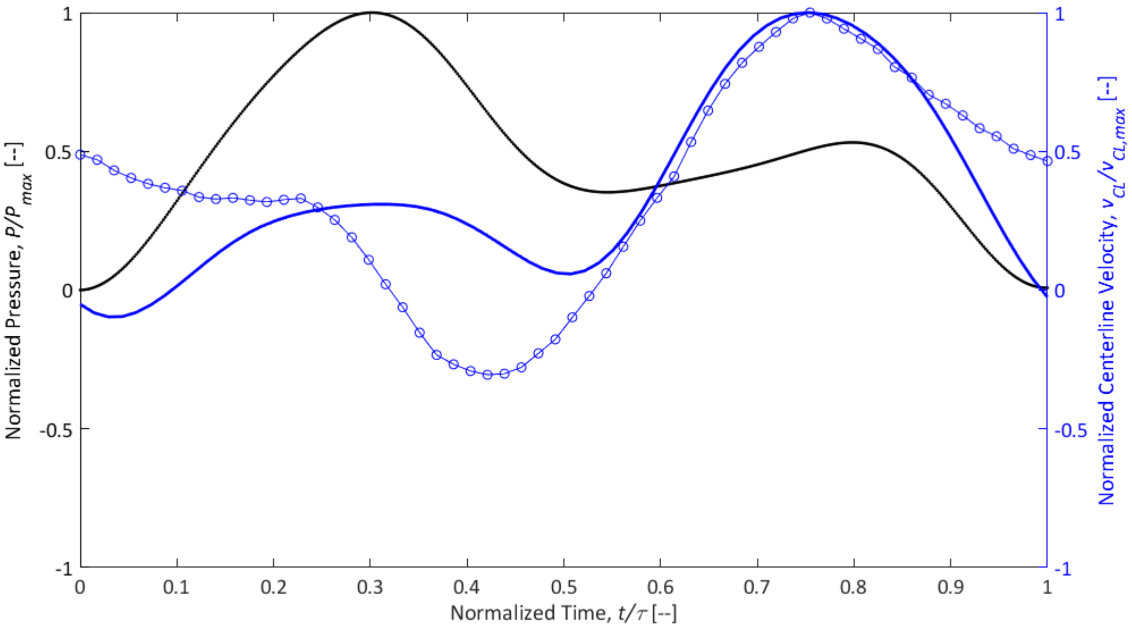

Figure A-14: Plot of normalized pressure and centerline velocity over one normalized pump cycle for rigid non – Newtonian *f* = 2.00 Hz (120 BPM) case

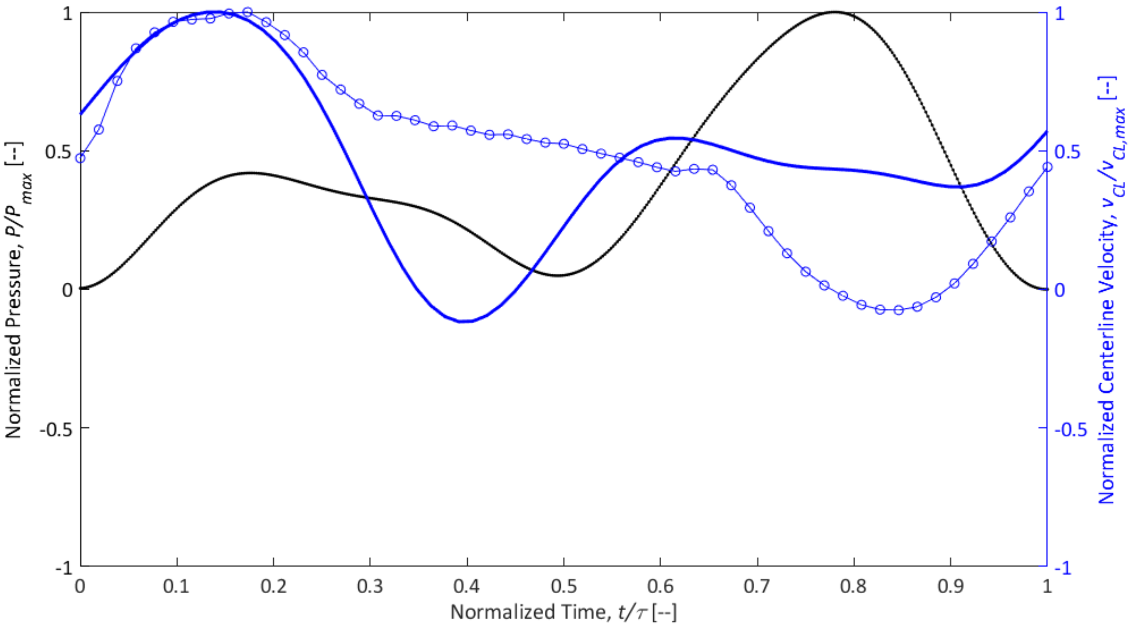

Figure A-15: Plot of normalized pressure and centerline velocity over one normalized pump cycle for rigid non – Newtonian *f* = 2.17 Hz (130 BPM) case

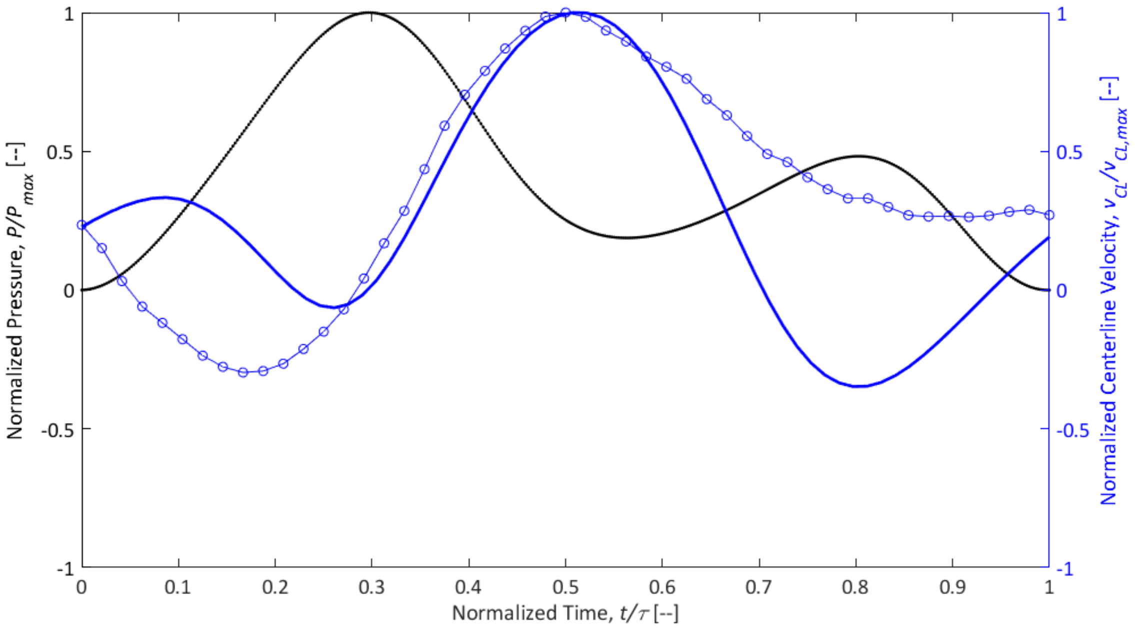

Figure A-16: Plot of normalized pressure and centerline velocity over one normalized pump cycle for rigid non – Newtonian *f* = 2.33 Hz (140 BPM) case

A-1.2 Peristaltic Pump Experiment – Compliant Case

This appendix provides plots of normalized pressure, theoretical centerline velocity (solid blue lines), experimental centerline velocity (blue circles) and tube distension response over one normalized pump cycle for additional cases of compliant peristaltic pump experiment.

Newtonian Cases

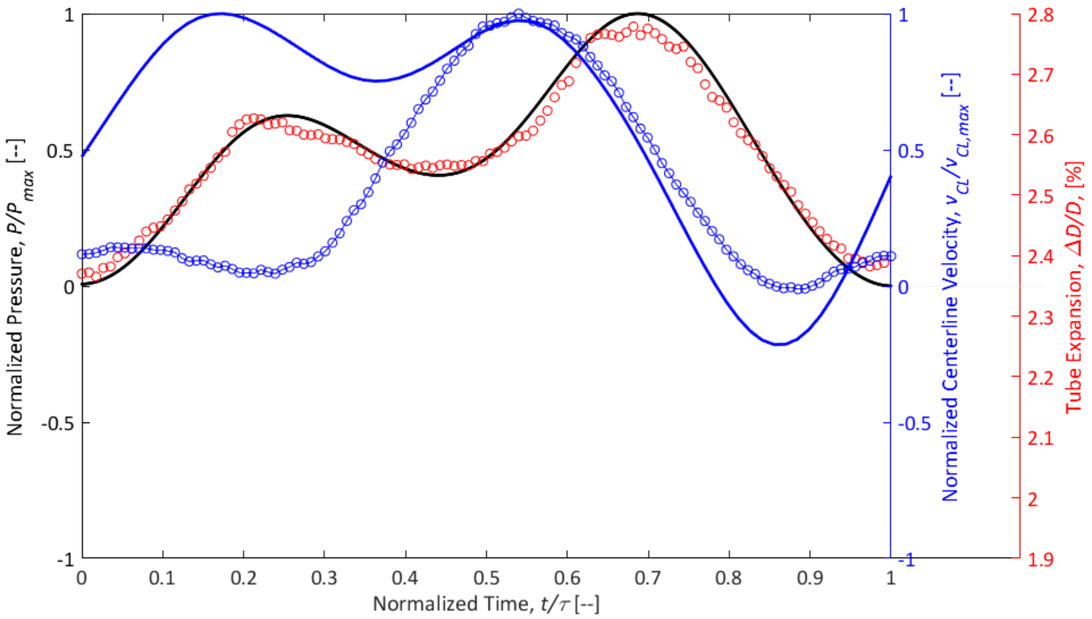

Figure A-17: Plot of normalized pressure, normalized centerline velocity and tube distension response over one normalized pump cycle for compliant Newtonian *f* = 1.00 Hz (60 BPM) case

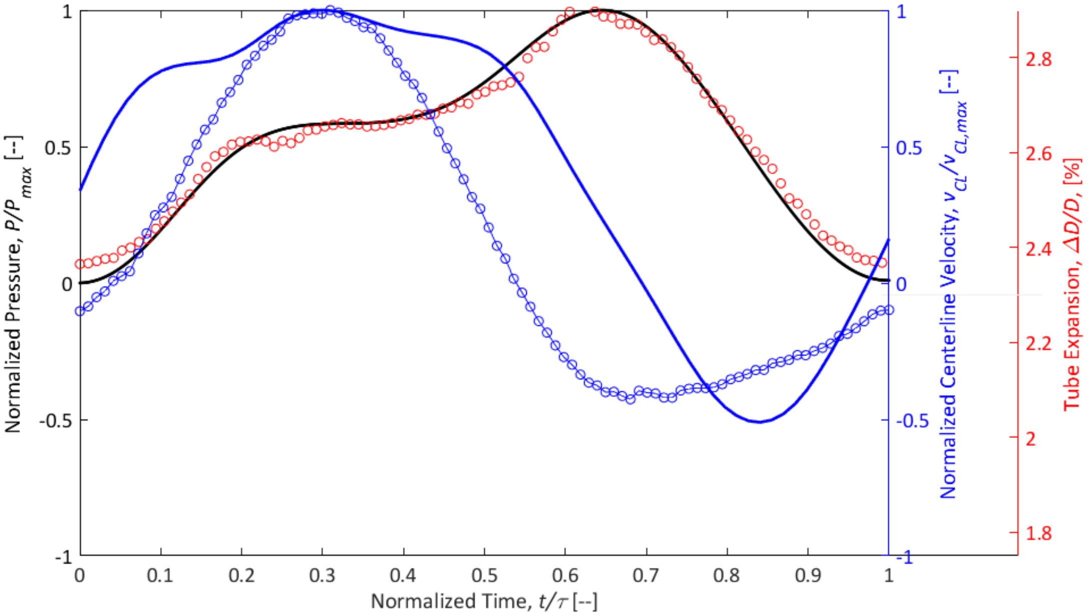

Figure A-18: Plot of normalized pressure, normalized centerline velocity and tube distension response over one normalized pump cycle for compliant Newtonian *f* = 1.17 Hz (70 BPM) case

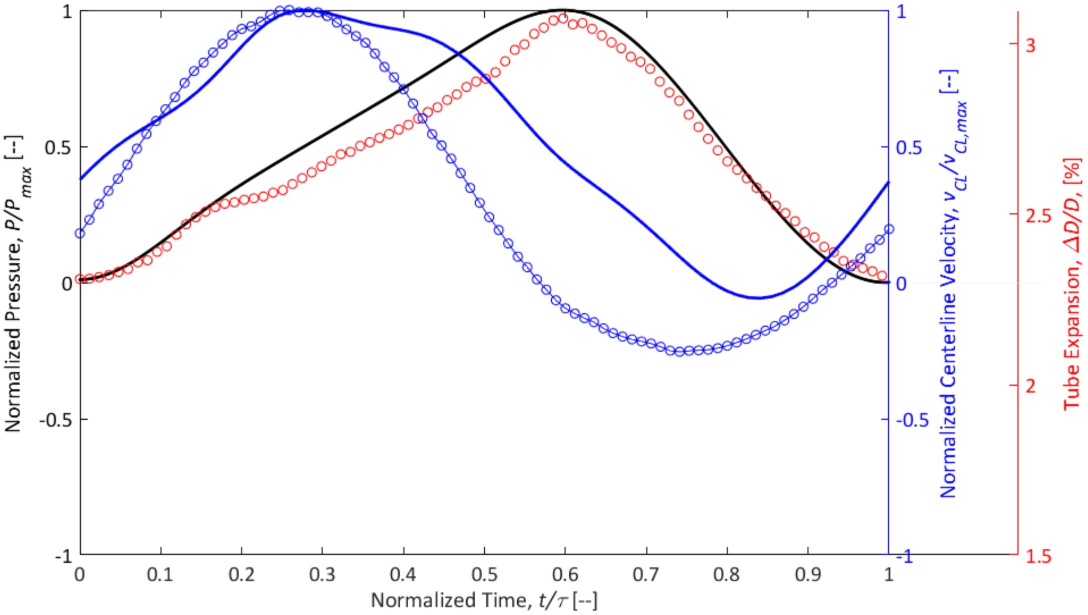

Figure A-19: Plot of normalized pressure, normalized centerline velocity and tube distension response over one normalized pump cycle for compliant Newtonian *f* = 1.33 Hz (80 BPM) case

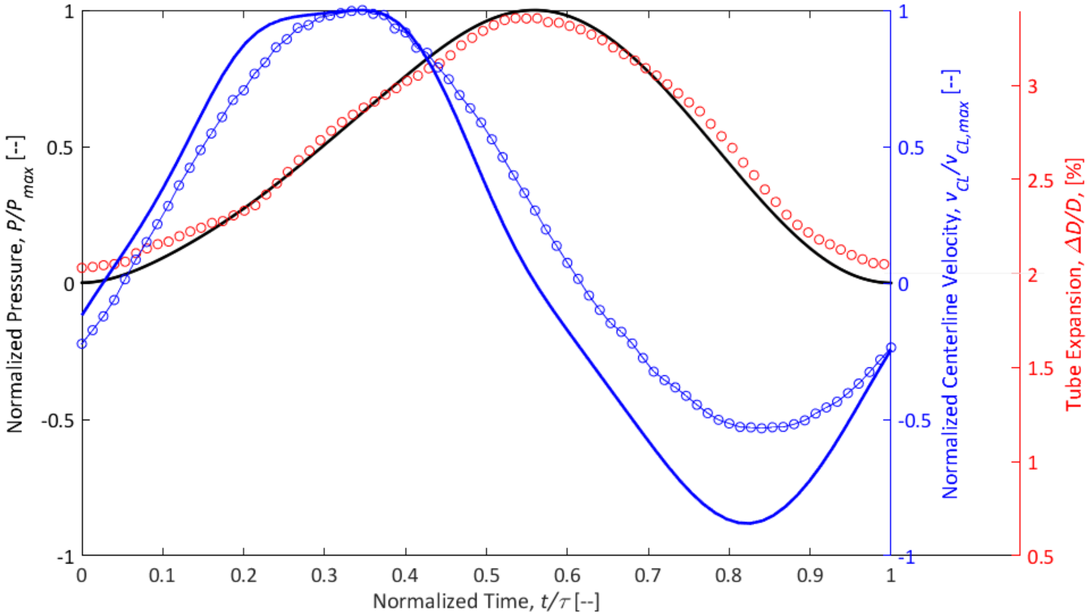

Figure A-20: Plot of normalized pressure, normalized centerline velocity and tube distension response over one normalized pump cycle for compliant Newtonian *f* = 1.50 Hz (90 BPM) case

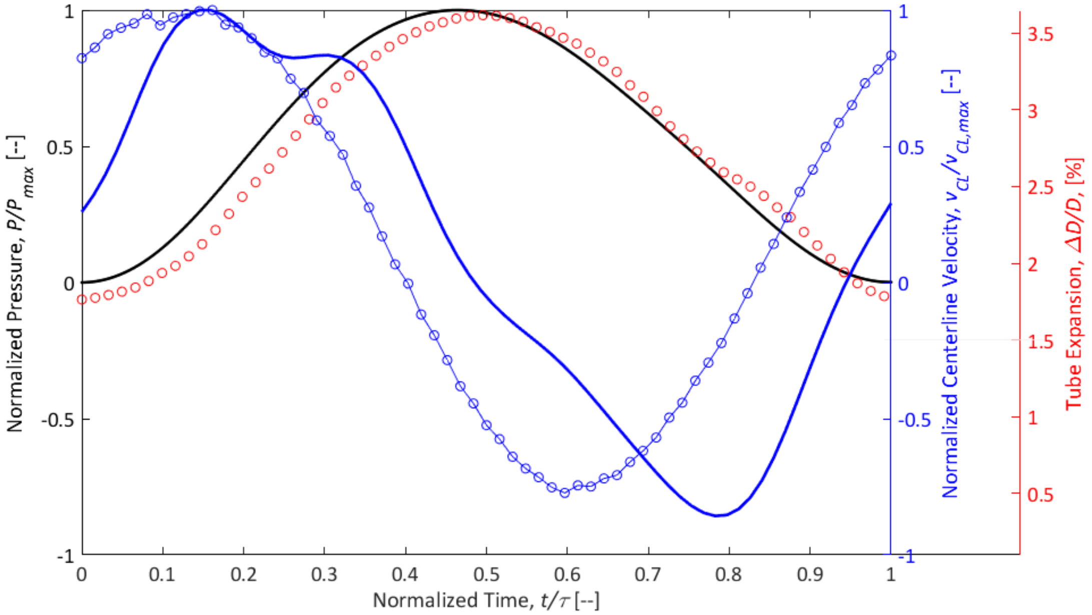

Figure A-21: Plot of normalized pressure, normalized centerline velocity and tube distension response over one normalized pump cycle for compliant Newtonian *f* = 1.83 Hz (110 BPM) case

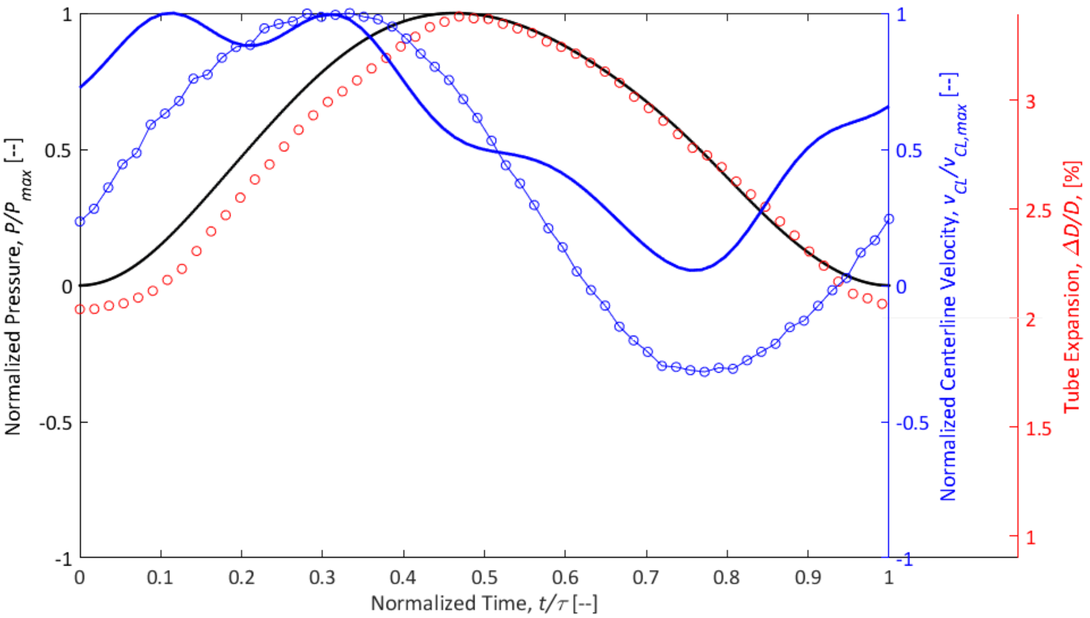

Figure A-22: Plot of normalized pressure, normalized centerline velocity and tube distension response over one normalized pump cycle for compliant Newtonian *f* = 2.00 Hz (120 BPM) case

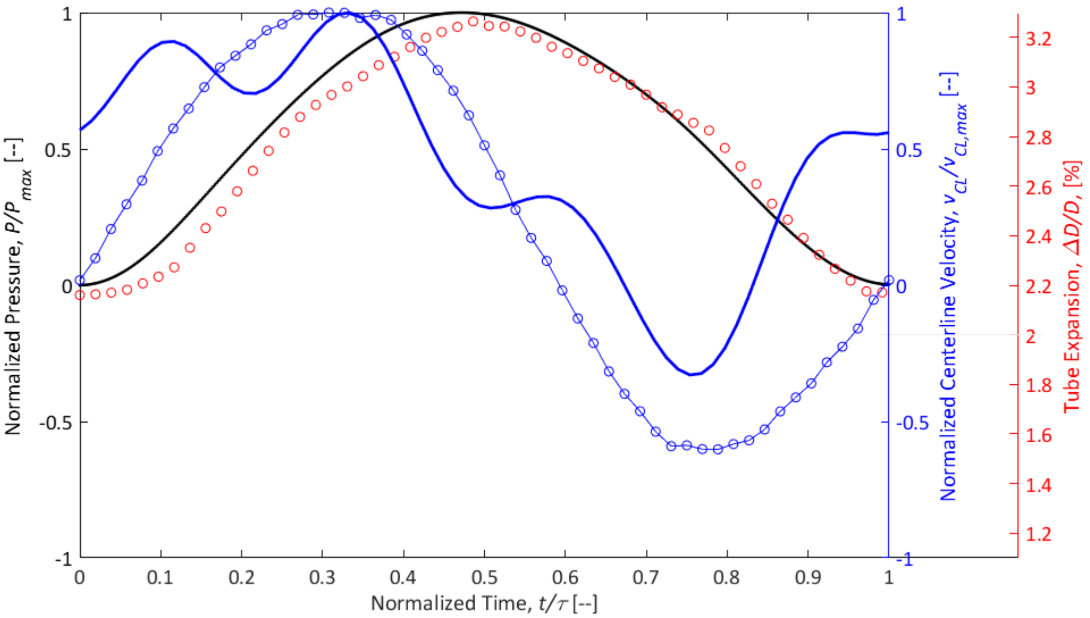

Figure A-23: Plot of normalized pressure, normalized centerline velocity and tube distension response over one normalized pump cycle for compliant Newtonian *f* = 2.17 Hz (130 BPM) case

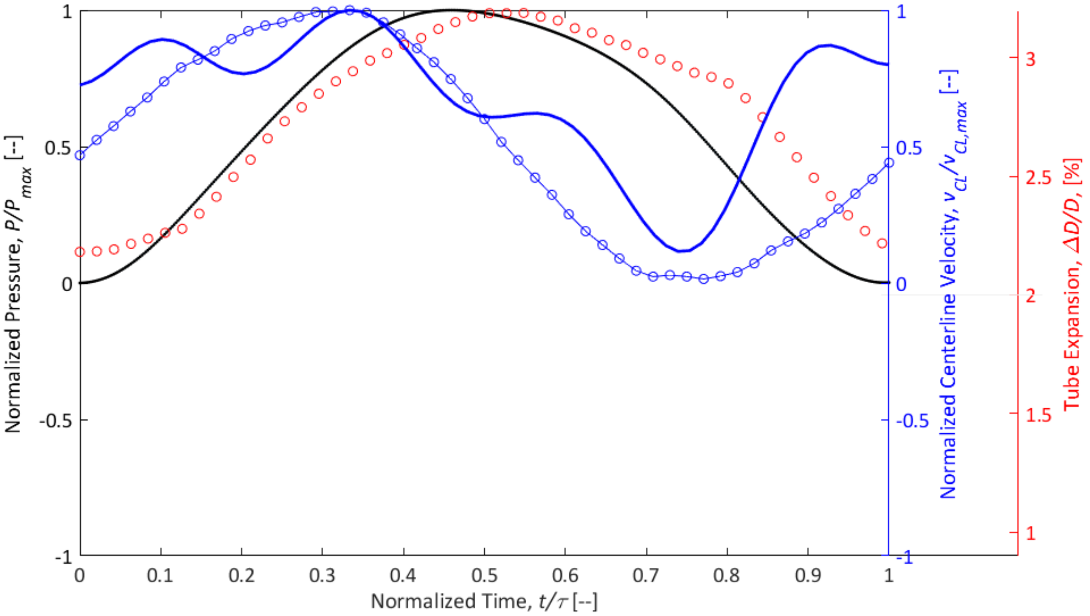

Figure A-24: Plot of normalized pressure, normalized centerline velocity and tube distension response over one normalized pump cycle for compliant Newtonian *f* = 2.33 Hz (140 BPM) case

Non-Newtonian Cases

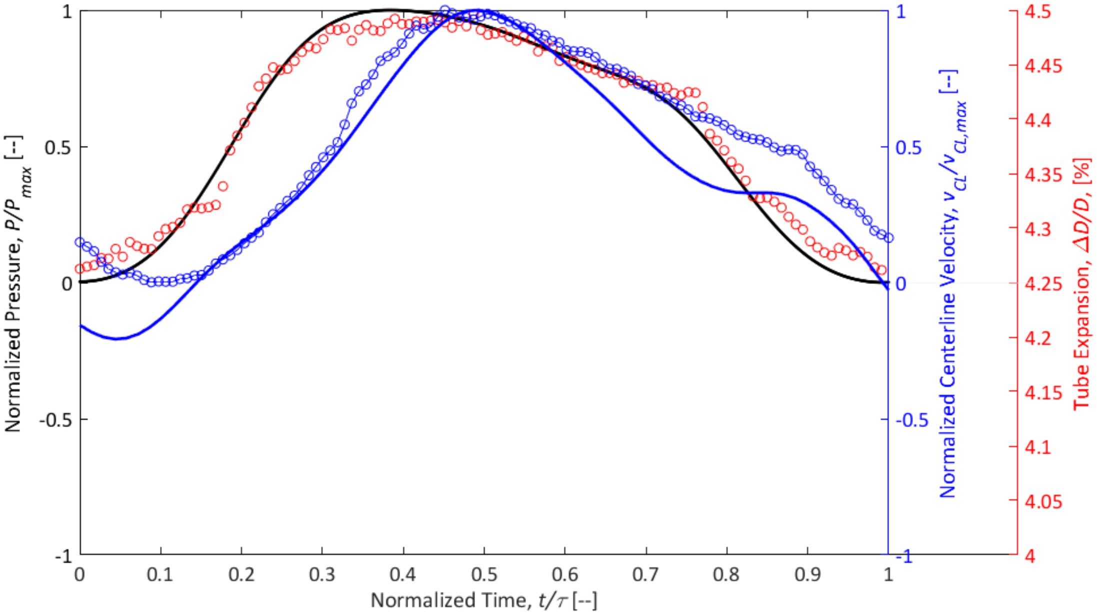

Figure A-25: Plot of normalized pressure, normalized centerline velocity and tube distension response over one normalized pump cycle for compliant non-Newtonian *f* = 1.00 Hz (60 BPM) case

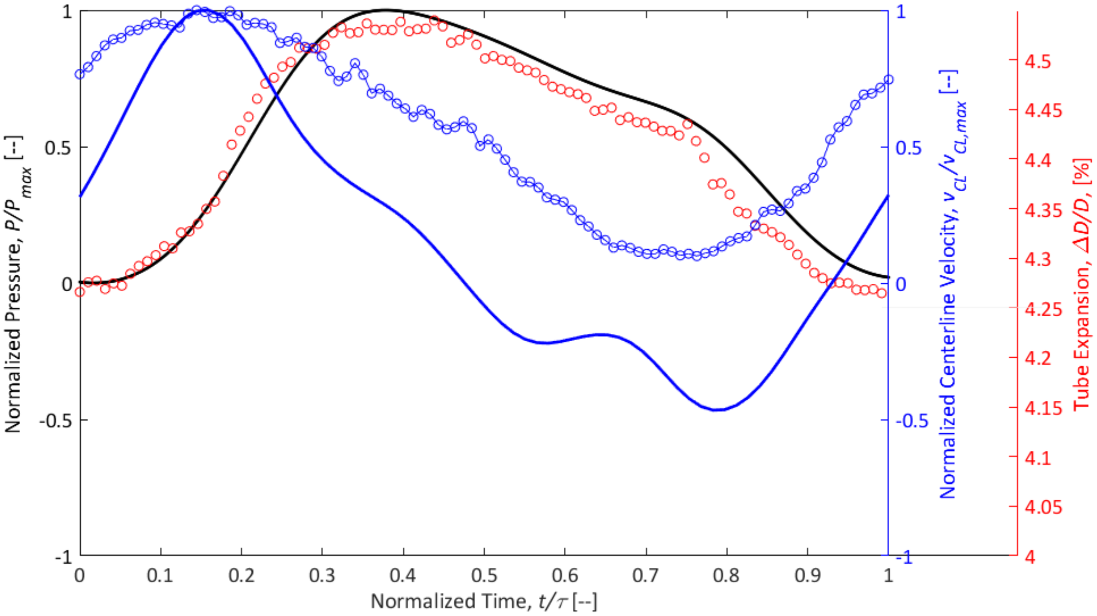

Figure A-26: Plot of normalized pressure, normalized centerline velocity and tube distension response over one normalized pump cycle for compliant non-Newtonian f = 1.17 Hz (70 BPM) case

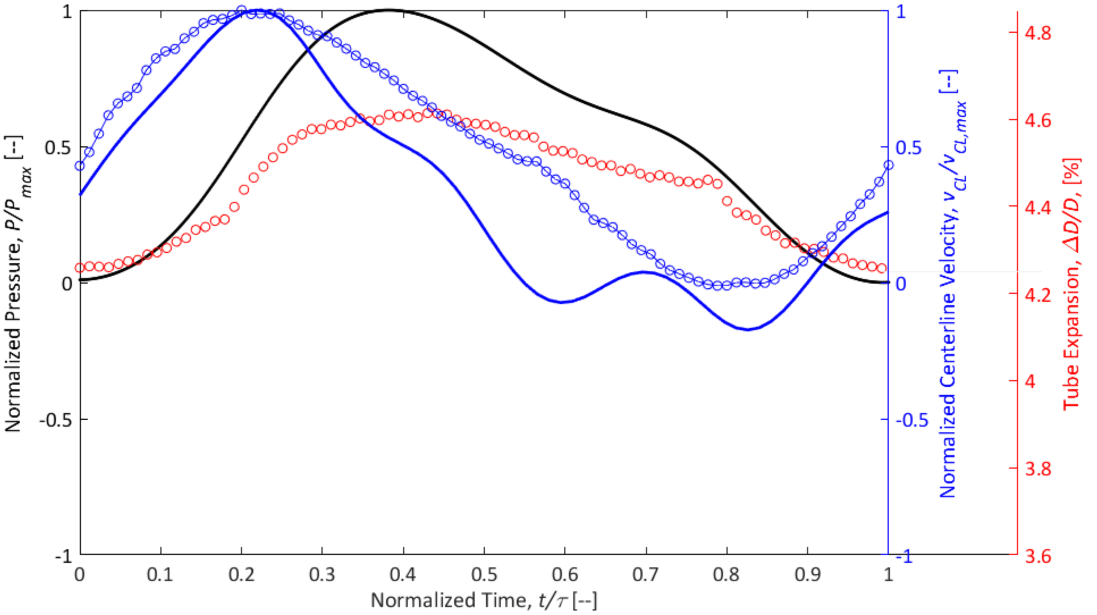

Figure A-27: Plot of normalized pressure, normalized centerline velocity and tube distension response over one normalized pump cycle for compliant non-Newtonian f = 1.33 Hz (80 BPM) case

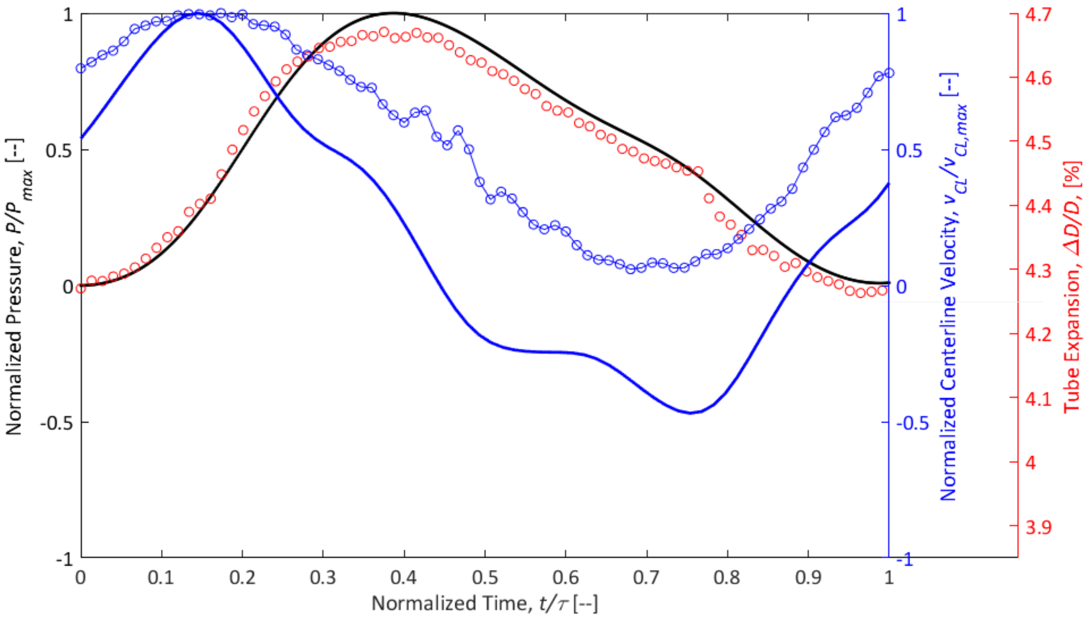

Figure A-28: Plot of normalized pressure, normalized centerline velocity and tube distension response over one normalized pump cycle for compliant non-Newtonian *f* = 1.50 Hz (90 BPM) case

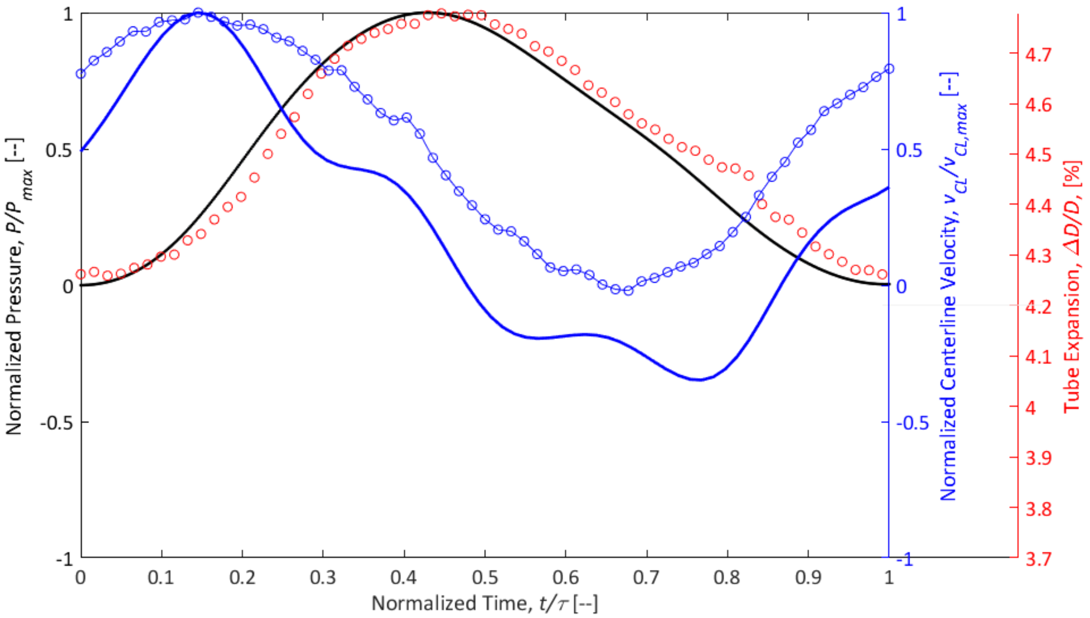

Figure A-29: Plot of normalized pressure, normalized centerline velocity and tube distension response over one normalized pump cycle for compliant non-Newtonian *f* = 1.83 Hz (110 BPM) case

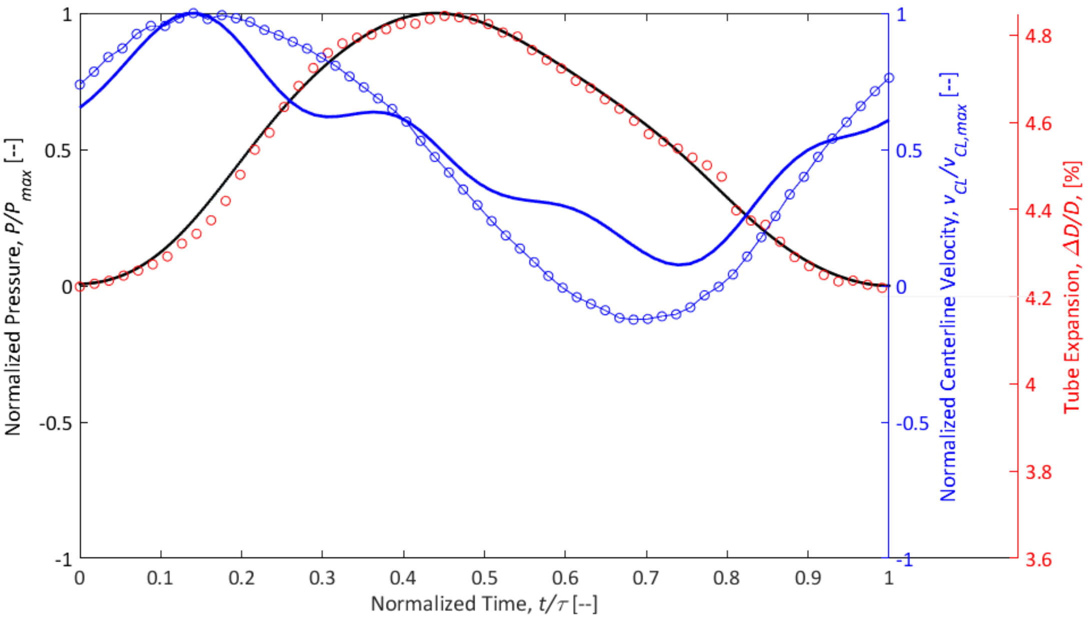

Figure A-30: Plot of normalized pressure, normalized centerline velocity and tube distension response over one normalized pump cycle for compliant non-Newtonian *f* = 2.00 Hz (120 BPM) case

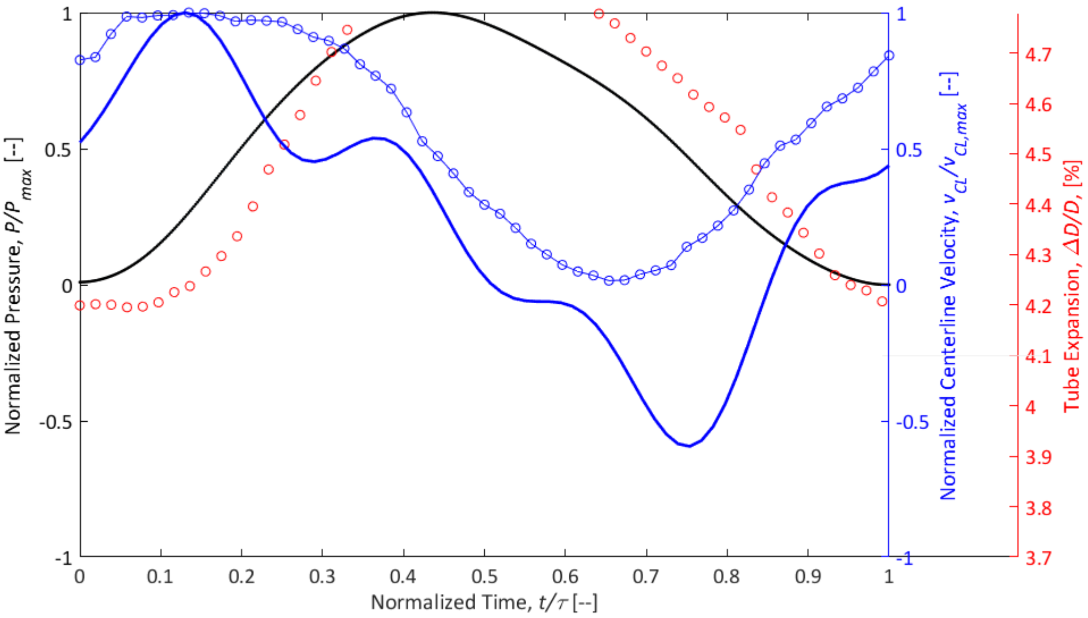

Figure A-31: Plot of normalized pressure, normalized centerline velocity and tube distension response over one normalized pump cycle for compliant non-Newtonian *f* = 2.17 Hz (130 BPM) case

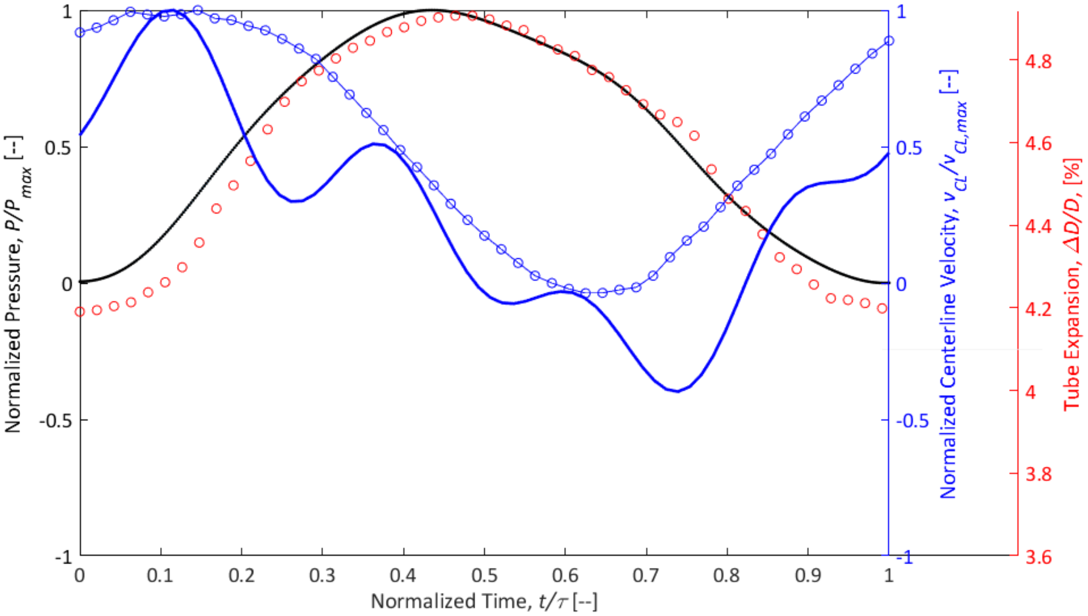

Figure A-32: Plot of normalized pressure, normalized centerline velocity and tube distension response over one normalized pump cycle for compliant non-Newtonian *f* = 2.33 Hz (140 BPM) case

A-1.3 VAD Experiment – Rigid Case

This appendix provides plots of normalized pressure and centerline velocity over one normalized pump cycle for all rigid VAD results.

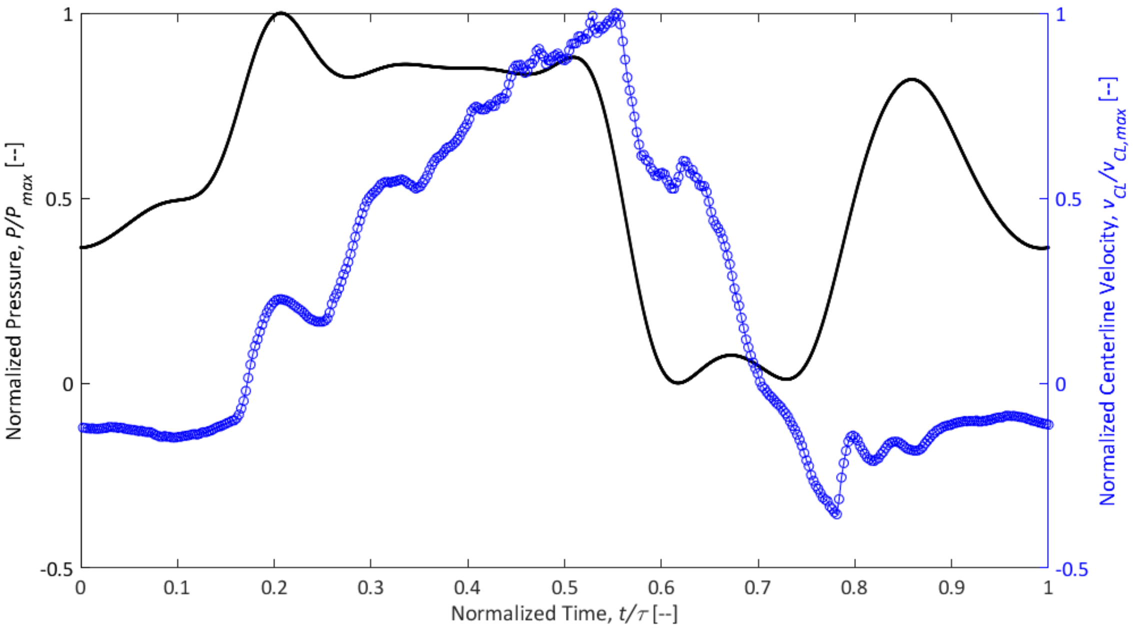

Figure A-33: Plot of normalized central aortic pressure waveform (P/P_{max}) and peripheral centerline velocity ($v_{CL}/v_{CL,max}$) for rigid case with $\omega_{AL\ pump}$= 980 RPM

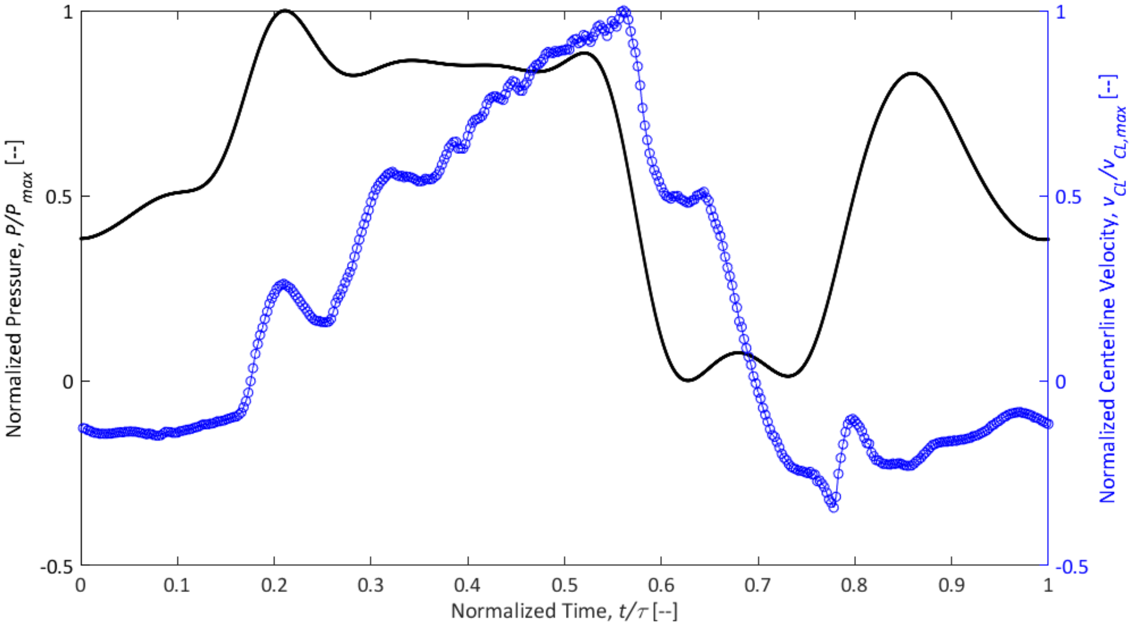

Figure A-34: Plot of normalized central aortic pressure waveform (P/P_{max}) and peripheral centerline velocity ($v_{CL}/v_{CL,max}$) for rigid case with $\omega_{AL\ pump}$ = 1065 RPM

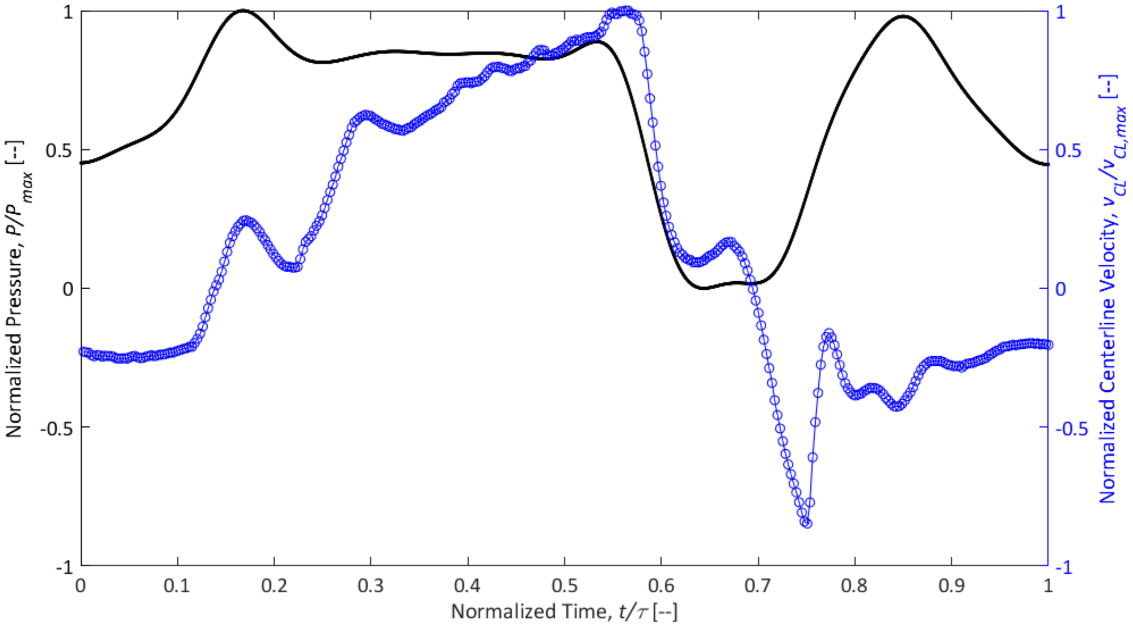

Figure A-35: Plot of normalized central aortic pressure waveform (P/P_{max}) and peripheral centerline velocity ($v_{CL}/v_{CL,max}$) for rigid case with $\omega_{AL\ pump}$ = 1450 RPM

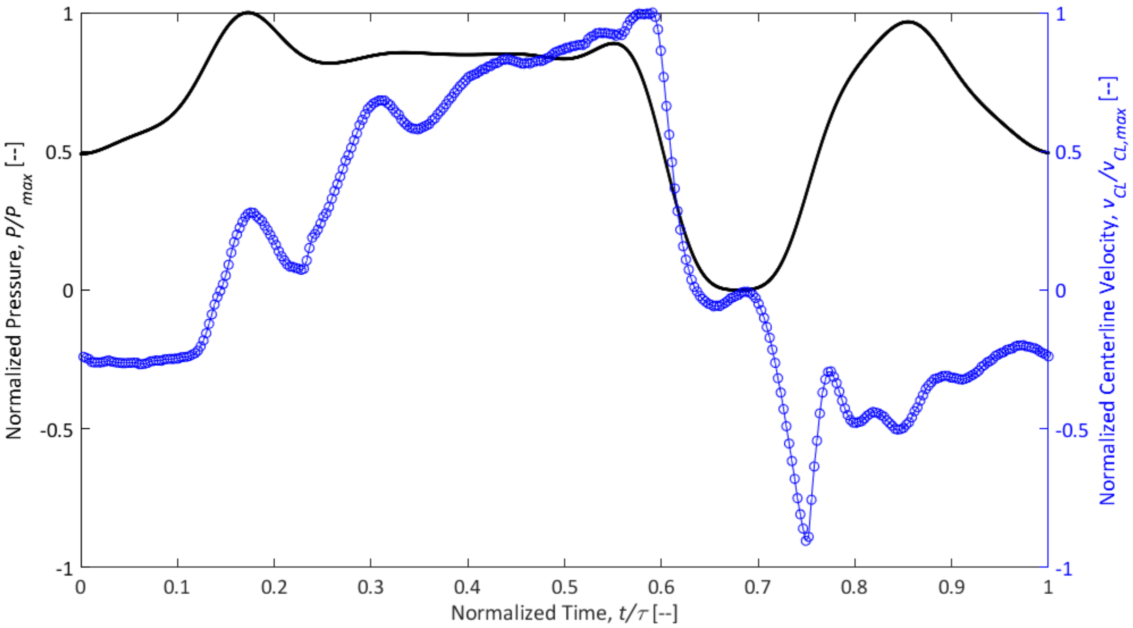

Figure A-36: Plot of normalized central aortic pressure waveform (P/P_{max}) and peripheral centerline velocity ($v_{CL}/v_{CL,max}$) for rigid case with $\omega_{AL\ pump}$ = 1540 RPM

A-1.4 VAD Experiment – Compliant Mock Aorta Case

This appendix provides plots of normalized pressure, normalized centerline velocity and tube distension over one normalized pump cycle for all tested compliant mock aorta VAD experimental conditions.

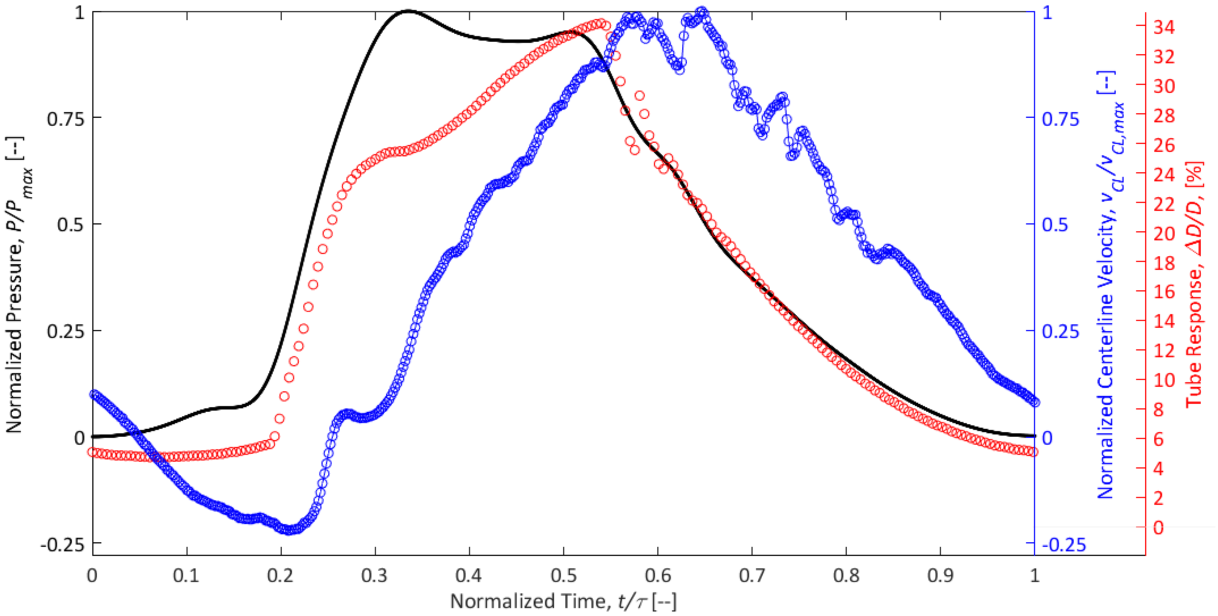

Figure A-37: Plot of normalized central aortic pressure waveform (*P/P_{max}*), normalized peripheral centerline velocity (*$v_{CL}/v_{CL,max}$*) and tube distension (*$\Delta D/D$*) for mock aorta case with *P_{ch}* = 103 mmHg and *$\omega_{AL\ pump}$* = 980 RPM

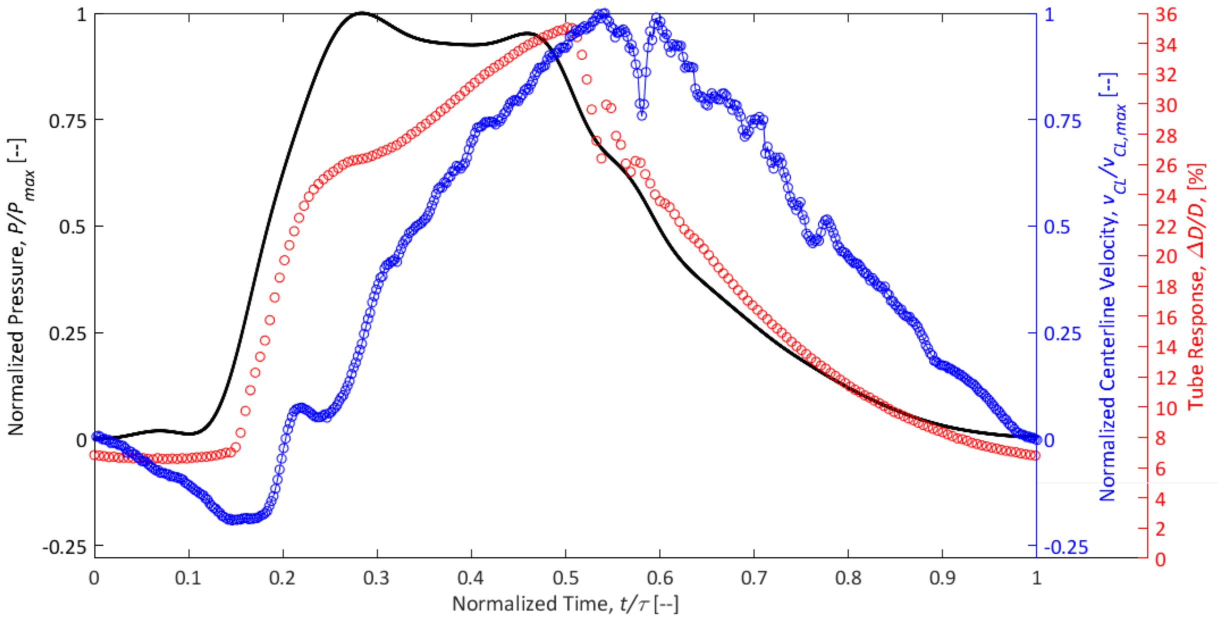

Figure A-38: Plot of normalized central aortic pressure waveform (P/P_{max}), normalized peripheral centerline velocity ($v_{CL}/v_{CL,max}$) and tube distension ($\Delta D/D$) for mock aorta case with P_{ch} = 103 mmHg and $\omega_{AL\ pump}$ = 1065 RPM

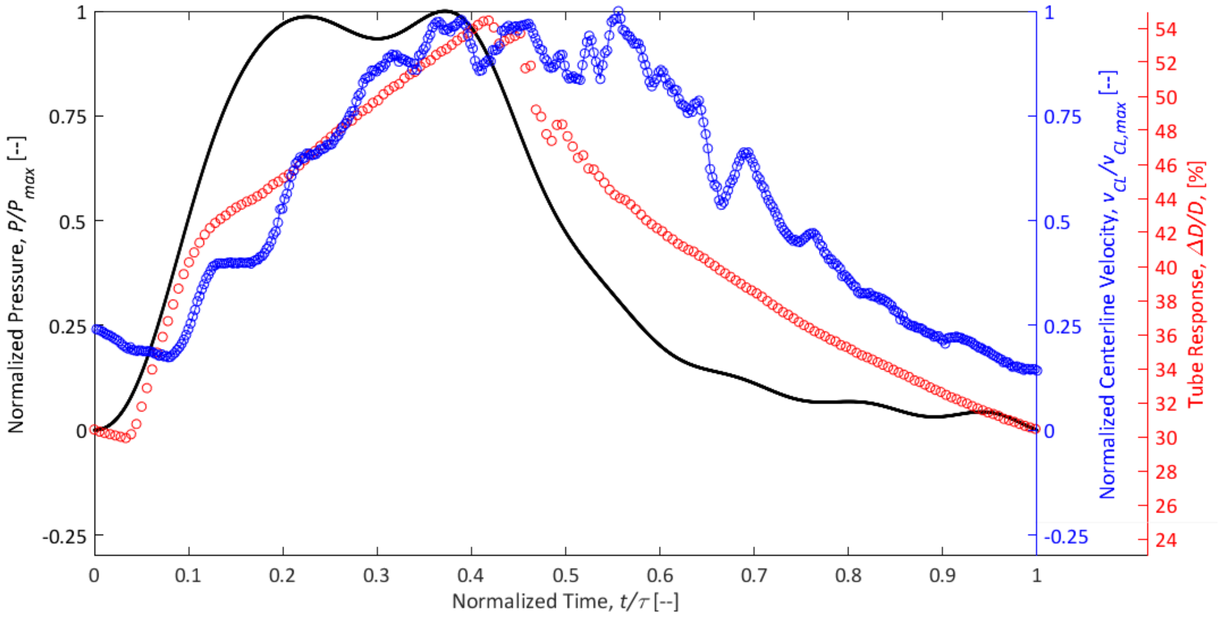

Figure A-39: Plot of normalized central aortic pressure waveform (P/P_{max}), normalized peripheral centerline velocity ($v_{CL}/v_{CL,max}$) and tube distension ($\Delta D/D$) for mock aorta case with P_{ch} = 103 mmHg and $\omega_{AL\ pump}$ = 1450 RPM

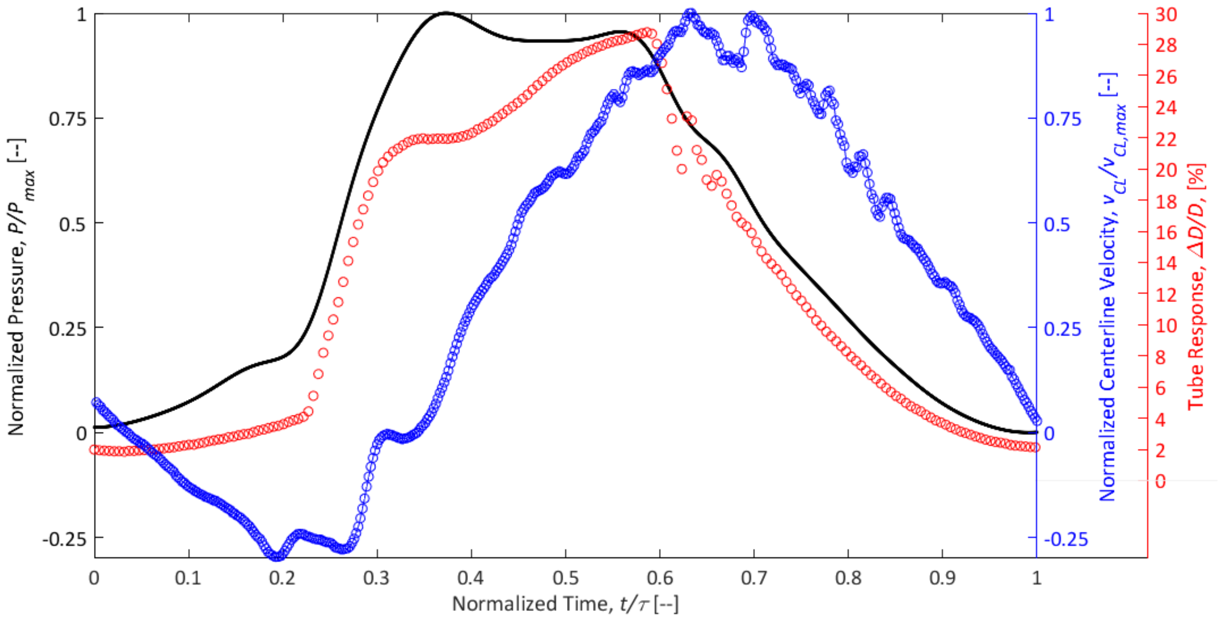

Figure A-40: Plot of normalized central aortic pressure waveform (P/P_{max}), normalized peripheral centerline velocity ($v_{CL}/v_{CL,max}$) and tube distension ($\Delta D/D$) for mock aorta case with P_{ch} = 155 mmHg and $\omega_{AL\ pump}$ = 980 RPM

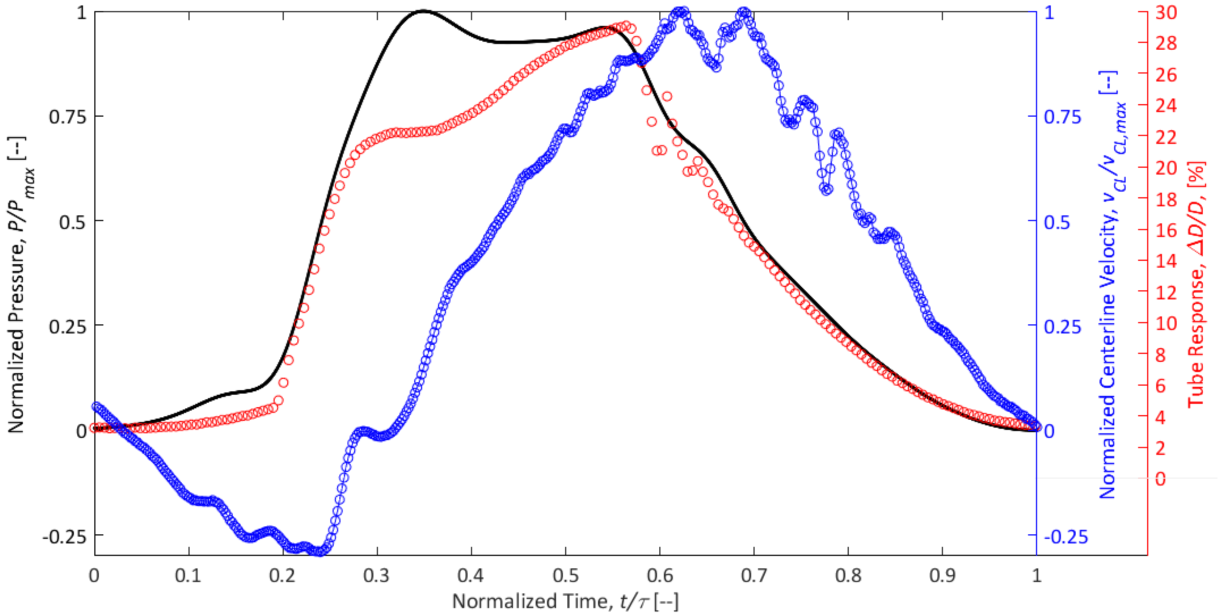

Figure A-41: Plot of normalized central aortic pressure waveform (P/P_{max}), normalized peripheral centerline velocity ($v_{CL}/v_{CL,max}$) and tube distension ($\Delta D/D$) for mock aorta case with P_{ch} = 155 mmHg and $\omega_{AL\ pump}$ = 1065 RPM

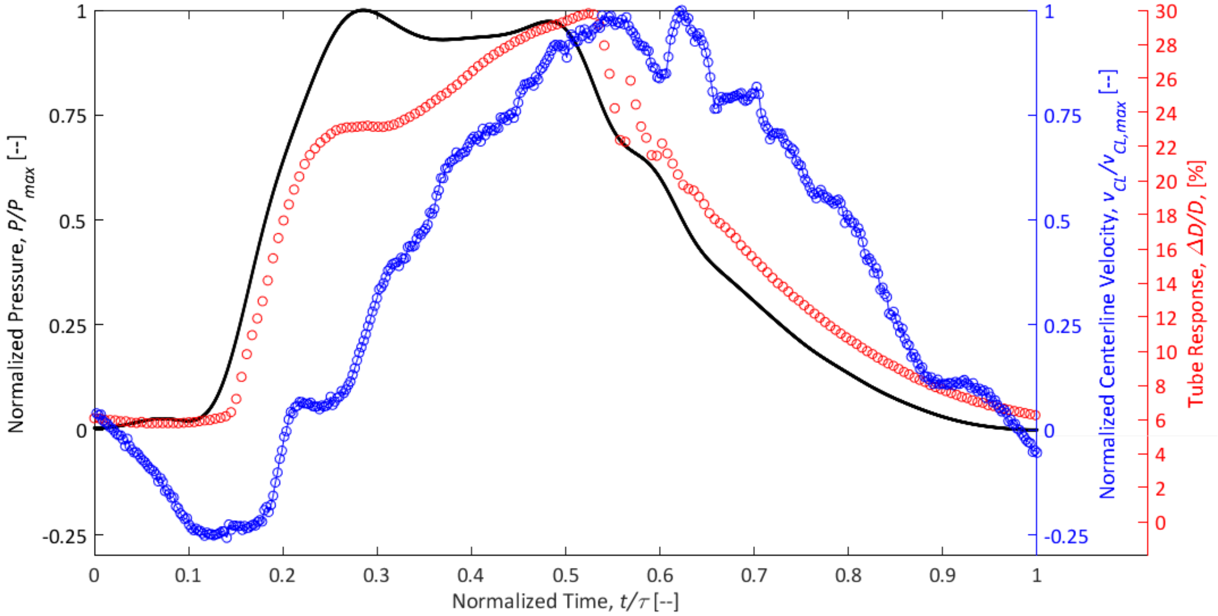

Figure A-42: Plot of normalized central aortic pressure waveform (P/P_{max}), normalized peripheral centerline velocity ($v_{CL}/v_{CL,max}$) and tube distension ($\Delta D/D$) for mock aorta case with P_{ch} = 155 mmHg and $\omega_{AL\ pump}$ = 1235 RPM

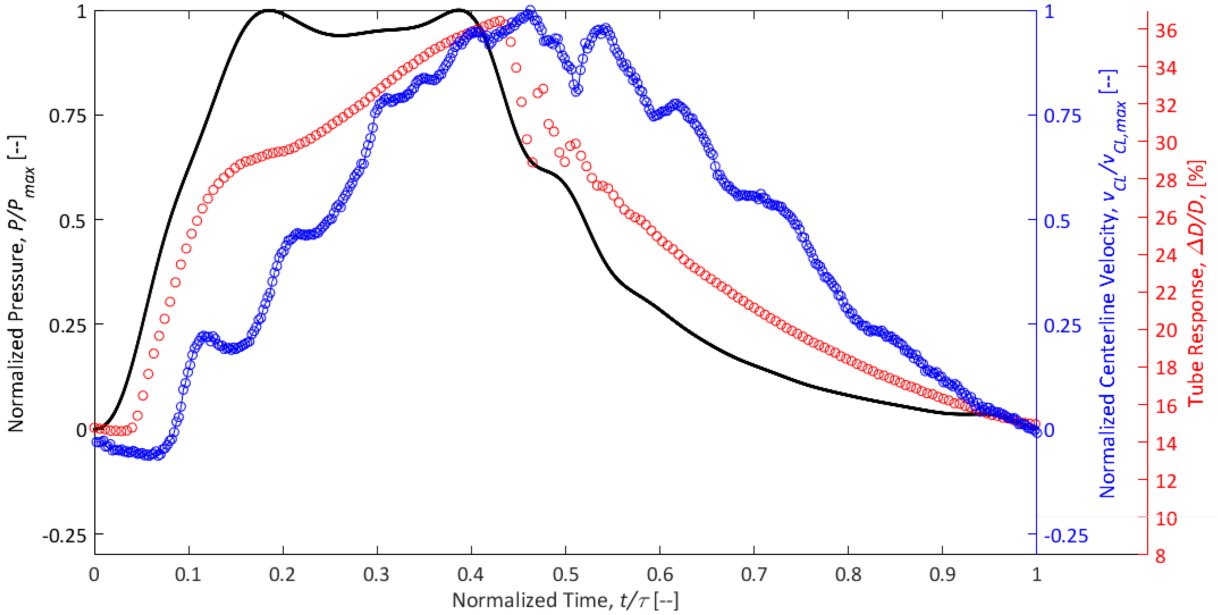

Figure A-43: Plot of normalized central aortic pressure waveform (P/P_{max}), normalized peripheral centerline velocity ($v_{CL}/v_{CL,max}$) and tube distension ($\Delta D/D$) for mock aorta case with P_{ch} = 155 mmHg and $\omega_{AL\ pump}$ = 1450 RPM

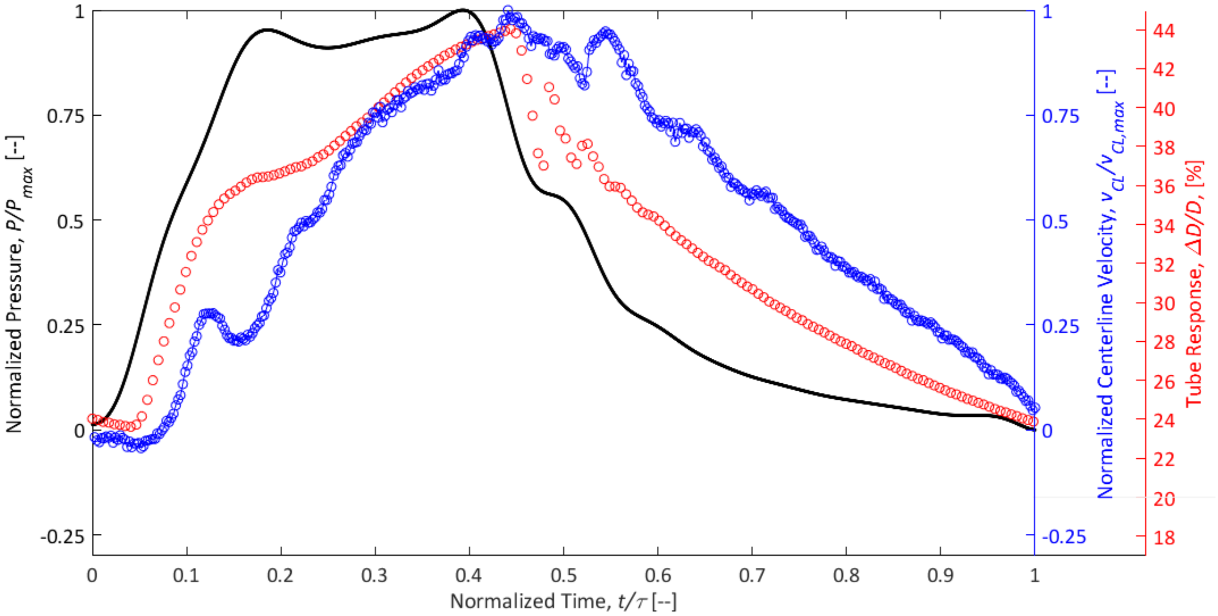

Figure A-44: Plot of normalized central aortic pressure waveform (*P/P_{max}*), normalized peripheral centerline velocity (*$v_{CL}/v_{CL,max}$*) and tube distension (*$\Delta D/D$*) for mock aorta case with *P_{ch}* = 155 mmHg and *$\omega_{AL\ pump}$* = 1540 RPM

A-2. Drawings

A-2.1 Imaging Section Base

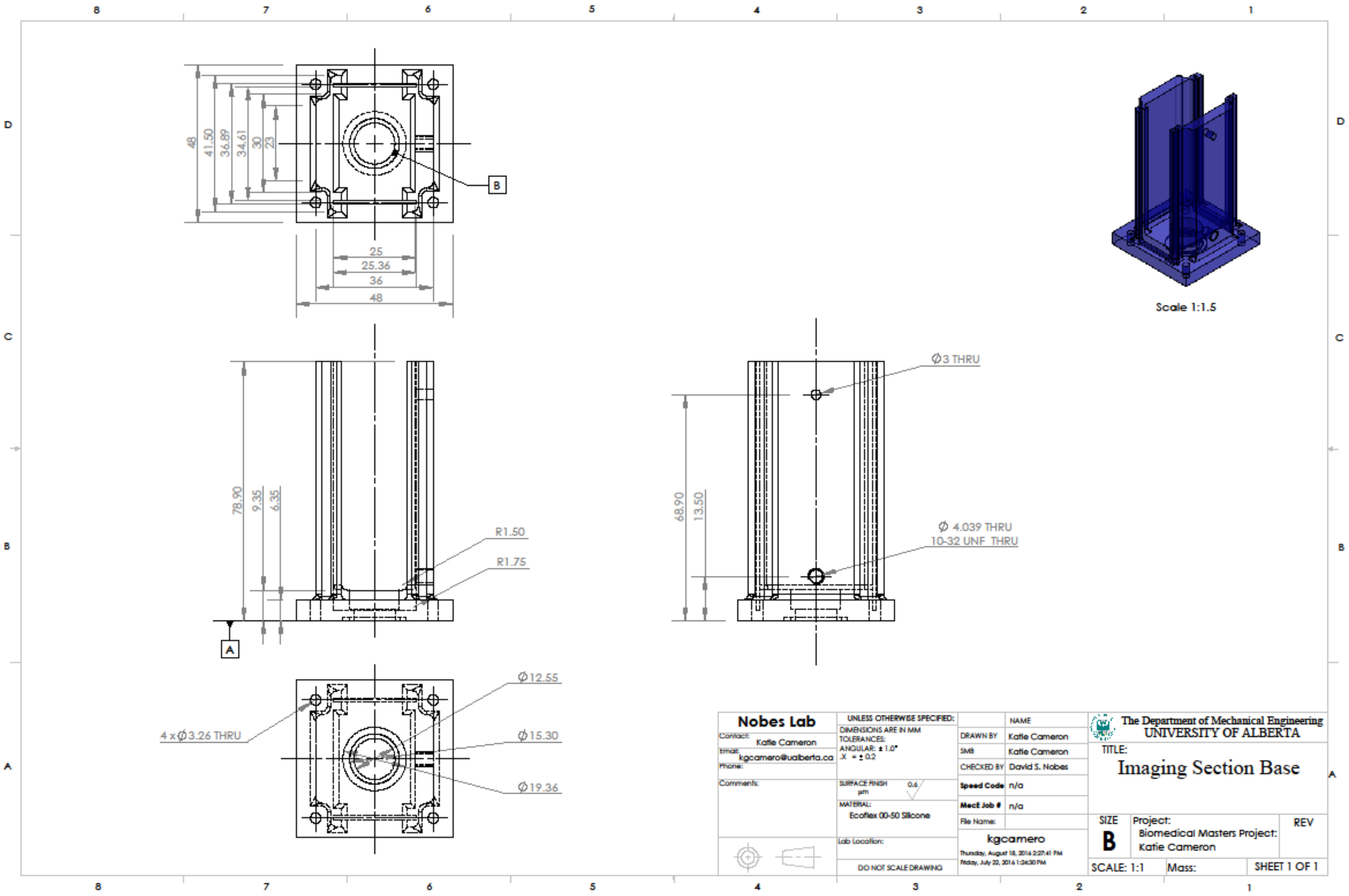

Nobes Lab
Contact: Katie Cameron
Email: kgcamero@ualberta.ca
Phone:
Comments:

UNLESS OTHERWISE SPECIFIED:
DIMENSIONS ARE IN MM
TOLERANCES:
ANGULAR: ± 1.0°
.X = ± 0.2
SURFACE FINISH µm 0.6
MATERIAL: Ecoflex 00-50 Silicone
Lab Location:
DO NOT SCALE DRAWING

	NAME
DRAWN BY	Katie Cameron
SMB	Katie Cameron
CHECKED BY	David S. Nobes
Speed Code	n/a
MecE Job #	n/a
File Name:	

kgcamero
Thursday, August 18, 2016 2:27:41 PM
Friday, July 22, 2016 1:24:30 PM

The Department of Mechanical Engineering
UNIVERSITY OF ALBERTA
TITLE:
Imaging Section Base
SIZE B
Project: Biomedical Masters Project: Katie Cameron
REV
SCALE: 1:1
Mass:
SHEET 1 OF 1

Figure A-45: Detailed drawing of imaging section base

A-2.2 Imaging Section Lid

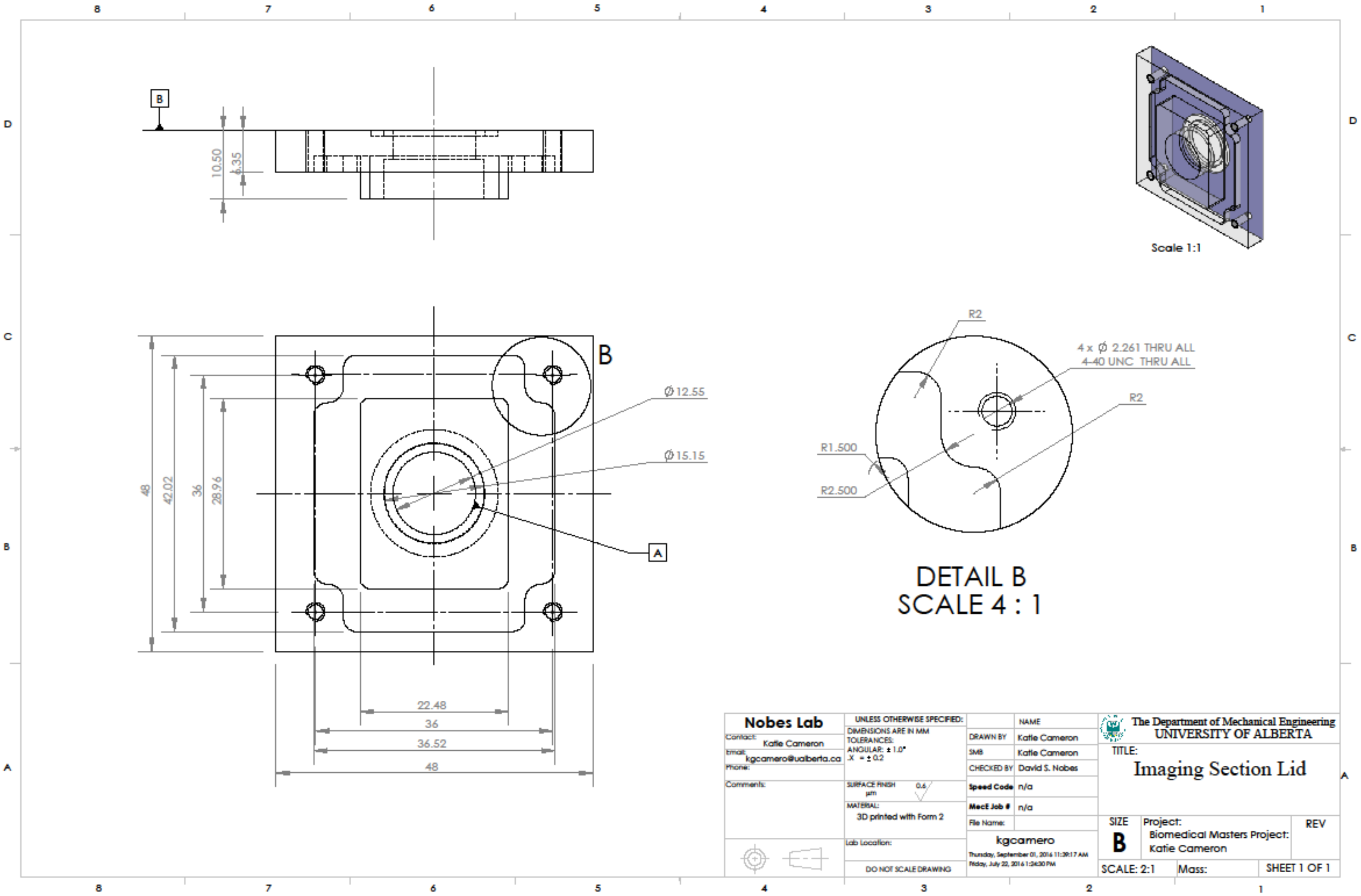

Nobes Lab
Contact: Katie Cameron
Email: kgcamero@ualberta.ca
Phone:
Comments:

UNLESS OTHERWISE SPECIFIED:
DIMENSIONS ARE IN MM
TOLERANCES:
ANGULAR: ± 1.0°
.X = ± 0.2
SURFACE FINISH µm 0.6
MATERIAL: 3D printed with Form 2
Lab Location:
DO NOT SCALE DRAWING

	NAME
DRAWN BY	Katie Cameron
SMB	Katie Cameron
CHECKED BY	David S. Nobes
Speed Code	n/a
MecE Job #	n/a
File Name:	

kgcamero
Thursday, September 01, 2016 11:39:17 AM
Friday, July 22, 2016 1:24:30 PM

The Department of Mechanical Engineering
UNIVERSITY OF ALBERTA
TITLE: Imaging Section Lid
SIZE B
Project: Biomedical Masters Project: Katie Cameron
REV
SCALE: 2:1
Mass:
SHEET 1 OF 1

Figure A-46: Detailed drawing of imaging section lid

A-2.3 Mock Aorta Mould Base

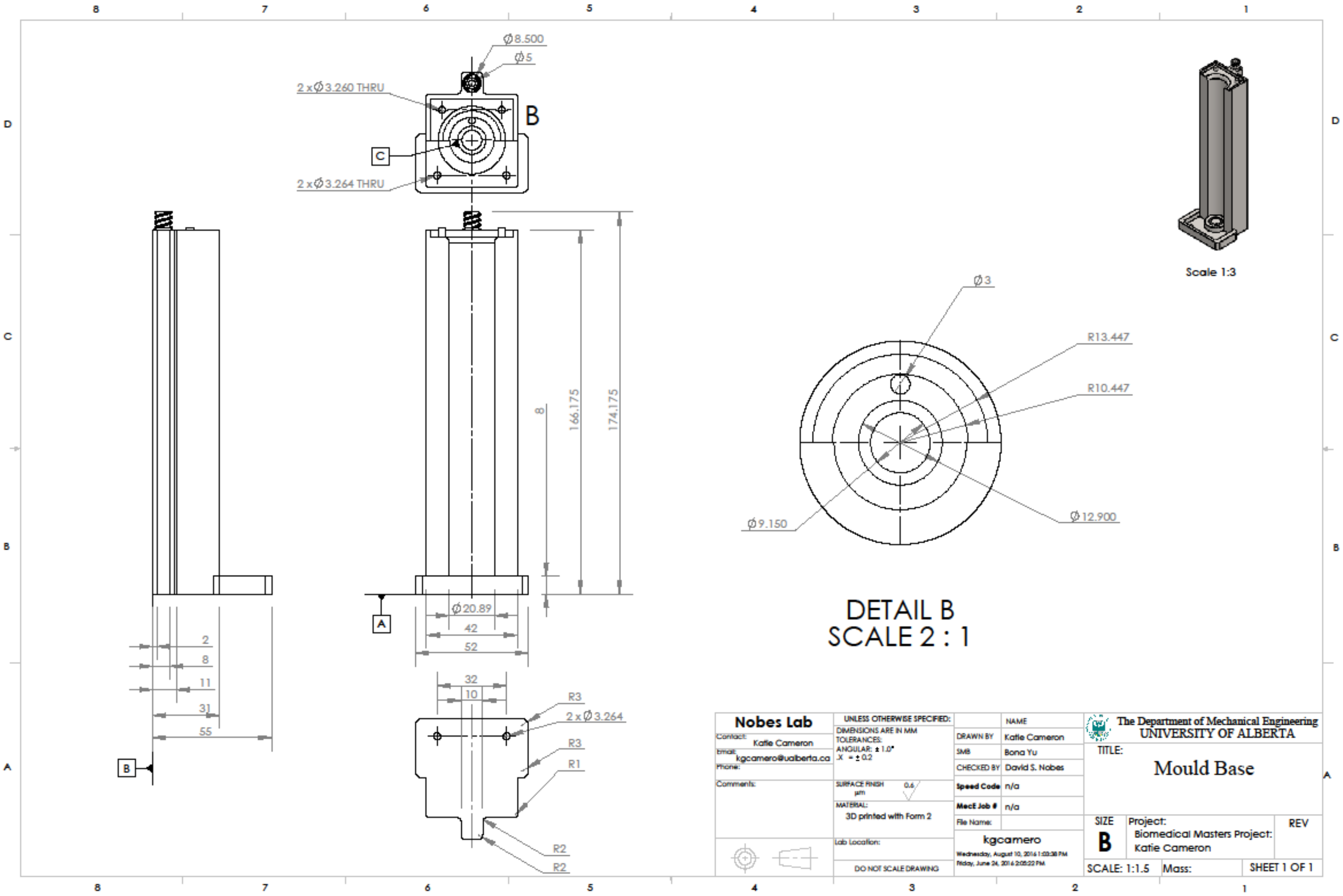

Nobes Lab

Contact: Katie Cameron
Email: kgcamero@ualberta.ca
Phone:
Comments:

UNLESS OTHERWISE SPECIFIED:
DIMENSIONS ARE IN MM
TOLERANCES:
ANGULAR: ± 1.0°
.X = ± 0.2
SURFACE FINISH µm 0.6
MATERIAL: 3D printed with Form 2
Lab Location:
DO NOT SCALE DRAWING

	NAME
DRAWN BY	Katie Cameron
SMB	Bona Yu
CHECKED BY	David S. Nobes
Speed Code	n/a
MecE Job #	n/a
File Name:	

kgcamero
Wednesday, August 10, 2016 1:03:38 PM
Friday, June 24, 2016 2:05:22 PM

The Department of Mechanical Engineering
UNIVERSITY OF ALBERTA
TITLE: Mould Base
SIZE B
Project: Biomedical Masters Project: Katie Cameron
REV
SCALE: 1:1.5
Mass:
SHEET 1 OF 1

Figure A-47: Detailed drawing of mould base

A-2.4 Mock Aorta Mould Side

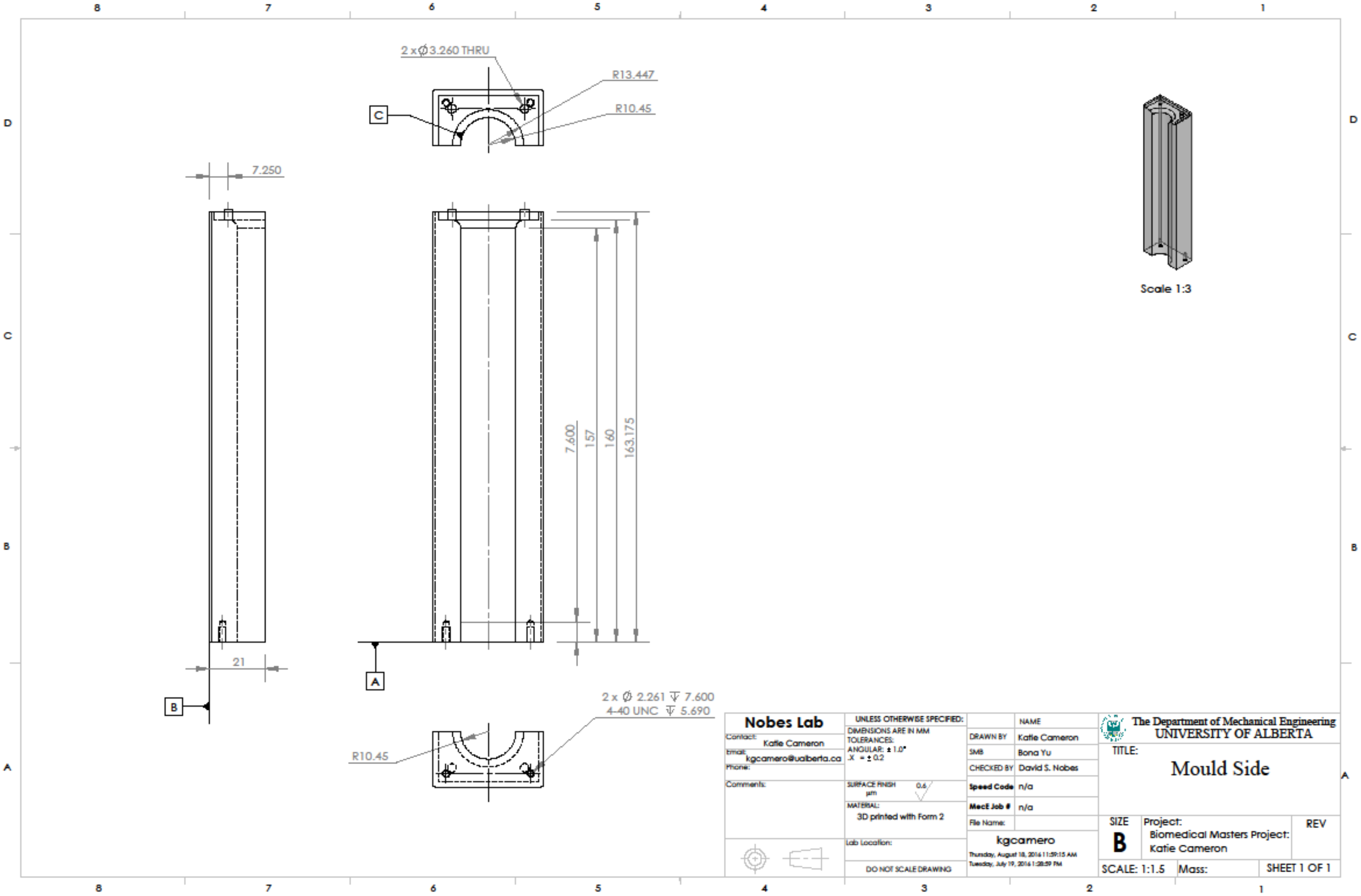

Figure A-48: Detailed drawing of mould side

A-2.5 Mock Aorta Mould Center Piece

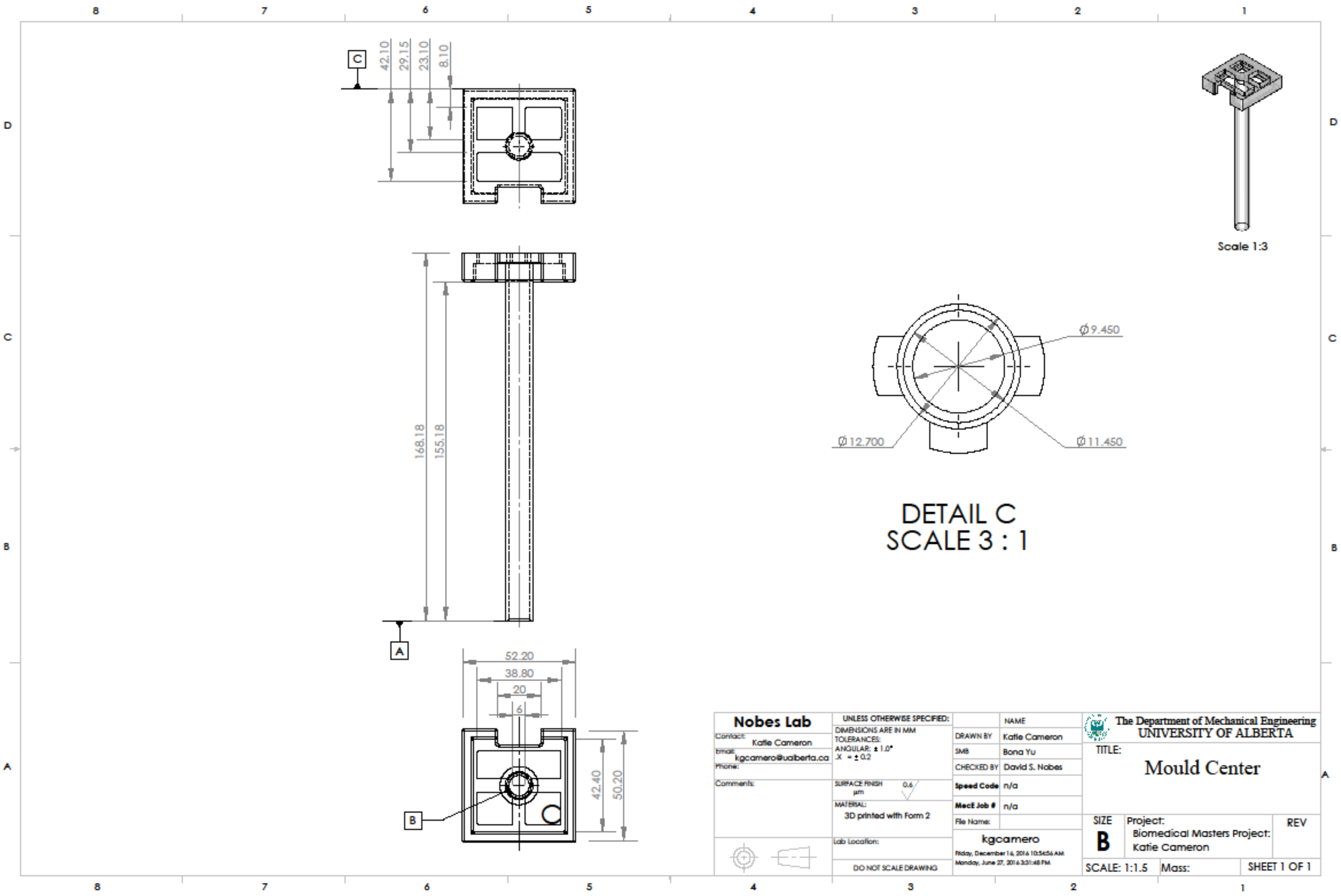

Nobes Lab
Contact: Katie Cameron
Email: kgcamero@ualberta.ca
Phone:
Comments:
UNLESS OTHERWISE SPECIFIED:
DIMENSIONS ARE IN MM
TOLERANCES:
ANGULAR: ± 1.0°
.X = ± 0.2
SURFACE FINISH µm 0.6
MATERIAL: 3D printed with Form 2
Lab Location:
DO NOT SCALE DRAWING

	NAME
DRAWN BY	Katie Cameron
SMB	Bona Yu
CHECKED BY	David S. Nobes
Speed Code	n/a
MecE Job #	n/a
File Name:	

kgcamero
Friday, December 16, 2016 10:54:56 AM
Monday, June 27, 2016 3:31:48 PM

The Department of Mechanical Engineering
UNIVERSITY OF ALBERTA
TITLE: Mould Center
SIZE B
Project: Biomedical Masters Project: Katie Cameron
REV
SCALE: 1:1.5
Mass:
SHEET 1 OF 1

Figure A-49: Detailed drawing of mould center piece

A-2.6 Peristaltic Pump Experiment Mock Aorta Bracket Connector

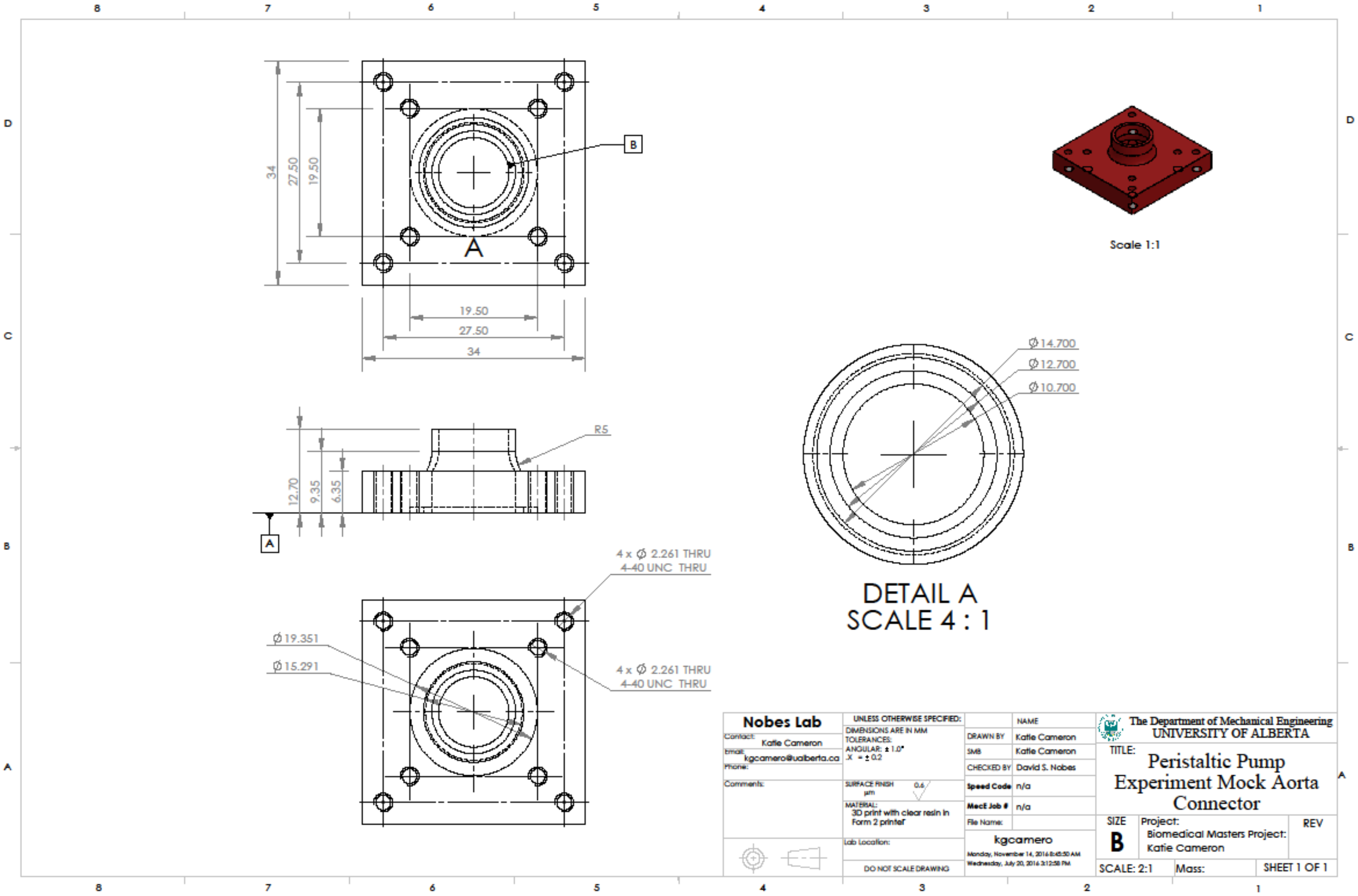

Figure A-50: Detailed drawing of peristaltic pump experiment mock aorta bracket connector

A-2.7 Peristaltic Pump Experiment Mock Aorta Connector Sleeve

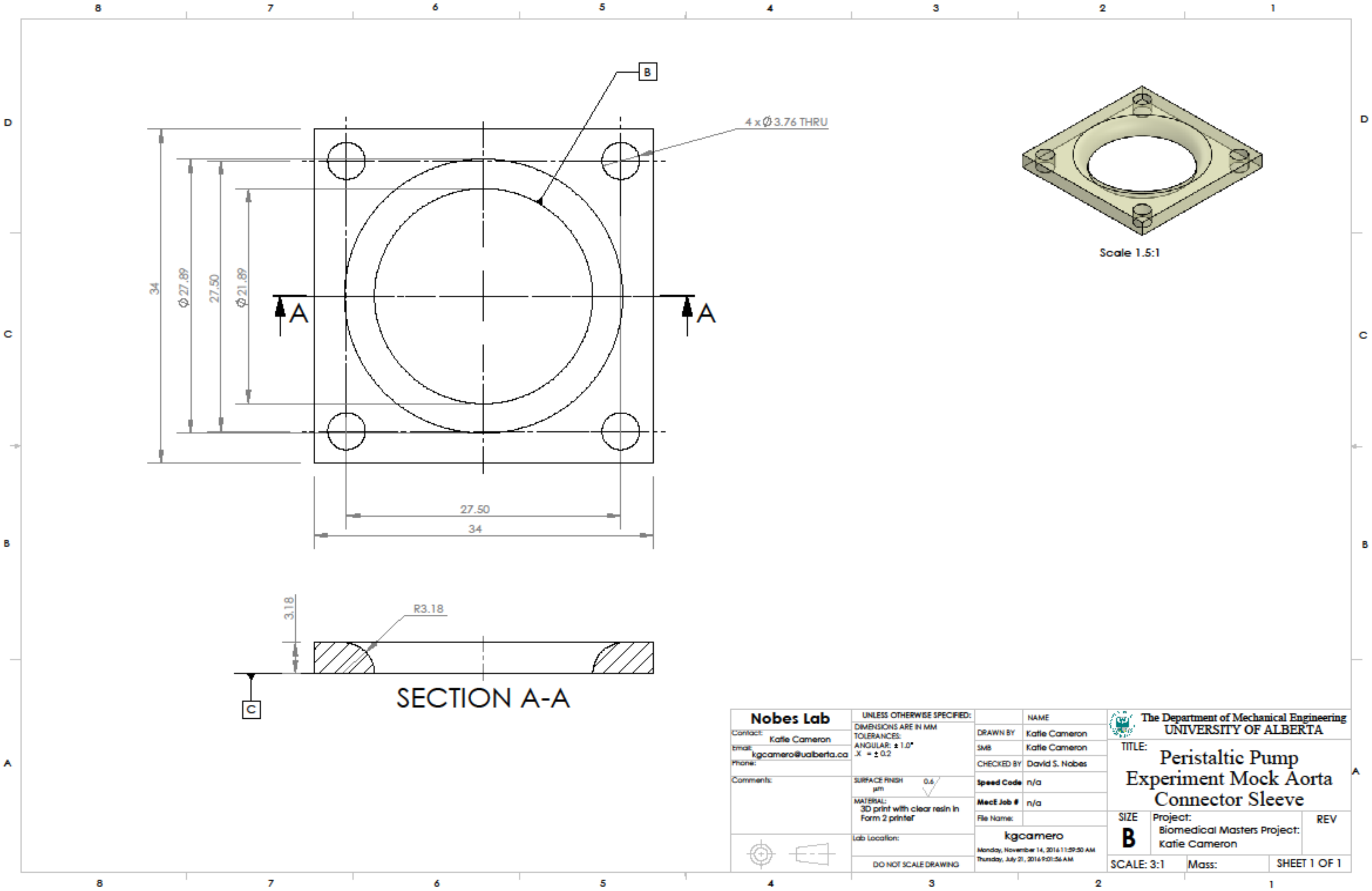

Nobes Lab
Contact: Katie Cameron
Email: kgcamero@ualberta.ca
Phone:
Comments:

UNLESS OTHERWISE SPECIFIED:
DIMENSIONS ARE IN MM
TOLERANCES:
ANGULAR: ± 1.0°
.X = ± 0.2
SURFACE FINISH µm 0.6
MATERIAL: 3D print with clear resin in Form 2 printer
Lab Location:
DO NOT SCALE DRAWING

	NAME
DRAWN BY	Katie Cameron
SMB	Katie Cameron
CHECKED BY	David S. Nobes
Speed Code	n/a
MecE Job #	n/a
File Name:	

kgcamero
Monday, November 14, 2016 11:59:50 AM
Thursday, July 21, 2016 9:01:56 AM

The Department of Mechanical Engineering
UNIVERSITY OF ALBERTA
TITLE: Peristaltic Pump Experiment Mock Aorta Connector Sleeve
SIZE B
Project: Biomedical Masters Project: Katie Cameron
REV
SCALE: 3:1
Mass:
SHEET 1 OF 1

Figure A-51: Detailed drawing of peristaltic pump experiment mock aorta bracket connector sleeve

A-2.8 Mock Aorta Pressure Chamber Top

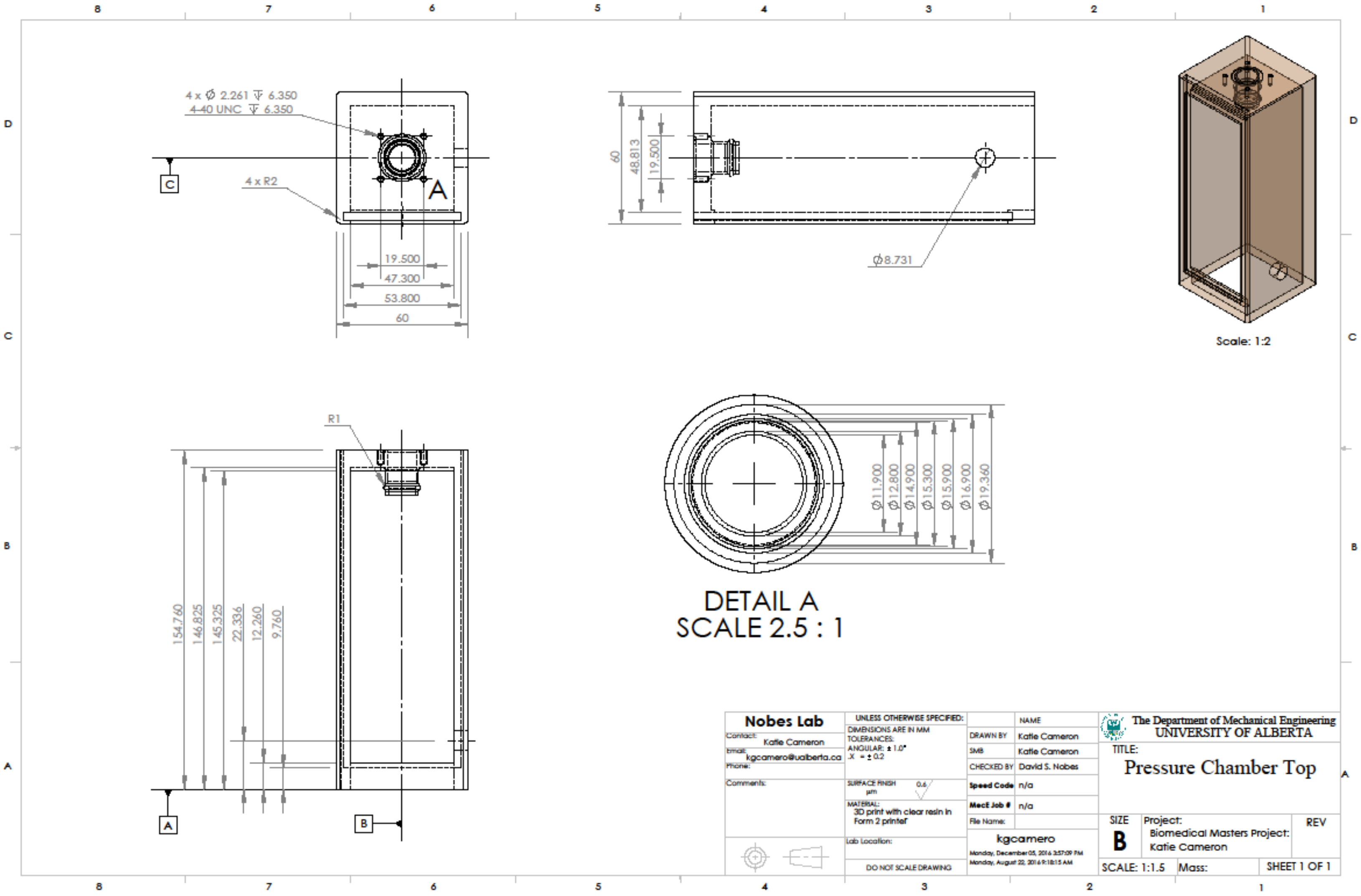

Figure A-52: Detailed drawing of mock aorta pressure chamber top

A-2.9 Mock Aorta Pressure Chamber Base Bracket

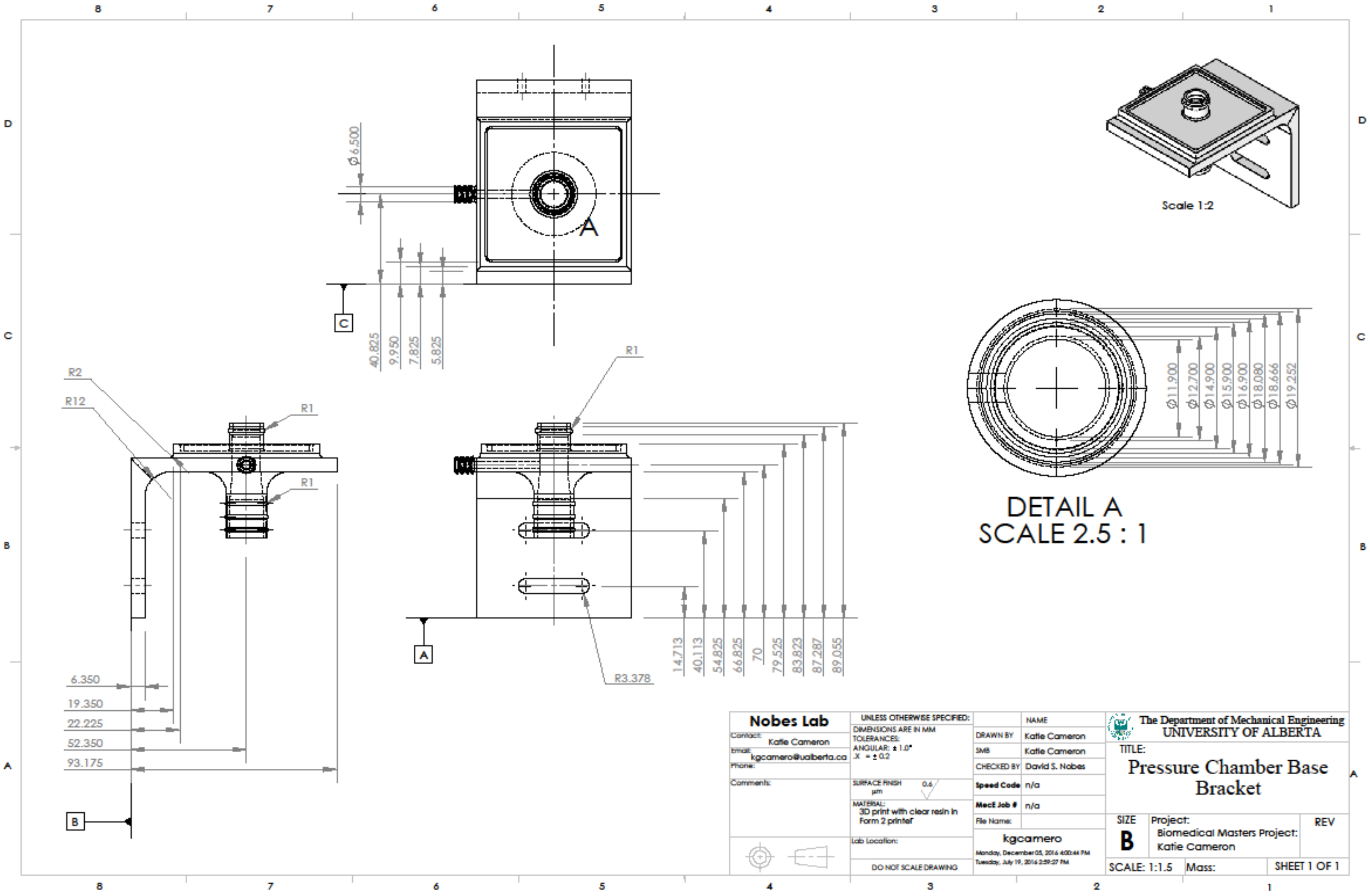

Figure A-53: Detailed drawing of mock aorta pressure chamber base bracket

A-2.10 VAD Mount

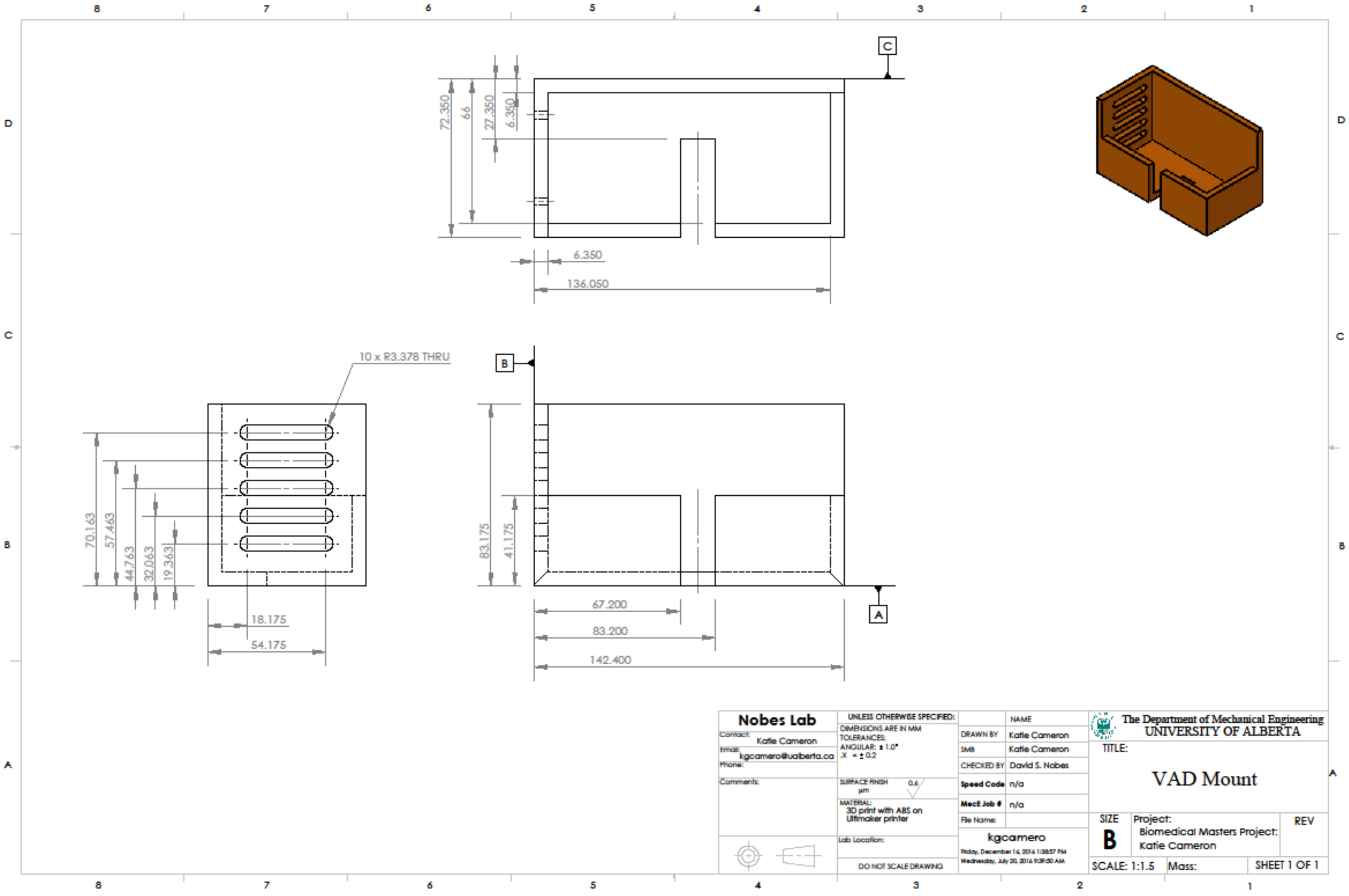

Figure A-54: Detailed drawing of VAD optical rail mount

A-3. Matlab Code

A-3.1 Matlab function used for zero-phase digital filtering of pressure waveforms

```
function fPressure=LPButterworthFilt(sampleRate,cutoffFq,pressure)
[B,A]=butter(4,cutoffFq/(sampleRate/2),'low');
fPressure=filtfilt(B,A,pressure);
end
```

A-3.2 Matlab code used to generate pressure data plots from Sections 3.1 and 4.2

```
close all
clear

fig1=figure;
fig2=figure; set(fig2,'position',[300 100 1100 500]);
fig3=figure;set(fig3,'position',[300 100 1100 500])
fig4=figure; set(fig4,'position',[100 200 300 175])
fig5=figure; set(fig5,'position',[100 200 300 175])

fileNameR='F:\UPDATED RESULTS (NOV)\Nov10\Nov10_PP_25RPM_Volt.log'; %pressure data
fileNameC='F:\UPDATED RESULTS (NOV)\Nov14\Water Pressure Files\Nov14_PPC_25RPM_Volt.log';
%pressure data
freq=1.667;
harmonics=4;

%transducer A
A_slope=0.0149;
A_int=0.0645;

%Marcus transducer C
C_slope=0.0149; %Marcus calibration
C_int=0.0003;

timeR=dlmread(fileNameR,'\t','A8..A15007'); %times
timeC=dlmread(fileNameC,'\t','A8..A15007'); %times
greenTriggerR=dlmread(fileNameR,'\t','C8..C15007');
greenTriggerC=dlmread(fileNameC,'\t','C8..C15007');
baslerTriggerR=dlmread(fileNameR,'\t','D8..D15007');
baslerTriggerC=dlmread(fileNameC,'\t','D8..D15007');
sampleRate=1000; %sampling frequency
frameRate = 113; %green camera
sampleNumber = length(timeR);
```

```
cycleTime=1/freq;
cycleIndex = round(cycleTime*sampleRate);

VoutImSectR=dlmread(fileNameR,'\t','F8..F15007'); %imaging section outlet
VinAortaR=dlmread(fileNameR,'\t','I8..I15007'); %aorta inlet

VoutImSectC=dlmread(fileNameC,'\t','F8..F15007'); %imaging section outlet
VinAortaC=dlmread(fileNameC,'\t','I8..I15007'); %aorta inlet

PoutImSectR=(VoutImSectR-C_int)/C_slope;
PinAortaR=(VinAortaR-A_int)/A_slope;

PoutImSectC=(VoutImSectC-C_int)/C_slope;
PinAortaC=(VinAortaC-A_int)/A_slope;

PoutImSect3=(VoutImSectC-C_int)/C_slope;
PinAorta3=(VinAortaC-A_int)/A_slope;

%filtered pressure wave
fPoutImSectR=LPButterworthFilt(sampleRate,freq*harmonics,PoutImSectR);
fPinAortaR=LPButterworthFilt(sampleRate,freq*harmonics,PinAortaR);

fPoutImSectC=LPButterworthFilt(sampleRate,freq*harmonics,PoutImSectC);
fPinAortaC=LPButterworthFilt(sampleRate,freq*harmonics,PinAortaC);

%RIGID------------------------------------------------------------------------
for i = 1:length(timeR)
    if greenTriggerR(i,1) > 9
        triggerIndexR = i;
        break
    end
end

%find minimum to start cycle from beginning of pressure pulse
firstTriggerCycleR=fPinAortaR(triggerIndexR:triggerIndexR+cycleIndex);
[pksR,pklocsR] = findpeaks(-firstTriggerCycleR);
pksR=-pksR;
[~,minIdxR] = min(pksR);
localMinIndexR=pklocsR(minIdxR);
firstMinIndexR=localMinIndexR+triggerIndexR;

%create new array for one cycle starting at first diastolic min
multiCycleTimeR=timeR(firstMinIndexR:firstMinIndexR+5*cycleIndex);
normMultiCycleTimeR=(multiCycleTimeR-min(multiCycleTimeR))*freq;
multiCyclePressureR = fPinAortaR(firstMinIndexR:(firstMinIndexR+5*cycleIndex)); %inlet waveform
using startframe of inlet wave

%COMPLIANT-------------------------------------------------------------------
for j = 1:length(timeC)
    if greenTriggerC(j,1) > 9
        triggerIndexC = j;
        break
    end
end
```

```
%find minimum to start cycle from beginning of pressure pulse
firstTriggerCycleC=fPinAortaC(triggerIndexC:triggerIndexC+cycleIndex);
[pksC,pklocsC] = findpeaks(-firstTriggerCycleC);
pksC=-pksC;
[~,minIdxC] = min(pksC);
localMinIndexC=pklocsC(minIdxC);
firstMinIndexC=localMinIndexC+triggerIndexC;

%2cycles
noCycles=2;
twoCycles=fPinAortaC(firstMinIndexC:firstMinIndexC+(noCycles*(1/freq)*sampleRate));
twoCyclesTime=timeC(firstMinIndexC:firstMinIndexC+(noCycles*(1/freq)*sampleRate));
twoCyclesOffsetTime=twoCyclesTime-min(twoCyclesTime);
twoCyclesNormTime=noCycles*twoCyclesOffsetTime/max(twoCyclesOffsetTime);

% %create new array for multiples cycles starting at first diastolic min
noCycles2=5;
multiCycleTimeC=timeC(firstMinIndexC:firstMinIndexC+noCycles2*cycleIndex);
normMultiCycleTimeC=(multiCycleTimeC-min(multiCycleTimeC))*freq;
multiCyclePressureC = fPinAortaC(firstMinIndexC:(firstMinIndexC+noCycles2*cycleIndex)); %inlet
waveform using startframe of inlet wave

%plot all collected data together
figure(fig1)
plot(timeC,greenTriggerC,'g-')
hold on
plot(timeC,baslerTriggerC,'r-')
plot(timeC,VinAortaC,'k.-')
plot(timeC,VoutImSectC,'b.-')

xlim([0 15]);
ylim([-1 5]);

hold off
ylabel('Voltage, {\itV} [V]');
xlabel('Time, {\itt} [s]');
set(fig1,'Position',[100 200 1100 500]);
L=legend('Camera 2 Trigger Function','Camera 1 Trigger Function','Test Section Entrance Pressure
Transducer','Imaging Section Exit Pressure Transducer')
set(L,'Location','eastoutside')
L.FontSize=12;
ax=gca;
ax.FontSize=14;
ax.FontName='Calibri';
set(ax,'LooseInset',get(ax,'TightInset'));

%compare unfiltered data to filtered waveform for compliant case
figure(fig2)
h1=plot(twoCyclesNormTime,PinAortaC(firstMinIndexC:firstMinIndexC+(noCycles*(1/freq)*sampleRate))
,'k.');
h1.MarkerSize=7;
hold on
h2=plot(twoCyclesNormTime, twoCycles,'b.-');
```

```
h2.MarkerSize=5
hold off
xlim([0 2]);
xlabel('Normalized Time, {\itt/\tau} [--]');
ylabel('Pressure, {\itP} [mmHg]')
L2=legend('Unfiltered Data', 'Filtered Waveform');
set(L2,'Location','eastoutside');
L2.FontSize=12;
ax=gca;
ax.FontSize=14;
ax.FontName='Calibri';
set(ax,'LooseInset',get(ax,'TightInset'));

%multi cycle rigid compliant comparison
figure(fig3)
h3=plot(normMultiCycleTimeR,multiCyclePressureR,'k.-');
hold on
h4=plot(normMultiCycleTimeC,multiCyclePressureC,'b.-');
h3.MarkerSize=5;
h4.MarkerSize=5;
xlim([0 3]);
ylim([0 35]);
xlabel('Normalized Time, {\itt/\tau} [--]');
ylabel('Pressure, {\itP} [mmHg]')
L3=legend('Rigid Case', 'Compliant Case');
set(L3,'Location','southeast');
ax=gca;
ax.FontSize=14;
ax.FontName='Calibri';
set(ax,'LooseInset',get(ax,'TightInset'));

%zoomed view of basler trigger function
figure(fig4);
plot(timeC,VinAortaC,'k.-')
hold on
plot(timeC,VoutImSectC,'b.-')
% plot(timeC,greenTriggerC,'g-')
plot(timeC,baslerTriggerC,'r-')
xlim([8.24 8.32]);
ylim([-0.1 10.2]);
xlabel('Time,{\itt} [s]');
ylabel('Voltage,{\itV} [V]');
ax=gca;
ax.FontSize=8;
ax.FontName='Calibri';
set(ax,'LooseInset',get(ax,'TightInset'));

%zoomed view of green camera trigger function
figure(fig5);
plot(timeC,VinAortaC,'k.-')
hold on
plot(timeC,VoutImSectC,'b.-')
plot(timeC,greenTriggerC,'g-')
xlim([3.4 3.46]);
```

```
ylim([-0.1 10.4]);
xlabel('Time,{\itt} [s]');
ylabel('Voltage,{\itV} [V]');
ax=gca;
ax.FontSize=8;
ax.FontName='Calibri';
set(ax,'LooseInset',get(ax,'TightInset'));
```

A-3.3 Matlab code used to generate plot of frequency vs. pressure presented in Section 4.7.1

```
close all
clear

fig1=figure;
% fig2=figure; set(fig2,'position',[300 100 1100 500]);
% fig3=figure;set(fig3,'position',[300 100 1100 500])
% fig4=figure;
% fig5=figure; fig6=figure;

path='F:\UPDATED RESULTS (NOV)\Nov15\Poly Pressure Files\';
fnames = dir(path);
count=0;

%transducer A
A_slope=0.0149;
A_int=0.0645;
harmonics=4;
sampleRate=1000;
frameRate = 113; %green camera

for i=3:length(fnames)
    count=count+1;
    ind(count)=strfind(fnames(i).name,'RPM');
    if ind(count)==17
        freq(count)=str2num(fnames(i).name(ind(count)-2:ind(count)-1));
    elseif ind(count)==19
        freq(count)=str2num(fnames(i).name(ind(count)-4:ind(count)-1));
    end
    freq(count)=(4*freq(count))/60;
    cycleTime(count)=1/freq(count);
    cycleIndex(count)=round(cycleTime(count)*sampleRate);
    %load pressure data
    fileLoc=fnames(i).name;
    fileName=strcat(path,fileLoc);

            delimiter = '\t';
            startRow = 8;
            formatSpec = 
'%f%*s%f%*s%*s%*s%*s%*s%f%*s%[^\n\r]';%f%*s%*s';%*s%*s%f%*s%*s%f%*s%*s%[^\n\r]';
            fileID = fopen(char(fileName)),'r';
            dataArray = textscan(fileID, formatSpec, 'Delimiter', delimiter, 'EmptyValue'
,NaN,'HeaderLines' ,startRow-1, 'ReturnOnError', false);
            fclose(fileID);
            time(:,count)=dataArray{1,1};
            greenTrigger(:,count)=dataArray{1,2};
                for j = 1:length(time)
                    if greenTrigger(j,count) > 9
                    triggerIndex(count) = j;
                    break
```

```
                    end
                end
            VinAorta(:,count)=dataArray{1,3};
            PinAorta(:,count)=(VinAorta(:,count)-A_int)/A_slope;

fPinAorta(:,count)=LPButterworthFilt(sampleRate,freq(count)*harmonics,PinAorta(:,count));
            [pks,pklocs]=findpeaks(-fPinAorta(:,count));
            pks=-pks;
            minIdx(count)=pklocs(pks==min(pks));


end

oneCycle1=fPinAorta(minIdx(1):minIdx(1)+cycleIndex(1)-1,1);
oneCycleTime1=time(minIdx(1):minIdx(1)+cycleIndex(1)-1,1);
offsetCycleTime1=oneCycleTime1-min(oneCycleTime1);
normCycleTime1=offsetCycleTime1/max(offsetCycleTime1);

oneCycle2=fPinAorta(minIdx(2):minIdx(2)+cycleIndex(2)-1,2);
oneCycleTime2=time(minIdx(2):minIdx(2)+cycleIndex(2)-1,2);
offsetCycleTime2=oneCycleTime2-min(oneCycleTime2);
normCycleTime2=offsetCycleTime2/max(offsetCycleTime2);

oneCycle3=fPinAorta(minIdx(3):minIdx(3)+cycleIndex(3)-1,3);
oneCycleTime3=time(minIdx(3):minIdx(3)+cycleIndex(3)-1,3);
offsetCycleTime3=oneCycleTime3-min(oneCycleTime3);
normCycleTime3=offsetCycleTime3/max(offsetCycleTime3);

oneCycle4=fPinAorta(minIdx(4):minIdx(4)+cycleIndex(4)-1,4);
oneCycleTime4=time(minIdx(4):minIdx(4)+cycleIndex(4)-1,4);
offsetCycleTime4=oneCycleTime4-min(oneCycleTime4);
normCycleTime4=offsetCycleTime4/max(offsetCycleTime4);

oneCycle5=fPinAorta(minIdx(5)-cycleIndex(5):minIdx(5)-1,5);
oneCycleTime5=time(minIdx(5)-cycleIndex(5):minIdx(5)-1,5);
offsetCycleTime5=oneCycleTime5-min(oneCycleTime5);
normCycleTime5=offsetCycleTime5/max(offsetCycleTime5);

oneCycle6=fPinAorta(minIdx(6):minIdx(6)+cycleIndex(6)-1,6);
oneCycleTime6=time(minIdx(6):minIdx(6)+cycleIndex(6)-1,6);
offsetCycleTime6=oneCycleTime6-min(oneCycleTime6);
normCycleTime6=offsetCycleTime6/max(offsetCycleTime6);

oneCycle7=fPinAorta(minIdx(7):minIdx(7)+cycleIndex(7)-1,7);
oneCycleTime7=time(minIdx(7):minIdx(7)+cycleIndex(7)-1,7);
offsetCycleTime7=oneCycleTime7-min(oneCycleTime7);
normCycleTime7=offsetCycleTime7/max(offsetCycleTime7);

oneCycle8=fPinAorta(minIdx(8)-cycleIndex(8):minIdx(8)-1,8);
oneCycleTime8=time(minIdx(8)-cycleIndex(8):minIdx(8)-1,8);
offsetCycleTime8=oneCycleTime8-min(oneCycleTime8);
normCycleTime8=offsetCycleTime8/max(offsetCycleTime8);

oneCycle9=fPinAorta(minIdx(9)-cycleIndex(9):minIdx(9)-1,9);
```

```
oneCycleTime9=time(minIdx(9)-cycleIndex(9):minIdx(9)-1,9);
offsetCycleTime9=oneCycleTime9-min(oneCycleTime9);
normCycleTime9=offsetCycleTime9/max(offsetCycleTime9);


figure(fig1)
plot(normCycleTime1,oneCycle1,'k.-')
hold on
plot(normCycleTime2,oneCycle2,'b.-')
plot(normCycleTime3,oneCycle3,'r.-')
plot(normCycleTime4,oneCycle4,'g.-')
plot(normCycleTime5,oneCycle5,'c.-')
plot(normCycleTime6,oneCycle6,'m.-')
p7=plot(normCycleTime7,oneCycle7,'.-')
p7.Color=[0.4 0.4 0.4];
p8=plot(normCycleTime8,oneCycle8,'.-')
p8.Color=[0.8 0.5 0];
p9=plot(normCycleTime9,oneCycle9,'.-')
p9.Color=[0.5 0.6 0];
hold off
ylabel('Pressure, {\itP} [mmHg]');
xlabel('Normalized Time, {\itt/\tau} [--]');
set(fig1,'Position',[100 200 1100 650]);
L=legend('{\itf}=1.00 Hz','{\itf}=1.17 Hz','{\itf}=1.33 Hz','{\itf}=1.50 Hz','{\itf}=1.67 Hz','{\itf}=1.83 Hz','{\itf}=2.00 Hz','{\itf}=2.17 Hz','{\itf}=2.33 Hz');
set(L,'Location','eastoutside')
L.FontSize=12;
ax=gca;
ax.FontSize=14;
ax.FontName='Calibri';
set(ax,'LooseInset',get(ax,'TightInset'));
```

A-3.4 Matlab code used to plot vectors fields from Section 3.3

```
clear
close all

fig1=figure; set(fig1,'position',[100 200 800 400]);
path = 'F:\PIV Results\VAD_Results_calibration_105mm\Oct6_2PSI_1235RPM_truncated (frames 1-1064)\TR_PIV_MP(3x32x32_75%ov)_01\';
% Get files in folder
fnames = dir([path '*.VC7']);
frameRate=1000;
pixel2mm=82;
skip=1;
startFrame=350;
endFrame=startFrame; %set equal to startFrame to get one vector field
count=0;

for i = startFrame:skip:endFrame
    count = count+1;
    v_File = [path fnames(i).name];
    % Load the vector file
    VEC = loadvec(v_File);
    [x1find,~]=find(VEC.vy);
    x1=min(x1find)-3;
    x2=max(x1find)+1;

    y1=1;
    [s1 s2]=size(VEC.y);
    y2=s2;

    box = [x1 x1 x2 y2];

    CHW=(x2-x1)+1;
    CHH=(y2-y1)+1;

    VEC2 = extractf(VEC,box); % get the vectors
    VEC2=rotatef(VEC2,pi);
    VEC2.ysign='upward';

    VEC2xoffset=VEC2.x-min(VEC2.x); %offset channel width to begin at 0
    VEC2.x=VEC2xoffset/max(VEC2xoffset); %normalize channel width
    VEC2yoffset=VEC2.y-min(VEC2.y);
    VEC2.y=(VEC2yoffset/(max(VEC2xoffset)));

    VEC2.vx=((VEC2.vx*frameRate)/pixel2mm)*0.001; %convert to velocities
    VEC2.vy=((VEC2.vy*frameRate)/pixel2mm)*0.001;

figure(fig1)
F=showf(VEC2,'norm','spacing',[4,8],'scalearrow',1,'cmap','jet')

%ylabel('Vertical [px]');
xlabel('{\itx/D}','FontSize',14,'FontName','Calibri');
```

```
ylabel('{\ity/D}',...
       'FontSize', 14,'FontName',...
       'Calibri')


xlim([0 1]);
ylim([0 0.66]);

c=colorbar;
ylabel(c,'|V|(m/s)');
colorbar('hide')
c=colorbar('FontSize',12,'FontName','Calibri');
ylabel(c,'|{\itV}| [m/s]','FontSize',12);

ax=gca;
set(ax,'FontSize',12);

end
```

A-3.5 Matlab code used to generate the theoretical velocity data discussed in Sections 3.4

Code for obtaining centerline velocity:

```
clear
clc
close all

fig1=figure;

nPts=140;
dataType=0;
fourierCheck = 1;

[up,uc,freq,times,PinF] = readme_pulsatile(nPts,dataType,fourierCheck);

sampleRate=1000;
cycleIndex=(1/freq)*sampleRate;
startIndex=500; %index of pressure start (from Pressure Data function)

%one cycle of pressure wave
PinF=PinF/133.32; %convert back to mmHg
firstCycle=PinF(startIndex:(startIndex+cycleIndex));
firstCycleTime=times(startIndex:(startIndex+cycleIndex));
offsetPCycleTime=firstCycleTime-min(firstCycleTime);
normPCycleTime=offsetPCycleTime/max(offsetPCycleTime);

%convert vCL plot to time axis
%one cycle of velocity
for i=1:length(uc)
ucTime(i,1)=(i/length(uc))*(2/freq);
end

[pks,pkLocs]=findpeaks(-firstCycle);
pks=-pks;
firstMinIdxLoc=pkLocs(pks==min(pks));

firstMinIndex = firstMinIdxLoc + startIndex;

oneCyclePTime=times(firstMinIndex:firstMinIndex+cycleIndex)-
min(times(firstMinIndex:firstMinIndex+cycleIndex));
normOneCyclePTime=oneCyclePTime*freq;
oneCyclePinF=PinF(firstMinIndex:firstMinIndex+cycleIndex);
offsetOneCyclePinF=oneCyclePinF-min(oneCyclePinF);
normOneCyclePinF=offsetOneCyclePinF/max(offsetOneCyclePinF);

offsetTime=times(firstMinIndex)-times(startIndex);
findoffsetTime=ucTime(ucTime<=offsetTime+0.0005);
beginIdx=length(findoffsetTime);
oneCycleUcTime=ucTime(beginIdx:beginIdx+(nPts/2)-1);
oneCycleUc=uc(beginIdx:beginIdx+(nPts/2)-1);
```

```
offsetUcTime=oneCycleUcTime-min(oneCycleUcTime);
normucTime=offsetUcTime/(max(offsetUcTime));
normuc=oneCycleUc/max(oneCycleUc);

phsAng=normucTime(normuc==max(normuc))-
normOneCyclePTime(normOneCyclePinF==max(normOneCyclePinF));

save theoPP_35RPM_vCL.mat normucTime normuc
save PP_35RPM_PhsAngle.mat phsAng

figure
[hAx, h1, h2]=plotyy(normOneCyclePTime,normOneCyclePinF,normucTime,normuc);
h1.Marker='o';
h2.Marker='o';
hAx(1).YColor='k';
hAx(2).YColor='b';
h1.Color='black';
h2.Color='blue';
set(hAx(1),'XLim',[0 1]);
set(hAx(2),'XLim',[0 1]);
set(hAx(1),'YLim',[-1 1]);
set(hAx(2),'YLim',[-1 1]);
set(hAx(1),'YTick',-1:0.5:1);
set(hAx(2),'YTick',-1:.5:1);
set(get(hAx(1),'YLabel'),'String','Normalized Pressure, {\itP/P_{max}} [--]');
set(get(hAx(2),'YLabel'),'String','Normalized Centerline Velocity, {\itv_{CL}/v_{CL,max}} [--]');
set(get(hAx(1),'XLabel'),'String','Normalized Time, {\itt/\tau} [--]');
set(get(hAx(2),'XLabel'),'String','Normalized Time, {\itt/\tau} [--]');
set(hAx,'Fontsize',11);
set(hAx,'Fontname','Calibri');
```

Code for obtaining velocity profiles:

```
clear
clc
close all

fig1=figure;

nProfiles=80;
dataType=0;
fourierCheck = 1;
r=0.00635;

[up,uc,freq,times,PinF] = readme_pulsatile(nProfiles,dataType,fourierCheck);

sampleRate=1000;
cycleIndex=(1/freq)*sampleRate;
startIndex=300; %index of pressure start (from Pressure Data code)

%one cycle of pressure wave from first min
PinF=PinF/133.32; %convert back to mmHg
```

```
firstCycle=PinF(startIndex:(startIndex+cycleIndex));
firstCycleTime=times(startIndex:(startIndex+cycleIndex));
[pks,pkLocs]=findpeaks(-firstCycle);
pks=-pks;
firstMinIdxLoc=pkLocs(pks==min(pks));

firstMinIndex = firstMinIdxLoc + startIndex;

oneCyclePTime=times(firstMinIndex:firstMinIndex+cycleIndex)-
min(times(firstMinIndex:firstMinIndex+cycleIndex));
normOneCyclePTime=oneCyclePTime*freq;
oneCyclePinF=PinF(firstMinIndex:firstMinIndex+cycleIndex);
offsetOneCyclePinF=oneCyclePinF-min(oneCyclePinF);
normOneCyclePinF=offsetOneCyclePinF/max(offsetOneCyclePinF); %normalized pressure

%time between beginning of velocity calculation and first pressure min - so
%offset can be calculated for velocity profiles start index
offsetTime=(firstMinIndex-startIndex)/sampleRate;
startPt=round(offsetTime*nProfiles)-2;
velCycleIndex=nProfiles/2;
endPt=startPt+velCycleIndex;

if endPt>80
    startPt=startPt-velCycleIndex;
    endPt=startPt+velCycleIndex;
end

interval=(nProfiles/2)/10;

count=0
for h=startPt:interval:endPt-1
    count=count+1;
    profiles(count,:)=up(h,:);
end

%normalize velocity profiles

for k=1:length(profiles)
    upRad(k)=-r+((2*r)*(k-1)/(length(profiles)-1));

end

%Normalize everything
maxArray=max(up);
normVal=max(maxArray);
normUpRad=(upRad/(2*max(upRad)))+.5;
normUpVel=up/normVal;

save PP_poly_25RPM_theoVelProf.mat nProfiles normUpRad profiles
```

Code for functions:

```
function [up,uc,freq, times, PinF] = readme_pulsatile(frameNumber,dataType,fourierCheck)
```

```
% Toolkit for Pulsatile flow in arteries
%
% IMPORTANT > This toolkit is using some functions of Image processing
% toolkit in matlab. Image processing toolkit is used to export dicom files
% generated from the toolkit. If you need to export dicom files
% this toolkit should also be installed.
%
% This toolkit includes a list of functions to provide pulsatile flow images
% acquired from Womersley solution in the rigid tube. The toolkit includes
% functions for exact solution of the domain for flow characteristics such
% as velocity, pressure, wall shear rate, volumetric flow and flow rate in
% the computational domain. Also there is a function to generate PC-MR
% images as numerical phantom for the domain. Fourier series for generation
% of temporal wave form are supported when pressure is given as:
% p(t)=p0+Sum[pn(n)*exp(i*(2*pi*freq*t*n-phi(n)))].
%
%
%******************** List of functions
%
% [u,p,dudr,q,dq,alpha]=PulsatileFlow(r,ru,mu,freq,p0,pn,phi,timestep,grid);
%
% [outputP] = PressureData(freq,Location,File_icon_text,duration,sampleRate);
%
%   Copyright 2007-2013 Ali Pashaei.


%clf; clear all; clc;
if nargin==0
    fourierCheck=0;
end
sampleRate = 1000;
Location = 'F:\UPDATED RESULTS (NOV)\Nov10\';
File_icon_text = 'Nov10_PP_35RPM_Volt.log';
ind=strfind(File_icon_text,'RPM');
RPM=str2num(File_icon_text(ind-2:ind-1));
r = 0.00635; grid = 64; timestep = round(frameNumber);
ru =1000; freq = (RPM*4)/60; mu = 0.001005;
harmonics = 4;

fourierCoefficients = 20;

lowerBound = 0;

cycle = 1;

cutoffFrequency = freq*harmonics;

transducerLength = .26;

A_slope=0.0149;
A_int=0.0645;
C_slope=0.0149; %Marcus calibration
C_int=0.0003;
```

```
staticHead=25.15*133.32;


[p times PinF] =
PressureData(freq,Location,File_icon_text,sampleRate,fourierCheck,staticHead,lowerBound,cycle,cut
offFrequency,transducerLength);
[p0,pn,phi] = FourierSeries(p,1/sampleRate,fourierCoefficients,(1/freq),fourierCheck);

[u]=PulsatileFlow(r,ru,mu,freq,p0,pn,phi,timestep,grid);

% get a velocity profile for all [frameNumber] time steps
up = u(:,1:grid+1,grid/2+1);
%centerline velocity
uc = u(:,grid/2+1,grid/2+1);

end
```

```
function [outputP times PinF] =
PressureData(frequency,Location,File_icon_text,sampleRate,fourierCheck,staticHead,lowerBound,cycl
e,fc,transducerLength)
%   frequency      - Frequency of the measured pulse, in Hz
%   Location       - Find file location by right clicking on file name from windows file
explorer, selecting properties
%                    and copying the "Location" address to this string
%   File_icon_text - Find File_icon_text by right clicking on file name from windows file
explorer, selecting properties
%                    and copying the file name found in the text box to this string
%   duration       - The amount of time that pressure data was collected for,
%                    in seconds
%   sampleRate     - The data aqusition rate for the pressure data, in Hz

fileName = strcat(Location,'\',File_icon_text);
%transducer A
A_slope=0.0149;
A_int=0.0645;

%Marcus transducer C
C_slope=0.0149; %Marcus calibration
C_int=0.0003;


times=dlmread(fileName,'\t','A8..A15007'); %times
ai4=dlmread(fileName,'\t','F8..F15007'); %imaging section outlet
ai7=dlmread(fileName,'\t','I8..I15007'); %aorta inlet
Pc=((ai4-C_int)/C_slope)*133.32;
PcF=LPButterworthFilt(sampleRate,fc,Pc);
Pin=((ai7-A_int)/A_slope)*133.32;
PinF=LPButterworthFilt(sampleRate,fc,Pin);

outputP = (PinF - PcF- staticHead)/transducerLength; %[Pa]

cycleTimes=times(((1/frequency)*sampleRate:2*(1/frequency)*sampleRate))-
```

```
min(times(((1/frequency)*sampleRate:2*(1/frequency)*sampleRate)));
cycle=outputP((1/frequency)*sampleRate:2*(1/frequency)*sampleRate);

figure(1)
set((1),'Position',[100 300 1100 500]);
plot(times,outputP,'k')
hold on
% plot(times,staticHead*ones(length(times)));
outputP=outputP(500:end-500);
xlim([0 2]);
xlabel('Time, {\itt} [s]');
ylabel('Axial Pressure Gradient, {\itdP/dz} [Pa/m]');
ax=gca;
ax.FontSize=14;
ax.FontName='Calibri';
set(ax,'LooseInset',get(ax,'TightInset'));
% set(ax,'Position',[100 200 1100 500]);
end
```

```
function [p0,pn,phi] = FourierSeries(p,dt,N,T,fourierCheck)
%FourierSeries FourierSeries function to generate coeficients of Fourier series for a given
discrete data.
%   [p0,pn,phi] = FourierSeries(p,dt,N,T) provides a constant p0 and two
%   arrays pn and phi with length N within period of T. N is the number of
%   coefficients for the Fourier serie.
%   Input parameters for the functions are defined as below:
%
%       p           array of discrete amplitudes for the pulsatile wave.
%       dt          time step size in which p data are presented.
%       N           Number of coefficients required from the function.
%       T           period of oscillation of the fluid.
%
%
%   p is an array, dt is a double number, N is integer and N is double.
%
%   given array p, [p0,pn,phi] = FourierSeries(p,dt,N,T) provides the
%   coefficients for function p(t)=p0+Sum[pn(n)*exp(i*(2*pi*t*n/T-phi(n)))]
%
%   Output parameters for the functions are defined as below:
%
%       p0          a value showing the steady-state component of peiodic wave.
%       pn          an array of size N presenting the absolute values of Fourier serie.
%       phi         an array of size N presenting the phase angle in Fourier serie.
%
%   Examples:
%
%       p=[-7.7183,-8.2383,-8.6444,-8.8797,-9.6337,-10.5957,-11.8705,-10.0942,-6.2839,-
1.1857,2.6043,4.4323,6.1785,7.8211,9.1311,9.9138,10.3447,10.4011,10.2807,9.8951,8.0597,5.6717,2.5
232,1.3301,1.4405,1.9094,1.8145,0.8738,0.7055,0.7343,0.7788,0.7495,0.6711,-0.4796,-1.6541,-
2.8643,-3.4902,-4.1714,-5.6581,-6.8024];
%       [p0,pn,phi] = FourierSeries(p,0.025,4,1)
%
```

```
%       generates the Fourier coefficients for wave p, presenting data in intervals of 0.025
within a period of 1 sec.
%       parameters set in SI.
%
%       is possible to visualize the results given function below:
%
%           tt=0:dt:T;
%           pt=p0;
%           for n=1:N
%               pt=pt+pn(n)*cos(2*pi*tt*n/T-phi(n));
%           end
%           plot (tt,pt,'-k',0:dt:T-dt,p,'x')
%
%
%   Reference:
%   A. Pashaei and N Fatouraee, "An analytical phantom for the evaluation
%   of medical flow imaging algorithms.", Phys Med Biol. 2009 Mar 21;54(6):1791-821.
%
%   Copyright 2007-2013 Ali Pashaei.

T=2*T;
[p0,pn,phi] = FourierCoefficients2(p,dt,N,T);
tt=0:dt:T;
pt=p0;
for n=1:N
  pt=pt+pn(n)*cos(2*pi*tt*n/T-phi(n));
end

if fourierCheck == 1
    figure(2);
    plot (tt,pt,'-k',0:dt:T-dt,p(1:length(tt)-1),'x');
    xlabel('time (s)');
    ylabel('dP/dz (Pa/m)');
end

end

function [A0,AN,BN] = FourierCoefficients(p,dt,N,T)
t=0:dt:(T-dt);
A0=0;
for n=1:length(t)
    A0=A0+p(n)*dt/T;
end
AN=zeros(N,1);
BN=zeros(N,1);
for n=1:N;
    for m=1:length(t)
        AN(n)=AN(n)+2*p(m)*cos (2*pi*t(m)/T*n)*dt/T;
        BN(n)=BN(n)+2*p(m)*sin (2*pi*t(m)/T*n)*dt/T;
    end
end
end

function [A0,MN,PHIN] = FourierCoefficients2(p,dt,N,T)
```

```
[A0,AN,BN] = FourierCoefficients(p,dt,N,T);
MN=zeros(N,1);
PHIN=zeros(N,1);
for n=1:N
    MN(n)=sqrt(AN(n)^2+BN(n)^2);
    PHIN(n)=angle(AN(n)+1i*BN(n));
end
end
```

A-3.6 Matlab code used to calculate and plot multiple cycle centerline velocity results from Section 4.4

```
clear
close all

% Size and position figures
figure(1), figure(2); figure(3);
sz_x = 560; sz_y = 420;
y_pos = 550;
x_pos =75;
set(1,'pos', [x_pos, y_pos, sz_x, sz_y]);
set(2,'pos', [x_pos+15+sz_x, y_pos, sz_x, sz_y]);
set(3,'pos', [x_pos, 10, sz_x*2, sz_y]);

% Load data set
pathR = 'F:\PIV Results\PP Results
November_calibration_90mm\Nov10_PP_25RPM\TR_PIV_MP(2x16x16_50%ov)\';
pathC='F:\PIV Results\PP Results
November_calibration_90mm\Nov14_PPC_25RPM\TR_PIV_MP(4x16x16_50%ov)_01\';
% Get files in folder
fnamesR = dir([pathR '*.VC7']);
fnamesC = dir([pathC '*.VC7']);
% Set a counter
countR=0;
countC=0;
% Define the num of images to SKIP (if needed)
skip = 1;

%so start frame is now 12 from the newly processed dataset
frameRate=113;
freq=1.667; %pulse frequency
cycleFrames=round((1/freq)*frameRate); %cycle time multiplied by camera frame rate
% endFrame=startFrame+cycleFrames;
harmonics=4;

%load pressure data to find start trigger
fileNameR='F:\UPDATED RESULTS (NOV)\Nov10\Nov10_PP_25RPM_Volt.log';
fileNameC='F:\UPDATED RESULTS (NOV)\Nov14\Nov14_PPC_25RPM_Volt.log';
%transducer A
A_slope=0.0149;
A_int=0.0645;

%Marcus transducer C
C_slope=0.0149; %Marcus calibration
C_int=0.0003;

pixel2mm_water=74;%74 pixel=1 mm for water case
pixel2mm_poly=77;

timeR=dlmread(fileNameR,'\t','A8..A15007'); %times
timeC=dlmread(fileNameC,'\t','A8..A15007'); %times
```

```
baslertriggerR=dlmread(fileNameR,'\t','D8..D15007');
baslertriggerC=dlmread(fileNameC,'\t','D8..D15007');
greenTriggerR=dlmread(fileNameR,'\t','C8..C15007');
greenTriggerC=dlmread(fileNameC,'\t','C8..C15007');
sampleRate=1000; %sampling frequency
frameRate = 113; %green camera
sampleNumber = length(timeR);

VoutImSectR=dlmread(fileNameR,'\t','F8..F15007'); %imaging section outlet
VinAortaR=dlmread(fileNameR,'\t','I8..I15007'); %aorta inlet
VoutImSectC=dlmread(fileNameC,'\t','F8..F15007'); %imaging section outlet
VinAortaC=dlmread(fileNameC,'\t','I8..I15007'); %aorta inlet

PoutImSectR=(VoutImSectR-C_int)/C_slope;
PinAortaR=(VinAortaR-A_int)/A_slope;
fPinAortaR=LPButterworthFilt(sampleRate,freq*harmonics,PinAortaR);
PoutImSectC=(VoutImSectC-C_int)/C_slope;
PinAortaC=(VinAortaC-A_int)/A_slope;
fPinAortaC=LPButterworthFilt(sampleRate,freq*harmonics,PinAortaC);

noPlotCycles=3; %how many normalized cycles to plot

%RIGID-----------------------------------------------------------------------

% finding the start frame of the camera for rigid dataset
for c = 1:sampleNumber
    if greenTriggerR(c,1) > 5
        triggerIndexR = c;
        break
    end
end

cycleIndexR = round((1/freq)*sampleRate); %frames per cycle
firstTriggerCycleR=fPinAortaR(triggerIndexR:triggerIndexR+cycleIndexR);

[pksR,pkLocsR]=findpeaks(firstTriggerCycleR); %positive peaks
[npksR,npkLocsR]=findpeaks(-firstTriggerCycleR);%cycle minima
npksR=-npksR;
[~, firstMinIndexUR] = min(fPinAortaR(triggerIndexR:(triggerIndexR+cycleIndexR)));
firstMinIndexR = firstMinIndexUR + triggerIndexR;

%calculate startFrame of cycle using triggerIndex
offsetTimeR = timeR(firstMinIndexR)- timeR(triggerIndexR);
startFrameR = round(frameRate*offsetTimeR);
endFrameR=round(startFrameR+noPlotCycles*(1/freq)*frameRate);
oneCycleTimeR=timeR(firstMinIndexR:firstMinIndexR+cycleIndexR);
oneCyclePressureR=fPinAortaR(firstMinIndexR:firstMinIndexR+cycleIndexR);

for c = startFrameR:skip:endFrameR
    countR = countR+1;
    v_FileR = [pathR fnamesR(c).name];
    % Load the vector file
    VECR = loadvec(v_FileR);
    [x1findR,~]=find(VECR.vy);
```

```
    x1R=min(x1findR)-1;
    x2R=max(x1findR)+1;

    y1R=1;
    [s1R s2R]=size(VECR.y);
    y2R=s2R;

    boxR = [x1R x1R x2R y2R];

    VECR2 = extractf(VECR,boxR); % get the vectors

mVelR(countR)=mean2(VECR2.vy);
mVelR(countR)=((mVelR(countR)*frameRate)/pixel2mm_water)*0.001;

figure(3)

    plot(mVelR,'r.');
        drawnow
end

for x=1:length(mVelR);
    velTimeR(x)= (startFrameR+(x*skip))*(1/frameRate)-(startFrameR*(1/frameRate)); %calculating the time steps associated with each image
end
normVelTimeR=noPlotCycles*(velTimeR-min(velTimeR))/max(velTimeR);

%COMPLIANT-----------------------------------------------------------------
%start frame for compliant dataset
for j = 1:sampleNumber
    if greenTriggerC(j,1) > 5
        triggerIndexC = j;
        break
    end
end

cycleIndexC = round((1/freq)*sampleRate); %frames per cycle
firstTriggerCycleC=fPinAortaC(triggerIndexC:triggerIndexC+cycleIndexC);

[pksC,pkLocsC]=findpeaks(firstTriggerCycleC); %positive peaks
[npksC,npkLocsC]=findpeaks(-firstTriggerCycleC);%cycle minima
npksC=-npksC;
[~, firstMinIndexUC] = min(fPinAortaC(triggerIndexC:(triggerIndexC+cycleIndexC)));
firstMinIndexC = firstMinIndexUC + triggerIndexC;

%calculate startFrame of cycle using triggerIndex
offsetTimeC = timeC(firstMinIndexC)- timeC(triggerIndexC);
startFrameC = round(frameRate*offsetTimeC);
endFrameC=round(startFrameC+noPlotCycles*(1/freq)*frameRate);
oneCycleTimeC=timeC(firstMinIndexC:firstMinIndexC+cycleIndexC);
oneCyclePressureC=fPinAortaC(firstMinIndexC:firstMinIndexC+cycleIndexC);

for c = startFrameC:skip:endFrameC
    countC = countC+1;
    v_FileC = [pathC fnamesC(c).name];
```

```
    % Load the vector file
    VECC = loadvec(v_FileC);
    [x1findC,~]=find(VECC.vy);
    x1C=min(x1findC)-1;
    x2C=max(x1findC)+1;

    y1C=1;
    [s1C s2C]=size(VECC.y);
    y2C=s2C;

    boxC = [x1C x1C x2C y2C];

    VECC2 = extractf(VECC,boxC); % get the vectors

mVelC(countC)=mean2(VECC2.vy);
mVelC(countC)=((mVelC(countC)*frameRate)/pixel2mm_water)*0.001;

figure(3)
    plot(mVelC,'r.');
        drawnow
end

for y=1:length(mVelC);
    velTimeC(y)= (startFrameC+(y*skip))*(1/frameRate)-(startFrameC*(1/frameRate)); %calculating the time steps associated with each image
end
normVelTimeC=noPlotCycles*(velTimeC-min(velTimeC))/max(velTimeC);
%--------------------------------------------------------------------------

figure(2)
plot(normVelTimeR,mVelR,'ko-');
hold on
plot(normVelTimeC,mVelC,'b*-');
hold off
xlim([0 3]);
ylim([-0.02 0.06]);
xlabel('Normalized Time, {\itt/\tau} [--]');
ylabel('Centerline Velocity, {\itv_{CL}} [m/s]')
set(figure(2),'position',[300 100 1100 500]);
L4=legend('Rigid Case', 'Compliant Case');
set(L4,'Location','eastoutside');
ax=gca;
ax.FontSize=14;
ax.FontName='Calibri';
set(ax,'LooseInset',get(ax,'TightInset'));

save ('meanVelocity_multicycle_PP_25RPM.mat', 'mVelR', 'skip','velTimeR');
save meanVelocity_multicycle_PPC_25RPM.mat mVelC skip velTimeC

%
```

A-3.7 Matlab code used to calculate one cycle of centerline velocities synced with theoretical phase angle from Section 4.5

```
clear
close all

% Size and position figures
fig1=figure;
fig2=figure;
fig3=figure;

% figure(1), figure(2); figure(3);
sz_x = 560; sz_y = 420;
y_pos = 550;
x_pos =75;
set(fig1,'pos', [x_pos, y_pos, sz_x+300, sz_y-70]);
set(fig2,'pos', [x_pos+15+sz_x, y_pos, sz_x+300, sz_y-70]);
set(fig3,'pos', [x_pos, 10, sz_x*2, sz_y]);

% Load data set
path = 'F:\PIV Results\PP Results
November_calibration_90mm\Nov10_PP_35RPM\TR_PIV_MP(3x24x24_50%ov)_01\';
fnames = dir([path '*.VC7']);
count=0;
% Define the num of images to SKIP (if needed)
skip = 1;
frameRate=113;
freq=2.33; %pulse frequency
cycleFrames=round((1/freq)*frameRate); %cycle time multiplied by camera frame rate
harmonics=4;

%load pressure data to find start trigger
fileName='F:\UPDATED RESULTS (NOV)\Nov10\Nov10_PP_35RPM_Volt.log';

%transducer A
A_slope=0.0149;
A_int=0.0645;

%Marcus transducer C
C_slope=0.0149; %Marcus calibration
C_int=0.0003;

pixel2mm_water=74;%74 pixel=1 mm for water case
pixel2mm_poly=77;

time=dlmread(fileName,'\t','A8..A15007'); %times
baslertriggerR=dlmread(fileName,'\t','D8..D15007');
greenTrigger=dlmread(fileName,'\t','C8..C15007');
sampleRate=1000; %sampling frequency
frameRate = 113; %green camera
sampleNumber = length(time);
```

```
VoutImSectR=dlmread(fileName,'\t','F8..F15007'); %imaging section outlet
VinAortaR=dlmread(fileName,'\t','I8..I15007'); %aorta inlet

PoutImSect=(VoutImSectR-C_int)/C_slope;
PinAorta=(VinAortaR-A_int)/A_slope;
fPinAorta=LPButterworthFilt(sampleRate,freq*harmonics,PinAorta);

% finding the start frame of the camera
for i = 1:sampleNumber
    if greenTrigger(i,1) > 5
        triggerIndex = i;
        break
    end
end

cycleIndex = round((1/freq)*sampleRate); %frames per cycle
firstTriggerCycle=fPinAorta(triggerIndex:triggerIndex+cycleIndex);

[pks,pkLocs]=findpeaks(firstTriggerCycle); %positive peaks
[npks,npkLocs]=findpeaks(-firstTriggerCycle);%cycle minima
npks=-npks;

[~, firstMinIndexU] = min(fPinAorta(triggerIndex:(triggerIndex+cycleIndex)));
firstMinIndex = firstMinIndexU + triggerIndex;


offsetTime=time(firstMinIndex)-time(triggerIndex);
startFrame = 1;
noCycles=2;
endFrame=startFrame+round((noCycles*(1/freq)*frameRate));
oneCyclePTime=time(firstMinIndex:firstMinIndex+cycleIndex);
offsetOneCyclePTime=oneCyclePTime-min(oneCyclePTime);
normOneCyclePTime=offsetOneCyclePTime/max(offsetOneCyclePTime);
oneCyclePressure=fPinAorta(firstMinIndex:firstMinIndex+cycleIndex);

for i = startFrame:skip:endFrame
    count = count+1;
    v_File = [path fnames(i).name];
    % Load the vector file
    VEC = loadvec(v_File);


%%%%%%%%%%%%%%%%%%%%%%%%%%%%%%%%%%%%%%%%%%%%%
% Plot the sub region Vector Field
%%%%%%%%%%%%%%%%%%%%%%%%%%%%%%%%%%%%%%%%%%%%%
figure(1) % Set Figure 1 active
% Define the sub region
    box = [90 1 101 225]; %to extract centerline velocity - check VEC.x for the pixel range
(~1080-1200) 135 1 153 225
%for entire region, use [77 1 192 225]
    VEC2 = extractf(VEC,box); % get the vectors

%%%%%%%%%%%%%%%%%%%%%%%%%%%%%%%%%%%%%%%%%%%%%
% figure(2) % Set Figure 2 active
```

```
mVel(count)=mean2(VEC2.vy);
mVel(count)=((mVel(count)*frameRate)/pixel2mm_water)*0.001;

figure(fig1)

plot(mVel,'r.');
drawnow
end

for x=1:length(mVel);
    velTime(x)= (startFrame+(x*skip))*(1/frameRate)-(startFrame*(1/frameRate)); %calculating the
time steps associated with each image
end

load PP_35RPM_PhsAngle.mat

%find first min of velocity waveform to offset over one cycle
[negPks,negPkLocs]=findpeaks(-mVel);
negPks=-negPks;
minFrameOneCycle=negPkLocs(1); %first velocity min
endFrameOneCycle=minFrameOneCycle+cycleFrames-3;
oneVelCycle=mVel(minFrameOneCycle:endFrameOneCycle);
oneVelT=velTime(minFrameOneCycle:endFrameOneCycle);

%normalize time
offsetVelT=oneVelT-min(oneVelT);
normVelT=offsetVelT/max(offsetVelT);

%find max pk location wrt normalized time
[pk,pkLoc]=findpeaks(oneVelCycle); %searching within the first cycle from first min for peaks
velPk=pkLoc(pk==max(pk)); %index location of max pk wrt to first cycle
velT=normVelT(velPk);

% plot(normVelT,oneVelCycle);

%find normalized location of pressure pk
[ppks,ppkLocs]=findpeaks(oneCyclePressure);
ppkLoc=ppkLocs(ppks==max(ppks));
pLoc=ppkLoc/cycleIndex;

%move two peaks to same position
currentShift=round((velT-pLoc)*frameRate);
phsShift=round(phsAng*(1/freq)*frameRate);

% startFrameOneCycle=startFrameOneCycle+currentShift+phsShift; %how many frames to shift
velocity wave by
startFrameOneCycle=minFrameOneCycle+currentShift+phsShift;%how many frames to shift velocity
wave
startFrameOneCycle=startFrameOneCycle+cycleFrames;
save PP_35RPM_cycleStartFrame.mat startFrameOneCycle;

oneCycleTime=velTime(startFrameOneCycle:startFrameOneCycle+cycleFrames);
oneCycleVel=mVel(startFrameOneCycle:startFrameOneCycle+cycleFrames);
```

```
figure(fig2)
plot(oneCycleTime,oneCycleVel,'ko-')

save meanVelocity_oneCycle_PP_35RPM.mat oneCycleTime oneCycleVel
save pressure_PP_35RPM.mat oneCyclePTime oneCyclePressure
```

A-3.8 Matlab code used to plot normalized one cycle results from Section 4.5 (rigid case)

```
close all
clear

freq=1.667;
% fig2=figure;

% % set(fig1,'pos',[100,500,700,400]);
% set(fig2,'pos',[300,300,1100,600]);

load pressure_PP_35RPM.mat; %
load meanVelocity_oneCycle_PP_35RPM.mat
load theoPP_35RPM_vCL.mat

%normalized velocity time
maxVT=max(oneCycleTime);
minVT=min(oneCycleTime);
offsetVT=oneCycleTime-minVT;
normVT=offsetVT/max(offsetVT);

%normalized pressure time
minPT=min(oneCyclePTime);
offsetPT=oneCyclePTime-minPT;
maxPT=max(offsetPT);
normPT=offsetPT/maxPT;

%normalized pressure

minP=min(oneCyclePressure);
offsetP=oneCyclePressure-minP;
maxP=max(offsetP);
normP=offsetP/maxP;
[~,pLoc]=(max(normP));
pLoc=(pLoc/1000)*(1/freq);

% normalized centerline velocity
maxV = max(oneCycleVel);
[a b] = size(oneCycleVel);
normV = oneCycleVel/maxV;
vCLPlotTime = [1:b]./b;
[~,vLoc]=(max(normV));
vLoc=(vLoc/1000)*(1/freq);


[hAx, h1, h2]=plotyy(normPT,normP,normVT,normV);%,'scatter','scatter');
hold on
p1=plot(normucTime,normuc,'b-');
p1.LineWidth=2;

h1.Marker='.';
```

```
h2.Marker='o';
hAx(1).YColor='k';
hAx(2).YColor='b';
h1.Color='black';
h2.Color='blue';
set(hAx(1),'XLim',[0 1]);
set(hAx(2),'XLim',[0 1]);
set(hAx(1),'YLim',[-1 1]);
set(hAx(2),'YLim',[-1 1]);
set(hAx(1),'YTick',-1:0.5:1);
set(hAx(2),'YTick',-1:.5:1);
set(get(hAx(1),'YLabel'),'String','Normalized Pressure, {\itP/P_{max}} [--]');
set(get(hAx(2),'YLabel'),'String','Normalized Centerline Velocity, {\itv_{CL}/v_{CL,max}} [--
]');
set(get(hAx(1),'XLabel'),'String','Normalized Time, {\itt/\tau} [--]');
set(get(hAx(2),'XLabel'),'String','Normalized Time, {\itt/\tau} [--]');
set(hAx,'Fontsize',14);
set(hAx,'Fontname','Calibri');
ax=gca;
ax.FontSize=14;
ax.FontName='Calibri';
```

A-3.9 Matlab code used to plot normalized one cycle results from Section 4.5 (compliant case)

```
close all
clear

load pressure_PPC_poly_15RPM.mat;
load meanVelocity_oneCycle_PPC_poly_15RPM.mat
load tubeResponse_oneCycle_PPC_poly_15RPM.mat
load theoPPC_poly_15RPM_vCL.mat

%normalized velocity time
minVT=min(oneCycleTime);
maxVT=max(oneCycleTime);
offsetVT=oneCycleTime-minVT;
normVT=offsetVT/max(offsetVT);

%normalized pressure time
minPT=min(oneCyclePTime);
offsetPT=oneCyclePTime-minPT;
maxPT=max(offsetPT);
normPT=offsetPT/maxPT;

%normalized pressure

minP=min(oneCyclePressure);
offsetP=oneCyclePressure-minP;
maxP=max(offsetP);
normP=offsetP/maxP;

% normalized centerline velocity
maxV = max(oneCycleVel);
[a b] = size(oneCycleVel);
normV = oneCycleVel/maxV;
vCLPlotTime = [1:b]./b;


%normalized tube response time
minDT=min(oneCycleCTime);
offsetDT=oneCycleCTime-minDT;
maxDT=max(offsetDT);
normDT=offsetDT/maxDT;
 %don't need to normalize tube response (%)

x1=normPT; y1=normP;
x2=normVT; y2=normV;
x3=normDT; y3=oneCycleCompl;
ylabels{1}='Normalized Pressure, {\itP/P_{max}} [--]';
ylabels{2}='Normalized Centerline Velocity, {\itv_{CL}/v_{CL,max}} [--]';
ylabels{3}='Tube Expansion, {\it\DeltaD/D}, [%]';
xlabel='Normalized Time, {\itt/\tau} [--]';
```

```
fig1=figure;
x=20;
y=40;
width=200;
height=500;

figure(fig1);
[ax,hlines]=plotyyy(x1,y1,x2,y2,x3,y3,ylabels);
hold on
h1=plot(normucTime,normuc,'b-');
h1.LineWidth=2;

set(ax(1),'YLim',[-1 1]);
set(ax(2),'YLim',[-1 1]);
set(ax(3),'XLim',[0 1.17]);
set(ax(1),'YTick',-1:.5:1);
set(ax(2),'YTick',-1:.5:1);
set(ax(1),'YColor',[0 0 0]);
set(ax(2),'YColor',[0 0 1]);
set(ax(3),'YLim',[4 4.5]);
set(get(ax(1),'xlabel'),'string',xlabel);

ax(1).FontSize=14; ax(2).FontSize=14; ax(3).FontSize=14;
ax(1).FontName='Calibri',ax(2).FontName='Calibri',ax(3).FontName='Calibri'
```

A-3.10 Matlab code used to plot the experimental velocity profiles presented in Section 4.6

```
close all
clear

fig1=figure;

%specify pressure file location and PIV data location
fileName='F:\UPDATED RESULTS (NOV)\Nov10\Nov10_PP_25RPM_Volt.log'; %pressure data
fileName2='F:\UPDATED RESULTS (NOV)\Nov14\Nov14_PPC_25RPM_Volt.log'; %pressure data
%PIV files
path = 'F:\PIV Results\PP Results
November_calibration_90mm\Nov10_PP_25RPM\TR_PIV_MP(2x16x16_50%ov)\'; %load PIV data
path2='F:\PIV Results\PP Results
November_calibration_90mm\Nov14_PPC_25RPM\TR_PIV_MP(4x16x16_50%ov)_01\';

%pulse frequency
freq=1.667;
cycleTime=1/freq;

%-------------------------------------------------------------------------
%Fill in
DaVisImgStart=1; % first image processed in DaVis
% Define the num of images to SKIP for velocity plot (if needed)
skip =1;

% Get files in folder
fnames = dir([path '*.VC7']);
fnames2=dir([path2 '*VC7']);
% Set a counter
count=0;
count2c2=0;
%--------------------------------------------------------------------------
%harmonics for filter
harmonics=4; %number of harmonics to include in filtered wave

r=0.0127; %tube radius[m]

%conversion factors
pixel2mm=74;
pixel2mm_poly=77;

%transducer A
A_slope=0.0149;
A_int=0.0645;

%Marcus transducer C
C_slope=0.0149; %Marcus calibration
C_int=0.0003;

time=dlmread(fileName,'\t','A8..A15007'); %times
```

```
time2=dlmread(fileName2,'\t','A8..A15007'); %times
greenTrigger=dlmread(fileName,'\t','C8..C15007');
greenTrigger2=dlmread(fileName2,'\t','C8..C15007');
sampleRate=1000; %sampling frequency
frameRate = 113; %green camera
sampleNumber = length(time);

VinAorta=dlmread(fileName,'\t','I8..I15007'); %aorta inlet
VinAorta2=dlmread(fileName2,'\t','I8..I15007'); %aorta inlet

PinAorta=(VinAorta-A_int)/A_slope;
PinAorta2=(VinAorta2-A_int)/A_slope;

%filtered pressure wave
fPinAorta=LPButterworthFilt(sampleRate,freq*harmonics,PinAorta);
fPinAorta2=LPButterworthFilt(sampleRate,freq*harmonics,PinAorta2);

cycleIndex = round(cycleTime*sampleRate);
cycleFrames=round((1/freq)*frameRate); %cycle time multiplied by camera frame rate


% %WATER-----------------------------------------------------------------------
for i = 1:length(time)
    if greenTrigger(i,1) > 9
        triggerIndex = i;
        break
    end
end
%
% %POLY------------------------------------------------------------------------
for d = 1:length(time2)
    if greenTrigger2(d,1) > 9
        triggerIndex2 = d;
        break
    end
end

%--------------------------------------------------------------------------

%WATER---------------------------------------------------------------------
%find minimum to start cycle from beginning of pressure pulse
firstTriggerCycle=fPinAorta(triggerIndex:triggerIndex+cycleIndex);
[pks,pklocs] = findpeaks(-firstTriggerCycle);
pks=-pks;
[~,minIdx] = min(pks);
localMinIndex=pklocs(minIdx);
firstMinIndex=localMinIndex+triggerIndex;

%create new array for one cycle starting at first min
oneCycleTime=time(firstMinIndex:firstMinIndex+cycleIndex);
oneCyclePressure = fPinAorta(firstMinIndex:(firstMinIndex+cycleIndex)); %inlet waveform using
startframe of inlet wave
offsetCycleTime=oneCycleTime-min(oneCycleTime);
normOneCycleTime=offsetCycleTime/max(offsetCycleTime);
```

```
% cutPressureOut = fPoutImSect_Pa(firstMinIndex:(firstMinIndex+cycleIndex)); %peripheral waveform
using startframe of inlet waveform (marks beginning of systole)

%find normalized location of pressure pk
[ppks,ppkLocs]=findpeaks(oneCyclePressure);
ppkLoc=ppkLocs(ppks==max(ppks));
pLoc=ppkLoc/cycleIndex;

%determine start and end frame for velocity profile
load PP_25RPM_cycleStartFrame.mat
startFrame=startFrameOneCycle;
endFrame=startFrame+round((cycleTime*frameRate))-1;

% %compliant-----------------------------------------------------------------------
%find minimum to start cycle from beginning of pressure pulse
firstTriggerCycle2=fPinAorta2(triggerIndex2:triggerIndex2+cycleIndex);
[pks2,pklocs2] = findpeaks(-firstTriggerCycle2);
pks2=-pks2;
[~,minIdx2] = min(pks2);
localMinIndex2=pklocs2(minIdx2);
firstMinIndex2=localMinIndex2+triggerIndex2;

%create new array for one cycle starting at first min
oneCycleTime2=time(firstMinIndex2:firstMinIndex2+cycleIndex);
oneCyclePressure2 = fPinAorta2(firstMinIndex2:(firstMinIndex2+cycleIndex)); %inlet waveform using
startframe of inlet wave
offsetCycleTime2=oneCycleTime2-min(oneCycleTime2);
normOneCycleTime2=offsetCycleTime2/max(offsetCycleTime2);
% cutPressureOut = fPoutImSect_Pa(firstMinIndex:(firstMinIndex+cycleIndex)); %peripheral waveform
using startframe of inlet waveform (marks beginning of systole)

%find normalized location of pressure pk
[ppks2,ppkLocs2]=findpeaks(oneCyclePressure2);
ppkLoc2=ppkLocs2(ppks2==max(ppks2));
pLoc2=ppkLoc2/cycleIndex;

%determine start and end frame for velocity profile
load PPC_25RPM_cycleStartFrame.mat
startFrame2=startFrameOneCycle;
endFrame2=startFrame2+round((cycleTime*frameRate))-1;

%WATER---------------------------------------------------------------------

for i =startFrame:skip:endFrame
%     i = startFrame:skip:endFrame
    count = count+1; %image number
    v_File = [path fnames(i).name];
    % Load the vector file
    VEC = loadvec(v_File);

    if i==startFrame
    [x1find,~]=find(VEC.vy);
    x1=min(x1find)-1;
    x2=max(x1find)+1;
```

```
    y1=1;
    [s1 s2]=size(VEC.y);
    y2=s2;

    box = [x1 y1 x2 y2];
    end

    % Define the sub region
     VEC2 = extractf(VEC,box); % get the vectors

        count2=0; %count2 represents the y location at which we're averaging (how many locations
in the y direction are we using to find the average velocity profile)
        %calculate velocity profiles across length of FOV
        c1=1;
        c2=length(VEC2.x);
        rdsmax=c2-c1+1;

        for j=c1:1:c2;%cycle through columns of VEC2.vy matrix
        count2=count2+1; %column number
        profilePixel(count,count2)=mean2(VEC2.vy(j,:)); %average value per column
        velProfile(count,count2)=((profilePixel(count,count2)*frameRate)/pixel2mm)*0.001;

        rds=j-c1;

        radVal(count,count2)=(rds/rdsmax)*r; %r position in tube [mm]
        end

    normRad(count,:)=radVal(count,:)/max(radVal(count,:));
    totImgNum(count)=startFrame+count-1;
end

%plot velocity profiles according to location on pressure plot
imgTime=(totImgNum-startFrame)/frameRate;
normImgTime=imgTime/max(imgTime);
incr=0.1;
counter=0;

%PROFILES
for x=0:incr:1
    counter=counter+1;
    if counter*x==0
        profLoc(counter)=1;
    elseif counter*x>0
    newIdx=(x-0.001<=normImgTime<=x+0.001).';
    profLoc(counter) = find(newIdx, 1, 'last');

    end
     x=x+incr;
end

%COMPLIANT----------------------------------------------------------------------

for f =startFrame2:skip:endFrame2
%     i = startFrame:skip:endFrame
```

```
    count2c2 = count2c2+1; %image number
    v_File2 = [path2 fnames2(f).name];
    % Load the vector file
    VECc2 = loadvec(v_File2);

if f==startFrame2
    [x1find2,~]=find(VECc2.vy);
    x1c2=min(x1find2)-1;
    x2c2=max(x1find2)+1;

    y1c2=1;
    [s1c2 s2c2]=size(VECc2.y);
    y2c2=s2c2;

    box2 = [x1c2 x1c2 x2c2 y2c2];
end

    VEC2c2 = extractf(VECc2,box2); % get the vectors

        count2c2_2=0; %count2 represents the y location at which we're averaging (how many
locations in the y direction are we using to find the average velocity profile)
        %calculate velocity profiles across length of FOV

        c1c2=1;
        c2c2=length(VEC2c2.x);
        rdsmaxc2=c2c2-c1c2+1;

        for g=c1c2:1:c2c2;%cycle through columns of VEC2.vy matrix
        count2c2_2=count2c2_2+1; %column number
        profilePixelc2(count2c2,count2c2_2)=mean2(VEC2c2.vy(g,:)); %average value per column

velProfilec2(count2c2,count2c2_2)=((profilePixelc2(count2c2,count2c2_2)*frameRate)/pixel2mm_poly)
*0.001;

        rdsc2=g-c1c2;

        radValc2(count2c2,count2c2_2)=(rdsc2/rdsmaxc2)*r; %r position in tube [mm]

        end

        normRadc2(count2c2,:)=radValc2(count2c2,:)/max(radValc2(count2c2,:));

        totImgNumc2(count2c2)=startFrame2+count2c2-1;
end


%plot velocity profiles according to location on pressure plot
imgTimec2=(totImgNumc2-startFrame2)/frameRate;
normImgTimec2=imgTimec2/max(imgTimec2);
counter3c2=0;


for z=0:incr:1
    counter3c2=counter3c2+1;
```

```
    if counter3c2*z==0
        profLocc2(counter3c2)=1;
    elseif counter3c2*z>0
    newIdxc2=(z-0.001<=normImgTimec2<=z+0.001).';
    profLocc2(counter3c2) = find(newIdxc2, 1, 'last');

    end
     z=z+incr;
end

%normalize wrt to maximum overall velocity (both poly and water)
minArray=[min(velProfile) min(velProfilec2)];
maxArray=[max(velProfile) max(velProfilec2)];

minVal=min(minArray);
maxVal=max(maxArray);

    if abs(minVal)>abs(maxVal)
        normVal=minVal;
    else
        normVal=maxVal;
    end

normProfile=velProfile/normVal;
normProfilec2=velProfilec2/normVal;

%SUBPLOT-----------------------------------------------------------------
h=figure(fig1)
figPx=600;
figPy=0;
figW=600;
figH=1000;
h.Position=[figPx figPy figW figH];

ncols = 2;
nrows = 5;

axisw = (1 / ncols) * 0.6; %.95
axish = (1 / nrows) * 0.6; %how much of the row is it taking up
frame=0;

for frame=1:length(profLoc)-1

    % calculate the row and column of the subplot
    row(frame) = nrows-floor( (frame-0.5)/ncols ) + 1;
    col(frame) = mod( frame-1, ncols ) + 1;

    if frame>1 && col(frame)==col(frame-1)
        col(frame)=col(frame)-1;
    end

    % calculate the left, bottom coordinate of this subplot

    if col(frame)==1
```

```
    axisl = (axisw+0.02) * (col(frame)-.7)+0.05;
    else
     axisl = (axisw+0.02) * (col(frame)-.3)+0.05;
    end

    initialoffset=.2; %1
    offsetVal=.34; %.32

    if row(frame)==6
        axisb = (axish+0.02) * (row(frame)-initialoffset)+0.035;
    elseif row(frame)==5
            axisb = (axish+0.02) * (row(frame)-(initialoffset+offsetVal))+0.035;
        elseif row(frame)==4
            axisb = (axish+0.02) * (row(frame)-(initialoffset+(2*offsetVal)))+0.035;
    elseif row(frame)==3
        axisb = (axish+0.02) * (row(frame)-(initialoffset+(3*offsetVal)))+0.035;
    elseif row(frame)==2
        axisb = (axish+0.02) * (row(frame)-(initialoffset+(4*offsetVal)))+0.035;
        else
        axisb = (axish+0.02) * (row(frame)-(initialoffset+(5*offsetVal)))+0.035;
    end

    fplot= subplot('position', [axisl, axisb, axisw, axish] );
    pR=plot(normRad(profLoc(frame),:),normProfile(profLoc(frame),:),'k.');
    hold on
    pC=plot(normRadc2(profLocc2(frame),:),normProfilec2(profLocc2(frame),:),'b.');
    hold off
    ttl=title(['{\itt/\tau} = 0.' int2str(frame-1)]);
    ttl.FontSize=12;
    ttl.FontWeight='normal';
    ttl.FontName='Calibri';

    xlim([0 1]);
    set(gca,'XTick',0:.25:1,'FontSize',10);
    ylim([-1.1 1.1]);
    set(gca,'YTick',-1:.5:1,'FontSize',10)
    ylabel('{\itU/U_{max}}','FontSize',10);
    xlabel('{\itr/D}','FontSize',10);

end
```

A-3.11 Matlab code used to plot the theoretical velocity profiles presented in Section 4.6

```
close all
clear

load PP_poly_25RPM_theoVelProf.mat
maxArrayR=max(profiles);
minArrayR=min(profiles);
upR=profiles;
load PP_poly_25RPM_PhsAngle.mat
phsAngR=phsAng;
load PPC_poly_25RPM_theoVelProf.mat
maxArrayC=max(profiles);
minArrayC=min(profiles);
upC=profiles;
load PPC_poly_25RPM_PhsAngle.mat
phsAngC=phsAng;

minArray=[min(minArrayR) min(minArrayC)];
maxArray=[max(maxArrayR) max(maxArrayC)];
minVal=min(minArray);
maxVal=max(maxArray);

    if abs(minVal)>abs(maxVal)
        normVal=minVal;
    else
        normVal=maxVal;
    end

normUpR=upR/normVal;
normUpC=upC/normVal;

fig1=figure;
h=figure(fig1)
figPx=600;
figPy=0;
figW=600;
figH=1000;
h.Position=[figPx figPy figW figH];

ncols = 2;
nrows = 5;

axisw = (1 / ncols) * 0.6; %.95
axish = (1 / nrows) * 0.6; %how much of the row is it taking up
frame=0;

for frame=1:1:nProfiles/2
     if frame>10
         break
     end
```

```
    % calculate the row and column of the subplot
    row(frame) = nrows-floor( (frame-0.5)/ncols ) + 1;
    col(frame) = mod( frame-1, ncols ) + 1;

    if frame>1 && col(frame)==col(frame-1)
        col(frame)=col(frame)-1;
    end

    % calculate the left, bottom coordinate of this subplot

    if col(frame)==1
    axisl = (axisw+0.02) * (col(frame)-.7)+0.05;
    else
     axisl = (axisw+0.02) * (col(frame)-.3)+0.05;
    end

    initialoffset=.2; %1
    offsetVal=.34; %.32

    if row(frame)==6
        axisb = (axish+0.02) * (row(frame)-initialoffset)+0.035;
    elseif row(frame)==5
            axisb = (axish+0.02) * (row(frame)-(initialoffset+offsetVal))+0.035;
        elseif row(frame)==4
            axisb = (axish+0.02) * (row(frame)-(initialoffset+(2*offsetVal)))+0.035;
    elseif row(frame)==3
        axisb = (axish+0.02) * (row(frame)-(initialoffset+(3*offsetVal)))+0.035;
    elseif row(frame)==2
        axisb = (axish+0.02) * (row(frame)-(initialoffset+(4*offsetVal)))+0.035;
        else
        axisb = (axish+0.02) * (row(frame)-(initialoffset+(5*offsetVal)))+0.035;
    end

    fplot= subplot('position', [axisl, axisb, axisw, axish] );
    pR=plot(normUpRad,normUpR(frame,:),'k-');
    pR.LineWidth=1.5;
    hold on
    pC=plot(normUpRad(1,:),normUpC(frame,:),'b-');
    pC.LineWidth=1.5;
    hold off
    ttl=title(['{\itt/\tau} = 0.' int2str(frame-1)]);
    ttl.FontSize=12;
    ttl.FontName='Calibri';
    ttl.FontWeight='normal';
    xlim([0 1]);
    set(gca,'XTick',0:.25:1,'FontSize',10);
    ylim([-1.1 1.1]);
    set(gca,'YTick',-1:.5:1,'FontSize',10)
    ylabel('{\itU/U_{max}}','FontSize',10);
    xlabel('{\itr/D}','FontSize',10);

end
```

A-3.12 Matlab code used to perform peristaltic pump energy calculations presented in Section 4.7.4

```
close all
clear

fig1=figure;
fig2=figure;
fig3=figure;
fig4=figure;
fig5=figure;
fig6=figure;
fig7=figure;

%CONSTANTS & TUBE PROPERTIES ----------------------------------------------
%conversion factors
mmHg_Pa_Conv=133.322; %1 mmHg=133.322 Pa
pixel2mmWater=74; %pixel/mm
pixel2mmPoly=77;
rhoWater=1000; %kg/m3
rhoPoly=998.2;
g=9.81; %m/s2

r=0.0127;
zPump=.22; %from PP to transducer A
zA_C=.26; %from A to C
zImSect=0.095; %imaging section height

zPLRes=.45+.11; %height to outlet spout + approximate height of fluid in res
zPt=zPump+(zA_C+(zImSect/2)); %z to where images are being taken
Leff=zPt-zPLRes;

%Files--------------------------------------------------------------------
fileName='C:\Users\kgcamero\Desktop\Nov15PP\Nov15_PP_poly_15RPM_Volt.log'; %pressure data
path = 'D:\MyProjects\PP_poly Results calibration_90
mm\Nov15_PP_poly_15RPM\TR_PIV_MP(3x16x16_50%ov)\'; %load PIV data

skip =1;

%pulse frequency
freq=1.0;
cycleTime=1/freq;

%harmonics for filter
harmonics=4; %number of harmonics to include in filtered wave

% LOAD PRESSURE DATA-------------------------------------------------------

%transducer A
A_slope=0.0149;
A_int=0.0645;
```

```
%transducer C
C_slope=0.0148;
C_int=0.0172;

time=dlmread(fileName,'\t','A8..A15007'); %times
greenTrigger=dlmread(fileName,'\t','C8..C15007');
sampleRate=1000; %sampling frequency
frameRate = 113; %green camera
sampleNumber = length(time);

VoutImSect=dlmread(fileName,'\t','G8..G15007'); %imaging section outlet
VinAorta=dlmread(fileName,'\t','I8..I15007'); %aorta inlet

PoutImSect=(VoutImSect-C_int)/C_slope;
PinAorta=(VinAorta-A_int)/A_slope;

%filtered pressure wave

fPoutImSect=LPButterworthFilt(sampleRate,freq*harmonics,PoutImSect);
fPinAorta=LPButterworthFilt(sampleRate,freq*harmonics,PinAorta);

%convert to Pa
fPinAorta_Pa=fPinAorta*mmHg_Pa_Conv;
fPoutImSect_Pa=fPoutImSect*mmHg_Pa_Conv;

% finding the start frame of the camera
cycleIndex = round(cycleTime*sampleRate); %frames per cycle

for i = 1:length(time)
    if greenTrigger(i,1) < 1
        triggerIndex = i;
        break
    end
end

% LOAD MEAN VELOCITY DATA-------------------------------------------------

% Get files in folder
fnames = dir([path '*.VC7']);
% Set a counter
count=0;

cycleFrames=round((1/freq)*frameRate); %cycle time multiplied by camera frame rate
firstTriggerCycle=fPinAorta(triggerIndex:triggerIndex+cycleIndex);
[pks,pklocs] = findpeaks(-firstTriggerCycle);
pks=-pks;
[~,minIdx] = min(pks);
localMinIndex=pklocs(minIdx);
firstMinIndex=localMinIndex+triggerIndex;

%create new array for one cycle starting at first diastolic min
oneCycleTime=time(firstMinIndex:firstMinIndex+cycleIndex);
onecyclePressure = fPinAorta_Pa(firstMinIndex:(firstMinIndex+cycleIndex));
offsetOneCycleTime=(oneCycleTime-min(oneCycleTime));
```

```
%determine start and end frame for velocity profile
offsetTime = time(firstMinIndex)- time(triggerIndex);
startFrame = round(frameRate*offsetTime);
endFrame=startFrame+round((cycleTime*frameRate))-1;

%LOAD PIV IMAGES, CALCULATE VELOCITY---------------------------------------

for i = startFrame:skip:endFrame
    count = count+1;
    v_File = [path fnames(i).name];
    % Load the vector file
    VEC = loadvec(v_File);

    if i==startFrame
    [x1find,~]=find(VEC.vy);
    x1=min(x1find)-1;
    x2=max(x1find)+1;
    y1=1;
    [s1 s2]=size(VEC.y);
    y2=s2;

    box = [x1 y1 x2 y2];
    end

    VEC2 = extractf(VEC,box); % get the vectors

    count2=0; %count2 represents the y location at which we're averaging (how many locations in the y direction are we using to find the average velocity profile)
        %calculate velocity profiles across length of FOV
        c1=1;
        c2=length(VEC2.x);
        rdsmax=c2-c1+1;

    for j=c1:1:c2 %j is the x location under consideration
        count2=count2+1;
        profilePixel(count,count2)=mean2(VEC2.vy(j,:)); %average value per column
        velProfile(count,count2)=((profilePixel(count,count2)*frameRate)/pixel2mmPoly)*0.001;

        rds=j-c1;

        radVal(count,count2)=(rds/rdsmax)*r; %r position in tube [mm]

    end

      fit1{count}=fit(radVal(count,:).',velProfile(count,:).','smoothingspline'); %smoothing spline for velocity profiles

    velProfileArea(count)=trapz(radVal(count,:).',velProfile(count,:).'); %area under averaged velocity profile for each image (count)
    volFlowRate(count)=pi*r*velProfileArea(count); %m3/s %integrate velocity profile around 180 degrees to get volume flow rate
    massFlowRate(count)=volFlowRate(count)*rhoPoly; %kg/s %multiply flow rate times density to get mass flow erate
```

```
    if massFlowRate(count)<0
        massFlowRate(count)=0;
    end

    avgVel(count)=mean2(velProfile(count,:));

    end


for x=1:length(velProfileArea);
    velTime(x)= (startFrame+(x*skip))*(1/frameRate)-(startFrame*(1/frameRate)); %calculating the
time steps associated with each image
end


%DYNAMIC ENERGY ---------------------------------------------------------

%calculating terms for integration
vSqrd=avgVel.^2;
VIntFunct=vSqrd.*massFlowRate;

VInt=trapz(velTime.',VIntFunct.');
VNRG=VInt*(1/2)

figure(fig1)
plot(velTime,avgVel,'k.-');
xlabel('Time, {\itt} [s]');
ylabel('Velocity, {\itv} [m/s]');

figure(fig2)
plot(velTime, VIntFunct,'b.-');
xlabel('Time, {\itt} [s]')
ylabel('Squared Velocity * mdot [m2/s2(kg/s)]');

figure(fig3)
plot(velTime,massFlowRate,'r.-');
xlabel('Time, {\itt} [s]')
ylabel('Mass Flow Rate [\itkg/s]');
ylim([-0.05 .3]);

% PRESSURE ENERGY --------------------------------------------------------

pCurveFit=fit(offsetOneCycleTime,oneCyclePressure,'sin4');

%CHECK FIT QUALITY
plot(offsetOneCycleTime,oneCyclePressure)
hold on
plot(pCurveFit);
hold off


for pts=1:length(massFlowRate) %fit pressure curve to the same data points as the velocity data
so it can be multiplied by mass flow rate
```

```
    pressTimeAdjusted(pts)=velTime(pts);
    pressAdjusted(pts)=pCurveFit(pressTimeAdjusted(pts));
    pts=pts+1;
end

PIntFunct=pressAdjusted.*massFlowRate;
PInt=trapz(velTime.',PIntFunct.');
PNRG=PInt/rhoWater

figure(fig4)
plot(offsetOneCycleTime,oneCyclePressure,'b');
hold on
% plot(offsetOneCycleTime,oneCyclePressure,'r-');
xlabel('Time, {\itt} [s]');
ylabel('P(t) [Pa]')
hold off

figure(fig5)
plot(velTime,PIntFunct,'k-');
xlabel('Time, {\itt} [s]');
ylabel('P(t)*mdot')

% STATIC ENERGY ----------------------------------------------------------

SInt=trapz(velTime.',massFlowRate.');
SNRG=(zPt-zPLRes)*g*SInt

%LOCAL ACCELERATION ------------------------------------------------------

dv_dt=diff(avgVel)./diff(velTime);
accelTime=velTime(1:length(dv_dt));

tick=0;
interval=2; %how many data points to skip over for acceleration plot (on top of skip already applied to avg velocity plot)
for t=1:interval:length(dv_dt)
    tick=tick+1;
    accelFunct(tick)=abs(dv_dt(t));
    accelTimeFunct(tick)=accelTime(t);
    massFlowRateAdjusted(tick)=massFlowRate(t);
    end

accelIntFunct=accelFunct.*massFlowRateAdjusted;
accelInt=trapz(accelTimeFunct.',accelIntFunct.');

figure(fig6)
plot(accelTimeFunct,accelFunct,'k.-');
xlabel('Time, {\itt} [s]');
ylabel('dv/dt [m/s2]')

figure(fig7)
plot(accelTimeFunct,accelIntFunct,'k.-');
xlabel('Time, {\itt} [s]');
ylabel('(dv/dt)*mdot');
```

```
ANRG=Leff*accelInt

%TOTAL ENERGY ------------------------------------------------------------

totNRG=PNRG+VNRG+SNRG+ANRG

excelfileName='C:\Users\kgcamero\Dropbox\Graduate Research & Designs\Thesis\Peristaltic
Pump\Energy Values.xlsx';
sheet=1;
excelData1=[VNRG PNRG SNRG ANRG totNRG];

xlRange1='I16';
xlswrite(excelfileName,excelData1,sheet,xlRange1);
```

A-3.13 Matlab code used to calculate and plot tube distension, as discussed in Sections 3.2, 4.3 and 5.3

```
close all
clear


fig1 = figure; fig2 = figure;
fig3 = figure; fig4 = figure; fig5 = figure; fig6=figure;
set(fig1,'pos',[75, 825,560,200]);
set(fig2,'pos',[650,825,560,200]);
set(fig3,'pos',[75, 530,560,200]);
set(fig4,'pos',[650,530,560,200]);
set(fig5,'pos',[75,300,1000,140]);
set(fig6,'pos',[75,5,1100,650]);

%Pressure transducer calibration
%transducer A
A_slope=0.0149;
A_int=0.0645;
%transducer C
C_slope=0.0148;
C_int=0.0172;

%-------------------------------------------------------------------------
%load tube images
%-------------------------------------------------------------------------
path='F:\VAD Data\2PSI\Oct6_2PSI_1235RPM';

fnam = '\Oct6_2PSI';
ext = '.tif';
text = [path '\Oct6*.tif'];
filelist = dir(text);

row_num = 250;
relaxedDiam=210; %relaxed diameter calculated from raw image of calibration
count=0;
skip=1;

%-------------------------------------------------------------------------
%load voltage data
%--------------------------------------------------------------------------
fileName='F:\VAD Data\2PSI\Oct6_2PSI_1235RPM_Volt.log';
time=dlmread(fileName,'\t','A8..A60007'); %times
baslerTrigger=dlmread(fileName,'\t','D8..D60007');
%set frame rate, frequency, etc.
baslerFrameRate=210;
freq=1.12;
harmonics=10;
sampleRate=4000;
sampleNumber=length(time);
```

```
%load aorta inlet pressure
VinAorta=dlmread(fileName,'\t','I8..I60007'); %aorta inlet
%convert to pressure
PinAorta=(VinAorta-A_int)/A_slope;
%filter pressure waveform
fPinAorta=LPButterworthFilt(sampleRate,freq*harmonics,PinAorta);

noPlotCycles=3; %number of cycles to plot

% finding the first trigger of basler camera
for j = 1:sampleNumber
    if baslerTrigger(j,1) > 9
        triggerIndex = j;
        break
    end
end

%find first pressure minimum within first trigger cycle
cycleIndex = round((1/freq)*sampleRate); %frames per cycle
firstTriggerCycle=fPinAorta(triggerIndex:triggerIndex+cycleIndex);
[npks,npkLocs]=findpeaks(-firstTriggerCycle);%cycle minima
npks=-npks;
[~, firstMinIndexU] = min(fPinAorta(triggerIndex:(triggerIndex+cycleIndex)));
firstMinIndex = firstMinIndexU + triggerIndex; %first pressure minimum index

%time between first basler trigger and first pressure minimum
offsetTime = time(firstMinIndex)- time(triggerIndex);
startFrame = round(baslerFrameRate*offsetTime);
baslerCycleIndex=round((1/freq)*baslerFrameRate);
endFrame=round(startFrame+(noPlotCycles*baslerCycleIndex));


%--------------------------------------------------------------------------
%calculate tube distension vs. time
%--------------------------------------------------------------------------
for i = startFrame:skip:endFrame
   count=count+1;

   tube_time(count)=(i./baslerFrameRate)-(startFrame/baslerFrameRate);
   file = [path '\' filelist(i).name];

   f0 = imread(file);
%
%    figure(fig1);

   imagesc(f0);
   colormap('gray');

      trim = 97; % trim off the right hand side of the image
   f2a=imcrop(f0,[1 size(f0,1)/2 size(f0,2)-trim 20]);

   level = graythresh(f2a);
   f2 = im2bw(f2a,level);
```

```
   f1 = edge(f2,'sobel',0.05);

   figure(fig1);
   imagesc(f2);
   colormap('gray');

   figure(fig2);
   imagesc(f1);
   colormap('gray');

   % Plot the peak detection
   figure(fig5)
   % generate plot of dI vs h at selected row and frame
    L1 = sum(f1);
    plot(L1);

    minHeight = 7;
   [pks,locs] = findpeaks(L1,'MinPeakHeight',minHeight);
   [aa bb]=size(locs);

   % Picking the TWO peaks to use
   pleft = min(locs);
   pright= max(locs);

   hold on
   plot(pleft, 0,'rs');
   plot(pright,0,'rs');
   plot([0 500],[minHeight minHeight],'r');
   hold off

    width2=pright-pleft;
    all_pixWidth(count) = width2;

    %%%%%%%%%%%%%%%%%%%%%%%%%%%%%%%%%%%%%%%%%%%%%%
    % Do the sub pixel find
    %%%%%%%%%%%%%%%%%%%%%%%%%%%%%%%%%%%%%%%%%%%%%%
    numpix = 15;%25
    L2 = sum(f2a);
    %%%%%%%%%%%%%%%%%%%%%%%%%%%%%%%%%%%%%%%%%%%%%%%%
% FIGURE 3 Rising (Left) edge to sub pixel
%%%%%%%%%%%%%%%%%%%%%%%%%%%%%%%%%%%%%%%%%%%%%%%%
figure(3)
clf
posL = pleft;
% get a short array of numpix pixels either side
left = L2(1,posL-numpix:posL+numpix)/10;
left = left - min(left); % set close to zero
left = left./max(left);  % scale the maximum 0-1
 x = 1:size(left,2);
 x = x + posL-numpix;
 y = left*100; % Scale this so that the seed number work
 % Do the curve Fit
  %fL = fit(x', y', 'a+b*atan((x0-x)/w)');
  fL = fit(x', y', 'a+b*atan((x0-x)/w)', 'Startpoint', [50 -30 1 150]);
```

```
% %Display on the figure
        hold on
        plot(x, y,'b.');
        plot(fL);
        hold off

%%%%%%%%%%%%%%%%%%%%%%%%%%%%%%%%%%%%%%%%%%%%%%%%
% FIGURE 4 falling (RIGHT) edge to sub pixel
%%%%%%%%%%%%%%%%%%%%%%%%%%%%%%%%%%%%%%%%%%%%%%%%
  figure(4)
 clf
 %posL = locs_La+39;
 posL = pright;
 % get a short arry 50 pixels either side
left = L2(1,posL-numpix:posL+numpix)/10;
left = left - min(left); % set close to zero
left = left./max(left);  % scale the maximum 0-1
 x = 1:size(left,2);
 x = x + posL-numpix;
 y = left*100; % Scale this so that the seed number work
 % Do the curve Fit
    fR = fit(x', y', 'a+b*atan((x0-x)/w)', 'Startpoint', [50 30 1 350]);
% Display on the figure
        hold on
        plot(x, y,'b.');
        plot(fR);
        hold off
%%%%%%%%%%%%%%%%%%%%%%%%%%%%%%%%%%%%%%%%%%%%%%%%
% AND the answer is:
%%%%%%%%%%%%%%%%%%%%%%%%%%%%%%%%%%%%%%%%%%%%%%%%

subpixWidth(count) = fR.x0 - fL.x0;

    figure(fig6)

    hold on
    plot(all_pixWidth,'b.-');
    plot(subpixWidth,'r.-');
    hold off

    drawnow

end

normWidth=(subpixWidth-relaxedDiam)/relaxedDiam;
percentWidth=(normWidth)*100;
ALContribution=min(percentWidth);
normTubeTime=noPlotCycles*(tube_time-min(tube_time))/max(tube_time);

figure(fig5);
    plot(tube_time,percentWidth,'ko-',tube_time,ones(size(tube_time))*ALContribution,'k--');
    xlabel('Time, t [s]');
```

```
    ylabel('Tube Expansion, \DeltaD/D [%]');


figure(fig6);
plot(normTubeTime,percentwidth,'ko-',normTubeTime,ones(size(normTubeTime))*ALContribution,'k--
');
    xlabel('Normalized Time, {\itt/\tau} [--]');
    ylabel('Tube Expansion, {\it\DeltaD/D} [%]');
    xlim([0 3]);
    ylim([0 40]);
    ax=gca;
    ax.FontName='Calibri';
    ax.FontSize=14;
    set(ax,'LooseInset',get(ax,'TightInset'));

%save as .mat file
save compliantresponse_multicycle_Oct6_2PSI_1235RPM.mat tube_time percentwidth
```

A-3.14 Matlab code used to generate the normalized cycle of a filtered VAD pressure waveform from Section 5.5

```
close all
clear

fig1=figure;
fig2=figure;

pm = 1;
sampleRate = 4000;
transducerIntercept = 0.0172;
transducerSlope = 0.0148;
freq=1.12;
harmonics=10;
cycleTime = 1/freq; %1/frequency of pulse
frameRate = 1000; %phantom camera
foldCount = 1;

% Loading data from .log file
fileName='F:\VAD Data\2PSI\Oct6_2PSI_1235RPM_Volt.log';
times(:,1)=dlmread(fileName,'\t','A8..A60007');
phantomTrigger(:,1)=dlmread(fileName,'\t','C8..C60007');
daslerTrigger(:,1)=dlmread(fileName,'\t','D8..D60007');
phantomSquareWave(:,1)=dlmread(fileName,'\t','E8..E60007');
voltageC(:,1)=dlmread(fileName,'\t','G8..G60007');
voltageB(:,1)=dlmread(fileName,'\t','H8..H60007');
voltageA=dlmread(fileName,'\t','I8..I60007');

sampleNumber = length(voltageA(:,1));
pressureA = (voltageA - transducerIntercept)/transducerSlope;
pressureAMean(:,1) = pressureA(:,1) - mean(pressureA(:,1));

% finding the start frame of the camera
for i = 1:length(times(:,1))
    if phantomTrigger(i,1) < 1
        triggerIndex = i;
        break
    end
end

%filtered pressure function
fPinAorta=LPButterworthFilt(sampleRate,freq*harmonics,pressureA);

cycleIndex = round((1/freq)*sampleRate); %frames per cycle
firstTriggerCycle=fPinAorta(triggerIndex:triggerIndex+cycleIndex);
[npks,npkLocs]=findpeaks(-firstTriggerCycle);%cycle minima
npks=-npks;
[~, firstMinIndexU] = min(fPinAorta(triggerIndex:(triggerIndex+cycleIndex)));
firstMinIndexU=npkLocs(2);
firstMinIndex = firstMinIndexU + triggerIndex; %first pressure minimum index
```

```
for ii = 1:1000
    if phantomTrigger(firstMinIndex+ii,pm) < 1
        break;
    elseif phantomTrigger(firstMinIndex+ii,pm) > 1
        firstMinIndex = firstMinIndex + 1;
    end
    if ii == 1000
        disp('maximum number of iterations exceeded to try and find first camera trigger, line
~2649');
    end
end

offsetTime = times(firstMinIndex)- times(triggerIndex);
startFrame = round(frameRate*offsetTime)

% Normalizing
shortTimes=(times(firstMinIndex:firstMinIndex+cycleIndex)-times(firstMinIndex));
normShortTime_Pressure=shortTimes/max(shortTimes);
shortDataLength = length(firstMinIndex:(firstMinIndex+cycleIndex));

shortTrigger = phantomTrigger(firstMinIndex:(firstMinIndex+cycleIndex));
cutPressureA = fPinAorta(firstMinIndex:(firstMinIndex+cycleIndex));

triggerMax = max(shortTrigger);
normTrigger = shortTrigger./triggerMax;

offsetPressure = cutPressureA - min(cutPressureA);
normPressure = offsetPressure./max(offsetPressure);

% plot pressure and camera triggers over first cycle

for pm = 1:foldCount
FigHandle=figure('Position', [50 50 1000 450]);
set(gca,'XTickLabel','')
ylabel('{\it P / P_{max} }');

set(subplot(2,1,2),'Position',[0.1 0.15 0.85 0.1]);

plot(normShortTime_Pressure(1:shortDataLength),normTrigger(1:shortDataLength),'k-');
axis([0 1 0 1.8]);
%                             hold on;
set(subplot(2,1,1),'Position',[0.1 0.4 0.85 0.55]);
plot(normShortTime_Pressure(1:shortDataLength),normPressure(1:shortDataLength),'o','MarkerEdgeCol
or','k','MarkerSize',2); %'MarkerFaceColor',char(color{pm,1}),
axis([0 1 0 1.2]);
title('Pressure Waveform: One Cycle');
hold on

end

save pressure_2PSI_1235RPM.mat normShortTime_Pressure normPressure fPinAorta firstMinIndex
```

A-3.15 Matlab code used to calculate the VAD pulse frequency and pressure values presented in Sections 5.6.1 and 5.6.2

```matlab
close all
clear
%import test

%transducer A
A_slope=0.0149;
A_int=0.0645;

%transducer B
B_slope=0.0149;
B_int=0.0074;

%transducer C

C_slope=0.0148;
C_int=0.0172;

fig1=figure;
fig2=figure;
fig3=figure;

fileName='F:\VAD Data\2PSI\Oct6_2PSI_1235RPM_Volt.log';

time(:,1)=dlmread(fileName,'\t','A8..A60007'); %times

Fs=4000; %sampling frequency

VinAorta(:,1)=dlmread(fileName,'\t','I8..I60007'); %aorta inlet
VoutAorta(:,1)=dlmread(fileName,'\t','H8..H60007'); %aorta outlet
VoutImSect(:,1)=dlmread(fileName,'\t','G8..G60007'); %imaging section outlet

%file2
time2(:,1)=dlmread('X:\01_Current_Students\Katie Cameron\LVAD\Compliant
experiments\Data\3PSI\Oct6_3PSI_1450RPM_Volt.log','\t','A8..A60007'); %times
VinAorta2(:,1)=dlmread('X:\01_Current_Students\Katie Cameron\LVAD\Compliant
experiments\Data\3PSI\Oct6_3PSI_1450RPM_Volt.log','\t','I8..I60007'); %aorta inlet
PinAorta2(:,1)=(VinAorta2-A_int)/A_slope;
fPinAorta2=Katie_LPF(PinAorta2);
shiftedTimefile2=(time2(3916:7224)-time2(3916));
normTimefile2=shiftedTimefile2/max(shiftedTimefile2);
shiftedPressurefile2=fPinAorta2(3916:7224)-fPinAorta2(3916);
normPressurefile2=shiftedPressurefile2/max(shiftedPressurefile2);

%file3
time3(:,1)=dlmread('X:\01_Current_Students\Katie Cameron\LVAD\Compliant
experiments\Data\3PSI\Oct6_3PSI_1625RPM_Volt.log','\t','A8..A60007'); %times
VinAorta3(:,1)=dlmread('X:\01_Current_Students\Katie Cameron\LVAD\Compliant
experiments\Data\3PSI\Oct6_3PSI_1625RPM_Volt.log','\t','I8..I60007'); %aorta inlet
PinAorta3(:,1)=(VinAorta3-A_int)/A_slope;
```

```
fPinAorta3=Katie_LPF(PinAorta3);
shiftedTimefile3=(time3(1752:3450)-time3(1752));
normTimefile3=shiftedTimefile3/max(shiftedTimefile3);
shiftedPressurefile3=fPinAorta3(1752:3450)-fPinAorta3(1752);
normPressurefile3=shiftedPressurefile3/max(shiftedPressurefile3);

  % convert to pressures
PinAorta(:,1)=(VinAorta-A_int)/A_slope;
PoutAorta(:,1)=(VoutAorta-B_int)/B_slope;
PoutImSect(:,1)=(VoutImSect-C_int)/C_slope;

sampleNumber = length(time);

%filtered pressure waves
fPinAorta=Katie_LPF(PinAorta);
fPoutAorta=Katie_LPF(PoutAorta);
fPoutImSect=Katie_LPF(PoutImSect);


figure(fig1) %pressure wave comparison
plot(time,fPinAorta,'k.',time,fPoutAorta,'b.',time,fPoutImSect,'r.');
xlabel('Time, {\itt} [s]');
ylabel('Pressure, {\itp} [mmHg]');
xlim([0 15]);
ylim([-60 182])
set(gca,'xtick',0:1:15)
set(gca,'ytick',0:20:180)


%HR (freq) calculation
[xpts,ypts]=getpts(fig1);

shift1=length(time(time<xpts(1)));
shift2=length(time(time<xpts(3)));

[min1,idx]=min(fPinAorta(time>xpts(1)&time<xpts(2))); %first minimum
[min2,idx2]=min(fPinAorta(time>xpts(3)&time<xpts(4))); %second minimum

[max3,idx3]=max(fPinAorta(time>xpts(1)&time<xpts(2))); %first max
[max4,idx4]=max(fPinAorta(time>xpts(3)&time<xpts(4))); %first min

%calculate phase averaged SBP,DBP,PP
firstMinIndex=idx+shift1;
secondMinIndex=idx2+shift2;
j=1;

firstMaxIndex=idx3+shift1;
secondMaxIndex=idx4+shift2;
% m=1;

while all(xpts<15)
    pulseTime(j)=time(secondMinIndex)-time(firstMinIndex);
    HR(j)=1/pulseTime(j);
```

```
    DBP(j)=fPinAorta(firstMinIndex);
    DBP2(j)=fPoutAorta(firstMinIndex);
    DBP3(j)=fPoutImSect(firstMinIndex);

    SBP(j)=fPinAorta(firstMaxIndex);
    SBP2(j)=fPoutAorta(firstMaxIndex);
    SBP3(j)=fPoutImSect(firstMaxIndex);

    PP(j)=SBP(j)-DBP(j);


MAPIn_Area(j)=trapz(time(firstMinIndex:secondMinIndex),fPinAorta(firstMinIndex:secondMinIndex));
    MAPIn_Calc(j)=(1/3)*SBP(j)+(2/3)*DBP(j);

    xpts(1)=xpts(1)+pulseTime(j);
    xpts(2)=xpts(2)+pulseTime(j);
    xpts(3)=xpts(3)+pulseTime(j);
    xpts(4)=xpts(4)+pulseTime(j);

    shiftA=length(time(time<xpts(1)));
    shiftB=length(time(time<xpts(2)));

    [min5,idx5]=min(fPinAorta(time>xpts(1)&time<xpts(2)));
    [min6,idx6]=min(fPinAorta(time>xpts(3)&time<xpts(4)));

    firstMinIndex=idx5+shiftA;
    secondMinIndex=idx6+shiftB;

    [max7,idx7]=max(fPinAorta(time>xpts(1)&time<xpts(2)));
    [max8,idx8]=max(fPinAorta(time>xpts(3)&time<xpts(4)));

    firstMaxIndex=idx7+shiftA;
    secondMaxIndex=idx8+shiftB;
    j=j+1;
end

HR_PhsAvg=mean(HR);
HR_StdDev=std2(HR);

DBP_PhsAvg=mean(DBP);
DBP_StdDev=std2(DBP);
DBP2_PhsAvg=mean(DBP2);
DBP2_StdDev=std2(DBP2);
DBP3_PhsAvg=mean(DBP3);
DBP3_StdDev=std2(DBP3);

SBP_PhsAvg=mean(SBP);
SBP_StdDev=std2(SBP);
SBP2_PhsAvg=mean(SBP2);
SBP2_StdDev=std2(SBP2);
SBP3_PhsAvg=mean(SBP3);
SBP3_StdDev=std2(SBP3);

PP_PhsAvg=mean(PP);
```

```
PP_StdDev=std2(PP);

MAPIn_Area_PhaseAvg=mean(MAPIn_Area);
MAPIn_Area_StdDev=std2(MAPIn_Area);
MAPIn_Calc_PhaseAvg=mean(MAPIn_Calc);
MAPIn_Calc_StdDev=std2(MAPIn_Calc);


% CLINICAL WAVEFORMS - TYPES A, B, C CENTRAL AORTIC AND PERIPHERAL
%%%%%%%%%%%%%%%%%%%%%%%%%%%%%%%%%%%%%%%%%%%%%%%%%%%%%%%%%%
% naming scheme for physl waveforms:
    % physl"Type""Location"...ex: physlBCA = Type B central aortic,
    % physlAP=Type A peripheral

%physl Type B central aortic waveform from Weber et al. 2006
physlBCAArray=csvread('X:\01_Current_Students\Katie Cameron\LVAD\Compliant experiments\Physl
Waveforms\Weber et al. Type B Central Aortic Waveform.csv');%,'\t','A1..A54');
physlBCANormTime=physlBCAArray(:,1)/max(physlBCAArray(:,1));
physlBCAPressure=physlBCAArray(:,2);
physlBCAShiftedPressure=physlBCAPressure-min(physlBCAPressure);
physlBCANormPressure=(physlBCAPressure-min(physlBCAPressure))/max(physlBCAShiftedPressure);

%physl DD waveform central aortic waveform from Weber et al. 2006
physlDDCAArray=csvread('X:\01_Current_Students\Katie Cameron\LVAD\Compliant experiments\Physl
Waveforms\Weber et al. DD Central Aortic Waveform.csv');%,'\t','A1..A54');
physlDDCANormTime=physlDDCAArray(:,1)/max(physlDDCAArray(:,1));
physlDDCAPressure=physlDDCAArray(:,2);
physlDDCAShiftedPressure=physlDDCAPressure-min(physlDDCAPressure);
physlDDCANormPressure=(physlDDCAPressure-min(physlDDCAPressure))/max(physlDDCAShiftedPressure);

%physl Type B peripheral waveform from Weber et al. 2006
physlBPArray=csvread('X:\01_Current_Students\Katie Cameron\LVAD\Compliant experiments\Physl
Waveforms\Weber et al. Type B Peripheral Waveform.csv');%,'\t','A1..A54');
physlBPNormTime=physlBPArray(:,1)/max(physlBPArray(:,1));
physlBPPressure=physlBPArray(:,2);
physlBPShiftedPressure=physlBPPressure-min(physlBPPressure);
physlBPNormPressure=(physlBPPressure-min(physlBPPressure))/max(physlBPShiftedPressure);

%physl DD waveform peripheral waveform from Weber et al. 2006
physlDDPArray=csvread('X:\01_Current_Students\Katie Cameron\LVAD\Compliant experiments\Physl
Waveforms\Weber et al. DD Peripheral Waveform.csv');%,'\t','A1..A54');
physlDDPNormTime=physlDDPArray(:,1)/max(physlDDPArray(:,1));
physlDDPPressure=physlDDPArray(:,2);
physlDDPShiftedPressure=physlDDPPressure-min(physlDDPPressure);
physlDDPNormPressure=(physlDDPPressure-min(physlDDPPressure))/max(physlDDPShiftedPressure);

%physl hypertensive central aortic waveform from Nichols, 2005
physlHTCAArray=csvread('X:\01_Current_Students\Katie Cameron\LVAD\Compliant experiments\Physl
Waveforms\Nichols Hypertensive Central Aortic Waveform.csv');%,'\t','A1..A54');
physlHTCANormTime=physlHTCAArray(:,1)/max(physlHTCAArray(:,1));
physlHTCAPressure=physlHTCAArray(:,2);
physlHTCAShiftedPressure=physlHTCAPressure-min(physlHTCAPressure);
physlHTCANormPressure=(physlHTCAPressure-min(physlHTCAPressure))/max(physlHTCAShiftedPressure);
```

```
%physl hypertensive peripheral  waveform from Nichols, 2005
physlHTPArray=csvread('X:\01_Current_Students\Katie Cameron\LVAD\Compliant experiments\Physl
Waveforms\Nichols Hypertensive Peripheral Waveform.csv');%,'\t','A1..A54');
physlHTPNormTime=physlHTPArray(:,1)/max(physlHTPArray(:,1));
physlHTPPressure=physlHTPArray(:,2);
physlHTPShiftedPressure=physlHTPPressure-min(physlHTPPressure);
physlHTPNormPressure=(physlHTPPressure-min(physlHTPPressure))/max(physlHTPShiftedPressure);

%theoretical Type C central aortic waveform
physlCCAArray=csvread('X:\01_Current_Students\Katie Cameron\LVAD\Compliant experiments\Physl
Waveforms\Nichols Type C Central Aortic Waveform.csv');%,'\t','A1..A54');
physlCCANormTime=physlCCAArray(:,1)/max(physlCCAArray(:,1));
physlCCAPressure=physlCCAArray(:,2);
physlCCAShiftedPressure=physlCCAPressure-min(physlCCAPressure);
physlCCANormPressure=(physlCCAPressure-min(physlCCAPressure))/max(physlCCAShiftedPressure);

% %theoretical Type C peripheral waveform
physlCPArray=csvread('X:\01_Current_Students\Katie Cameron\LVAD\Compliant experiments\Physl
Waveforms\Nichols Type C Peripheral Waveform.csv');%,'\t','A1..A54');
physlCPNormTime=physlCPArray(:,1)/max(physlCPArray(:,1));
physlCPPressure=physlCPArray(:,2);
physlCPRadShiftedPressure=physlCPPressure-min(physlCPPressure);
physlCPRadNormPressure=(physlCPPressure-min(physlCPPressure))/max(physlCPRadShiftedPressure);

% %theoretical Type A peripheral waveform
physlAPArray=csvread('X:\01_Current_Students\Katie Cameron\LVAD\Compliant experiments\Physl
Waveforms\Nichols Type A Peripheral Waveform.csv');%,'\t','A1..A54');;
physlAPNormTime=physlAPArray(:,1)/max(physlAPArray(:,1));
physlAPRadPressure=physlAPArray(:,2);
physlAPRadShiftedPressure=physlAPRadPressure-min(physlAPRadPressure);
physlAPRadNormPressure=(physlAPRadPressure-
min(physlAPRadPressure))/max(physlAPRadShiftedPressure);

%theoretical Type A central aortic waveform
physlACAArray=csvread('X:\01_Current_Students\Katie Cameron\LVAD\Compliant experiments\Physl
Waveforms\Nichols Type A Central Aortic Waveform.csv');%,'\t','A1..A54');
physlACANormTime=physlACAArray(:,1)/max(physlACAArray(:,1));
physlACAPressure=physlACAArray(:,2);
physlACAShiftedPressure=physlACAPressure-min(physlACAPressure);
physlACANormPressure=(physlACAPressure-min(physlACAPressure))/max(physlACAShiftedPressure);

% EXPERIMENTAL WAVEFORMS %%%%%%%%%%%%%%%%%%%%%%%%%%%%%%%%%%%%%%%%%%%%%%%%%

%normalized one cycle central aortic experimental waveform 1230rpm
shiftedTime=(time(idx+shift1:idx2+shift2)-time(idx+shift1));
normTime=shiftedTime/max(shiftedTime);
shiftedPressure=fPinAorta(idx+shift1:idx2+shift2)-fPinAorta(idx+shift1);
normPressure=shiftedPressure/max(shiftedPressure);

shiftedPressure2=fPoutAorta(idx+shift1+61:idx2+shift2+61)-fPoutAorta(idx+shift1+61);
normPressure2=shiftedPressure2/max(shiftedPressure2);

% PLOTTING OF EXPERIMENTAL AND CLINICAL WAVEFORMS %%%%%%%%%%%%%%%%
figure(fig2)
```

```
plot(physlACANormTime, physlACANormPressure,'r-',physlBCANormTime,physlBCANormPressure,'b-
',physlCCANormTime,physlCCANormPressure,'k-',physlDDCANormTime,physlDDCANormPressure,'b-',
physlHTCANormTime,physlHTCANormPressure,'g-
',normTime,normPressure,'kx',normTimefile2,normPressurefile2,'rx',normTimefile3,normPressurefile3
,'bx');
legend('Type A Central Aortic Waveform (Nichols,2005)','Type B Central Aortic Waveform (Weber et
al.,2006)','Type C Central Aortic Waveform (Nichols,2005)','Diastolic Dysfunction Central Aortic
Waveform (Weber et al., 2006)','Hypertensive Central Aortic Waveform (Nichols,
2005)','Experimental Central Aortic Waveform 1','Experimental Central Aortic Waveform
2','Experimental Central Aortic Waveform 3');
% plot(normTime,normPressure,'kx')%,normTimefile2,normPressurefile2,'bx')
xlabel('Normalized Time, {\itt/\tau} [--]');
ylabel('Normalized Pressure, {\itp/p_{max}} [--]');
xlim([0 1]);
ylim([-0.05 1.1])
set(gca,'xtick',0:.1:1)
set(gca,'ytick',0:.1:1)

figure(fig3)
plot(physlAPNormTime,physlAPRadNormPressure,'r-',physlBPNormTime,physlBPNormPressure,'b-
',physlCPNormTime,physlCPRadNormPressure,'k-',physlDDPNormTime,physlDDPNormPressure,'b-
',physlHTPNormTime,physlHTPNormPressure,'g-',normTime,normPressure,'kx')
legend('Type A Peripheral Waveform (Nichols, 2005)','Type B Peripheral Waveform (Weber et
al.,2006)','Type C Peripheral Waveform (Nichols, 2005)','Diastolic Dysfunction Peripheral
Waveform (Weber et al., 2006)','Hypertensive Peripheral Waveform (Nichols, 2005)','Experimental
Peripheral Waveform');
xlabel('Normalized Time, {\itt/\tau} [--]');
ylabel('Normalized Pressure, {\itp/p_{max}} [--]');
xlim([0 1]);
ylim([-0.05 1.1])
set(gca,'xtick',0:.1:1)
set(gca,'ytick',0:.1:1)

% WRITE PHASE AVERAGED VALUES TO EXCEL FILE %%%%%%%%%%%%%%%%%%%%%%%%%%%%%%%%%%%%%%%%%%

% fileName='C:\Users\KatieG\Dropbox\Graduate Research & Designs\Thesis\CODE\DataCollection.xlsx';
% sheet=1;
% excelData1=[HR_PhsAvg HR_StdDev SBP_PhsAvg SBP_StdDev DBP_PhsAvg DBP_StdDev MAPIn_Calc_PhaseAvg
MAPIn_Calc_StdDev MAPIn_Area_PhaseAvg MAPIn_Area_StdDev PP_PhsAvg];
% excelData2=[SBP2_PhsAvg SBP2_StdDev DBP2_PhsAvg DBP2_StdDev SBP3_PhsAvg SBP3_StdDev DBP3_PhsAvg
DBP3_StdDev];
% xlRange1='C26';
% xlRange2='O26';
%
% xlswrite(fileName,excelData1,sheet,xlRange1);
% xlswrite(fileName,excelData2,sheet,xlRange2);
```

A-3.16 Matlab code used to generate VAD centerline velocity results presented in Section 5.4

```
clear
close all

% Size and position figures
figure(1), figure(2); figure(3);
sz_x = 560; sz_y = 420;
y_pos = 550;
x_pos =75;
set(1,'pos', [x_pos, y_pos, sz_x, sz_y]);
set(2,'pos', [x_pos+15+sz_x, y_pos, sz_x, sz_y]);
set(3,'pos', [x_pos, 10, sz_x*2, sz_y]);

% Load data set
path = 'F:\PIV Results\VAD_Results_calibration_105mm\Oct6_2PSI_1235RPM_truncated (frames 1-
1064)\TR_PIV_MP(3x32x32_75%ov)_01\';
% Get files in folder
fnames = dir([path '*.VC7']);
% Set a counter
count=0;
% Define the num of images to SKIP
skip = 2;
startFrame=145;
frameRate=1000;
pixel2mm=82;
frequency=1.12; %pulse frequency
cycleFrames=(1/frequency)*frameRate; %cycle time multiplied by camera frame rate
endFrame=startFrame+cycleFrames-1;

for i = startFrame:skip:endFrame
    count = count+1;
    v_File = [path fnames(i).name];
    % Load the vector file
    VEC = loadvec(v_File);

figure(1) % Set Figure 1 active
% Define the sub region
    box = [65 30 85 70];

    VEC2 = extractf(VEC,box); % get the vectors
    VEC2vy_invert=-1*VEC2.vy; % vy vectors are being taken in wrong direction (downward) so need
to multiply the array by -1

figure(2) % Set Figure 2 active
mVel(count)=mean2(VEC2vy_invert);
mVel(count)=((mVel(count)*frameRate)/pixel2mm)*0.001;
xlabel('Horizontal [px]','FontSize', 12,'FontName', ‘Calibri’);
ylabel('Vertical  ({\ity}/{\itR})',...
       'FontSize', 12,'FontName',...
       ‘Calibri’)
```

```
colormap('hot');
c=colorbar;
ylabel(c,'|V|(m/s)')

figure(3)
plot(mVel,'r.');
end

save ('meanVelocity_Oct6_2PSI_1235RPM.mat', 'mVel', 'skip');
```

A-3.17 Matlab code used to plot the VAD normalized pressure and centerline velocity (rigid case) results presented in Section 5.5

```
close all
clear

fig1=figure;
fig2=figure;

set(fig1,'pos',[100,500,1100,600]);

daslerFrameRate=210;
sampleRate_Voltage=4000;
frequency=1.44;
cycleTime = 1/frequency;
fileName='F:\VAD Data\Rigid\Oct14_Rigid_1540RPM_Volt.log';
times(:,1)=dlmread(fileName,'\t','A8..A60007'); %times
daslerTrigger(:,1)=dlmread(fileName,'\t','D8..D60007');
sampleNumber=length(daslerTrigger(:,1));

load pressure_Rigid_1540RPM.mat;
load meanVelocity_Oct14_Rigid_1540RPM.mat

startIndex=firstMinIndex; %from pressureworld code

% centerline velocity plot
maxV = max(mVel);
[a b] = size(mVel);
normV = mVel/maxV;
vCLPlotTime = [1:b]./b;

figure(fig1)
[hAx, h1,
h2]=plotyy(normShortTime_Pressure,normPressure,vCLPlotTime,normV);%,'scatter','scatter');
hold on
h1.Marker='.';
h2.Marker='o';
hAx(1).YColor='k';
hAx(2).YColor='b';
h1.Color='black';
h2.Color='blue';
set(hAx(1),'XLim',[0 1]);
set(hAx(2),'XLim',[0 1]);
set(hAx(1),'YLim',[-1.0 1]);
set(hAx(2),'YLim',[-1.0 1]);
set(hAx(1),'YTick',-1:0.5:1);
set(hAx(2),'YTick',-1:.5:1);
set(get(hAx(1),'YLabel'),'String','Normalized Pressure, {\itP/P_{max}} [--]');
set(get(hAx(2),'YLabel'),'String','Normalized Centerline Velocity, {\itv_{CL}/v_{CL,max}} [--
]');
set(get(hAx(1),'XLabel'),'String','Normalized Time, {\itt/\tau} [--]');
set(get(hAx(2),'XLabel'),'String','Normalized Time, {\itt/\tau} [--]');
```

```
set(hAx,'Fontsize',14);
set(hAx,'Fontname','Calibri');
ax=gca;
ax.FontSize=14;
ax.FontName='Calibri';
set(ax,'LooseInset',get(ax,'TightInset'));
```

A-3.18 Matlab code used to plot VAD normalized pressure, centerline velocity and tube distension (compliant case)

```
close all
clear

valveCloseTime=0.4048; %from StartFrame excel sheet
valveCloseFrame=74; %from ValveCloseFrame excel sheet
baslerFrameRate=210;
sampleRate=4000;
freq=1.12;
cycleTime = 1/freq;
tubeCycleIndex=round(cycleTime*baslerFrameRate);

fileName='F:\VAD Data\2PSI\Oct6_2PSI_1235RPM_Volt.log';
times(:,1)=dlmread(fileName,'\t','A8..A60007'); %times
baslerTrigger(:,1)=dlmread(fileName,'\t','D8..D60007');
sampleNumber=length(baslerTrigger(:,1));

load pressure_2PSI_1235RPM.mat;
load compliantresponse_multicycle_Oct6_2PSI_1235RPM.mat;
load meanVelocity_Oct6_2PSI_1235RPM.mat

%syncing tube response with first pressure minimum after beginning of
%dasler camera trigger

% finding the start frame of the camera
for j = 1:sampleNumber
    if baslerTrigger(j,1) > 9
        triggerIndex = j;
        break
    end
end

%find number of pressure data points for one cycle
%then find minimum between the start index and the end of the cycle
%get index of first pressure minimum
cycleIndex_Pressure = round(cycleTime*sampleRate); %frames per cycle
firstTriggerCycle=fPinAorta(triggerIndex:(triggerIndex+cycleIndex_Pressure));
[~, firstMinIndexU] = min(firstTriggerCycle); %local index of first pressure min after camera
trigger
firstPressureMinIndex = firstMinIndexU + triggerIndex; % index of first pressure min after
trigger
firstCycle=fPinAorta(firstPressureMinIndex:firstPressureMinIndex+cycleIndex_Pressure);

%TUBE
twoCyclesTime=tube_time(1:2*tubeCycleIndex+1);
twoCyclesExpansion=percentwidth(1:2*tubeCycleIndex+1);
[pks,pklocs]=findpeaks(-twoCyclesExpansion);
pks=-pks;
startPkLocal=pklocs(pks==min(pks));
oneCycleTime=tube_time(startPkLocal:startPkLocal+tubeCycleIndex);
```

```
offsetOneCycleTime=oneCycleTime-min(oneCycleTime);
normOneCycleTime=offsetOneCycleTime/max(offsetOneCycleTime);
oneCycleExpansion=percentwidth(startPkLocal:startPkLocal+tubeCycleIndex);

%find current valve close index and shift to match pressure valve close
%index
currentValveCloseIdx=pklocs(4)-pklocs(2);
reqdValveCloseIdx=round(valveCloseTime*baslerFrameRate);

phsShift=reqdValveCloseIdx-currentValveCloseIdx;

tubeStartFrame=startPkLocal-phsShift;

tubePlotTime=tube_time(tubeStartFrame:tubeStartFrame+tubeCycleIndex);
tubePlot=percentwidth(tubeStartFrame:tubeStartFrame+tubeCycleIndex);
offsetTubePlotTime=tubePlotTime-min(tubePlotTime);
normTubePlotTime=offsetTubePlotTime/max(offsetTubePlotTime);


% centerline velocity plot
maxV = max(mVel);
[a b] = size(mVel);
normV = mVel/maxV;
vCLPlotTime = [1:b]./b;

x1=normShortTime_Pressure; y1=normPressure;
x2=vCLPlotTime; y2=normV;
x3=normTubePlotTime;
y3=tubePlot;%percentwidth(tubeStartFrame:tubeStartFrame+tubeCycleIndex);normTubeShortTime
ylabels{1}='Normalized Pressure, {\itP/P_{max}} [--]';
ylabels{2}='Normalized Centerline Velocity, {\itv_{CL}/v_{CL,max}} [--]';
ylabels{3}='Tube Response, {\it\DeltaD/D}, [%]';
xlabel='Normalized Time, {\itt/\tau} [--]';

[ax,hlines]=plotyyy(x1,y1,x2,y2,x3,y3,ylabels);

set(ax(1),'YLim',[-.3 1]);
set(ax(2),'YLim',[-.3 1]);
set(ax(3),'XLim',[0 1.12]);
set(ax(1),'YTick',-0.25:0.25:1);
set(ax(2),'YTick',-.25:0.25:1);
set(ax(1),'YColor',[0 0 0]);
set(ax(2),'YColor',[0 0 1]);
set(ax(3),'YLim',[2 38]);
set(ax(3),'YTick',0:2:54);
set(get(ax(1),'xlabel'),'string',xlabel);

ax(1).FontSize=14; ax(2).FontSize=14; ax(3).FontSize=14;
ax(1).FontName='Calibri',ax(2).FontName='Calibri',ax(3).FontName='Calibri'
```

A-3.19 Matlab code used to perform the VAD pump energy calculations presented in Section 5.6.5

```
clear
close all

fig1=figure;
fig2=figure;
fig3=figure;
fig4=figure;
fig5=figure;
fig6=figure;
fig7=figure;
figmin=figure;
getptsfig=figure;

% INPUTS -----------------------------------------------------------------
%ENTER CASE TYPE (1- RIGID OR 2-COMPLIANT)
type=2;

fileName='F:\VAD Data\2PSI\Oct6_2PSI_1235RPM_Volt.log'; %pressure data
path = 'F:\PIV Results\VAD_Results_calibration_105mm\Oct6_2PSI_1235RPM_truncated (frames 1-
1064)\TR_PIV_MP(3x32x32_75%ov)_01\'; %load PIV data

%Fill in
DaVisImgStart=1; % first image processed in DaVis minus one (to include first image)
% Define the num of images to SKIP for velocity plot
skip =1;

%don't touch
DaVisOffset=DaVisImgStart-1;

%pulse frequency (from excel)
freq=1.12;
cycleTime=1/freq;

%harmonics for filter
harmonics=10; %number of harmonics to include in filtered wave
highHarm=15;

%CONSTANTS & TUBE PROPERTIES ---------------------------------------------

%constants & tube/flow properies
rho=1000; %kg/m3
g=9.81; %[m/s2]
r=0.0127; %[m]
Atube=pi*(r^2);

%conversion factors
mmHg_Pa_Conv=133.322; %1 mmHg=133.322 Pa
pixel2mm=82; %pixel/mm
```

```
%heights
z1=0.225; %from outlet valve to transducer B (outlet mock aorta) [m]
z2=0.095; %from transducer B to C [m]
z=z1+(z2/2); %from valve outlet to halfway up imaging section (where flow fields taken)
zC_ALRes=.6; %height from transducer C to AL reservoir
zALRes=z1+z2+zC_ALRes; %height from outlet valve to bottom of AL reservoir


% LOAD PRESSURE DATA-------------------------------------------------------

%transducer A
A_slope=0.0149;
A_int=0.0645;

%transducer C
C_slope=0.0148;
C_int=0.0172;

time=dlmread(fileName,'\t','A8..A60007'); %times
phantomTrigger=dlmread(fileName,'\t','C8..C60007');
sampleRate=4000; %sampling frequency
frameRate = 1000; %phantom camera
sampleNumber = length(time);

VoutImSect=dlmread(fileName,'\t','G8..G60007'); %imaging section outlet
VinAorta=dlmread(fileName,'\t','I8..I60007'); %aorta inlet

PoutImSect=(VoutImSect-C_int)/C_slope;
PinAorta=(VinAorta-A_int)/A_slope;

%filtered pressure waveform
fPoutImSect=LPButterworthFilt(sampleRate,freq*harmonics,PoutImSect);
fPinAorta=LPButterworthFilt(sampleRate,freq*harmonics,PinAorta);

%higher harmonics filtered wave to find valve closure time
fPinAorta2=LPButterworthFilt(sampleRate,freq*highHarm,PinAorta);

%convert to Pa
fPinAorta_Pa=fPinAorta*mmHg_Pa_Conv;
fPoutImSect_Pa=fPoutImSect*mmHg_Pa_Conv;
fPinAorta2_Pa=fPinAorta2*mmHg_Pa_Conv;
deltaP=fPinAorta_Pa-fPoutImSect_Pa;

% finding the start frame of the camera
cycleIndex = round(cycleTime*sampleRate); %frames per cycle
for i = 1:length(time)
    if phantomTrigger(i,1) < 1
        triggerIndex = i;
        break
    end
end

% LOAD MEAN VELOCITY DATA--------------------------------------------------
```

```
% Get files in folder
fnames = dir([path '*.VC7']);
% Set a counter
count=0;

cycleFrames=round((1/freq)*frameRate); %cycle time multiplied by camera frame rate

%RIGID CASE ---------------------------------------------------------------
if type==1

%find diastolic minimum to start cycle from beginning of ejection
firstTriggerCycle=fPinAorta_Pa(triggerIndex:triggerIndex+cycleIndex);
[pks,pklocs] = findpeaks(-firstTriggerCycle);
pks=-pks;
[~,rigidDiastolicMinIdx] = min(pks);
rigidDiastolicMinIdx=rigidDiastolicMinIdx+1; %enter this if diastolic minimum is not the second
% minimum - for 980 RPM, subtract 4
localMinIndex=pklocs(rigidDiastolicMinIdx);
firstMinIndex=localMinIndex+triggerIndex;

%create new array for one cycle starting at first diastolic min
shortTime=(time(firstMinIndex:firstMinIndex+cycleIndex)-time(firstMinIndex));%for non-normalized
plot (zero to cycle time)
cutPressureIn = fPinAorta_Pa(firstMinIndex:(firstMinIndex+cycleIndex)); %inlet waveform using
startframe of inlet wave
cutPressureOut = fPoutImSect_Pa(firstMinIndex:(firstMinIndex+cycleIndex)); %peripheral waveform
using startframe of inlet waveform (marks beginning of systole)

%finding absolute min of inlet pressure wave in order to determine valve
%closure time
[abspks,abspklocs]=findpeaks(-cutPressureIn);
abspks=-abspks;
[~,absMinIdx]=min(abspks);
localAbsMinIndex=abspklocs(absMinIdx);
AbsMinIndex=localAbsMinIndex+firstMinIndex;

%bounds of integration for specifying time of systole
cycleStartTime=0;
cycleStartIndex = 1; %define lower bound of integration
valveCloseTime=time(AbsMinIndex)-time(firstMinIndex) %valve closure time
valveCloseIndex=AbsMinIndex-firstMinIndex+1;

%new arrays for period of systole
shortTimeSystole=time(firstMinIndex:AbsMinIndex)-time(firstMinIndex);
cutPressureInSystole=cutPressureIn(1:valveCloseIndex);
cutPressureOutSystole=cutPressureOut(1:valveCloseIndex);

offsetTime = time(firstMinIndex)- time(triggerIndex);
startFrame = round(frameRate*offsetTime);
startFrame= startFrame-DaVisOffset
endFrame=startFrame+round((valveCloseTime*frameRate)); %end of systole (as defined by absolute
min on inlet pressure wave)

% UNCOMMENT THIS TO CHECK WHERE MIN IS BEING FOUND ------------------------
```

```
figure(figmin);
plot(shortTimeSystole,cutPressureInSystole.','r')

% COMPLIANT CASE----------------------------------------------------------

elseif type==2
%finding first minimum where image was taken (from inlet pressure wave)
firstTriggerCycle=fPinAorta(triggerIndex:(triggerIndex+cycleIndex));

[triggerpks,triggerpklocs]=findpeaks(-firstTriggerCycle);
triggerpks=-triggerpks;
newtriggerpks=triggerpks(triggerpks>min(triggerpks));
[~,compliantDiastolicMinIdx]=min(triggerpks);
newtriggerpklocs=triggerpklocs(triggerpks>min(triggerpks));
localDiastMinIdx=triggerpklocs(compliantDiastolicMinIdx);
firstMinIndex = localDiastMinIdx + triggerIndex;

%create new array for one cycle starting at first diastolic min
shortTime=(time(firstMinIndex:firstMinIndex+cycleIndex)-time(firstMinIndex));%for non-normalized
plot (zero to cycle time)
cutPressureIn = fPinAorta_Pa(firstMinIndex:(firstMinIndex+cycleIndex)); %inlet waveform using
startframe of inlet wave
cutPressureOut = fPoutImSect_Pa(firstMinIndex:(firstMinIndex+cycleIndex)); %peripheral waveform
using startframe of inlet waveform (marks beginning of systole)

cutPressureIn2 = fPinAorta2_Pa(firstMinIndex:(firstMinIndex+cycleIndex));
% cutDeltaP=deltaP(firstMinIndex:(firstMinIndex+cycleIndex));

low=0.3;
up=.42;

%find valve closure index from higher harmonic waveform
[vcPks,vcPkLocs]=findpeaks(-cutPressureIn2(shortTime<up & shortTime>low));
vcPks=-vcPks;
[~,vcMinIdx]=min(vcPks);
localVcIdx=vcPkLocs(vcMinIdx);

shift1=firstMinIndex+(low*sampleRate);

vcIndex=localVcIdx+shift1; %index wrt beginning of cycle

%systole indices
valveCloseIndex=vcIndex-firstMinIndex+1;
%valve close time
valveCloseTime=time(valveCloseIndex)

%new arrays for period of systole
shortTimeSystole=time(firstMinIndex:firstMinIndex+valveCloseIndex-1)-time(firstMinIndex);
cutPressureInSystole=cutPressureIn(1:valveCloseIndex);
cutPressureOutSystole=cutPressureOut(1:valveCloseIndex);

% UNCOMMENT THIS TO CHECK WHERE MIN IS BEING FOUND ------------------------
figure(figmin);
plot(shortTime, cutPressureIn2,'k')
```

```
hold on
plot(shortTime,cutPressureIn2(valveCloseIndex)*ones(length(shortTime)),'b');
plot(shortTimeSystole,cutPressureInSystole.','r')
hold off

offsetTime = time(firstMinIndex)- time(triggerIndex);
startFrame = round(frameRate*offsetTime);
if startFrame==0
    startFrame=1
else
    startFrame= startFrame-DaVisOffset
end

endFrame=startFrame+round((valveCloseTime*frameRate));

end

%LOAD PIV IMAGES, CALCULATE VELOCITY---------------------------------------

for i = startFrame:skip:endFrame
    count = count+1;
    v_File = [path fnames(i).name];
    % Load the vector file
    VEC = loadvec(v_File);
    VEC=rotatef(VEC,pi);

    % Define the sub region

    if i==startFrame
    [x1find,~]=find(VEC.vy);
    x1=min(x1find)-1;
    x2=max(x1find)+1;
    y1=1;
    [s1 s2]=size(VEC.y);
    y2=s2;

    box = [x1 y1 x2 y2];
    end

    VEC2 = extractf(VEC,box); % get the vectors
        count2=0; %count2 represents the y location at which we're averaging (how many locations
in the y direction are we using to find the average velocity profile)
        %calculate velocity profiles across length of FOV
        %calculate velocity profiles across length of FOV
        c1=1;
        c2=length(VEC2.x);
        rdsmax=c2-c1+1;
    for j=c1:1:c2 %j is the x locations under consideration
        count2=count2+1;
        profilePixel(count,count2)=mean2(VEC2.vy(j,:)); %average value per column
        velProfile(count,count2)=((profilePixel(count,count2)*frameRate)/pixel2mm)*0.001;

        rds=j-c1;
```

```
        radVal(count,count2)=(rds/rdsmax)*r; %r position in tube [mm]

    end

    fit1{count}=fit(radVal(count,:).',velProfile(count,:).','smoothingspline'); %smoothing spline for velocity profiles

    velProfileArea(count)=trapz(radVal(count,:).',velProfile(count,:).'); %area under averaged velocity profile for each image (count)
    volFlowRate(count)=pi*r*velProfileArea(count); %m3/s %integrate velocity profile around 180 degrees to get volume flow rate
    massFlowRate(count)=volFlowRate(count)*rho; %kg/s %multiply flow rate times density to get mass flow erate


    avgVel(count)=mean2(velProfile(count,:));

end

%disregard negative mass flow rate values
for q=1:length(massFlowRate)

    if massFlowRate(q)<0
        massFlowRate(q)=0;
    end
       q=q+1;
end

for x=1:length(velProfileArea);
    velTime(x)= (startFrame+(x*skip))*(1/frameRate)-(startFrame*(1/frameRate)); %calculating the time steps associated with each image
end

%DYNAMIC ENERGY ---------------------------------------------------------

%calculating terms for integration
vSqrd=avgVel.^2;
VIntFunct=vSqrd.*massFlowRate;

VInt=trapz(velTime.',VIntFunct.');
VNRG=VInt*(1/2)

figure(fig1)
plot(velTime,avgVel,'k.-');
xlabel('Time, {\itt} [s]');
ylabel('Velocity, {\itv} [m/s]');

figure(fig2)
plot(velTime, VIntFunct,'b.-');
xlabel('Time, {\itt} [s]')
ylabel('Squared Velocity * mdot [m2/s2(kg/s)]');

figure(fig3)
plot(velTime,massFlowRate,'r.-');
```

```
xlabel('Time, {\itt} [s]')
ylabel('Mass Flow Rate [\itkg/s]');
ylim([-0.05 .3]);

% PRESSURE ENERGY ------------------------------------------------------

PCurveFitOutSystole=fit(shortTimeSystole,cutPressureOutSystole,'smoothingspline');

for pts=1:length(massFlowRate) %fit pressure curve to the same data points as the velocity data
so it can be multiplied by mass flow rate
    PressTimeAdjusted(pts)=velTime(pts);
    PressAdjusted(pts)=PCurveFitOutSystole(PressTimeAdjusted(pts));
    pts=pts+1;
end

PIntFunct=PressAdjusted.*massFlowRate;
PInt=trapz(velTime.',PIntFunct.');
PNRG=PInt/rho

figure(fig4)
plot(shortTimeSystole,cutPressureInSystole,'b');
hold on
plot(shortTimeSystole,cutPressureOutSystole,'r-');
xlabel('Time, {\itt} [s]');
ylabel('P(t) [Pa]')
hold off

figure(fig5)
plot(velTime,PIntFunct,'k-');
xlabel('Time, {\itt} [s]');
ylabel('P(t)*mdot')

% STATIC ENERGY --------------------------------------------------------

SInt=trapz(velTime.',massFlowRate.');
SNRG=z*g*SInt

%LOCAL ACCELERATION ----------------------------------------------------

dv_dt=diff(avgVel)./diff(velTime);
accelTime=velTime(1:length(dv_dt));

tick=0;
interval=1; %how many data points to skip over for acceleration plot (on top of skip already
applied to avg velocity plot)
for t=1:interval:length(dv_dt)
    tick=tick+1;
    accelFunct(tick)=dv_dt(t);
    accelTimeFunct(tick)=accelTime(t);
    massFlowRateAdjusted(tick)=massFlowRate(t);
    end

accelIntFunct=accelFunct.*massFlowRateAdjusted;
accelInt=trapz(accelTimeFunct.',accelIntFunct.');
```

```
figure(fig6)
plot(accelTimeFunct,accelFunct,'k.-');
xlabel('Time, {\itt} [s]');
ylabel('dv/dt [m/s2]')

figure(fig7)
plot(accelTimeFunct,accelIntFunct,'k.-');
xlabel('Time, {\itt} [s]');
ylabel('(dv/dt)*mdot');

ANRG=z*accelInt

%TOTAL ENERGY ------------------------------------------------------------

totNRG=PNRG+VNRG+SNRG+ANRG

% excelfileName='C:\Users\kgcamero\Dropbox\Graduate Research & Designs\Thesis\Start
Frames.xlsx';
% sheet=2;
% excelData1=[VNRG PNRG SNRG ANRG totNRG];
%
% xlRange1='K10';
% xlswrite(excelfileName,excelData1,sheet,xlRange1);
```

A-3.20 Matlab code used to generate pump energy plots from Sections 5.6.5

```
clear
close all
fig1=figure; set(fig1,'position',[100 200 1100 650]);

excelfileName='C:\Users\KatieG\Dropbox\Graduate Research & Designs\Thesis\Start Frames.xlsx';
sheet=3;

xlRange_RPM='B3:B7'; RPM=xlsread(excelfileName,2,xlRange_RPM);
xlRange_980Dist='B3:B5'; Dist980=xlsread(excelfileName,sheet,xlRange_980Dist);
xlRange_980NRG='C3:C5'; NRG980=xlsread(excelfileName,sheet,xlRange_980NRG);

xlRange_1065Dist='D3:D5'; Dist1065=xlsread(excelfileName,sheet,xlRange_1065Dist);
xlRange_1065NRG='E3:E5'; NRG1065=xlsread(excelfileName,sheet,xlRange_1065NRG);

xlRange_1235Dist='F3:F5'; Dist1235=xlsread(excelfileName,sheet,xlRange_1235Dist);
xlRange_1235NRG='G3:G5'; NRG1235=xlsread(excelfileName,sheet,xlRange_1235NRG);

xlRange_1450Dist='H3:H5'; Dist1450=xlsread(excelfileName,sheet,xlRange_1450Dist);
xlRange_1450NRG='I3:I5'; NRG1450=xlsread(excelfileName,sheet,xlRange_1450NRG);

xlRange_1540Dist='J3:J4'; Dist1540=xlsread(excelfileName,sheet,xlRange_1540Dist);
xlRange_1540NRG='K3:K4'; NRG1540=xlsread(excelfileName,sheet,xlRange_1540NRG);

figure(fig1)
p1=plot(Dist980,NRG980,'ko-');
hold on
p2=plot(Dist1065,NRG1065,'bo-');
p3=plot(Dist1235,NRG1235,'ro-');
p4=plot(Dist1450,NRG1450,'mo-');
p5=plot(Dist1540,NRG1540,'go-');
ylim([0 135]);
xlabel('Distensibility, {\itd} [mmHg^{-1}]');
ylabel('Pump Energy, {\itE_{VAD}} [J/min]');
LF1=legend('{\it\omega_{AL pump}}= 980 RPM','{\it\omega_{AL pump}}= 1065 RPM','{\it\omega_{AL
pump}}= 1235 RPM','{\it\omega_{AL pump}}= 1450 RPM','{\it\omega_{AL pump}}= 1540 RPM');
set(LF1,'location','eastoutside');
set(gca,'XTick',0:0.0005:0.006);
set(gca,'YTick',0:10:130);
ax=gca;
ax.FontName='Calibri';
ax.FontSize=14;
set(ax,'LooseInset',get(ax,'TightInset'));
```